2023

# Exploring coral symbiosis under climate change stress across spatial and temporal scales

BOSTON UNIVERSITY

GRADUATE SCHOOL OF ARTS AND SCIENCES

Dissertation

# EXPLORING CORAL SYMBIOSIS UNDER CLIMATE CHANGE STRESS ACROSS SPATIAL AND TEMPORAL SCALES

by

**HANNAH ELISE AICHELMAN**

B.Sc., University of North Carolina at Chapel Hill, 2014
M.Sc., Old Dominion University, 2018

Submitted in partial fulfillment of the

requirements for the degree of

Doctor of Philosophy

2023

Approved by

First Reader _____

Sarah W. Davies, Ph.D.
Assistant Professor of Biology

Second Reader _____

Peter Buston, Ph.D.
Associate Professor of Biology

## DEDICATION

This dissertation is dedicated to my Dad, who fostered my love of the ocean and encouraged the adventures that led me to pursue many years' worth of graduate degrees in marine biology.

## ACKNOWLEDGMENTS

This work, and making it through the last five years pursuing a PhD, would have been made infinitely more difficult without the support of my amazing community. First and foremost, thank you to my advisor, Dr. Sarah Davies. I am immensely grateful to have worked with an advisor who is also a dear friend, despite the occasional complications that brought. Thank you for being my biggest cheerleader, and for being there to celebrate all the wins and mourn all the losses. You work so hard to foster a lab environment full of collaboration and lovely humans, and we are all better for it. It has been a joy to do science together, and to get to watch your girls grow up in the process. What an adventure it's been since the days of front porch evenings in Carrboro, cheers to many more!

There are so many other incredible folks at Boston University and beyond that have been instrumental in my academic journey. Starting with Mr. Rice, my high school AP Biology teacher, thank you for fostering my love of science and for being such a strong support through a tough time in my life. Thank you also to my previous academic advisors, Dr. Karl Castillo and Dr. Dan Barshis, for guiding me to the point where I even started a PhD and for shaping my interest in coral biology. Special thanks to my committee members, Dr. Pete Buston, Dr. Sean Mullen, Dr. Carly Kenkel, and Dr. Karen Warkentin, for challenging me to think critically about my work and guiding my scientific growth. My time at BU has been greatly enriched by lab family, including Dan Wuitchik, James Fifer, Maria Valadez Ingersoll, Carsten Grupstra, Colleen Bove, Annabel Hughes, JK Da-Anoy, Hanny Rivera, Lili Vizer, and Nicola Kriefall. Whether I've known you for all five years or less than one, y'all have had such a positive impact on my time at BU. My dissertation

would also not have been possible without the incredibly bright undergraduates and high school students who helped along the way, including Alexa Huzar, Olivia Nieves, Laura Tsang, Carlos Tramonte, Hayden Dickerson, Alyssa Pereslete, Andrea Rodas, and Jack Weldon.

I am forever grateful to have moved to Boston at the same time as my dear friends Jamie and Alex Durbin, and for all of the adventures we've had since. Thank you for afternoons in the garden, delicious meals together (including a Covid Thanksgiving and German feasts), and for unwavering support through the ups and downs of getting a PhD. Friends like y'all make Boston home. Boston has also been made home by my first roommates in the city, MacKenzie and Deniz – thank you for kitchen dance parties, back porch dinners, and for being my companions through a global pandemic. Dan Wuitchik deserves some extra love here, for being a friend since day one and for truly being part of my Boston Family, along with Brian Kennedy. Thank you both for hiking adventures, Sunday Rituals, and nights with too much whiskey.

My family have been massively supportive throughout my entire academic journey. Thank you to my Dad, Julie, and Mom for raising me to be a strong, intelligent woman. I am also eternally grateful for the love and support of my brother Jay and sister-in-law Katie. A massive thank you to the full Aichelman and Eckler clans, especially for supporting me at my defense, both in person and remotely. I love you all dearly.

Last but certainly not least, thank you to my love, Nick Fox. Thank you for sharing my love of the ocean, and for always being up for a tide pooling, snorkeling, or clamming adventure. Your dedication to building a wonderful life for us is incredible, and something

I will be eternally grateful for. Thank you for being there to celebrate my successes and to build me up on my lowest days. Your support has made getting through the end of this degree possible. I love you to the bottom of the ocean and back again.

**EXPLORING CORAL SYMBIOSIS UNDER CLIMATE CHANGE STRESS ACROSS SPATIAL AND TEMPORAL SCALES**

**HANNAH ELISE AICHELMAN**

Boston University Graduate School of Arts and Sciences, 2023

Major Professor: Sarah W. Davies, Assistant Professor of Biology

ABSTRACT

Human activity since the Industrial Revolution has increased global greenhouse gas concentrations resulting in rapid climate change, which now threatens terrestrial and marine ecosystems. Tropical coral reefs, along with the biodiversity and communities they support, are particularly threatened by these changes in climate. Corals are a consortium of organisms, with the coral host along with its photosynthetic endosymbiont (Family Symbiodiniaceae) and diverse community of microorganisms (bacteria, archaea, fungi, and viruses) together forming the 'coral holobiont'. However, the symbiosis between tropical corals and Symbiodiniaceae algae is sensitive to even small changes in temperature and 'coral bleaching' events – the loss of symbiosis – are now occurring with increased frequency and severity. These bleaching events can result in coral mortality and loss of entire reefs if stressful conditions do not subside. While research efforts have increased our ability to understand and predict coral bleaching events, fundamental questions remain surrounding how genetic diversity of the coral holobiont and interactions with its environment can drive coral resilience or resistance under climate change. The overarching goal of my dissertation is to understand how various abiotic (*i.e.,* stress duration,

spatiotemporal variation on the reef) and biotic (*i.e.,* holobiont diversity, symbiosis) factors determine a coral's response to environmental change at the level of phenotype and genotype. To achieve this goal, I first tested how environmental history and stress duration modulated the physiological responses of two reef-building corals under combined ocean warming and ocean acidification conditions. I found that one species was more stress-resistant (*Siderastrea siderea*), but that both duration of stress exposure and environmental history (inshore vs. offshore reef origin) modulated coral physiology. Next, I investigated the importance of holobiont genetic identity and abiotic environment in driving phenotypic responses of *S. siderea* exposed to a diel temperature variability (DTV) and subsequent heat challenge experiment. I found that while DTV increased coral growth, cryptic host diversity and their unique pairings with algal symbiont strains were the strongest predictors of holobiont physiology and response to heat challenge. Lastly, I leveraged genome-wide gene expression profiling and the facultative symbiosis between the subtropical coral *Oculina arbuscula* and its symbiont *Breviolum psygmophilum* to disentangle the independent responses of both partners to heat and cold challenges in and out of symbiosis. I found that *O. arbuscula* host gene expression was more plastic under temperature challenges relative to *B. psygmophilum* when in symbiosis, and that symbionts exhibited more gene expression plasticity in culture compared to in symbiosis. Taken together, this dissertation provides valuable insights into the phenotypic and genotypic mechanisms that contribute to coral success in a changing climate.

## TABLE OF CONTENTS

## LIST OF TABLES

## LIST OF FIGURES

# CHAPTER ONE: INTRODUCTION

Climate change is causing dramatic alterations across terrestrial and marine landscapes, as a result of increasing concentrations of anthropogenic greenhouse gasses (particularly $CO_2$) trapping heat in the atmosphere. In the ocean, this greenhouse effect has resulted in increasing temperatures (ocean warming) and decreasing pH (ocean acidification) (Pörtner et al. 2019). In 2021, ocean temperatures were the hottest ever recorded (Cheng et al. 2022), and this trend will only continue unless we dramatically reduce greenhouse gas emissions (Cooley et al. 2022). The effects of climate change are already apparent on organisms across the globe, and include overall declines in biodiversity (Harvey et al. 2022; Butchart et al. 2010), species range expansions (Hickling et al. 2006) and contractions (Parmesan 2006), and phenological shifts (Parmesan and Yohe 2003). The global extinction risk is predicted to accelerate with rising temperatures, and if we continue warming the planet under the "business as usual" scenario, it is estimated that one in six species will be threatened with extinction (Urban 2015). Such rapid environmental changes are affecting organisms across the tree of life, and it remains critical to understand the abiotic and biotic factors influencing these responses to enable predictions of species persistence in a changing world.

Understanding how symbioses will be affected by rapid environmental change is even more challenging, as there is not just one organism to consider, but instead a 'holobiont'–the host and all associated microbiota. According to the hologenome theory, the holobiont (and its associated hologenome) serves as a distinct biological entity upon which selection can act (Rosenberg and Zilber-Rosenberg 2018). Symbiosis can alter an

organism's response to heat stress, and have been shown to increase holobiont thermal tolerance through diverse mechanisms, including altering the expression of host stress-response genes and producing protective metabolites (reviewed in Hector et al. 2022). In an interesting example of a vertebrate symbiosis, the microbiome has been shown to alter acute thermal tolerance under both heat and cold challenge in tadpoles, and additionally influenced survival over prolonged heat stress (Fontaine, Mineo, and Kohl 2022). It is therefore important to characterize the identity of all members of a holobiont, and to understand how unique combinations of hosts and symbionts interact to influence holobiont responses to climate change.

The tropical coral holobiont, consisting of the coral host, its obligate photosynthetic dinoflagellate algae in the family Symbiodiniaceae, and its diverse community of microorganisms (bacteria, archaea, fungi, and viruses), is an iconic symbiosis that is severely threatened by climate change (Putnam et al. 2017). This symbiotic relationship, in which corals obtain the majority of their nutritional requirements as photosynthetic by-products from Symbiodiniaceae algae (Muscatine 1990), allows corals to thrive in oligotrophic waters and build ecosystems that support an incredible diversity of marine ecosystem services valued at billions of dollars annually (Costanza et al. 2014). Tropical corals live close to their upper thermal limit, making them susceptible to even small increases in temperature (Berkelmans and Willis 1999; Baker, Glynn, and Riegl 2008). Such increasing temperatures can compromise the relationship between coral hosts and their Symbiodiniaceae algae, which can lead to dysbiosis in a process termed "coral bleaching" (Brown 1997; Glynn 1984). If the coral persists in its bleached (aposymbiotic)

state for long enough, it can result in starvation and eventual mortality (Brown 1997; Boilard et al. 2020). Coral bleaching events are now occurring with increasing frequency and severity, which is only projected to worsen as climate change continues (van Hooidonk et al. 2016). As a result, live coral cover has declined substantially over the last 50 years, leading to a concurrent decline in the ability of these ecosystems to provide the services on which millions of coastal Indigenous people and small-island developing states rely (T. D. Eddy et al. 2021). However, coral reefs are not changing homogeneously, and while our understanding of which reefs and species are more bleaching resistant is advancing (Safaie et al. 2018; Grottoli et al. 2014), predicting their future remains challenging due to complexities governing coral resilience, including environmental variation, host genetics, and associations with algal and microbial symbionts (reviewed by Bove, Ingersoll, and Davies 2022).

Abiotic environmental conditions are known to vary greatly on coral reefs, both across small spatial scales and broad latitudinal gradients, which influences coral physiology and stress responses. One classic example of environmental gradients on coral reefs are reef zones, where offshore habitats tend to experience lower turbidity, less run-off, higher water flow, and more stable temperatures compared to inshore habitats, which tend to have higher turbidity, less flow, and more variable temperatures (Kenkel et al. 2013; Morgan et al. 2017; Briand, Guzmán, and Sunday 2023). These environmental differences drive the community composition and functional characteristics of coral reefs (Briand, Guzmán, and Sunday 2023) and influence historical coral growth rates (Castillo et al. 2012). Additionally, it is hypothesized that corals originating from these inshore

environments may be "primed" to withstand future stressors (Drury et al. 2022; Hackerott, Martell, and Eirin-Lopez 2021). Elevated thermotolerance of inshore corals has been linked specifically to high frequency temperature variability, also called diel temperature variability (DTV) (*e.g.,* Kenkel, Almanza, and Matz 2015; Oliver and Palumbi 2011). While the role of DTV in mitigating coral bleaching has been recently highlighted on reefs spanning the globe (Safaie et al. 2018; Schoepf et al. 2020), it is not a cure-all, and temperature variability can also have negative impacts on corals (Schoepf, Sanderson, and Larcombe 2022). Therefore, it is critical to understand the environmental factors that enable coral holobionts to respond to and survive such diverse challenges.

In addition to the role of environmental history, the physiological stress responses of coral holobionts can vary greatly across host species (Bove et al. 2019; Okazaki et al. 2017), algal symbiont communities (Abrego et al. 2008), and microbiomes (Morrow, Muller, and Lesser 2018; Ziegler et al. 2017). For example, twelve species of Caribbean scleractinian corals exhibited diverse calcification responses when exposed to crossed ocean warming and acidification treatments, with positive, neutral, and negative calcification observed (Okazaki et al. 2017). The calcification response was also not consistent under warming and acidification stress, highlighting the importance of considering how corals respond not just to temperature, but also to other stressors that occur concurrently on reefs, including acidification (*e.g.,* Okazaki et al. 2017; Horvath et al. 2016; Edmunds, Brown, and Moriarty 2012). Disentangling the effects of multiple stressors on corals is only further complicated by the diversity of Symbiodiniaceae algae they can associate with, because unique combinations of coral hosts and algal symbionts

can greatly influence the coral holobiont's response to stress. For example, the algal symbiont *Durusdinium trenchii* has been shown to confer thermal tolerance to their hosts, both through elevated photochemical efficiency (Fv/Fm) (Berkelmans and van Oppen 2006) and lower bleaching prevalence (Manzello et al. 2019; reviewed in Stat and Gates 2010). Alternatively, *Acropora tenuis* juveniles hosting *Cladocopium sp.* exhibited lower metabolic costs and higher tolerance to heat and light stress compared to those hosting *Durusdinium sp.* (Abrego et al. 2008). Coral holobionts have also been shown to shuffle their algal symbiont communities from less tolerant Symbiodiniaceae species to more tolerant ones following a bleaching event, which improved performance under a later heat stress event (Silverstein, Cunning, and Baker 2015). Similar to algal symbiont communities, microbial communities have also been associated with coral thermal resilience, and these communities can shift in response to distinct thermally variable habitats (Ziegler et al. 2017). Given that each of these symbiotic partners plays a role in coral resilience, it is critical to consider multiple members of the coral holobiont (*i.e.*, host, algal symbiont, and microbiome) when evaluating coral responses to climate change stressors.

Our understanding of coral responses to climate change has been additionally complicated by a growing appreciation for cryptic host diversity on coral reefs. Cryptic coral lineages are distinct genetic clusters that were previously characterized as a single species (Bickford et al. 2007), and have now been found to differ in their spatial distributions (Matias et al. 2022; Fifer et al. 2022) and bleaching tolerances (Gómez-Corrales and Prada 2020). Cryptic lineages have also been shown to differ in their

associations with Symbiodiniaceae, and Rose et al. (2021) demonstrated that *Acropora hyacinthus* cryptic lineages differed in their associations with *Durusdinium*, and the most thermotolerant lineage hosted *Durusdinium* more often than the other lineages. Such cryptic diversity has the potential to play an important role in determining how reef communities will respond to future climate change conditions, and additionally in how we design more effective coral restoration efforts.

The endosymbiosis between coral hosts and their algal symbionts allows them to persist in oligotrophic tropical waters, but also presents a distinct threat under increasing temperatures. It has been hypothesized that reactive oxygen species (ROS) produced by Symbiodiniaceae under stress can damage cellular components, cause photoinhibition, and trigger bleaching (reviewed in Szabó, Larkum, and Vass 2020). Therefore, coral hosts may benefit from controlling the environment of their algal symbionts to maintain conditions that are suitable for photosynthesis and nutrient sharing. For example, Barott et al. (2015) demonstrated that coral hosts acidify the symbiosome (*i.e.*, organelle in which the algal symbiont is housed) *via* expression of V-type proton ATPases, which serves as a carbon concentrating mechanism and promotes photosynthesis. Additionally, cnidarian hosts have been shown to regulate symbiont cell densities by controlling nitrogen available to the symbiont through glutamine-dependent nitrogen cycling, both in corals (Rivera and Davies 2021) and in anemones (Xiang et al. 2020; Cui et al. 2019). There is additional evidence that hints at host control of the symbiont's microenvironment, particularly at the level of gene expression, where coral hosts exhibit many more differentially expressed genes than their photobionts under heat stress (*e.g.,* Barshis et al. 2014; Bellantuono et al. 2019; S. W.

Davies et al. 2018; Leggat et al. 2011). However, few studies have directly compared the effects of temperature stress on algal symbionts both in and out of symbiosis (*in hospite* and *ex hospite*), which would be required to test for a host's ability to buffer their algal symbionts.

Despite a growing number of studies focused on understanding the response of corals to climate change, there are still many outstanding questions regarding what makes corals both resistant and resilient in the face of climate change. This dissertation takes an integrative approach to coral resilience from genes to populations, and leverages diverse experimental approaches to understand, at the level of phenotype and genotype, the role of stress duration, spatiotemporal variation on the reef, and symbiosis in determining a coral's response to stress. This dissertation gives rise to valuable insights about the phenotypic and molecular mechanisms underlying symbiosis maintenance in corals, particularly under global climate change.

In Chapter 2, I characterized the phenotypes of two major tropical reef-building coral species (*Siderastrea siderea, Pseudodiploria strigosa*) and their symbionts from two reef zones on the Belize Mesoamerican Barrier Reef System through time in a 95-day common garden exposure to warming (~28, 31°C), acidification ($pCO_2 \sim 343$ [present day], ~663 [end of century], ~3109 [extreme] $\mu$atm), and their interaction. By tracking coral holobiont physiology (net calcification rate, host protein and carbohydrate, chlorophyll *a*, and symbiont density) every 30 days through the 95-day exposure, I showed species differences in physiological responses that were modulated by exposure duration. *Siderastrea siderea* was generally resistant to end of century $pCO_2$ and temperature stress,

while *P. strigosa* holobiont physiology was negatively affected by elevated temperatures. While *S. siderea* calcification was negatively impacted by extreme $pCO_2$ conditions initially, we demonstrated recovery through positive calcification rates by the end of the experiment, suggesting acclimation. Additionally, while *P. strigosa* physiology was negatively affected overall by elevated temperatures, nearshore corals maintained calcification under those conditions, providing evidence for local adaptation of this species to the warmer nearshore environment. This chapter illustrates the benefits of tracking holobiont physiology of multiple coral species throughout long-term experiments to reveal more nuanced responses to climate change stressors.

In Chapter 3, I assessed the roles of abiotic environment and holobiont genetic identity in driving phenomic responses of *Siderastrea siderea.* Corals were sourced from six sites spanning an inshore to offshore gradient across Bocas del Toro, Panamá and exposed to a common garden exposure including 50 days of diel temperature variability (DTV) followed by a 15-day heat challenge and 16-day recovery. We found that DTV increased coral growth overall, but all other phenotypes were more strongly shaped by the presence of three cryptic host lineages that differed in their spatial distributions, phenomes, and algal associations. The lineage found predominantly at offshore sites was more likely to host *Durusdinium trenchii* algal symbionts, had elevated energetic reserves, exhibited higher growth, had smaller corallites, and greater resistance under heat challenge, highlighting the potential for ecological specialization of these cryptic lineages. Additionally, unique combinations of host-symbiont pairings resulted in differences in thermotolerance. These findings highlight the complexities associated with projecting

bleaching, the role of DTV in driving coral growth, and the need to better characterize cryptic diversity when evaluating responses of corals to global change.

In Chapters 2 and 3, many of the factors contributing to how a coral holobiont responds to climate change stress are explored in tropical, reef-building corals. However, understanding the independent stress responses of each symbiotic partner in tropical corals is ultimately challenging because the symbiosis is obligate, and therefore any aposymbiotic host response is inherently coupled with nutritional stress. Therefore, in Chapter 4, I leveraged the facultatively symbiotic subtropical coral *Oculina arbuscula* and its symbiont *Breviolum psygmophilum* to disentangle the independent host and symbiont responses to temperature challenges. Previous work has shown that coral host transcriptomes respond more strongly to environmental stress compared to their algal symbionts at the level of gene expression, which suggests that coral hosts could be regulating their symbiont's environment to buffer environmental stress. To explore this further, I used genome-wide gene expression profiling (TagSeq) to characterize the response of both *O. arbuscula* and *B. psygmophilum* in symbiosis (*in hospite*) and out of symbiosis (*ex hospite*) to thermal challenge using two separate experiments. First, the host and *in hospite* symbiont response was considered by exposing symbiotic and aposymbiotic fragments of *O. arbuscula* to three temperature treatments: 1) control (18°C), 2) heat challenge (32°C), and 3) cold challenge (6°C). This experimental design was replicated with *B. psygmophilum* cultured from *O. arbuscula* to characterize *ex hospite* photobiont response. I then identified orthologous genes and demonstrated that *O. arbuscula* hosts responded more to cold challenge compared to heat, and responded more overall than their *in hospite* symbiont. By

comparing *B. psygmophilum* gene expression across the two experiments, I observed a more plastic response to temperature challenge *ex hospite.* Additionally, while cold challenge negatively affected *B. psygmophilum* photosynthesis both *in* and *ex hospite*, a gene expression signature of oxidative stress was found *ex hospite*, but not *in hospite*. While future work will benefit from additional technologies, including proteomics, these findings presented in Chapter 4 suggest that *O. arbuscula* hosts buffer the environment of *B. psygmophilum* under thermal challenge.

# CHAPTER TWO: EXPOSURE DURATION MODULATES THE RESPONSE OF CARIBBEAN CORALS TO GLOBAL CHANGE STRESSORS

This chapter is published, and the full citation is as follows:

Aichelman, Hannah E., Colleen B. Bove, Karl D. Castillo, Jessica M. Boulton, Alyssa C. Knowlton, Olivia C. Nieves, Justin B. Ries, and Sarah W. Davies. 2021. "Exposure Duration Modulates the Response of Caribbean Corals to Global Change Stressors." *Limnology and Oceanography* 66 (8): 3100–3115. https://doi.org/10.1002/lno.11863.

## 2.1 Abstract

Global change, including rising temperatures and acidification, threatens corals globally. Although bleaching events reveal fine-scale patterns of resilience, traits enabling persistence under global change remain elusive. We conducted a 95-d controlled-laboratory experiment investigating how duration of exposure to warming (~28, 31°C), acidification ($pCO_2 \sim 343$ [present day], ~663 [end of century], ~3109 [extreme] $\mu$atm), and their combination influences physiology of reef-building corals (*Siderastrea siderea*, *Pseudodiploria strigosa*) from two reef zones on the Belize Mesoamerican Barrier Reef System. Every 30 d, net calcification rate, host protein and carbohydrate, chlorophyll *a*, and symbiont density were quantified for the same coral individual to characterize acclimation potential under global change. Coral physiologies of the two species were differentially affected by stressors and exposure duration was found to modulate these responses. *Siderastrea siderea* exhibited resistance to end of century $pCO_2$ and temperature stress, but calcification was negatively affected by extreme $pCO_2$. However, *S. siderea* calcification rates remained positive after 95 d of extreme $pCO_2$ conditions,

suggesting acclimation. In contrast, *P. strigosa* was more negatively influenced by elevated temperatures, which reduced most physiological parameters. An exception was nearshore *P. strigosa*, which maintained calcification rates under elevated temperature, suggesting local adaptation to the warmer environment of their natal reef zone. This work highlights how tracking coral physiology across various exposure durations can capture acclimatory responses to global change stressors.

## 2.2 Introduction

Since the Industrial Revolution, anthropogenic activities have increased the partial pressure of atmospheric carbon dioxide ($pCO_2$), causing atmospheric warming of ~0.6°C (Pörtner et al. 2019). As atmospheric temperatures increase, so do sea surface temperatures (SSTs) (Pörtner et al. 2019). Increasing $pCO_2$ has also caused surface ocean pH to decrease by 0.017 to 0.027 units per decade since the 1980s (Pörtner et al. 2019). Warming and acidification have impacted organisms across the globe, as thermal niches shift and habitats rapidly change (Morley et al. 2018; Pörtner et al. 2019). The negative effects of global climate change are predicted to strengthen and, under the Intergovernmental Panel on Climate Change's (IPCC) most extreme emissions scenario (RCP8.5), oceans are expected to uptake 5 to 7 times more heat and decrease by 0.3 pH units by 2100 (van Vuuren et al. 2011; Pörtner et al. 2019).

Coral reefs are valuable economic and ecological resources (Costanza et al. 2014) that are vulnerable to ocean warming and acidification. The high biodiversity of coral reefs depends on the obligate symbiosis between corals and their symbiotic algae (LaJeunesse

et al. 2018). This symbiosis is sensitive to thermal anomalies and, because tropical reef-building corals live within 1°C of their upper thermal limit, small SST increases can result in bleaching (breakdown of symbiosis) and ultimately mortality if symbionts fail to repopulate the coral host. These coral bleaching events are occurring with increasing frequency and severity as SSTs continue to rise (Hughes et al. 2017).

Ocean acidification alters seawater carbonate chemistry (Doney et al. 2009) by reducing seawater pH, carbonate ion concentration ($[CO_3^{2-}]$), and the saturation state of seawater with respect to aragonite ($\Omega_{arag}$)—which can make it challenging for corals to build their aragonite skeletons (Doney et al. 2009). Laboratory experiments have shown that projected acidification conditions can have negative (Horvath et al. 2016; Hoegh-Guldberg et al. 2007), neutral (Reynaud et al. 2003), threshold (Ries, Cohen, and McCorkle 2010 [409-2856 µatm]), and parabolic (Castillo et al. 2014) impacts on coral calcification, while *in situ* manipulative field experiments have yielded more negative outcomes (Albright et al. 2018; Kline et al. 2019). The direction and magnitude of coral calcification responses to acidification are influenced by numerous factors, including species-level differences (Bove et al. 2019; Okazaki et al. 2017), differences in the ability to regulate calcifying fluid chemistry (Guillermic et al. 2021; Y.-W. Liu et al. 2020; Justin B. Ries 2011), $CO_2$-induced fertilization of photosynthesis (Castillo et al. 2014), gonochoric colony sex (Holcomb, Cohen, and McCorkle 2012), experimental duration (Kline et al. 2019), co-occurring thermal stress (Kroeker et al. 2013), boundary layer limitation of proton flux (Jokiel 2011), heterotrophy (Towle, Enochs, and Langdon 2015), and biomass energy utilization (Wall et al. 2017). Calcification in response to temperature stress is

similarly complicated by a number of factors. For example, calcification rates of corals have been shown to respond parabolically to temperature, with trends varying across species (Edmunds 2005). Additional complexities have been linked to life history and seasonality (Kornder, Riegl, and Figueiredo 2018). Energetic reserves are critical to coral health and resistance to stressors, and have been associated with bleaching susceptibility (Anthony et al. 2009; Levas et al. 2018) and whether a bleaching event will lead to mortality (Anthony et al. 2009; Grottoli et al. 2014). Additionally, a coral's response to thermal stress–like their response to acidification–can be mediated by heterotrophy (Aichelman et al. 2016; Grottoli, Rodrigues, and Palardy 2006).

Fewer studies consider the interactions of temperature and acidification stress, and these studies have similarly produced variable results. Although some research finds stronger negative effects of elevated temperature compared to acidification on calcification (Anderson et al. 2019; Schoepf et al. 2013) and survivorship (Anderson et al. 2019), others have shown additive effects of the two stressors (Agostini et al. 2013; Edmunds, Brown, and Moriarty 2012; Horvath et al. 2016; Rodolfo-Metalpa et al. 2011). The response of the coral holobiont to environmental stress varies by stressor, and also by species. Such species-level differences have been observed in coral calcification under crossed temperature and acidification stress (Bove et al. 2019; Okazaki et al. 2017) and recovery of energetic reserves through time after bleaching (Levas et al. 2018). Additionally, spatial scale can play a role in response to environmental stress, with differential stress tolerance observed across populations along a reef system (Dixon et al. 2015), between reef zones (Castillo et al. 2012; Kenkel et al. 2013), and between tidal pools (Bay and Palumbi 2014),

illustrating that adaptation and/or acclimation to fine scale environmental differences can play a role in determining stress response. Therefore, a more complete understanding of the interactions of environmental stressors necessitates investigations of multiple species from different populations in response to multiple stressors across longer timescales with a focus on holobiont physiology.

Considering how duration of stress exposure affects the coral holobiont is critical (McLachlan et al. 2020), but this pursuit is complicated by the difficulty of executing long-term laboratory experiments. However, several studies have been conducted for ~90 days or more, revealing patterns of stress and resilience. For example, acidification (1,050 μatm $pCO_2$) caused rapid, species-specific alterations of calcifying fluid chemistry in four coral and two calcifying algae species that remained for one year (Comeau et al. 2019). Castillo et al. (2014) showed calcification responses to elevated $pCO_2$ varied with exposure duration, with *S. siderea* calcification under moderate $pCO_2$ (604 μatm) increasing between 0 and 60 days and decreasing between 60 and 90 days. Additionally, Levas et al. (2018) tracked corals for 11 months following experimental bleaching and found interspecific differences in recovery. *Porites divaricata* initially catabolized lipids and decreased calcification but recovered within 11 months, while *P. astreoides* recovered within 1.5 months after increasing feeding and symbiont nitrogen uptake (Levas et al. 2018). In summary, tracking coral physiology through time provides valuable insights into how corals respond to short-, moderate-, and long-term stress.

Here, two ecologically important reef-building coral species (*Siderastrea siderea* and *Pseudodiploria strigosa*) from two reef zones with distinct thermal environments

(Baumann et al. 2016) of the Belize Mesoamerican Barrier Reef System (MBRS) were maintained under a fully crossed $pCO_2$ (~343 μatm [present day], ~663 μatm [end of century], ~3109 μatm [extreme]) and temperature (~28, 31°C) 95-day experiment. Control and elevated temperature treatments correspond to present-day mean annual temperature from the collection sites on the MBRS (Baumann et al. 2016; Castillo et al. 2012) and projected end of century annual mean temperature for this region (Stocker et al. 2013), respectively. End of century $pCO_2$ is based on the RCP6 emissions scenario, and extreme $pCO_2$ is a projection for the year 2500 under RCP8.5 (Stocker et al. 2013), and is intended to test a coral's response to extreme acidification. To characterize the species' responses to projected global change, holobiont physiology of each colony was monitored approximately every 30 days (exposure duration: 0-30 days=$T_0$-$T_{30}$=short-term, 30-60 days=$T_{30}$-$T_{60}$=moderate-term, 60-95 days=$T_{60}$-$T_{95}$=long-term), including metrics for coral host (calcification rate, protein, carbohydrates) and algal symbiont (symbiont cell density, chlorophyll *a*). This work elucidates the impact of exposure duration on corals' acclimatory response to global change stressors.

## 2.3 Materials and methods

### *2.3.1 Coral collection and experimental design*

The experiment presented here was run in parallel with that published by Bove et al. (2019); therefore, experimental design and culturing conditions are similar to those presented therein. However, our study used different coral colonies and only two species (instead of four). Experimental timing is staggered by 30 days between the two experiments; for comparison, $T_0$ here corresponds to "pre-acclimation period" in Bove et al. (2019). This difference in timing is intentional because we wanted to observe the effects of the initial exposure period, while Bove et al. (2019) treated this as "pre-acclimation" and excluded this experimental interval. Methods specific to this experiment are presented below with additional details in Appendix 1.1.

Three colonies of *Siderastrea siderea* and three colonies of *Pseudodiploria strigosa* were collected from a nearshore and forereef site along the southern Belize MBRS (Figure 2-1, Appendix 1.1). All colonies were transported to Northeastern University's Marine Science Center in Nahant, Massachusetts, USA and fragmented into 24 pieces. One forereef *P. strigosa* colony did not survive fragmentation, leaving 3 genotypes for nearshore and forereef *S. siderea,* 3 genotypes for nearshore *P. strigosa*, but only 2 genotypes for forereef *P. strigosa.* We acknowledge that replication across reef zone is limited; however, sample size was restricted by permitting, space was limited within experimental tanks, as well as the large colony size and number of fragments needed to consider genet-level coral physiology through time. After fragmentation, corals recovered for 23 days in natural flow-through seawater (5 μm-filtered seawater obtained from

Massachusetts Bay) maintained at 28.2±0.5°C and ~500 µatm $pCO_2$. Following recovery, temperature and $pCO_2$ were incrementally adjusted over 20 days until target treatments were achieved. The six experimental treatments consisted of a full factorial design of two temperatures (target: 28, 31°C) and three $pCO_2$ levels (target: 400, 700, 2800 µatm). In order to capture genotype-specific responses through time, four replicate coral fragments per genotype were represented in each of the six treatments, and each treatment was replicated in three 42 L acrylic tanks on a 10:14 h light:dark cycle (full spectrum LED lights; Euphotica, 120W, 20000K) with PAR of ~300 µmol photons $m^{-2}$ $s^{-1}$ (Castillo et al. 2014). Coral fragments were fed a combination of ~6 g frozen adult *Artemia* sp. and 250 mL newly hatched live *Artemia* sp. (500 $mL^{-1}$) every other day and maintained in treatment conditions for 95 days or until preservation.

Experimental conditions were maintained similarly to Bove et al. (2019). Temperature, salinity, and pH were measured in all tanks every few days (n=40 total) and water samples for total alkalinity (TA) and dissolved inorganic carbon (DIC) were collected a total of 7 times throughout the experimental period. TA and DIC were measured using a VINDTA 3C (Marianda Corporation, Kiel, Germany) calibrated with certified Dickson Laboratory standards for seawater $CO_2$ measurements (Scripps Institution of Oceanography; San Diego, California, USA). Temperature, salinity, TA, and DIC were used to calculate all carbonate system parameters using $CO_2$SYS (Pierrot et al. 2006) with Roy et al. (1993) carbonic acid constants $K_1$ and $K_2$, the Mucci (1983) value for the stoichiometric aragonite solubility product, and an atmospheric pressure of 1.015 atm. All measured and calculated seawater parameters are reported in Figures A1-1, A1-2, and

Tables A1-1, A1-2. Cumulative average (±SE) $pCO_2$ and temperature throughout the 95-day experimental period (n=20-21) were: 298±27 µatm, 28.0±0.04 °C (present day $pCO_2$, 28 °C); 388±25 µatm, 31.1±0.04 °C (present day $pCO_2$, 31 °C); 663±13 µatm, 28.0±0.06 °C (end of century $pCO_2$, 28 °C); 662±28 µatm, 31.0±0.03 °C (end of century $pCO_2$, 31 °C); 2973±125 µatm, 28.1±0.02 °C (extreme $pCO_2$, 28 °C); 3245±154 µatm, 30.7±0.06 °C (extreme $pCO_2$, 31 °C).

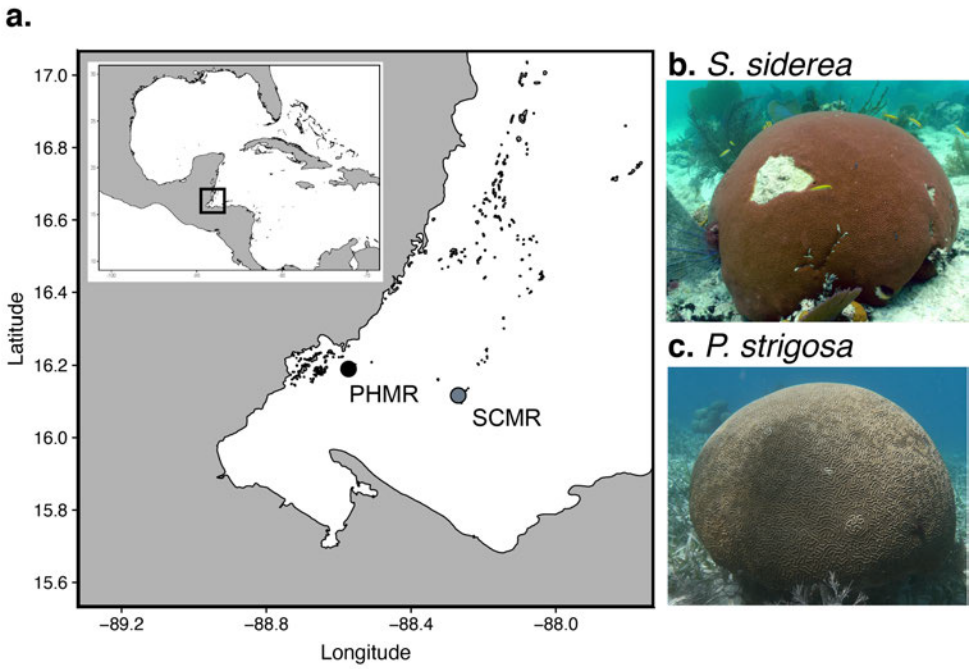


**Figure 2-1.**
**(a)** Map of forereef (SCMR=Sapodilla Cayes Marine Reserve) and nearshore (PHMR=Port Honduras Marine Reserve) coral collection sites on the Belize Mesoamerican Barrier Reef System. **(b)** Example of *Siderastrea siderea* (photo credit: K.D. Castillo). **(c)** Example of *Pseudodiploria strigosa* (photo credit: H.E. Aichelman).

### *2.3.2. Coral host and symbiont physiology*

Coral host and symbiont physiological measurements were taken at each of the four time points ($T_0$, $T_{30}$, $T_{60}$, $T_{95}$). Net calcification rates were estimated in triplicate for each fragment using the buoyant weight technique (S. Davies 1989) and normalized to surface area. A subset of fragments from both species were used to confirm the relationship between buoyant weight and dry weight (Bove et al. 2019). Growing surface area was quantified in triplicate from photos taken at each timepoint using ImageJ software (Rueden et al. 2017). The same surface area values of each coral fragment were used to normalize all host and symbiont physiological parameters within a time point. Additionally, at each time point, a fragment of each colony was removed from each treatment, flash frozen in liquid nitrogen, and stored at −80°C until processing, when fragments were airbrushed to remove host tissue and symbiont cells. Tissue slurries were homogenized and centrifuged to separate coral tissue and symbiont fractions for physiological assays. Fragments were frozen approximately every 30 days, but the actual number of days from $T_0$ to sampling were 36 ($T_0$ to $T_{30}$), 63 ($T_0$ to $T_{60}$), and 92 ($T_0$ to $T_{95}$). Because corals were frozen on the same day for each time point, there was no need to correct for the number of days in experimental treatment for physiological metrics other than calcification rate.

Total coral host protein content was quantified from host tissue slurry using a bicinchoninic acid protein assay following manufacturer's instructions. Total host carbohydrates were quantified using the phenol-sulfuric acid method (Masuko et al. 2005), which measures all monosaccharides, including glucose—the major photosynthate translocated from symbiont to coral (Burriesci, Raab, and Pringle 2012). Symbiont cell

density was quantified using the hemocytometer method (Rodrigues and Grottoli 2007). Symbiont photosynthetic pigments (chlorophyll *a,* abbreviated Chl *a*) were quantified spectrophotometrically following Marchetti et al. (2012). See Appendix 1.1 for additional details.

### *2.3.3. Statistical analyses*

Statistical differences between experimental treatments were tested using an ANOVA (*aov*) with fixed effects of temperature and $pCO_2$, and post-hoc pairwise comparisons were assessed using Tukey's HSD tests (reported in Table A1-7). Temperature and $pCO_2$ data were log-transformed if necessary to meet assumptions of normality, which was assessed via a Shapiro-Wilk Test (*shapiro.test*). The results of statistical differences between treatments are reported in Table A1-7 as well as Figures A1-1 and A1-2. Coral physiological data were assessed using a series of linear mixed effects models (*lmer*) for each species and individual physiological parameter (including fixed effects of time, temperature, $pCO_2$, and reef zone) using a forward model selection method (Appendix 1.1). A random effect of genotype was included in all models to account for physiological variation across genotypes. Physiological data were transformed to meet assumptions of normality for ANOVAs when necessary, including several parameters for *P. strigosa* (symbiont density [cube root], Chl *a* [square root], carbohydrate [square root]) and *S. siderea*: symbiont density [log], Chl *a* [cube root], carbohydrates [square root]). *Siderastrea siderea* calcification rates did not meet assumptions of normality despite transformations; therefore, a generalized additive model for location scale and shape with

a Weibull distribution (Rigby and Stasinopoulos 2005) was fit using the same forward model selection method (Appendix 1.1). Model results are reported with summary statistics in Table A1-3. Significant post-hoc pairwise comparisons from linear mixed effects models were assessed using Tukey's HSD tests implemented in the *lsmeans* function (reported in Table A1-4).

Principal Components Analyses (PCA) were constructed using the *FactoMineR* package (Lê, Josse, and Husson 2008) to assess how overall physiologies were modulated through time for each species. Significance of each factor in the PCA was assessed using PERMANOVA, via the *adonis* function in the *vegan* package (Oksanen et al. 2022). Statistics for all *adonis* tests are reported in Table A1-5.

Correlation matrices of all host and symbiont physiological parameters for both species through time were built using the *corrplot* function with a significance threshold of $p$=0.05. Impacts of temperature and $pCO_2$ on host and symbiont physiology of only *P. strigosa* were assessed via linear regression modeling, as no noteworthy correlations were found for *S. siderea*. To estimate significance of predictors and their interactions, increasingly parsimonious, nested linear models (using *lmer*) were compared with likelihood ratio tests. Conditional R-squared values, accounting for both fixed and random effects, of regressions were determined using the *r.squaredGLMM* function in the *MuMIn* package. Summary statistics for all linear regressions are reported in Table A1-6. All raw data and code associated with analyses presented here are stored in a Github repository at the following link: https://github.com/hannahaichelman/TimeCourse_Physiology. All statistical analyses used R version 4.0.1 (R Core Team 2017).

## 2.4 Results

### *2.4.1. Holobiont physiology through time*

*Siderastrea siderea* holobiont physiology (calcification rate, host protein and carbohydrate, chlorophyll *a*, symbiont density) clustered more strongly by $pCO_2$ than by temperature (Figure 2-2a-c). There was an apparent, but not statistically significant, effect of $pCO_2$ on holobiont physiology after short-term exposure ($T_{30}$, $p$=0.054; Figure 2-2a), and this effect became significant through time ($T_{95}$: $p$=0.002; Figure 2-2c). At $T_{95}$, the interaction of $pCO_2$ and temperature was also significant ($p$=0.001; Figure 2-5c). Principal components analyses loadings for calcification, symbiont density, and Chl *a* discriminate between clusters of fragments in extreme $pCO_2$ and other acidification treatments (Figure 2-2a-c). Comparing PCAs in Figure 2-2a-c with individual physiological results (Figures 2-3a,c and 2-4a,c) demonstrates that $pCO_2$ significantly reduced *S. siderea* calcification, symbiont density, and Chl *a*, but did not have a significant effect on host carbohydrates or protein. Reef zone did not have a significant effect on *S. siderea* holobiont physiology for any exposure duration (Figure 2-2a-c).

Holobiont physiology of *P. strigosa* clustered more strongly by temperature than by $pCO_2$, especially after long-term exposure ($T_{95}$; Figure 2-2d-f). At $T_{60}$, there was a significant effect of $pCO_2$ on holobiont physiology ($p$=0.029; Figure 2-2e). However, at $T_{95}$ $pCO_2$ was no longer significant, and only temperature had a significant effect ($p$=0.045; Figure 2-2f). Additionally, the interaction of reef zone and temperature had a marginally significant effect on holobiont physiology after long-term exposure ($T_{95}$; $p$=0.053; Figure 2-2f). Comparing PCAs in Figure 2-2d-f with results from individual physiological

parameters (Figures 2-3b,d and 2-4b,d) shows that elevated temperature resulted in consistent negative effects on all physiological parameters.

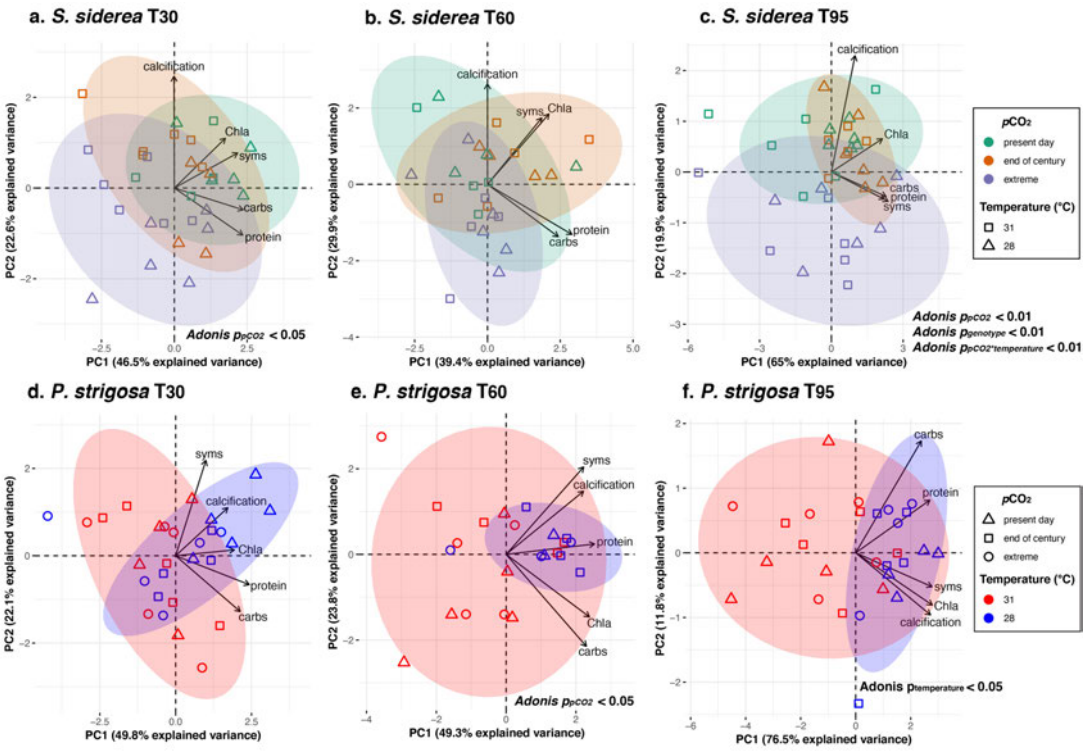


**Figure 2-2.**
**Influence of temperature, $pCO_2$, and exposure duration on holobiont physiology.** Principal components analyses of log-transformed holobiont physiological data, including total carbohydrate (carbs; mg $cm^{-2}$), total protein (protein; mg $cm^{-2}$), symbiont density (syms; cells $cm^{-2}$), chlorophyll *a* (Chla; µg $cm^{-2}$), and calcification (mg $cm^{-2}$ $day^{-1}$) for *Siderastrea siderea* (**a-c**) and *Pseudodiploria strigosa* (**d-f**). Colors represent $pCO_2$ for *S. siderea* (**a-c**: green=present day, orange=end of century, purple=extreme) and temperature for *P. strigosa* (**d-f**: red=31°C, blue=28°C). Shapes represent temperature for *S. siderea* (**a-c**: square=31°C, triangle=28°C) and $pCO_2$ for *P. strigosa* (**d-f**: triangle=present day, square=end of century, circle=extreme). Points represent an individual coral fragment's physiology at each time point (a,d=short-term [$T_{30}$], b,e=moderate-term [$T_{60}$], c,f=long-term [$T_{95}$]). Only individuals with data for all five parameters at each time point were included. The x- and y-axes indicate variance explained (%) by the first and second principal component, respectively.

### *2.4.2. Effects of temperature and $pCO_2$ stress on calcification*

*Siderastrea siderea* net calcification rates were clearly influenced by $pCO_2$, and were significantly reduced under extreme $pCO_2$ relative to present day $pCO_2$ ($p$=0.002; Figure 2-3a). However, end of century $pCO_2$ did not significantly reduce *S. siderea* net calcification relative to present day $pCO_2$ ($p$=0.4). Additionally, *S. siderea* net calcification was significantly reduced at $T_{90}$ relative to $T_{30}$ ($p$=0.02). Neither temperature treatment nor reef zone significantly altered net calcification rates. For this and all remaining individual physiological parameters, full model outputs (estimate, standard error, T-value, etc.) are reported in Table A1-3, and post-hoc pairwise comparisons are reported in Table A1-4.

*Pseudodiploria strigosa* net calcification rates were significantly negatively affected by $pCO_2$ ($p$<0.001; Figure 2-3b), and when compared to present day $pCO_2$ calcification rates were reduced under end of century ($p$=0.02) and extreme $pCO_2$ ($p$<0.001). Calcification rates were also reduced at elevated temperature (31°C) relative to control conditions ($p$<0.001), and nearshore corals exhibited higher net calcification rates than forereef corals ($p$=0.04). A significant interaction of temperature and experimental duration was detected for *P. strigosa* calcification rates ($p$<0.001), with calcification decreasing between $T_{30}$ and $T_{60}$ under control and elevated temperatures ($p$<0.05); however, these reductions were not detectable after moderate- and long-term exposure ($T_{60}$ and $T_{95}$). When considering the full duration of the experiment ($T_0$ to $T_{95}$), *P. strigosa* net calcification rates were lower under elevated, but not control temperatures (Figure 2-3b). Additionally, a significant interaction between reef zone and temperature on *P. strigosa* calcification rate was detected ($p$=0.03), with elevated temperatures more negatively

influencing calcification of forereef corals than nearshore corals ($p$=0.02). Lastly, there was a significant interaction between temperature and $pCO_2$ on *P. strigosa* calcification rates ($p$<0.001). Specifically, there were no significant differences in *P. strigosa* calcification rates amongst $pCO_2$ treatments under elevated temperatures, but calcification rates in control temperatures were significantly reduced under extreme $pCO_2$ compared to present day $pCO_2$ ($p$<0.001).

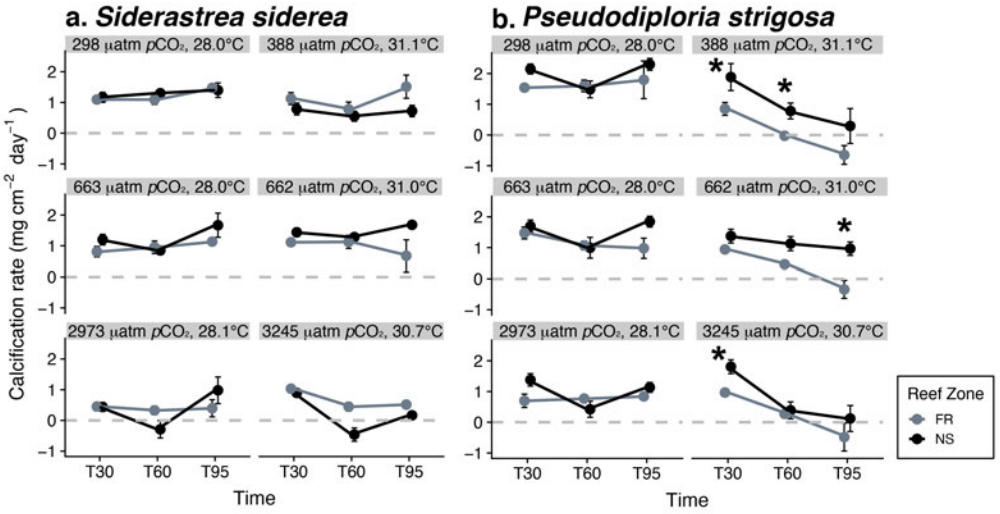


**Figure 2-3.**
*Siderastrea siderea* (**a**) and *Pseudodiploria strigosa* (**b**) net calcification rate (mg $cm^{-2}$ $day^{-1}$) at each experimental time point (short-term=$T_{30}$; moderate-term=$T_{60}$; long-term=$T_{95}$). Facets represent the six treatments and are labeled with average $pCO_2$ and temperature for the experiment duration ($pCO_2$: present day [top row], end of century [middle row], extreme [bottom row]; temperature: control [left column], elevated [right column]). Within a facet, data are separated by reef zone (FR=forereef; NS=nearshore). Points represent mean calcification rates since the previous time point (i.e., $T_{30}$ represents calcification between $T_0$ and $T_{30}$). Asterisks (*) indicate significant ($p$<0.05) differences in calcification rates between reef zones within a time point. Error bars represent standard error. For (**a**), each data point represents three colonies. For (**b**), each FR point represents 2 colonies and each NS point represents 3 colonies, except extreme $pCO_2$/28°C treatment at $T_{60}$ and $T_{95}$, where one forereef colony is represented due to mortality. For both (**a**) and (**b**), $n$=1-3 fragments/colony depending on time point ($T_{30}$ $n$=3, $T_{60}$ $n$=2, and $T_{90}$ $n$=1). Although there are exceptions due to mortality, sample size for each point should therefore be: $T_{30}$ $n$=9, $T_{60}$ $n$=6, and $T_{90}$ $n$=3 (degrees of freedom reported in Table A1-3).

### *2.4.3. Effects of temperature and $pCO_2$ stress on host energy reserves*

Elevated temperatures significantly reduced *S. siderea* protein concentrations relative to corals in control temperatures ($p$=0.009; Figure 2-4a). Regardless of $pCO_2$ and temperature treatments, *S. siderea* proteins increased through time, and at $T_{95}$ corals had higher mean protein than $T_0$ ($p$=0.03). Neither $pCO_2$ nor reef zone significantly altered *S. siderea* protein concentrations. Similar to proteins, elevated temperatures significantly reduced *S. siderea* carbohydrate concentrations relative to control temperatures (Figure 2-4c; $p$=0.004). Neither $pCO_2$, reef zone, nor experiment duration significantly altered *S. siderea* carbohydrate concentrations.

Temperature significantly influenced *P. strigosa* protein ($p$<0.001; Figure 2-4b), with reduced protein concentrations under elevated temperatures compared to controls ($p$<0.001). Neither $pCO_2$, reef zone, nor experiment duration significantly altered *P. strigosa* protein concentrations. Similarly, *P. strigosa* total carbohydrate was reduced under elevated temperatures compared to control conditions ($p$<0.001; Figure 2-4d). Regardless of treatment, carbohydrates decreased between $T_0$ and $T_{60}$ ($p$<0.01). Under control temperatures, *P. strigosa* carbohydrates increased between $T_{60}$ and $T_{95}$ ($p$=0.004); however, under elevated temperatures, carbohydrates did not increase significantly between $T_{60}$ and $T_{95}$ (Figure 2-4d). Neither $pCO_2$ nor reef zone significantly altered *P. strigosa* carbohydrate concentrations.

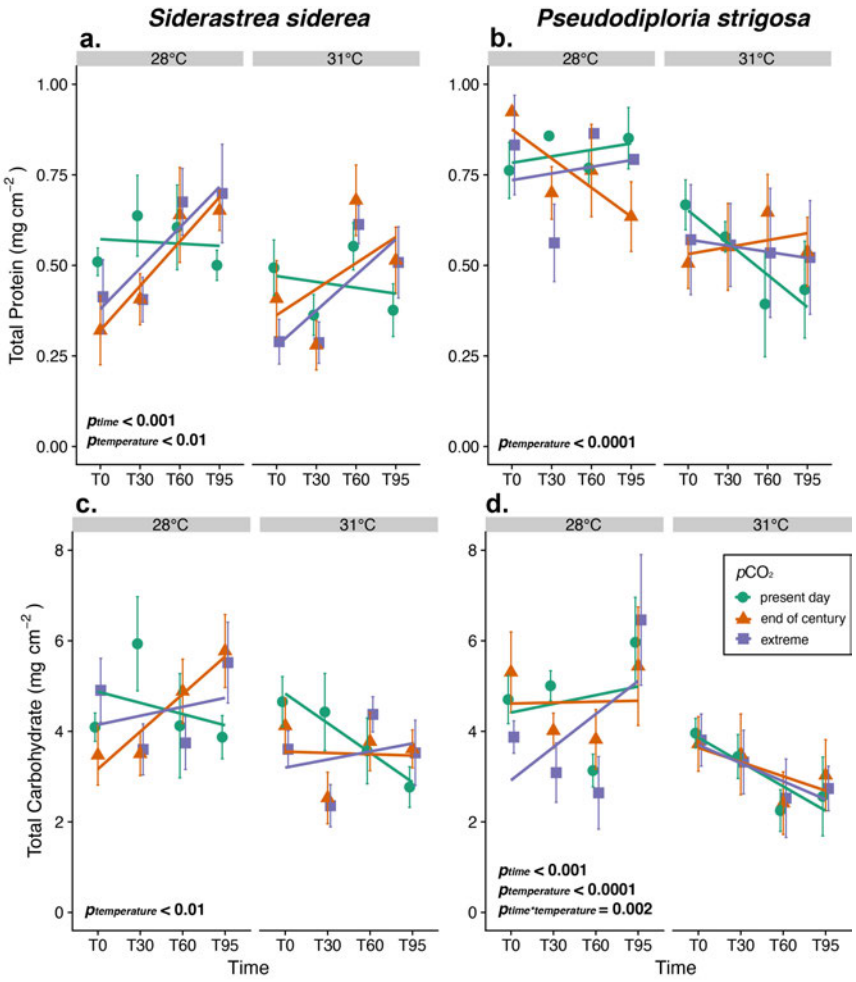


**Figure 2-4.**
Host energy reserves (total protein [**a,b**] and total carbohydrate [**c,d**]) of *Siderastrea siderea* (**a,c**) and *Pseudodiploria strigosa* (**b,d**) across four experimental durations (day 0=$T_0$; day 30 [short-term]=$T_{30}$; day 60 [moderate-term]=$T_{60}$; day 95 [long-term]=$T_{95}$). Within panels, results are faceted by temperature and colored by $pCO_2$ (present day=green, end of century=orange, extreme=purple). Each point is an average of nearshore and forereef corals, with $n$=4-6 (*S. siderea*) and $n$=3-6 (*P. strigosa*) distinct fragments ($n$=1/genotype). Significant factors are indicated in each panel. Lines represent linear fits (using ggplot2 *stat_smooth()* method to visualize differences regardless of model) for each treatment through time, and error bars represent standard error.

### *2.4.4. Effects of temperature and $pCO_2$ stress on symbiont physiology*

*Siderastrea siderea* symbiont densities decreased from $T_0$ to $T_{95}$ ($p$=0.0001), were reduced under elevated temperatures compared to control ($p$=0.001), and were reduced under extreme $pCO_2$ relative to end of century ($p$=0.04; Figure 2-5a). Reef zone did not significantly alter *S. siderea* symbiont densities. In contrast to symbiont density, *S. siderea* Chl *a* increased from $T_0$ to $T_{95}$ ($p$<0.001; Figure 2-5c). Although corals under present day and end of century $pCO_2$ treatments exhibited similar Chl *a* concentrations, corals under extreme $pCO_2$ had significantly less Chl *a* compared to those under both present day ($p$=0.001) and end of century ($p$=0.03) $pCO_2$. Neither reef zone nor temperature significantly altered *S. siderea* Chl *a*.

Regardless of $pCO_2$ treatment, *P. strigosa* had reduced symbiont densities under elevated temperatures compared to control temperatures ($p$<0.001; Figure 2-5b). Additionally, *P. strigosa* symbiont density was reduced at $T_{95}$ relative to $T_0$ ($p$<0.001). Neither $pCO_2$ nor reef zone significantly altered *P. strigosa* symbiont densities. Similarly, *P. strigosa* exhibited reduced Chl *a* under elevated temperatures compared to controls, regardless of $pCO_2$ treatment ($p$<0.001; Figure 2-5d). Additionally, *P. strigosa* Chl *a* was reduced under extreme $pCO_2$ compared to present day $pCO_2$ treatment regardless of temperature ($p$=0.02). Neither reef zone nor experiment duration significantly altered *P. strigosa* Chl *a*.

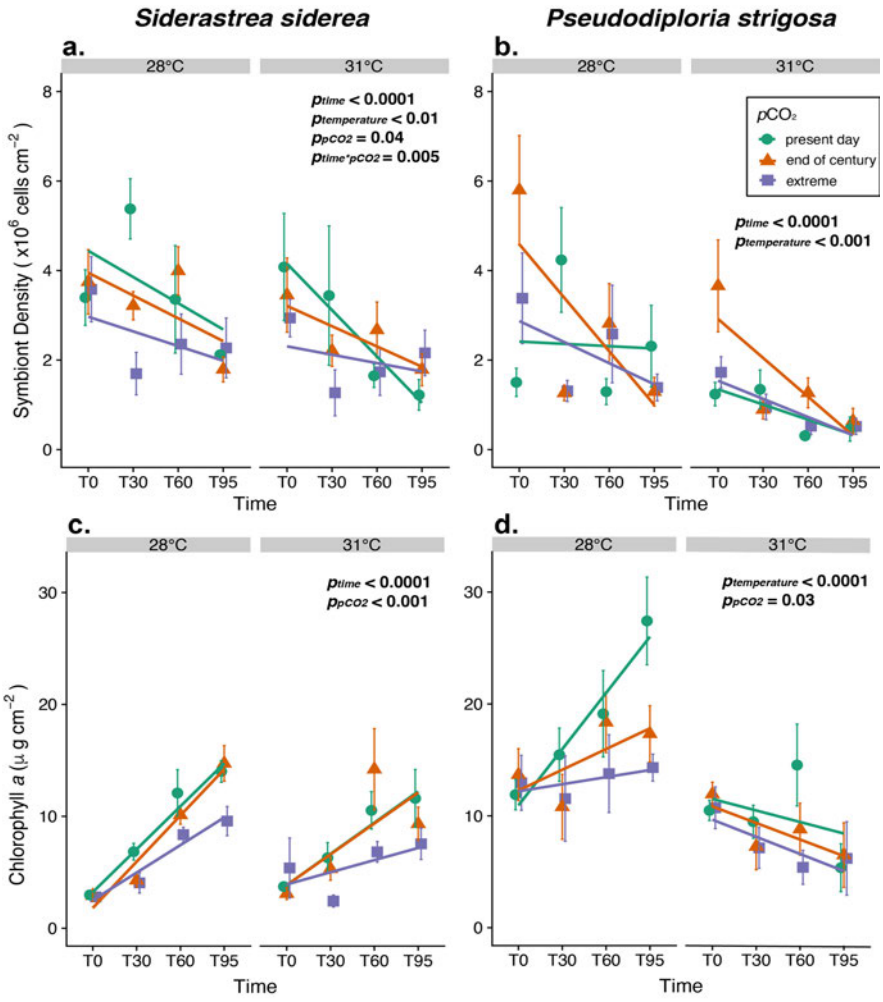


**Figure 2-5.**
Symbiodiniaceae physiology (symbiont cell density [**a,b**] and Chl *a* concentration [**c,d**]) of *Siderastrea siderea* (**a,c**) and *Pseudodiploria strigosa* (**b,d**) across four experimental durations (day 0=$T_0$; day 30 [short-term]=$T_{30}$; day 60 [moderate-term]=$T_{60}$; day 95 [long-term]=$T_{95}$). Within panels, results are faceted by temperature and colored by $pCO_2$ (present day=green, end of century=orange, extreme=purple). Each point is an average of nearshore and forereef corals, with *n*=4-6 (*S. siderea*) and *n*=3-6 (*P. strigosa*) distinct fragments (*n*=1/genotype). Significant factors are indicated in each panel. Lines represent linear fits (using ggplot2 *stat_smooth()* method to visualize differences regardless of model) for each treatment through time, and error bars represent standard error.

### *2.4.5.* Pseudodiploria strigosa *physiological trait correlations*

*Pseudodiploria strigosa* calcification rates were significantly correlated with all other physiological parameters ($p<0.05$) after long-term exposure ($T_{95}$; Figure A1-4), and temperature had a main effect on relationships between calcification and all other predictor variables (Figure 2-6). Under elevated temperatures at $T_{95}$, *P. strigosa* fragments with higher protein ($p=0.04$) and symbiont densities ($p=0.001$) maintained faster calcification rates (Figure 2-6b,c). A similar trend was observed for carbohydrates ($p=0.06$; Figure 2-6a). The interactive effect of temperature and the predictor variables on *P. strigosa* calcification rate was not significant until the end of the experiment ($T_{95}$; Figure A1-5). Correlations for *Pseudodiploria strigosa* (Figure 2-6) are presented in terms of temperature because it had a significant main effect on *P. strigosa* holobiont physiology at $T_{95}$ (Figure 2-2f). *Siderastrea siderea* correlation matrix (Figure A1-4) and linear regression analyses did not reveal any significant interactions with treatment.

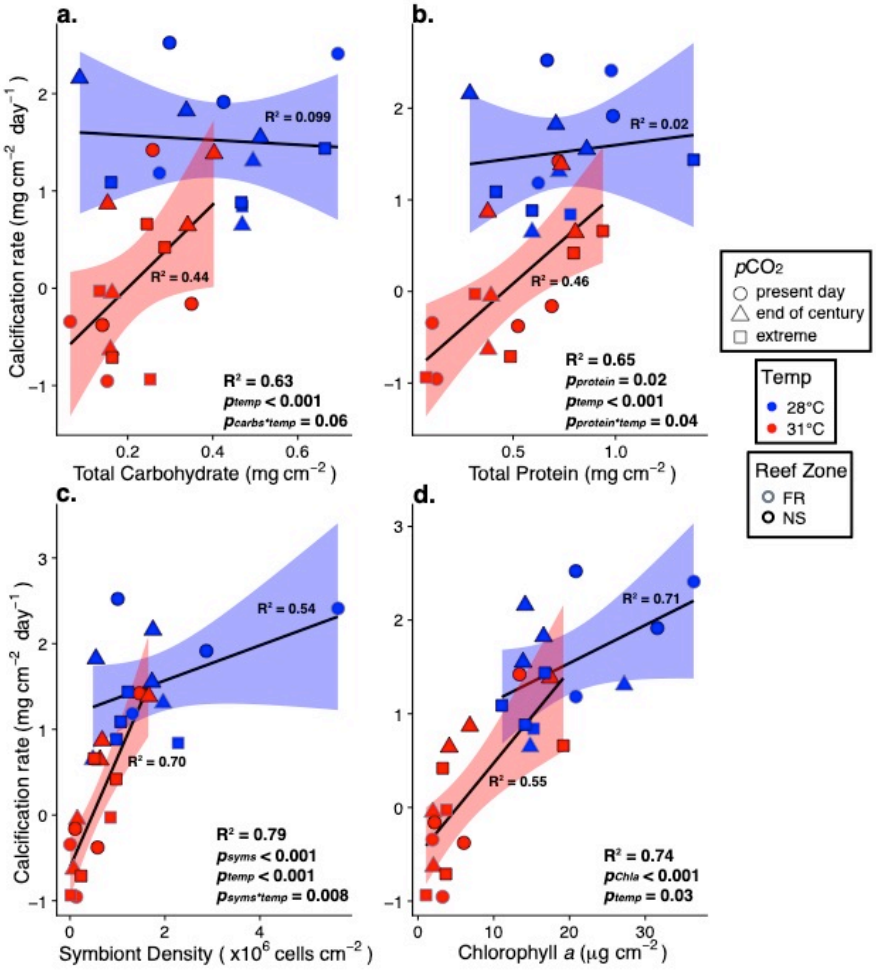


**Figure 2-6.**
Correlations of *Pseudodiploria strigosa* calcification rate with carbohydrates (**a**), proteins (**b**), symbiont density (**c**), and chlorophyll *a* (**d**) after long-term exposure to experimental treatments ($T_{95}$). Colors represent temperature treatment (red=31°C, blue=28°C), shapes represent $pCO_2$ (circle=present day, triangle=end of century, square=extreme), and shape outline colors represent reef zone (gray=forereef [FR], black=nearshore [NS]). Points represent individual coral fragments. Significant factors are indicated within each panel. Lines represent linear models of measured parameters within treatment through time, fit using ggplot2's *stat_smooth()* method with gray shading representing 95% confidence intervals for each temperature. Conditional $R^2$ values (Nakagawa and Schielzeth 2013) are reported for the whole model (bottom right corner of each facet) and for each temperature (next to the line of best fit).

## 2.5. Discussion

### *2.5.1. Divergent responses of coral species to warming and acidification*

*Siderastrea siderea* and *P. strigosa* exhibited divergent responses to two co-occurring global change stressors—ocean warming and acidification—and these responses were modulated by exposure duration. Overall *S. siderea* physiological performance was more negatively affected by acidification through time, while temperature had a more negative effect on *P. strigosa* over time. Such species-specific responses to temperature and acidification are not uncommon in reef-building corals. For example, when testing how twelve Caribbean coral species responded to crossed temperature and acidification conditions, Okazaki et al. (2017) observed that some species exhibited no growth response to either stressor (including *S. siderea* and *P. strigosa*), while other, more abundant species (*e.g., Orbicella faveolata* and *P. astreoides*), decreased calcification under both stressors. The difference between our findings and Okazaki et al. (2017) may be due to experiment duration (>30 days longer than Okazaki et al. [2017]) or be the result of the more extreme treatments used here (31°C and ~3109 µatm compared to 30.3°C and 1300 µatm $pCO_2$). It is also possible that *S. siderea* and *P. strigosa* populations in Florida (Okazaki et al. 2017) could be less susceptible to stress than populations from the Belize MBRS studied here. For example, according to the climate variability hypothesis (Stevens 1989), higher latitude populations (*e.g.,* Florida) that experience more variable thermal regimes (*i.e.,* stronger seasonality) are predicted to be more phenotypically flexible and exhibit a wider range of thermal tolerances compared to populations closer to the equator (*e.g.,* MBRS). A meta-analysis of Caribbean coral calcification responses to acidification, elevated temperature,

and their combination found similar regional differences in stress responses between corals from Florida and Belize (Bove, Umbanhowar, and Castillo 2020). While calcification of Florida corals did not clearly respond to acidification, elevated temperature, or their combination, elevated temperature reduced calcification rates in Belize corals (Bove, Umbanhowar, and Castillo 2020). While acknowledging differences in annual temperature variability, Bove et al. (2020) highlight differences in experimental treatment extremes as the main driver of calcification. Although consideration of treatment level is critical, such population-level differences in stress tolerance have been previously observed in corals (Dixon et al. 2015). Interestingly, such population-level differences—specifically with respect to thermal tolerance and coral bleaching—do not appear to be related to history of $pCO_2$ exposure (Noonan and Fabricius 2016; Wall et al. 2018). Regardless, our results contribute to a growing body of literature supporting the resistance of *S. siderea* to elevated temperature and acidification (Banks and Foster 2016; Bove et al. 2019; Castillo et al. 2014; S. W. Davies et al. 2016).

Resistance of *S. siderea* to global change stressors was previously reported by Castillo et al. (2014), which found that only the most extreme temperature (32°C) and acidification (2553 µatm $pCO_2$) treatments reduced calcification rates. Castillo et al. (2014) concluded that *S. siderea* will be more negatively impacted by elevated temperatures over the coming century, given the IPCC's next-century acidification projections did not reduce calcification. Our findings are consistent with this work, as only extreme–but not end of century $pCO_2$–reduced *S. siderea* calcification. Gene expression profiling of *S. siderea* from the Castillo et al. (2014) coral fragments revealed that thermal stress caused large-

scale downregulation of gene expression, while acidification elicited upregulation of proton transport genes (S. W. Davies et al. 2016). This potentially offsets effects of acidification at the site of calcification (*e.g.,* Justin B. Ries 2011), although this is potentially complicated by the electrochemical challenges of exporting $H^+$ from the calcifying fluid under acidified conditions (proton flux hypothesis; Jokiel 2011). These findings provide further support for *S. siderea*'s ability to acclimate to acidification.

Bove et al. (2019) investigated the combined effects of similar temperature and acidification treatments on four coral species: *S. siderea, P. strigosa, P. astreoides,* and *Undaria tenuifolia.* After 93 days, calcification declined in all species under increased $pCO_2$. However, only *P. strigosa* reduced calcification under elevated temperature, which is consistent with results presented here and highlights that thermal stress more negatively impacts *P. strigosa* than *S. siderea* (Figure 2-2d-f). Additionally, Bove et al. (2019) found that *S. siderea* was the most resistant of the four species, and maintained positive calcification rates even in the most extreme acidification treatment (~3300 µatm $pCO_2$) — findings that are also corroborated here (Figure 2-3a). By quantifying net calcification rates at 30-day increments, we show that *S. siderea* net calcification was negative under extreme $pCO_2$ at $T_{60}$, but that rates recovered by $T_{95}$ (Figure 2-3a). This result is potentially due to acclimation to stressful conditions over time, perhaps through transcriptome plasticity, as previously proposed in *S. siderea* (S. W. Davies et al. 2016) and in *P. astreoides* (Kenkel and Matz 2016); however, without following these colonies for even longer time periods, it is impossible to know without follow-up experimental work.

### *2.5.2. Stress differentially modulates physiology across coral species*

Under thermal and acidification stress, corals can draw on energy reserves, including lipids, proteins, and carbohydrates, to maintain and/or produce tissue and skeleton (Anthony et al. 2009; Schoepf et al. 2013). In addition to using energetic reserves, heterotrophy (Aichelman et al. 2016; Towle, Enochs, and Langdon 2015) or enhanced productivity of Symbiodiniaceae owing to $CO_2$ fertilization of photosynthesis (Brading et al. 2011) can augment energetic resources in zooxanthellate corals. Coral energetic reserves can therefore influence resistance to and recovery from thermal stress (Grottoli, Rodrigues, and Palardy 2006; Grottoli et al. 2014) as well as resistance to acidification (Wall et al. 2017).

In this study, host energy reserves of *S. siderea* and *P. strigosa* responded to temperature and acidification stress in different ways. Between $T_0$ and $T_{60}$, *P. strigosa* exhibited reduced carbohydrates regardless of treatment, indicating catabolism of this energy reserve (Figure 2-4d). This was followed by restoration of carbohydrates (acclimation) at control temperatures at $T_{95}$ (Figure 2-4d), which likely supported the positive calcification rates also observed under these conditions (Figure 2-6a, Figure A1-5). Protein reserves did not emulate trends in carbohydrates (Figure 2-4b), potentially owing to *P. strigosa* catabolizing carbohydrates before proteins, which has been observed over shorter time scales in other scleractinian corals (Grottoli, Rodrigues, and Juarez 2004). This sequence of energy reserve catabolism is consistent with relative enthalpies of combustion: carbohydrates are considered a short-term energy source and have the lowest enthalpy of combustion, lipids are a longer-term energy source and have the highest

enthalpy of combustion, and proteins are intermediate (Gnaiger and Bitterlich 1984; Grottoli, Rodrigues, and Juarez 2004). Elevated protein reserves did predict faster calcification rates in *P. strigosa* under elevated temperatures, but only after long-term exposure (Figure 2-6b, Figure A1-5). As photosynthate translocated from symbionts is a major source of carbohydrates to coral hosts (Burriesci, Raab, and Pringle 2012), reductions in *P. strigosa* symbiont densities, Chl *a*, and carbohydrates at elevated temperature suggests that symbionts were translocating fewer resources to the host, which likely contributed to reductions in calcification under elevated temperatures, particularly after long-term exposure ($T_{95}$; Figure 2-6, Figure A1-5). Total protein and carbohydrate of *S. siderea*, similar to *P. strigosa,* declined under elevated temperatures (Figure 2-4a,c)—consistent with previous work highlighting upregulation of protein catabolism pathways in *S. siderea* exposed to long-term thermal stress (S. W. Davies et al. 2016). Grottoli et al. (2004) previously linked species-level differences in energy catabolism to differences in photosynthesis/respiration ratios, and while we did not explore these traits here, this would be a worthy pursuit for future studies to better contextualize energy reserve catabolism of *S. siderea* and *P. strigosa* under stress. Additionally, a limitation to the present study is that lipid content was not measured through time, thereby precluding evaluation of a potential contributor to energy reserve catabolism under stress, as Wall et al. (2017) observed for *Pocillopora acuta*.

An overall trend in reduced symbiont density and increased Chl *a* through time was observed under most $pCO_2$ and temperature conditions, except for *P. strigosa* under elevated temperature (Figure 2-5). Given that both species under most treatments exhibited

this pattern, it cannot be ruled out that these changes in symbiont physiology were influenced by other factors, including incomplete symbiont acclimation to experimental light environment (Roth 2014) and seasonal patterns in symbiont density and pigment concentration (Fitt et al. 2000)—which may have masked the symbiont response to thermal stress within *S. siderea*. In contrast, *P. strigosa* exhibited reduced symbiont density and Chl *a* under elevated temperature (Figure 2-5b,d), a pattern more consistent with thermally induced bleaching (Weis 2008) and further illustrating the susceptibility of this species to thermal stress.

### *2.5.3. Nearshore P. strigosa are more resistant than forereef conspecifics*

Reef zone was a significant predictor of host physiology, particularly for *P. strigosa*, as nearshore corals exhibited greater net calcification (Figure 2-3b). Although reef zone differences in calcification were observed for *S. siderea* (particularly through time), corals from one reef zone did not clearly outperform the other. In contrast, reef zone-specific calcification of *P. strigosa* may arise from local adaptation of the host to distinct temperature regimes. The Belize MBRS nearshore habitats have higher maximum temperatures, greater annual temperature range, and more days above the regional thermal bleaching threshold compared to forereef sites (Baumann et al. 2016). Local adaptation to distinct reef zones is not uncommon in corals, and has been previously shown to affect coral responses to thermal stress. For example, *P. astreoides* was locally adapted to distinct thermal regimes in Florida, with inshore corals exhibiting higher thermal tolerance, constitutively higher expression of specific metabolic genes, and greater gene expression plasticity compared to offshore conspecifics (Kenkel et al. 2013; Kenkel, Meyer, and Matz

2013; Kenkel and Matz 2016). A similar pattern of local adaptation was previously suggested for three Hawaiian coral species native to the warmer and more acidic Kāne‘ohe Bay, as corals were more tolerant to experimental temperature and $pCO_2$ stress relative to conspecifics from a cooler and less acidic site (Jury and Toonen 2019).

*Pseudodiploria strigosa* is a hermaphroditic broadcast spawning species, and previous work on the Flower Garden Banks population demonstrated that these larvae have short pelagic durations compared with other broadcast spawning scleractinian corals (*e.g., Orbicella franksi*), which could facilitate local adaptation as larvae are more likely to recruit locally (S. W. Davies et al. 2017). However, it is unknown if *P. strigosa* on the Belize MBRS have similarly short pelagic larval durations. We hypothesize that nearshore *P. strigosa* are locally adapted and/or acclimated to more variable and stressful nearshore conditions, allowing maintenance of higher calcification rates under thermal stress compared to their forereef counterparts. However, responses based on reef zone could be obscured by uneven sampling across sites, as forereef genotypes of *P. strigosa* were underrepresented in the experiment (2 genotypes vs. the standard 3) due to mortality of one forereef colony before the experiment began. We do acknowledge, however, that greater replication within each site may have yielded different effects of reef zone in other parameters of *P. strigosa* physiology due to the well documented additive genetic variation within coral populations (Dixon et al. 2015; Kavousi et al. 2016).

### *2.5.4. Time-course experiments reveal acclimation to thermal stress*

This study contributes to a growing body of literature demonstrating the value of assessing time-course physiology of corals under stress. Although studies investigating

independent effects of temperature and acidification on corals have yielded insight into the effects of global change (Albright et al. 2018; Jokiel and Coles 1990), combined effects of these stressors remain less explored—particularly in the context of how coral stress is modulated by stress duration. By characterizing host and symbiont physiology of the same colony through time, acclimatory responses were identified in two coral species, providing further evidence of the species-specific nature of coral acclimation. For example, under extreme $pCO_2$ and elevated temperature, *S. siderea* net calcification appears to recover by the end of the experiment while *P. strigosa* calcification continues to decline with time, resulting in negative net calcification by $T_{95}$. Notably, these results would not have been apparent in shorter-term exposures. Additionally, the exposure duration component of this study suggests that species will exhibit differential responses to ephemeral stress events. Local heat waves that raise SST and upwelling events that reduce pH–factors that already threaten coral populations–may threaten coral species in different ways in the future depending on the duration of these events. The lack of a statistical difference in $pCO_2$ levels between several of the treatments at $T_0$ (end of century $pCO_2$ treatment at 31°C was lower than target $pCO_2$; Figure A1-2) may have also affected the corals' physiological response through time. It is possible that if corals in this end of century, 31°C treatment had been exposed to the target $pCO_2$ for longer, additional physiological responses through time would have been observed. However, this does not negate the key findings that *P. strigosa* was most responsive to elevated temperature while *S. siderea* was most responsive to extreme $pCO_2$. Additionally, the goal of this study was to characterize how corals acclimate to global change stressors through time, and the observed responses to treatments relevant

to predicted future ocean conditions – particularly *P. strigosa* in response to temperature – highlights that exposure to these conditions is likely not sustainable over the course of the lifespans of individuals of this species. Interestingly, our results suggest that such stress exposure could be more sustainable for *S. siderea.*

Acclimation is an important mechanism by which corals can withstand changing environmental conditions, and transcriptome plasticity is one way that corals can acclimate to stress (S. W. Davies et al. 2016; Kenkel and Matz 2016; Rivera et al. 2021). For example, a coral reciprocal transplant experiment revealed that adaptive gene expression plasticity of stress response genes was associated with reduced susceptibility to bleaching (Kenkel and Matz 2016). In addition to plasticity providing a mechanism for acclimation within a generation, corals can rapidly adapt through selection on standing genetic variation in thermal tolerance traits (Dixon et al. 2015; Matz et al. 2018). However, recent declines in coral abundance, diversity, and health suggest rates of intra- and trans-generational adaptation to global change stressors within most coral populations are insufficient for mitigating deleterious impacts of global change (Thomas et al. 2018). Additionally, in contrast to the demonstrated importance of gene expression plasticity in acclimating to different temperature environments, Comeau et al. (2019) demonstrated that corals were unable to acclimatize to acidification conditions by altering calcifying fluid chemistry over the course of one year. Understanding the interplay of acclimation and adaptation in scleractinian corals is therefore essential for projecting how corals will fare in the higher-$CO_2$ future. Studies focusing on long-term acclimation capacities of corals will further elucidate mechanisms of resistance and resilience to global stressors.

## 2.6 Acknowledgements

We thank the Belize Fisheries Department for coral collection permits. Isaac Westfield, Amanda Dwyer, Sara Williams, and Louise Cameron are acknowledged for assisting with experimental maintenance at Northeastern University. Thanks to the Marchetti and Septer labs at the University of North Carolina at Chapel Hill for assistance with equipment and lab space to complete physiological assays. We also thank Samir Patel, Savannah Swinea, Bailey Thomasson, Forrest Buckthal, and Cori Lopazanski for assisting with preparing corals for physiological assays. This work was supported by NSF award OCE-1437371 (to J.B.R.), NSF award OCE-1459522 (to K.D.C.), NOAA award NA13OAR4310186 (to J.B.R. and K.D.C.), and the National Academies of Sciences, Engineering, and Medicine Gulf Research Program Fellowship (to S.W.D.). H.E.A. was supported by the NSF Graduate Research Fellowships Program (2016222953) and S.W.D. was a Simons Foundation Fellow of the Life Sciences Research Foundation (LSRF) while completing part of this research

# CHAPTER THREE: GENETIC DRIVERS OF CORAL RESPONSE TO DIEL TEMPERATURE VARIABILITY

## 3.1 Abstract

The persistence of reef-building corals in the Anthropocene is shaped by an interplay between their holobiont constituents (*i.e.,* the coral animal and its microbial symbionts) and environment. Diel temperature variability (DTV) has been shown to promote thermal resistance, but the extent to which DTV may interact with different holobiont partners to determine this resistance remains unclear. We disentangled the relative contributions of DTV and holobiont genetics in shaping thermal resistance by exposing the coral *Siderastrea siderea* to different levels of DTV, followed by heat challenge and subsequent recovery periods. We uncovered three cryptic *S. siderea* lineages that associated with diverse algal partners, and while unique associations between cryptic lineages and algal partners were the primary driver of thermal resistance, high DTV consistently promoted growth. Our results highlight the potential for ecological specialization in cryptic lineages and showcase how unique host-symbiont pairings and environmental variability shape thermotolerance, with broad implications for reef restoration.

## 3.2 Introduction

Climate change is altering environments at unprecedented rates, resulting in warmer and increasingly variable environments with more extreme events (Rahmstorf and Coumou 2011; Pörtner et al. 2019). An organism's response to such rapid changes (*e.g.,* through shifts in thermal limits; Somero 2010) is influenced by their environment, genetic background, and interactions between these two forces (GxE; Chevin, Lande, and Mace 2010; Somero 2010; Josephs 2018). Understanding and predicting the relative importance of these factors on fitness is fundamental as environments continue to change, species ranges shift, and localized extinctions occur (Somero 2010; Parmesan and Yohe 2003).

Coral reefs represent one of the most productive and economically valuable ecosystems (Costanza et al. 2014) threatened by global (*i.e.,* warming, acidification) and local (*i.e.,* nutrient pollution, overfishing) stressors (França et al. 2020; Klein et al. 2022). These stressors have increased the frequency and severity of coral bleaching – loss of the coral's obligate symbiotic algae (Brown 1997) – which is projected to worsen under current emissions trajectories (van Hooidonk et al. 2016). However, reef environments are not changing homogeneously, and while our understanding of which reefs and species are more bleaching resistant is advancing (Safaie et al. 2018; Grottoli et al. 2014), predicting their future remains challenging due to complexities governing coral resilience, including environmental variation, host genetics, and associations with algal and microbial symbionts (reviewed in Bove, Ingersoll, and Davies 2022).

Environmental heterogeneity drives patterns of species distributions and thermotolerance (Buckley and Huey 2016; Sheldon and Dillon 2016). On coral reefs, a seminal example is reef zones, where corals occupying offshore habitats (generally lower turbidity, less run-off, higher flow, more stable temperatures) tend to be less thermotolerant than corals from inshore habitats (generally higher turbidity, less flow, more variable temperatures; Kenkel et al. 2013; Morgan et al. 2017; Castillo et al. 2012). Inshore coral thermotolerance has been linked to diel temperature variability (DTV; Safaie et al. 2018; Kenkel, Almanza, and Matz 2015; Oliver and Palumbi 2011), which is theorized to induce tolerance by "priming" (*i.e.,* beneficial acclimation hypothesis; Massey et al. 2022) organisms to more effectively respond to future heat stress events (Drury et al. 2022; Hackerott, Martell, and Eirin-Lopez 2021; Hilker and Schmülling 2019). However, temperature variability alone fails to fully capture the heterogeneity in coral bleaching, and it remains unclear whether this variability facilitates thermotolerance via priming or by selecting for individuals with higher thermal limits.

'Coral holobionts' encompass complex symbioses between coral hosts, algal symbionts (Symbiodiniaceae), and a diverse array of microorganisms, all interacting to shape aggregated holobiont phenotypes (*i.e.,* phenomes). Each member of the holobiont contributes to coral bleaching heterogeneity, including host genetic variation (Dixon et al. 2015; Fuller et al. 2020), algal symbiont communities (Berkelmans and van Oppen 2006; Manzello et al. 2019), and microbiomes (Morrow, Muller, and Lesser 2018; Ziegler et al. 2017). Recent genomic studies have revealed a surprising level of cryptic diversity in corals, and cryptic lineages (*i.e.,* distinct genetic clusters previously characterized as one

species; Bickford et al. 2007) differ in both their spatial distributions (Fifer et al. 2022; Matias et al. 2022; Rippe et al. 2021) and thermal tolerance (Rose et al. 2021; Gómez-Corrales and Prada 2020). Cryptic host diversity can also interact with diversity in other holobiont members to produce distinct phenotypes; for example, the thermotolerant lineage in the *Acropora hyacinthus* species complex more frequently hosts the heat tolerant algae *Durusdinium* (Rose et al. 2021). To disentangle the relative roles of environment, host, and associated algal and microbial communities on coral phenomes and thermotolerance, we investigated the response of the reef-building coral *Siderastrea siderea* from three inshore and three offshore sites in the Bocas del Toro reef complex (BTRC), Panamá to a 50-day DTV experiment, followed by heat challenge and recovery. We hypothesized that DTV would play a dominant role in shaping coral phenomes and would prime corals to be resistant to heat challenge.

## 3.3 Materials and methods

### *3.3.1 Experimental design*

To disentangle the effects of environment, host, and associated algal and microbial communities on coral phenomes and thermotolerance, we exposed the reef-building coral *Siderastrea siderea* from three inshore (Punta Donato = PD, STRI Point = SP, Cristobal Island = CI) and three offshore (Bastimentos North = BN, Bastimentos South = BS, Cayo de Agua = CA) sites in the Bocas del Toro reef complex (BTRC), Panamá to a 50-day DTV experiment, followed by heat challenge and recovery. *In situ t*emperature data were continuously collected every 15 minutes for one year prior to colony collection, with

HOBO ProV2 temperature loggers (Onset, Bourne, MA) deployed between 1 and 4 m depth at each of the six sites (Figure 3-1) from July 1, 2015 to June 30, 2016. Loggers were recovered from four sites, including three inshore (CI, PD, SP), and one offshore (CA). Differences in daily mean temperature and daily temperature range (reported in Table A2-1) across sites were determined using a one-way ANOVA with Tukey's HSD post-hoc tests (Figure 3-1b; Table A2-2). Four DTV treatments were designed based on *in situ* temperature data. The control treatment (no DTV) was maintained at 29.5℃, representing the overall daily mean of all sites (29.60 ± 0.02℃; Table A2-1). The three variability treatments had the same minimum temperature of 28.5℃ with daily increases of either 2°C (low variability; 28.5-30.5°C), 3°C (moderate variability; 28.5 - 31.5℃), or 4°C (high variability; 28.5 - 32.5℃). The low variability treatment was informed by the mean maximum daily DTV measured across all four sites (1.96°C), moderate variability by the highest *in situ* DTV observed (2.86℃ at CI), and high variability represented a physiological challenge with DTV outside of the range observed in *in situ* data (Figure 3-1, Figure A2-8; Table A2-1).

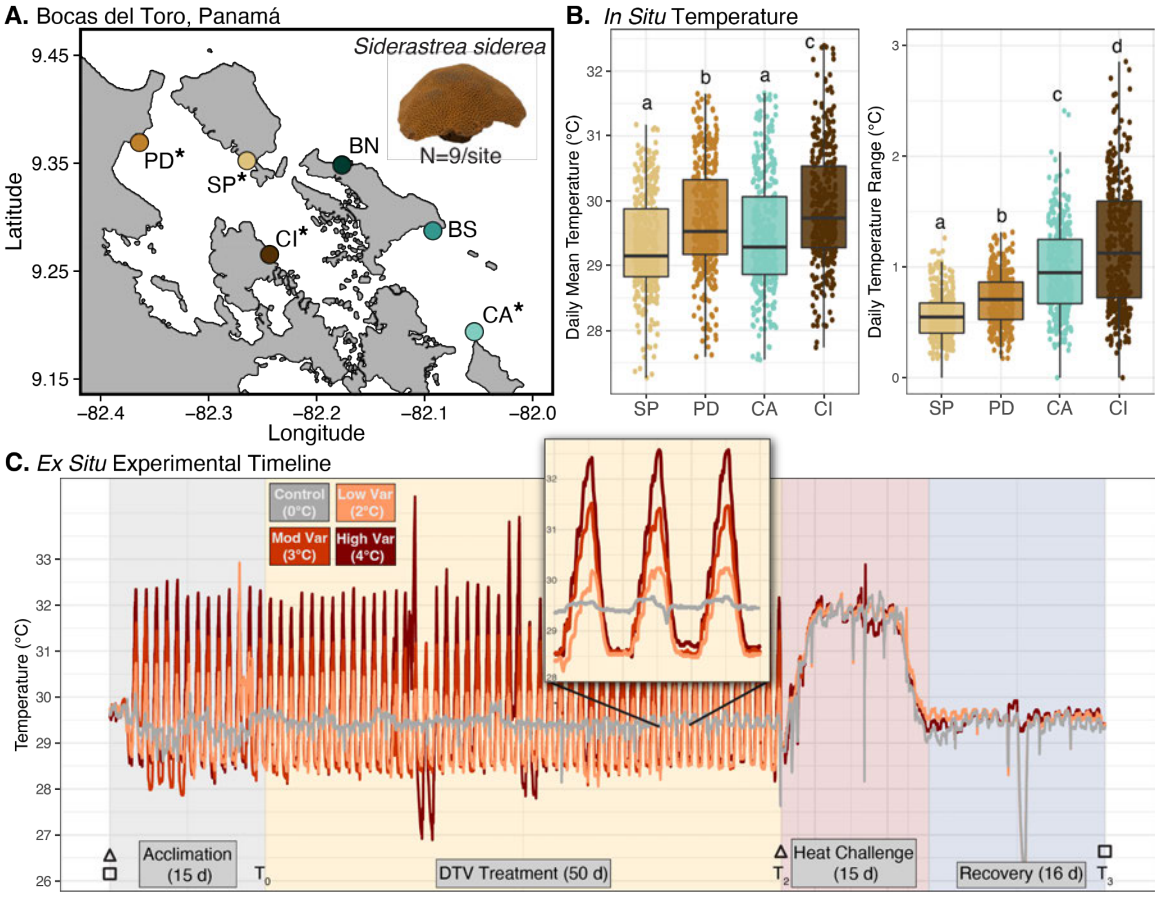


**Figure 3-1.**
**Experimental overview.** (**a**) Map indicating six sites across the Bocas del Toro Reef Complex in Panamá where *Siderastrea siderea* colonies were collected, including three inshore (brown shades: PD = Punta Donato, SP = STRI Point, CI = Cristobal Island) and three offshore (green shades: BN = Bastimentos North, BS = Bastimentos South, CA = Cayo de Agua) sites. Asterisks indicate sites where temperature loggers were recovered. (**b**) Daily mean temperature (left) and daily temperature range (right) for one year prior to coral collection (7/1/2015-6/30/2016). Distinct letters indicate significant differences in temperature parameters from ANOVA and Tukey's HSD post-hoc tests (Table A2-2). (**c**) Timeline of *ex situ* diel temperature variability (DTV) experiment, including 15 days of acclimation, 50 days of DTV treatment, 15 days of heat challenge, and 16 days of recovery. *Ex situ* temperature data were obtained from HOBO loggers, which recorded temperature every 5 minutes. Squares indicate when fragments were flash frozen to measure coral and symbiont phenomic metrics. Triangles indicate when fragments were subsampled for DNA, before acclimation to determine host genetics and at the end of DTV to assess Symbiodiniaceae and microbiome communities. $T_0$, $T_2$, $T_3$ indicate when corals were buoyant weighed to calculate growth. The inset illustrates temperatures over three days to highlight DTV treatments in more detail.

In August 2016, nine visually healthy *S. siderea* colonies (20-30 cm diameter) were collected from between 2.5 and 8 m deep at each of the six sites (54 colonies total, permit No. SE/A-36-16). Colonies were maintained in a flow-through seawater system at the Smithsonian Tropical Research Institute in BTRC prior to transport to the University of North Carolina at Chapel Hill. Upon return, each colony was sectioned into at least five fragments using a tile saw (RIDGID; Elyria OH, USA) and affixed to pre-labeled plastic petri dishes using cyanoacrylate glue. Fragments (N=18 genotypes per tank, 3 aquaria per treatment) were randomly distributed into treatment aquaria for 16 days at 28°C (recovery), followed by 15 days of acclimation to experimental conditions. Next, a 50-day DTV experiment was conducted followed by a 15-day heat challenge (32°C) and 16-day recovery period (Figure 3-1). Distinct treatments were maintained over the course of the 50-day DTV treatment (Table A2-11; Figure A2-8). Light conditions were standardized to 400 µmol photon $m^{-2}$ $s^{-1}$ on a 12 h:12 h light:dark cycle using full spectrum LED lights (Euphotica; 120W, 20000K) based on Rodas et al. (2020). For more detailed information on experimental specifics including water quality, see Appendix 2.1. Phenomic metrics of coral host and algal symbiont health were assessed by flash freezing fragments of each genotype at the start of acclimation and following final recovery. Coral DNA was also subsampled, preserved in 100% ethanol, and stored at -80°C during colony fragmentation and at the end of the 50-day DTV treatment to assess host genetics and Symbiodiniaceae and microbiome communities, respectively (Figure 3-1c).

### *3.3.2 2b-RAD-sequencing to identify cryptic lineages*

Holobiont DNA was extracted from tissue samples collected at the beginning of the experiment (pre-acclimation; N=54) using a modified phenol-chloroform method (Chomczynski and Sacchi 2006) as in Davies et al. (2013). DNA extracts were cleaned using Zymo Genomic DNA Clean and Concentrator kits and concentrations were assessed using a Quant-iT PicoGreen dsDNA assay kit (Thermo Fisher). Samples of sufficient concentration (51/54 putative genotypes) were prepared for 2b-RAD-sequencing (Wang et al. 2012), with 10 technical replicates to enable clone identification. A total of 61 samples were successfully sequenced across one lane of Illumina HiSeq 2500 using single-end 50 bp sequencing at the Tufts University Core Facility (TUCF).

Analysis of 2b-RADseq data generally followed the pipeline presented at https://github.com/z0on/2bRAD_denovo. Raw reads were trimmed and demultiplexed, cutadapt (Martin 2011) removed reads with Phred quality score less than 15 and reads <36 bp in length. Because no *S. siderea* genome is available, a *de novo* reference was created. Following Rippe et al. (2021), Symbiodiniaceae contamination was removed by mapping reads to concatenated genomes from four Symbiodiniaceae genera: *Symbiodinium* (Aranda et al. 2016), *Breviolum* (Shoguchi et al. 2013), *Cladocopium* (H. Liu et al. 2018), and *Durusdinium* (Dougan 2020) using Bowtie2 v2.4.2 (Langmead and Salzberg 2012). Putative symbiont reads were removed and CD-HIT v4.7 (Fu et al. 2012) clustered and assembled remaining reads into a *de novo* reference consisting of 30 pseudochromosomes. Reads were mapped to the *de novo* reference using Bowtie2 v2.4.2 (Langmead and Salzberg 2012) with default parameters and ANGSD v0.935 (Korneliussen, Albrechtsen,

and Nielsen 2014) was used for genotyping (using likelihood estimates) and identifying single nucleotide polymorphisms (SNPs). Standard filters were used to retain loci, which included loci present in at least 80% of individuals, a depth of coverage >2 reads, a minimum mapping quality score of 20, a minimum quality score of 25, a strand bias p-value >1 x $10^{-5}$, a heterozygosity bias >1 x $10^{-5}$, a SNP p-value of 1 x $10^{-5}$, a minimum minor allele frequency >0.05, excluded all triallelic sites, and removed reads with multiple best hits. To distinguish putative clones, a hierarchical clustering tree (*hclust*) was constructed based on pairwise identity by state (IBS) values across all samples. Clones were determined using the similarity of technical replicates as a cut-off, and only one pair of clones was detected at Punta Donato (PD; I4G and I4F; Figure A2-1a). The clone pair with lower total read count (I4G) was removed from the dataset for all further analyses.

Population structure on the data set with the clone removed (8105 SNPs) was determined using three methods: 1) hierarchical clustering of pairwise IBS values, 2) principal component analysis (PCoA) based on IBS matrix, and 3) admixture proportions of individuals across sites. A height of 0.265 was used as the cut-off from the clustering dendrogram to distinguish three lineages (Figure A2-1b). PCoA was performed on the covariance matrix using *capscale* (with a null model) in the *vegan* package (Oksanen et al. 2022), and was used in combination with the hierarchical clustering results to determine an optimal K of three. NgsAdmix v1.3.0 (Skotte, Korneliussen, and Albrechtsen 2013) with K=3 then determined the proportion of each individual's ancestry that corresponded to each lineage. These three clusters are referred to as lineage 1 (L1), lineage 2 (L2), and lineage 3 (L3).

To estimate genetic differentiation, a different set of filters were used to retain loci, which included loci present in at least 80% of individuals, a minimum mapping quality score of 25, a minimum quality score of 30, a strand bias p-value >1 x $10^{-5}$, a heterozygosity bias >1 x $10^{-5}$, excluded all triallelic sites, removed reads with multiple best hits, and passed the lumped paralogs filter (770,398 SNPs). Genetic differentiation between lineages was estimated using ANGSD (Korneliussen, Albrechtsen, and Nielsen 2014) to find site allele frequency (SAF) for each lineage, after which realSFS determined the site frequency spectrum (SFS) for all lineage pairwise comparisons. Calculated SAFs and SFSs were then used to calculate global $F_{ST}$, reported as weighted global $F_{ST}$ values. Pearson's Chi-squared test was used to determine if the distribution of L1 and L2 was dependent on reef zone, excluding L3 individuals.

### *3.3.3 Non-invasive phenomic assessments*

Coral growth rates were estimated using the buoyant weight method (Spencer Davies 1989) under standard conditions (28°C and 33 ppt) with a bottom-loading balance (precision=0.0001 g; Mettler-Toledo, Columbus, OH) at four time points: after acclimation ($T_0$), during DTV ($T_1$), at the end of DTV ($T_2$), and at the end of recovery ($T_3$). Growth was calculated as percent change in weight through DTV treatment ($T_2$-$T_0$/$T_0$) as well as through heat stress and recovery ($T_3$-$T_2$/$T_2$). Immediately after buoyant weighing, corals were imaged to quantify surface area for physiology standardization with a CoralWatch Health Chart (Siebeck et al. 2006) as a size standard. Distance between the camera and corals as well as lighting were standardized. Surface area measurements were obtained

using ImageJ (Schneider, Rasband, and Eliceiri 2012) and only live tissue was included in surface area normalizations.

Photosynthetic efficiency of photosystem II (Fv/Fm) was measured in triplicate for each fragment using a Diving PAM (Walz) at seven time points: once at the end of DTV, three times during heat challenge, and three times during recovery. Measurements were made using a saturation pulse width of 0.6 s at full strength light intensity, electronic signal damping of 2, and gain of 4.

### *3.3.4 Tissue processing and invasive physiological assays*

Flash frozen fragments were thawed, and a small sample (3-4 polyps) was removed via sterile razor blade for later DNA isolation. Remaining tissue was removed via airbrush and seawater, homogenized, and centrifuged to separate host and symbiont fractions, which were divided into four aliquots. One symbiont aliquot was used for symbiont cell counts and all other host and symbiont aliquots were disrupted using a bead mill homogenizer (Omni Bead Mill 24; GA, USA) with a high throughput hub at 6 m $s^{-1}$ for 2 min for downstream phenomic assessments.

Total host protein was quantified using the Bradford method (Bradford 1976) with absorbances read at 595 nm on a microplate reader (Biotek Synergy H1; CA, USA). Data were converted from absorbance to total protein concentrations (μg $\mu L^{-1}$) using a standard curve of Bovine Albumin Serum (BSA). Total host and algal symbiont carbohydrates were quantified using the phenol-sulfuric acid method (Masuko et al. 2005) with absorbances read at 500 nm. Carbohydrate values (mg $mL^{-1}$) were calculated from raw absorbance using

a D-glucose standard curve. This method measures all monosaccharides, which includes glucose, the main byproduct of photosynthesis that is translocated from symbiont to coral (Burriesci, Raab, and Pringle 2012). Symbiont cell density was quantified in triplicate using the hemocytometer method (Rodrigues and Grottoli 2007). Symbiont photosynthetic pigments (chlorophyll *a* = Chl *a*) were measured spectrophotometrically, read at 663 and 630 nm, calculated following the equation below (Jeffrey and Haxo 1968), where A663 and A630 represent blank-corrected absorbance values at 663 nm and 630 nm respectively, and then normalized to surface area.

$$\text{Chl } a \text{ } (\mu g \text{ } mL^{-1}) = 13.31 \text{ x } A663 - 0.27 \text{ x } A630$$

Tissue thickness (mm) for all $T_0$ fragments was measured with calipers after tissue was removed and corallite surface area ($mm^2$) was measured following methods presented by Conti-Jerpe et al. (2020). Briefly, the polygon tool in ImageJ (Schneider, Rasband, and Eliceiri 2012) measured the area of seven corallites from each fragment in pixels, which was converted to $mm^2$ using a size standard in each photograph.

### *3.3.5 Statistical analysis of physiological data*

The effect of DTV and host lineage on growth was assessed separately for two durations: 1) throughout the 50-day DTV treatment and 2) during the heat challenge and recovery periods. For both durations, linear models (*lme4*; Bates et al. 2015) were implemented with main effects of treatment and lineage with a random effect of genotype. Another linear model was implemented to assess the interactive effects of time, lineage, DTV treatment, and dominant symbiont type (with a random effect of genotype) on

photochemical efficiency (Fv/Fm) throughout the heat challenge and recovery periods. Models were selected based on a backwards selection method, where only significant interaction terms were maintained in the model. Assumptions and model fit were assessed visually using *check_model* (package=*performance*; Lüdecke et al. 2021) and pairwise comparisons were calculated with *emmeans* (Lenth et al. 2022).

To characterize phenome-wide responses across factors of interest at the beginning and end of the experiment, all host and symbiont physiology metrics were *log*-transformed and combined in principal component analyses (PCAs) using *FactoMineR* (Lê, Josse, and Husson 2008). Significance of each factor (fixed effects of lineage and site of origin for baseline phenome, and fixed effects of DTV treatment, site of origin, cryptic lineage, and dominant ITS2 type for end of DTV treatment phenome) were assessed with PERMANOVAs, using the *adonis* function (package=*vegan*; Oksanen et al. 2022). Effect size of each factor was determined using partial Omega-squared ($\omega^2$) values calculated with *adonis_OmegaSq* (package=*MicEco*; Russel, Jakob 2021).

### *3.3.6 Assessing prokaryotic and Symbiodiniaceae communities*

To identify Symbiodiniaceae and prokaryotic communities of corals following DTV treatment (N=184 coral fragments), metabarcoding libraries were generated using a series of PCR amplifications for the ITS2 region of Symbiodiniaceae ribosomal DNA (B. Hume et al. 2013; 2015) and the V4/V5 region of the bacterial 16S rRNA gene (Parada, Needham, and Fuhrman 2016; Apprill et al. 2015), respectively. Samples were sequenced

(paired-end 250 bp) on an Illumina Miseq at TUCF. For detailed information on library preparation, please refer to Appendix 2.1.2.

ITS2 data were submitted to SymPortal (B. C. C. Hume et al. 2019) to identify ITS2 type profiles. Successfully sequenced samples (N=172) were analyzed at two levels to consider differences across DTV treatments, host lineage, and site of origin: 1) majority ITS2 sequence and 2) defining intragenomic variants (DIVs). First, relative abundances of majority ITS2 sequences were compared with bar plots using *phyloseq* (McMurdie and Holmes 2013), and a Kruskal-Wallis test (*kruskal.test*) was used to test for differences in the proportion of D1 majority ITS2 sequences across lineages. Second, Bray-Curtis dissimilarity PCoAs were constructed on relative abundance DIVs using *phyloseq* (McMurdie and Holmes 2013) and *vegan* (Oksanen et al. 2022) determined community dissimilarity and dispersion. Additionally, *pairwise.adonis* (Trachsel, Julian, n.d.) compared ITS2 communities across levels of DTV treatment as well as sites of origin.

16S sequencing data were analyzed using *DADA2* (Callahan et al. 2016), which conducted quality filtering and identified 8619 amplicon sequence variants (ASVs) in 174 successfully sequenced samples. ASVs matching mitochondrial, chloroplast, and non-bacterial sequences were removed (785 ASVs) followed by an additional 154 ASVs identified in negative controls by *decontam*, leaving 7680 ASVs and 172 samples remaining. Taxonomy was assigned using the Silva v132 database (Quast et al. 2013) and by using *blast+* against the NCBI nucleotide database (Camacho et al. 2009). ASVs were checked for eukaryotic contamination, but none was detected. *MCMC.OTU* (Green et al. 2014) trimmed underrepresented ASVs (<0.01% of counts or identified in only one

sample), leaving 641 ASVs and 171 samples. Counts were then rarefied to 1000 reads per sample using *vegan* (Oksanen et al. 2022), leaving 641 ASVs and 165 samples remaining. Using cleaned data (contaminant ASVs removed, but not trimmed or rarefied), *phyloseq* (McMurdie and Holmes 2013) calculated ASV richness and Shannon and Simpson's diversity indices. An ANOVA tested for differences in diversity metrics across fixed effects of DTV treatment and host lineage. Core and accessory microbiomes were identified from the trimmed and rarefied dataset using *microbiome,* with the core microbiome defined as ASVs present at greater than 0.1% relative abundance in more than 50% of samples. Bray-Curtis dissimilarity principal coordinate analyses (PCoA) were conducted on core, accessory, and all ASVs (relative abundance of trimmed and rarefied dataset) using *phyloseq* (McMurdie and Holmes 2013). *Vegan* (Oksanen et al. 2022) and *pairwise.adonis* (Trachsel, Julian, n.d.) were implemented for statistical analyses of microbial community differences and dispersion as in ITS2 analyses. *ANCOM* (F. H. Lin 2019) identified differentially abundant taxa across DTV treatments and lineages, and *phylosmith* (Smith 2019) plotted a heat map of log-transformed abundance data for those differentially abundant taxa. 16S analyses (including PCoA's) were conducted on both rarefied and non-rarefied data, and the same patterns emerged regardless of the dataset, so only the trimmed and rarefied version is presented for brevity.

## 3.4 Results

### *3.4.1. Presence of three lineages of Siderastrea siderea with distinct phenomes*

This study focused on the ubiquitous Caribbean reef-building coral, *Siderastrea siderea,* collected from six sites in the BTRC, Panamá across an inshore (Punta Donato = PD, STRI Point = SP, Cristobal Island = CI) to offshore (Bastimentos North = BN, Bastimentos South = BS, Cayo de Agua = CA) gradient (Figure 3-1, Table A2-1). Admixture ancestry of individuals across sites (Figure 3-2a), PCoA based on the identity by state (IBS) matrix (Figure 3-2b; Table A2-3), and hierarchical clustering of pairwise IBS values (Figure A2-1a,b) all support the presence of three distinct coral host genetic clusters (hereafter referred to as L1, L2, and L3) across BTRC. Pairwise global weighted $F_{ST}$ values illustrate high divergence between these genetic clusters (L1 vs L2 = 0.17, L1 vs L3 = 0.18, L2 vs L3 = 0.12; Figure 3-2b), suggesting they represent three cryptic lineages of a *Siderastrea siderea* species complex. Cryptic lineages differed in their spatial distributions across BTRC, with more L1 individuals sampled at offshore sites (83%; 24/29 offshore/total L1 individuals) and more L2 individuals sampled at inshore sites (94%; 17/18 inshore/total L2 individuals; $X^2$=23.57, $p$<0.001). L3 was the least abundant lineage, with only three individuals observed at SP (Figure 3-2). CI is the only site where two lineages were sampled in equal proportion (n=4 L1, n=4 L2; Figure 3-2a,b). While admixture results at K=2 suggest that L3 individuals are of mixed ancestry between L1 and L2, L3 fully resolves as a distinct lineage when K=3 (Figure 3-2a). Cryptic lineages had low admixture, and the individual with the most admixture had <5% assigned to a second

ancestral population. Given the small sample size for L3, these individuals were excluded from downstream physiology analyses.

Corals of L1 and L2 ancestry exhibited distinct holobiont phenomes at the start of acclimation (Figure 3-2c; *ADONIS* $p<0.001$, $\omega^2=0.32$), while site of origin had no effect (*ADONIS* $p=0.19$, $\omega^2=0.04$; Table A2-4). Lineages were distinguished by the first principal component (PC), with loadings for energy reserves (symbiont density, host and symbiont carbohydrate, chlorophyll *a*, and protein) positively correlated with L1 and tissue thickness positively correlated with L2 (Figure 3-2c). L1 corals had the smallest corallites, and corallite area was significantly larger in L2 compared to L1 (Tukey HSD $p<0.0001$) and in L3 compared to L2 (Tukey HSD $p=0.015$; Figure A2-1c; Table A2-5). This pattern was consistently observed at CI where L1 and L2 co-occur, with L2 (N=4) maintaining smaller corallites than L1 (N=4; Figure A2-1d; $p=0.001$; Table A2-5).

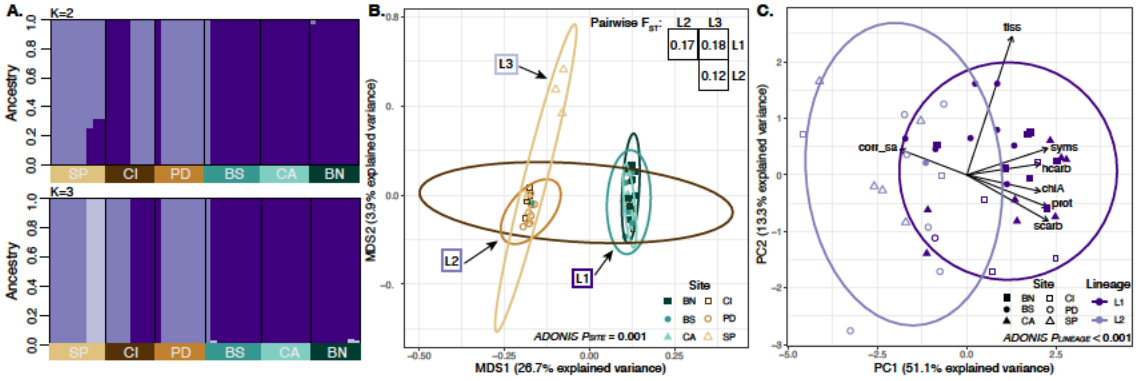


**Figure 3-2.**
**Three cryptic lineages of *Siderastrea siderea* species complex observed in Bocas del Toro Reef Complex exhibit distinct phenomes.** (**a**) ADMIXTURE results for K=2 (top) and K=3 (bottom). Columns represent an individual and the bar color represents an individual's assignment to one of two (top) or three (bottom) ancestral populations (L1=dark purple, L2=medium purple, L3=light purple). Boxes below group individuals by collection site (colors as in **b**). (**b**) Multidimensional scaling (MDS) plot illustrating significant clustering of lineages across collection sites. Shapes and colors distinguish sites, with closed shapes/green shades representing offshore sites and open shapes/brown shades representing inshore sites. Inset shows pairwise $F_{ST}$ values between lineages. (**c**) Principal component analysis (PCA) of *log*-transformed holobiont phenomes showcasing initial differences between L1 and L2 following 15-day recovery. Phenotypes include corallite surface area (corr_sa; $mm^2$), tissue thickness (tiss; mm), symbiont density (syms; cells $cm^{-2}$), host and symbiont carbohydrate (hcarb and scarb, respectively; mg $cm^{-2}$), chlorophyll *a* (chlA; ug $cm^{-2}$), and total protein (prot; mg $cm^{-2}$). Only individuals with data for all phenotypes were included (N=42), and x- and y- axes represent the % variance explained by the first and second principal component, respectively.

### *3.4.2. Host lineage and experimental diel temperature variability drive holobiont phenome*

Cryptic host lineages maintained distinct holobiont phenomes at the end of the 50-day DTV experiment (Figure 3-3a; *ADONIS* $p$=0.0004; $\omega^2$=0.091; Table A2-4). Similar to baseline holobiont phenomes (Figure 3-2c), lineages were consistently distinguished along the first PC, with loadings for host and symbiont energy reserves positively correlated with

L1. DTV treatment also influenced holobiont phenomes, and control corals were distinguished from corals in the low, moderate, and high variability treatments along the second PC, with growth positively correlated with variability treatments (Figure 3-3b; *ADONIS* $p$=0.0009; $\omega^2$=0.099; Table A2-4).

*3.4.3. Diel temperature variability increased growth, but not resistance to heat challenge*

Regardless of DTV treatment, L1 corals grew constitutively faster than L2 corals throughout the variability period (Figure 3-3c; $p$=0.04), as well as the heat challenge and recovery periods (Figure A2-2a; $p$<0.001; Table A2-6). Additionally, there was a clear effect of DTV treatment on growth, with corals in moderate and high DTV treatments growing more than control corals (Figure 3-3c; $p$=0.006 and $p$=0.008, respectively). However, this growth benefit of moderate and high variability was not sustained and no effect of DTV treatment on growth through heat challenge and recovery periods was observed (Figure A2-2a; $p$=0.58; Table A2-6).

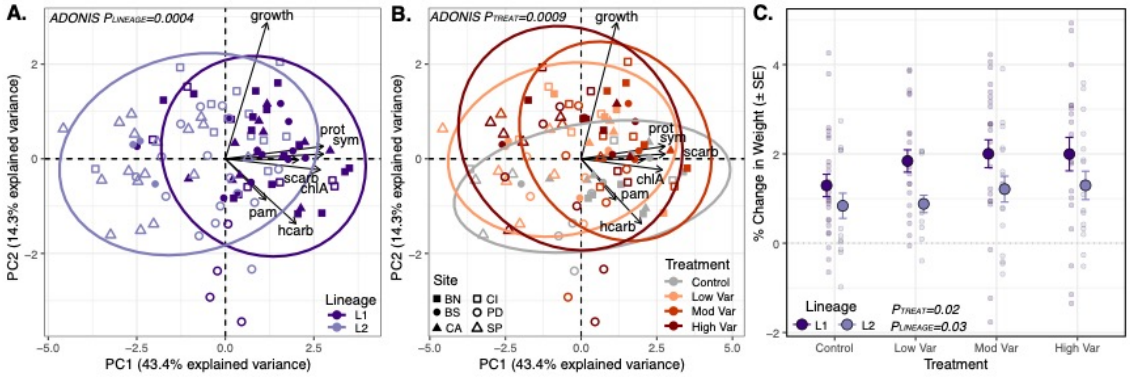


**Figure 3-3.**
**Holobiont phenomes were shaped by diel temperature variability (DTV) and cryptic host lineage.** (**a,b**) Principal component analysis (PCA) of *log*-transformed holobiont phenomes of corals following 50 days in DTV. Shapes represent site of origin (solid symbols = offshore, open symbols = inshore). Phenotypes include percent change in weight through 50 days in DTV (growth), total protein (prot; mg $cm^{-2}$), host and symbiont carbohydrate (hcarb and scarb, respectively; mg $cm^{-2}$), chlorophyll *a* (chlA; µg $cm^{-2}$), symbiont density (syms; cells $cm^{-2}$), and photochemical efficiency of photosystem II (pam). Only individuals with data for all phenotypes were included, and x- and y- axes represent the % variance explained by the first and second principal component, respectively. Colors represent lineage (**a**: L1 = dark purple, L2 = light purple) or DTV treatment (**b**: Control = gray, low variability [Low Var] = light red, moderate variability [Mod Var] = medium red, and high variability [High Var] = dark red) or. (**c**) Percent change in weight by host lineage throughout the DTV experiment, measured as % change in weight (y-axis) across DTV treatments (x-axis). Large points represent mean ± standard error of growth for each lineage across treatments, and smaller points represent an individual fragment's growth. Sample sizes and summary statistics reported in Table A2-4 and Table A2-6.

### *3.4.4. Cryptic host lineages associate with distinct Symbiodiniaceae communities and subtly different microbiomes*

Symbiodiniaceae communities were aggregated by the majority ITS2 sequence assigned by SymPortal for analysis and visualization. Nine Symbiodiniaceae ITS2 defining intragenomic variants (DIVs) matched the C1 majority ITS2 sequence (*Cladocopium*

*goreaui*), two DIVs matched C3, five DIVs matched D1 (*Durusdinium trenchii*), and one DIV matched each of the B19, C3af, and C15 majority ITS2 sequences. When data were summed based on the majority ITS2 sequence, after 50 days of DTV treatment, Symbiodiniaceae communities were differentiated based on cryptic host lineage (Figure 3-4a; Figure A2-3). Specifically, L1 individuals had more *D. trenchii* reads than L2 individuals, with 33% of L1 and 4.5% of L2 ITS2 reads assigned to *D. trenchii* (Figure 3-4a). Additionally, significantly more L1 corals (52.6%) hosted >50% relative abundance of *D. trenchii* reads relative to L2 corals (14.8%) (kruskal-wallis test: $X^2$=29.15, $p$<0.0001). When only considering corals from the site where an equal proportion of L1 and L2 individuals were present (CI), differences in Symbiodiniaceae communities between lineages was no longer significant, with 7.7% of L1 individuals and 42.9% of L2 individuals hosting >50% relative abundance of *D. trenchii* (kruskal-wallis test: $X^2$=2.28, $p$=0.13), although this analysis is likely underpowered because of the limited number of individuals. Additionally, dominant symbiont type had no significant effect on holobiont phenomes (Figure A2-3b; *ADONIS* $p$=0.90; Table A2-4).

No differences for any microbiome diversity metrics (ASV richness, Shannon's index, Simpson's index, and evenness) were observed between cryptic host lineages (Figure A2-5a-d; Table A2-7), and there was no effect of host lineage on overall microbiome structure (Figure A2-6a; *ADONIS* $p$=0.06; Table A2-8). However, the accessory microbiome was more dispersed in L2 compared to L1 (Figure A2-6c; *Pdis*=0.012; Table A2-8) and there were two differentially abundant taxa across host

lineages (*Dyella thiooxydans* [Family Rhodanobacteraceae] and SAR11 Clade III; Figure A2-6d).

### *3.4.5. Diel temperature variability did little to structure algal and microbial communities*

Bray-Curtis dissimilarity PCAs of all relative abundance ITS2 DIVs demonstrated that Symbiodiniaceae communities were structured by lineage (Figure A2-3d; *ADONIS* $p$=0.001) and site of origin (Figure A2-3b; *ADONIS* $p$=0.001), but not by DTV treatment (Figure A2-3c; *ADONIS* $p$=0.21; Table A2-9). No differences in the dispersion of Symbiodiniaceae communities was observed for lineage, site of origin, or DTV treatment (*Pdis*=0.76, *Pdis*=0.32, *Pdis*=0.70, respectively; Figure A2-3b-d; Table A2-9). No differences in microbiome diversity metrics were observed between DTV treatments (Figure A2-5e-h; Table A2-7). Bray-Curtis dissimilarity PCAs with all bacterial ASVs illustrated that community dispersion was not modulated by DTV treatment (Figure A2-7a; *Pdis*=0.81); however, there was a significant effect of DTV on overall microbiome structure (Figure A2-7a; *ADONIS* $p$=0.035), and microbiomes of control corals were distinct from microbiomes of corals in all variability treatments (Figure A2-7a; *ADONIS* $p$=0.042 [low variability], *ADONIS* $p$=0.023 [moderate variability], *ADONIS* $p$=0.007 [high variability]; Table A2-8).

### *3.4.6. Unique host lineage and algal symbiont pairings exhibit distinct responses to heat challenge*

After a 50-day exposure to DTV, L1 corals exhibited higher photochemical efficiency (Fv/Fm) than L2 corals, and these higher values were maintained throughout

heat challenge and recovery (Figure 3-4b; $p$=0.006; Table A2-10). However, aggregating Fv/Fm data by lineage hides important complexity. When data are split by majority ITS2 sequence, unique host lineage and algal symbiont partnerships influence response to heat challenge and recovery (Figure 3-4c; $p$=0.007; Table A2-10). These unique pairings between host lineage and majority ITS2 sequence were especially important for corals dominated by *D. trenchii*. L1 individuals hosting *D. trenchii* were able to maintain Fv/Fm values, consistent with resistance to heat challenge; however, L2 individuals hosting *D. trenchii* exhibited reduced Fv/Fm during heat challenge, and failed to recover, suggesting susceptibility (Figure 3-4c). In contrast, when hosting majority *Cladocopium goreaui* (C1), both lineages maintained relatively stable Fv/Fm, while C3af in L1 and C3 in L2 exhibited reduced Fv/Fm during heat challenge and subsequently recovery, showcasing thermal resilience.

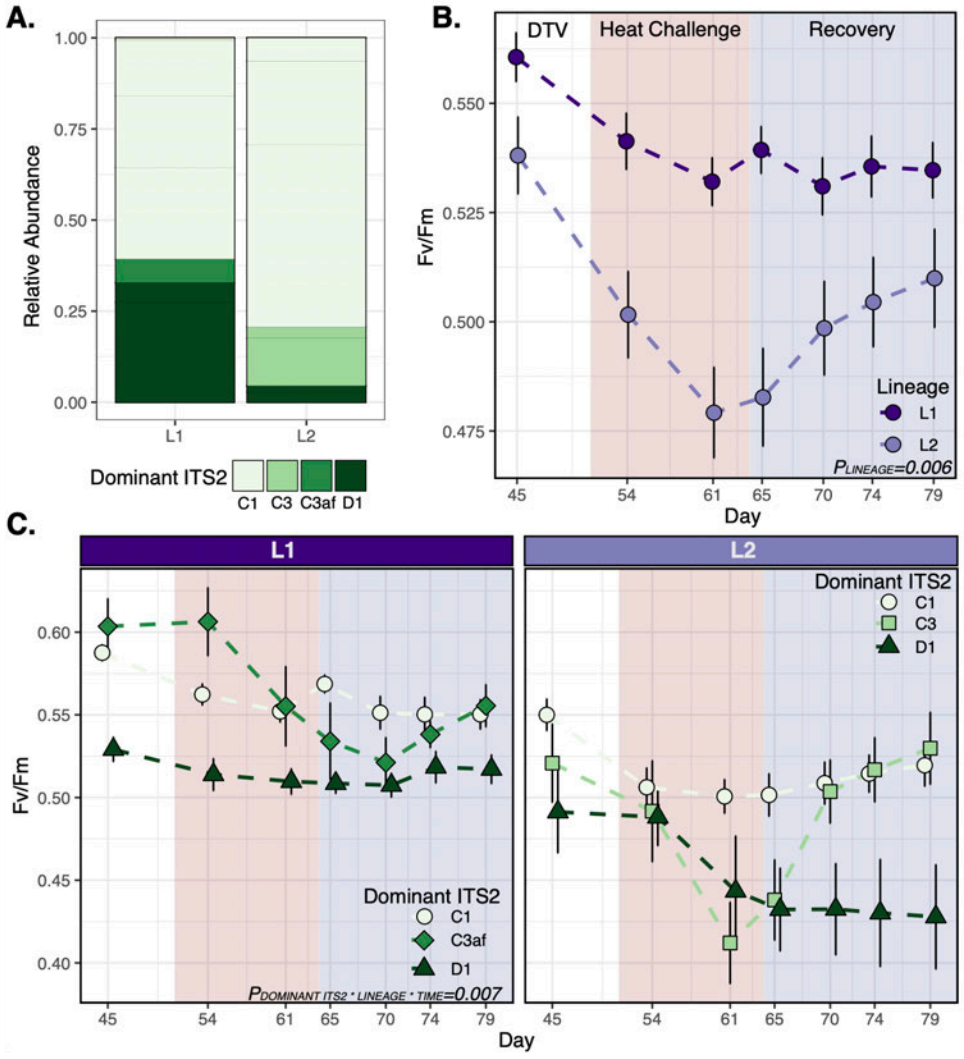


**Figure 3-4.**

**Coral responses through heat challenge and recovery.** (**a**) Relative abundance of *Durusdinium trenchii* (D1 majority ITS2 sequence) aggregated by lineage after 50-day DTV treatment. (**b**) Photochemical efficiency (Fv/Fm) across seven time points throughout the end of DTV treatment, heat stress (red shaded) and recovery (blue shaded) treatments. Points represent mean ± standard error in Fv/Fm for each lineage. (**c**) These same data as (**b**), but faceted by lineage (L1 left panel, L2 right panel), with colors and shapes representing majority ITS2 sequence (>50% relative read abundance) for each coral fragment (circle = C1, square = C3, diamond = C3af, triangle = D1). Background shading is as in (**b**).

## 3.5. Discussion

Understanding how diversity is partitioned across the seascape is critical to predicting coral bleaching. Here, we identified three cryptic host lineages (L1, L2, L3) in a *Siderastrea siderea* species complex across BTRC that varied in phenotypes relevant to thermal tolerance. L1 corals maintained elevated energetic reserves and grew more throughout the 50-day DTV experiment and additionally maintained elevated photochemical efficiency and growth throughout heat challenge and recovery. This work builds on the growing evidence for widespread cryptic diversity in corals, which has been detected at larger archipelago-wide (Fifer et al. 2022) and range-wide scales (Ladner and Palumbi 2012; Matias et al. 2022), as well as at relatively small spatial scales, including within reefs in Puerto Rico (Prada and Hellberg 2021), the Florida Keys (Rippe et al. 2021), and American Samoa (Rose et al. 2021). Depth has emerged as a common driver of lineage differentiation in corals (Rippe et al. 2021; Prada and Hellberg 2021; Eckert, Studivan, and Voss 2019), with relevant abiotic factors including temperature, light (Rippe et al. 2021), and small-scale current patterns (Eckert, Studivan, and Voss 2019). Across larger scales, only one of three *Acropora hyacinthus* cryptic lineages was able to occupy habitat along a range expansion front in Japan, which was attributed to outlier loci associated with adaptation to temperate, seasonally fluctuating environments (Fifer et al. 2022). Temperature variability has also been associated with the differential distribution of *A. hyacinthus* cryptic lineages in American Samoa (Rose et al. 2018; 2021), and experimental work has found differences in bleaching susceptibility among these lineages (Gómez-Corrales and Prada 2020; Rose et al. 2021). Similarly, we find that cryptic lineages, which

vary in ecologically relevant phenomes (*i.e.,* energetic reserves and growth), differ in their thermal tolerance.

The cryptic host lineages identified here were largely structured across an inshore to offshore gradient in BTRC, with L2 and L3 more prevalent inside Bahia Almirante (inshore), and L1 more prevalent outside of the bay (offshore). Inshore BTRC sites are characterized by limited influence from the open ocean, riverine inputs that deliver nutrients, agricultural run-off, and sewage to the bay, and most recently hypoxic events that have altered coral communities (Altieri et al. 2017; Briand, Guzmán, and Sunday 2023). We find evidence that lineages exhibit unique features that could contribute to success in these distinct local environments. Lineages more common at inshore sites (L2 and L3) had larger corallites compared to offshore L1 individuals, and this difference persisted even when lineages co-existed in the same environment (CI). This suggests a genetic basis for this trait, but this pattern could also be the result of developmental plasticity (West-Eberhard 2005). Recent work supports the hypothesis that corals with smaller corallites maintain more autotrophic lifestyles than larger corallite corals, which rely more on heterotrophy (Conti-Jerpe et al. 2020). L2 and L3 may have adapted to the low light-high nutrient environments of inshore BTRC in part with larger corallites to facilitate heterotrophy, while L1 adapted to clear offshore waters with smaller corallites to maximize autotrophy. Future explorations of this system would benefit from stable isotope analyses to confirm correlations between corallite size and trophic level (Conti-Jerpe et al. 2020). Additionally, reciprocal transplant experiments would disentangle the relative roles of adaptation and acclimation in the observed phenotypes between lineages, followed by

coral bleaching assays to establish whether environmental acclimation led to shifts in bleaching resistance within lineages. Finally, a more thorough characterization of environmental conditions at these sites (*e.g.,* irradiance, nutrient concentrations, and dissolved oxygen) is needed, as sites where L1 and L2 are sympatric suggest other environmental characteristics could be driving differentiation and distributions of *S. siderea* cryptic lineages.

We initially hypothesized that DTV would shape coral phenomes to increase thermal resilience (following Drury et al. 2022; Oliver and Palumbi 2011; Schoepf et al. 2020; Thomas et al. 2018; DeMerlis et al. 2022; Barshis et al. 2018). While an effect of experimental DTV on holobiont phenomes was observed, this was overshadowed by the strong influence of cryptic lineage that persisted from collection through heat challenge and recovery. DTV did increase growth, and both L1 and L2 corals in moderate and high variability treatments grew more than control corals, suggesting that DTV represents a promising coral restoration tool to improve growth in nursery settings (as in DeMerlis et al. 2022). However, we did not observe improved performance under heat challenge after experimental exposure to DTV. It is possible that the DTV treatments used here were insufficient to "prime" corals (reviewed in Hackerott, Martell, and Eirin-Lopez 2021). Indeed, unique temperature variability treatments have resulted in variable phenotypic outcomes in thermal tolerance of the coral *Montipora capitata* (Drury et al. 2022) and growth and developmental rate in insects (Kingsolver, Higgins, and Augustine 2015; Worner 1992). In *Manduca sexta*, the mean temperature around which variability occurred altered growth rates, with positive effects observed around low mean temperatures and

negative effects around higher mean temperatures (Kingsolver, Higgins, and Augustine 2015). This phenomenon is due to Jensen's Inequality (Ruel and Ayres 1999), and highlights the importance of designing treatment temperatures with knowledge of an organism's thermal performance curve to determine whether DTV places an individual above their thermal optimum. While DTV was distinct across all treatments here, it was confounded by differences in mean temperatures, which may have influenced the effects of DTV observed, especially under low variability where mean temperatures were lower than control conditions. Future work should aim to disentangle the relative effects of mean temperature and variability on performance by designing treatments based on knowledge of an organism's thermal performance curve.

While L1 exhibited higher resistance to heat challenge than L2, this pattern was confounded by L1 hosting higher proportions of *D. trenchii* than L2 corals. *Durusdinium trenchii* has been shown to confer thermal tolerance to their hosts through elevated Fv/Fm (Silverstein, Cunning, and Baker 2015; Berkelmans and van Oppen 2006) and reduced bleaching prevalence (Manzello et al. 2019). Rose et al. (2021) also demonstrated that a more bleaching resistant *Acropora hyacinthus* cryptic lineage hosted greater proportions of *D. trenchii.* Additionally, *D. trenchii* proportions significantly improved the model accuracy for predicting bleaching responses in *A. millepora* (Fuller et al. 2020). Here, hosting *D. trenchii* failed to confer tolerance equally across *S. siderea* cryptic lineages. Instead, unique host lineage and algal symbiont pairings exhibited distinct responses to heat challenge with L1-*D. trenchii* out-performing L2-*D. trenchii* corals under thermal challenge. In addition, L2 corals were dominated by *D. trenchii* only when they originated

from sites where both cryptic lineages were sampled (CI and BS). It is therefore possible that, although L2 recruits arriving to these environments have *D. trenchii* available to them, it is ultimately not the most adaptive host-symbiont pairing for coping with acute heat challenge in this lineage. Future work characterizing the environmental pools of Symbiodiniaceae available across sites would be a worthy endeavor.

Despite cryptic lineages hosting distinct Symbiodiniaceae communities across different environments, only subtle microbiome differences were detected between the two dominant host lineages, even after 50 days of DTV treatment. This microbiome stability suggests that *S. siderea* in BTRC are "microbiome regulators" with conserved microbial functions (Ziegler et al. 2019). This finding is in contrast to previous work in *S. siderea,* which observed variation in core microbiomes across sites in Belize that differed in temperature variability (Speare et al. 2020). It is therefore possible that this stability is due to microbiome acclimation to lab conditions and that distinct communities between cryptic lineages may be detected if *S. siderea* were sampled *in situ* (Galand et al. 2018).

*Siderastrea siderea* is a horizontally transmitting, gonochoric broadcast spawning coral, with colonies of separate sexes spawning gametes to produce aposymbiotic larvae that spend time in the water column before settling, leading to the potential for broad population connectivity across great distances (up to 1200 km, Nunes, Norris, and Knowlton 2011). While much more work is warranted, we propose that in BTRC, the semi-lagoonal nature of Bahia Almirante and physical characteristics of the archipelago (Guzmán et al. 2005; Dominici-Arosemena and Wolff 2005) maintain a barrier to dispersal

between inshore or offshore larvae, with some exceptions due to their time as pelagic larvae. Because few sites were found to host multiple lineages and no site hosted all three, we posit that once recruits settle, even if larvae are dispersed to new reefs, this limited migration coupled with spatially varying selection leads to a dominance of one lineage in each environment. As was previously demonstrated by Quigley et al. (2017), it is also likely that environmental pools of algae are much more diverse than communities hosted by adult corals, and therefore once recruits begin establishing symbiosis, algal symbionts likely compete through a "winnowing" process with dominance depending on local environmental conditions (*i.e.,* light, depth) that are further shaped by coral colony morphology (Enríquez et al. 2017). Surviving recruits of distinct lineages then develop associations with specific Symbiodiniaceae in environments that differ in temperature, light, and nutrients, likely resulting in further acclimation to local conditions. Together, these genetic and environmental factors interact to determine the patterns of responses observed here, where unique combinations of host-symbiont pairings shape the variation in bleaching observed across reefs and between individuals on a reef. This work highlights the importance of understanding cryptic coral diversity when determining species responses to future climate change and in conservation planning.

## 3.6. Acknowledgements

We extend appreciation to the staff at the Smithsonian Tropical Research Institute at Bocas del Toro, especially Urania Gonzalez for assistance coordinating field work. Thanks to our fearless boat captain Sebastian Castillo, in addition to Colleen Bove, Clare Fieseler, and Logan Buie for field assistance. Thank you to Jack Weldon for assistance with physiology assays. Analysis was made possible through BU's Shared Computing Cluster.

## 3.7. Data Availability

All raw data and code associated with analyses presented in Chapter 3 are maintained in a Github repository at the following link: https://github.com/hannahaichelman/DielTempVariability.

# CHAPTER FOUR: SYMBIOSIS MODULATES GENE EXPRESSION OF PHOTOBIONTS, BUT NOT HOSTS, UNDER THERMAL CHALLENGE

## 4.1 Abstract

Anthropogenic changes in ocean temperature are causing dysbiosis of coral hosts and their photobionts. Previous work suggests that coral host gene expression varies more strongly in response to environmental stress compared to that of their intracellular photobionts; however, questions remain as to the causes and consequences of this phenomenon. We hypothesized that photobionts are less responsive because hosts modulate their symbiont's environment to buffer stress. To test this hypothesis we capitalized on the facultative symbiosis between the subtropical scleractinian coral *Oculina arbuscula* and its photobiont *Breviolum psygmophilum* to characterize gene expression responses of both symbiotic partners *in* and *ex hospite* in response to thermal challenges. First, to characterize the host and *in hospite* photobiont responses, symbiotic and aposymbiotic *O. arbuscula* were exposed to three temperatures: 1) control (18°C), 2) heat (32°C), and 3) cold (6°C). This design was replicated with *B. psygmophilum* cultured from *O. arbuscula* to characterize *ex hospite* photobiont responses. By comparing symbiotic and aposymbiotic host gene expression, orthologous gene expression of hosts and photobionts *in hospite,* and gene expression of *in* and *ex hospite B. psygmophilum,* we tested the influence of symbiosis on *O. arbuscula* hosts and photobiont gene expression under temperature challenges. We found that both thermal challenges elicited classic environmental stress responses in *O. arbuscula* regardless of symbiotic state, and both symbiotic and aposymbiotic hosts responded more strongly to cold challenge compared to

heat. Hosts also exhibited stronger overall responses than their *in hospite* photobionts. When comparing gene expression of *in* and *ex hospite B. psygmophilum*, both exhibited downregulation of genes associated with photosynthesis under thermal challenge; however, *ex hospite* photobionts exhibited greater gene expression plasticity and differential expression of genes associated with environmental stress response. Taken together, these findings suggest that *O. arbuscula* hosts buffer the environment of *B. psygmophilum* photobionts; however, future work would benefit from exploring a broader repertoire of cellular components.

## 4.2 Introduction

Endosymbioses — associations where one organism lives within the cells of its host (Sagan 1967) — have driven evolutionary innovations and allowed species to access resources and environments that would otherwise be unavailable (Wernegreen 2012; Melo Clavijo et al. 2018). Endosymbioses span the tree of life and include exemplary innovations including tubeworms (*Riftia pachyptila*) living at deep-sea hydrothermal vents that rely on chemosynthetic bacterial endosymbionts (*e.g.,* Robidart et al. 2008) and salamanders (*Ambystoma maculatum*) benefiting from photosynthetic endosymbionts (*Oophila amblystomatis*) as embryos (*e.g.,* Burns et al. 2017). Endosymbionts often live within a host compartment, such as a vacuole or membrane, which facilitates the exchange of materials (*i.e.,* nutrients, metabolites) and serves as the backbone for the relationship between host and symbiont (Dean et al. 2016; Wernegreen 2012).

Corals are one of the most iconic examples of endosymbiosis, and their symbiosis with single celled photobionts (dinoflagellate algae in the family Symbiodiniaceae;

LaJeunesse et al. 2018) enables diverse tropical reef ecosystems to thrive in oligotrophic waters (Melo Clavijo et al. 2018). Symbiodiniaceae live in coral gastrodermal cells in specialized vacuoles called symbiosomes (Davy, Allemand, and Weis 2012; Wernegreen 2012). This endosymbiosis facilitates the transfer of materials between host and symbiont, where Symbiodiniaceae share photosynthetically-derived carbon sugars and in return receive inorganic compounds from the coral's metabolic waste in addition to protection (Muscatine 1990; Muscatine, R. McCloskey, and E. Marian 1981). Once symbiosis is established, hosts can actively modulate photobiont physiology by manipulating the environment of the symbiosome. For example, photobiont photosynthesis is highly dependent on nitrogen availability, and host-mediated nitrogen limitation enables maintenance of primary production and control of photobiont growth (Falkowski et al. 1993; Rädecker et al. 2015). Additionally, coral hosts acidify the symbiosome *via* expression of V-type proton ATPases, which can facilitate increased photosynthesis (Barott et al. 2015).

Tropical corals live close to their upper thermal limits, making them particularly susceptible to temperature changes (Berkelmans and Willis 1999; Baker, Glynn, and Riegl 2008). Increases in anthropogenic carbon dioxide levels are elevating global ocean temperatures and leading to extreme regional ocean warming (*i.e.,* marine heatwaves; Smale et al. 2019), which threatens corals globally (Frieler et al. 2013). Specifically, temperature increases lead to a breakdown of the coral-algal symbiosis in a process called 'coral bleaching', and extended periods of dysbiosis can lead to coral starvation and eventual mortality (Brown 1997). It is theorized that reactive oxygen species (ROS)

generated by Symbiodiniaceae under temperature stress can damage cellular components, cause photoinhibition, and trigger coral bleaching (reviewed in Szabó, Larkum, and Vass 2020). However, even though both symbiotic partners exhibit a wide array of stress responses, photobionts are assumed to initiate symbiosis breakdown due to ROS production (*e.g.,* Berkelmans and van Oppen 2006; Stat, Carter, and Hoegh-Guldberg 2006; Stat and Gates 2010). In contrast to these physiological responses, several lines of evidence demonstrate that hosts exhibit strong stress responses at the transcriptional level (*e.g.,* S. W. Davies et al. 2016; DeSalvo et al. 2010; Meyer, Aglyamova, and Matz 2011; reviewed in Dixon, Abbott, and Matz 2020), while the photobiont's transcriptional response is muted (*e.g.,* Barshis et al. 2014; Baumgarten et al. 2013; Leggat et al. 2011). This lack of an algal transcriptional response may suggest that coral hosts regulate their symbiont's environment to buffer the algae from stress; however, an alternative explanation might be that the photobiont's transcriptome is less responsive to stress regardless of symbiotic state.

Understanding the independent and interactive roles of coral hosts and Symbiodiniaceae algae in holobiont (*i.e.,* assemblage of coral host and associated algal and microbial symbionts) resilience is difficult in a tropical coral system (reviewed in Bove, Ingersoll, and Davies 2022). Namely, it is impossible to disentangle the host's aposymbiotic state from stress and nutrient limitation given tropical coral reliance on Symbiodiniaceae-derived carbon. Facultative symbioses have emerged as tractable systems in which to ask fundamental questions about coral symbiosis (Puntin et al. 2022). Here, we leveraged genome-wide gene expression profiling in the facultatively symbiotic

coral *Oculina arbuscula* and its photobiont *Breviolum psygmophilum* to address two main questions. First, what is the consequence of symbiosis for coral hosts under thermal challenge? We hypothesized that, compared to aposymbiotic corals, symbiotic corals under thermal challenge would exhibit patterns of gene expression consistent with environmental stress responses of tropical corals because of symbiont-derived ROS produced under thermal stress. Second, we asked how symbiosis modulates photobiont responses to thermal challenges? Based on previous work documenting a lack of gene expression response in *in hospite* photobionts, we predicted greater responses of symbiotic hosts compared to photobionts *in hospite* in addition to a muted response of photobionts *in hospite* compared to *ex hospite,* consistent with coral hosts modulating the environment of their photobionts. To address these two questions, we replicated identical temperature challenge assays in two independent experiments and characterized host and photobiont responses via whole genome gene expression profiling.

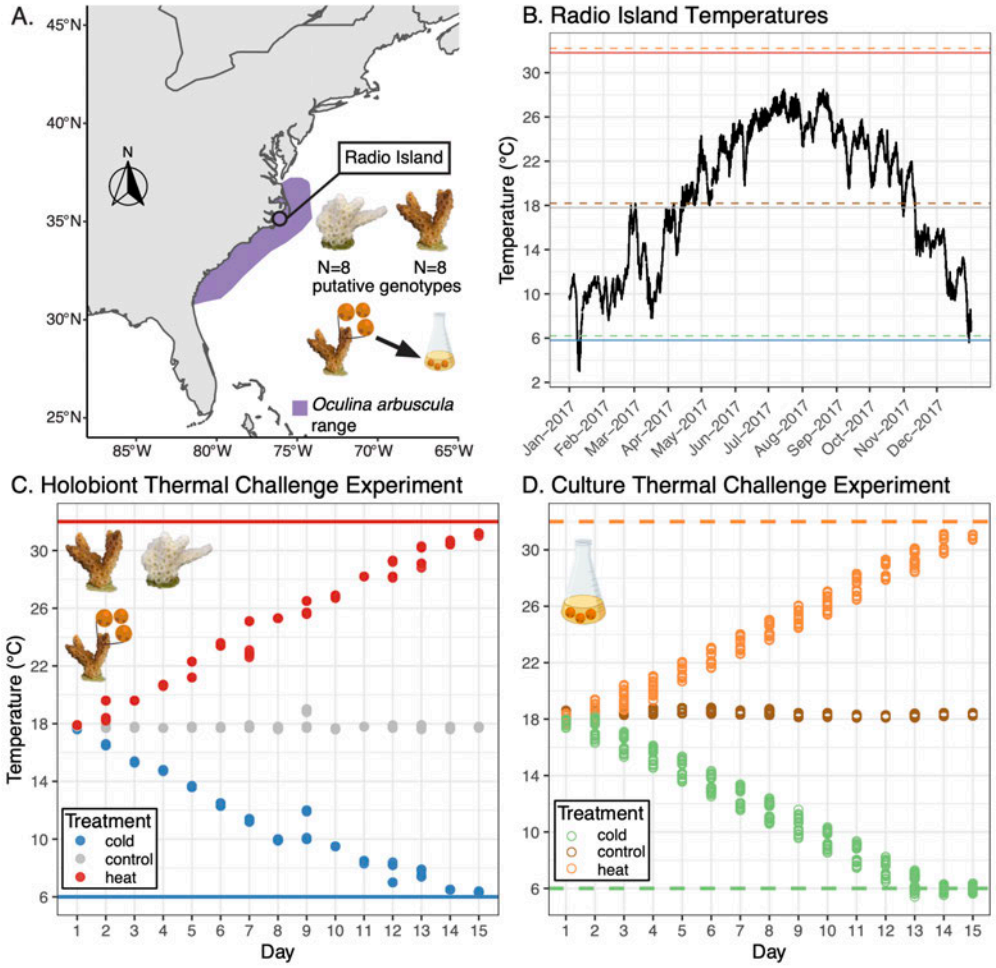


**Figure 4-1.**
**Experimental overview.** (**a**) Map showing collection site (Radio Island, North Carolina) of *Oculina arbuscula* colonies used in the holobiont thermal challenge experiment (N=8 symbiotic, N=8 aposymbiotic putative genotypes). *Breviolum psygmophilum* photobionts used in the culture thermal challenge experiment were isolated from symbiotic *O. arbuscula* tissue. Purple shading indicates the subtropical range of *O. arbuscula* (based on Thornhill et al. 2008). (**b**) Water temperatures (black line) recorded every 6 minutes at the NOAA buoy closest to Radio Island collection site (Station BFTN7; minimum temperature recorded = 3°C, maximum temperature recorded = 28.5°C) for the year prior to coral collection (January 1, 2017 - December 31, 2017). Thermal challenge treatments (heat = 32°C, control = 18°C, cold = 6°C) are overlaid annual temperature data. (**c**) Temperatures recorded during holobiont thermal challenge experiment, using NIST-calibrated glass thermometer. (**d**) Temperatures recorded during culture thermal challenge experiment, using HOBO loggers in each of the three incubators. Coral photos are courtesy of C. Tramonte, symbiont shapes were created by G. Puntin, and culture icons were created with BioRender.com.

## 4.3 Materials and methods

### *4.3.1. Experiment I.* Oculina arbuscula *and* Breviolum psygmophilum *holobiont responses to temperature challenges in symbiosis*

To test the prediction that symbiotic hosts would be more stressed under thermal challenge compared to aposymbiotic hosts, we exposed symbiotic and aposymbiotic fragments of *Oculina arbuscula* to three temperature treatments: 1) control (18°C), 2) heat challenge (temperature increased 1°C $day^{-1}$ from 18°C to 32°C), and 3) cold challenge (temperature decreased 1°C $day^{-1}$ from 18°C to 6°C).

#### *4.3.1.1. Coral collection and experimental design*

In June 2018, 16 colonies of the subtropical scleractinian coral *Oculina arbuscula* (N=8 symbiotic, N=8 aposymbiotic) were collected from Radio Island, North Carolina (NC) (34.712590°N, -76.684308°W) under NC Division of Marine Fisheries permits #706481 and #1627488 (Figure 4-1a). Colonies were shipped overnight to Boston University, fragmented, attached to petri dishes using cyanoacrylate glue, and maintained at ambient conditions (18°C, 33-35 PSU) for approximately 5 months. Experimental temperatures were informed in part by *in situ* temperature data recorded the year prior to collection by the NOAA buoy closest to the collection site (Figure 4-1b). On November 1, 2018, one fragment from each colony was placed in one of three treatments: 1) control (18°C), 2) heat challenge (target: 32°C), and 3) cold challenge (target: 6°C) (N=48 fragments total). Temperatures in the control treatment remained at 18°C for the duration of the 15-day study. Temperatures in the heat challenge treatment started at 18°C and

increased daily by 1°C with a final target temperature of 32°C. Temperatures in the cold challenge treatment started at 18°C and decreased daily by 1°C with a final target temperature of 6°C (lower temperatures were restricted by aquaria chillers) (Figure 4-1c). Temperatures were controlled using Aqua Logic digital temperature controllers.

Each temperature treatment consisted of three 15-gallon aquaria connected to one sump. All aquaria had a powerhead for water circulation, and each sump was equipped with a filter sock and protein skimmer for filtration. Water quality was tested daily in each tank by measuring temperature using a NIST-calibrated thermometer (Figure 4-1c) and salinity with a YSI meter. Target salinity of 33-34 PSU was maintained by mixing DI water with Instant Ocean Sea Salt, and mean (± SE) salinity was 33.94 ± 0.025 in control, 33.87 ± 0.015 in cold challenge, 34.15 ± 0.024 in heat challenge. A 50% water change was performed on day nine. Light exposure was monitored to ensure corals received equal light (50 µmol photons $m^{-2} sec^{-1}$) and remained on a 12:12 hour, light:dark schedule throughout the experiment. Coral fragments were rotated daily to ensure even light exposure. Each aquaria was fed ¼ tsp of reconstituted powdered brine shrimp daily, and feeding occurred for one hour before recirculating flow was resumed.

#### *4.3.1.2.* In hospite *photobiont physiology*

Pulse Amplitude Modulation (PAM) fluorometry was used to measure the dark-acclimated photochemical efficiency of photosystem II (Fv/Fm) using a Junior PAM approximately every three days throughout the experiment. Corals were given 8 hours of dark acclimation before Fv/Fm was measured in triplicate for all symbiotic coral fragments between the hours of 0800 and 1200. The effect of temperature challenge and experiment

duration on photobiont Fv/Fm was analyzed using a linear mixed effects model (*lmer*), with the interactions of fixed effects of treatment and day plus a random effect of genotype (to account for the lack of independence among measures from the same genet). Pairwise comparisons of the model output were compared using *emmeans* (Lenth et al. 2022). All analyses were performed in the R v4.2.0 statistical environment (R Core Team 2022).

#### *4.3.1.3.* Oculina arbuscula *holobiont gene expression profiling*

Following completion of the thermal challenge experiment (day 15, when temperature treatments were most divergent), tissue from all *O. arbuscula* fragments (N=48) was sampled using sterilized bone cutters, immediately placed into 200 proof ethanol, and maintained at -80°C. Total RNA was extracted using an RNAqueous kit (ThermoFisher Scientific) following manufacturer's instructions, but including an additional step of homogenizing samples with lysis buffer and glass beads for 1 minute at 5 m $s^{-1}$. Following extraction, DNA contamination was removed *via* DNAse1 Digestion for 30 minutes at 37°C. TagSeq libraries were prepared using 1.5 $\mu$g of input RNA (following Meyer, Aglyamova, and Matz 2011) with necessary adaptations for Illumina HiSeq sequencing (Lohman, Weber, and Bolnick 2016). Successfully prepared libraries (N=47) were sent to the Tufts University Core Facility and sequenced on the Illumina Hiseq 2500 using single-end 50 bp sequencing. Analysis of TagSeq data generally followed the pipeline presented here: https://github.com/z0on/tag-based_RNAseq. Raw reads were quality filtered using a custom perl script (tagseq_clipper.pl) to remove Illumina adapters, poly-A sequences, PCR duplicates, reads less than 20 bp long, and reads with a quality score less than 33.

#### *4.3.1.4. Putative coral clone identification*

Because many of our analyses are ordination based and gene expression has been shown to be highly heritable in corals and can drive global gene expression patterns (*i.e.,* Dixon et al. 2015), we tested for the presence of clones in our dataset. Following methods presented in Bove et al. (2023), putative *O. arbuscula* clones were identified and removed from downstream analyses by mapping quality filtered reads to concatenated *O. arbuscula* and *B. psygmophilum* transcriptomes (available at http://sites.bu.edu/davieslab/data-code/) using Bowtie2 (Langmead and Salzberg 2012). Single nucleotide polymorphisms (SNPs) were identified using the local mode (--local) with seed substring alignment length of 16 (-L 16), suppressing records for unaligned reads (--no-unal), and a minimum alignment score function of f(x) = 16 + x, where x is read length (--score-min L,16,1). Symbiont reads were then removed from the dataset, and genotyping and identification of host SNPs was performed using ANGSD (Korneliussen, Albrechtsen, and Nielsen 2014). Loci were filtered to include those that were present in at least 80% of individuals, with a minimum mapping score of 20, a minimum quality score of 25, a strand bias p-value >1 x $10^{-5}$, a heterozygosity bias >1 x $10^{-5}$, a minimum minor allele frequency >0.05, a p-value >1 x $10^{-5}$, and all triallelic sites were excluded as well as those with multiple best hits. Putative clones were distinguished using a hierarchical clustering tree (*hclust*) based on pairwise identity by state (IBS) distances calculated in ANGSD (Figure A3-1a). One genotype (A) was removed from downstream analyses because its replicate fragments failed to cluster together, suggesting sequencing failure, and the hierarchical clustering tree was re-made without that genotype (Figure A3-1b). This tree identified three sets of putative clones: 1)

aposymbiotic putative clonal group of genotypes N, O, and P, 2) aposymbiotic putative clonal group of genotypes H and K, and 3) symbiotic putative clonal group of M and L (Figure A3-1b). The genotype within each putative clonal group with the highest depth of coverage was maintained in downstream analyses (N, M, and H) and all others were removed leaving a total of 33 samples (N=7 putative symbiotic genotypes, N=4 putative aposymbiotic genotypes).

#### *4.3.1.5.* Oculina arbuscula *and* in hospite B. psygmophilum *gene expression analyses*

Quality filtered reads were mapped to the same concatenated transcriptome described above using Bowtie2 (Langmead and Salzberg 2012), but with different parameters (-k mode, with k=5, in addition to the flags --no-hd and --no-sq). *Oculina arbuscula* host and *B. psygmophilum* photobiont reads were then separated and independent runs of DESeq2 (Love, Huber, and Anders 2014) identified differentially expressed genes (DEGs) in response to heat and cold thermal challenge relative to the control separately for host and photobiont datasets using Wald's tests.

Host and photobiont gene expression data were *rlog*-transformed and used as input for separate principal component analyses (PCAs) using *plotPCA* (package=DESeq2) to determine the effect of temperature on gene expression profiles using PERMANOVAs *via* the *adonis2* function (package=vegan; Oksanen et al. 2022). Gene expression plasticity was calculated from host and photobiont PCAs using a custom function (Bove 2022), and was defined as the distance in PC space between an individual's expression profile and the average expression of all samples in the control treatment (as in Bove et al. 2023). Differences in gene expression plasticity between treatments were tested using an ANOVA

(*aov*) followed by a Tukey's HSD post-hoc test (*TukeyHSD*) for multiple test correction. Assumptions of these models were assessed visually using *check_model* (package=performance; Lüdecke et al. 2021).

GO enrichment analyses were performed using Mann-Whitney *U* tests (GO_MWU) based on the ranking of signed log p-values (Wright et al. 2015) for both the host and photobiont datasets. Results were visualized in dendrograms, which indicate the amount of gene sharing between significant GO categories and the direction of change relative to the control treatment. Results from the GO enrichment analyses were used for two functional analyses, detailed below.

First, following Wuitchik et al. (2021), GO delta ranks were used to compare *O. arbuscula* host response under thermal challenge relative to the stress responses of tropical reef-building corals. To accomplish this, functional enrichment results of the *O. arbuscula* host under cold and heat challenge were contrasted with a meta-analysis from Dixon et al. (2020) that characterized the transcriptomic signatures of stress in the coral genus *Acropora.* This meta-analysis identified two classes of coral stress responses: "type A", which was positively correlated across projects and functionally consistent with the general coral environmental stress response (ESR), and "type B", which was the opposite to the type A response and indicated lower intensity stress. We plotted these delta-ranks of the host GO-MWU results against the ESR genes in the Biological Processes (BP) GO category identified by Dixon et al. (2020) (termed the "red module") and determined whether the slopes of these correlations were positive (type A) or negative (type B).

Second, for *B. psygmophilum* photobiont data, GO results identified several terms related to photosynthesis as significantly underrepresented under cold challenge. To further explore genes in these GO categories, a heatmap of genes with an unadjusted p-value <0.10 that had GO annotations related to these underrepresented photosynthesis terms were plotted using *pheatmap*.

#### *4.3.1.6. Checking identity of* Breviolum psygmophilum in hospite

The species identity of the algal symbionts in symbiosis with *O. arbuscula* used in the holobiont thermal challenge experiment was confirmed using metabarcoding of the Symbiodiniaceae ITS2 region. DNA was extracted from N=39/48 coral fragments that had sufficient sample remaining using a modified phenol-chloroform extraction, described in detail by Davies et al. (2013). Because aposymbiotic corals can still host a small amount of photobionts, both symbiotic and aposymbiotic fragments were included in these extractions. The ITS2 region was targeted using forward primer *ITS-DINO* (5' - TCGTCGGCAGCGTC AGATGTGTATAAGAGACAG *NNNN* **GTGAATTGCAGAACTCCGTG** - 3') (Pochon et al. 2001) and reverse primer *ITS2Rev2* (5' - GTCTCGTGGGCTCGG AGATGTGTATAAGAGACAG *NNNN* **CCTCCGCTTACTTATAGCTT** 3') (Stat et al. 2009). Underlined bases denote adapter linker, bold bases are primer sequences, and the middle bases are spacer sequences. The reactions totaled 20 µl and included 20 ng of template DNA, 10 µM forward primer, 10 µM reverse primer, 0.2 mM dNTP, 1X ExTaq buffer (Takara), 0.025 U ExTaq enzyme (Takara), and the remaining Milli-Q $H_20$ (Millipore). The PCR profile was 95°C for 40 seconds, 59°C for 120 seconds, and 72°C for 60 seconds for 35 cycles with a final

elongation step of 72°C for 7 minutes. PCR products were purified using Ampure XP Reagent for PCR Purification (Beckman Coulter) and eluted in 28 µL. Each PCR product was barcoded with a unique Illumina barcoded adapter using five PCR cycles and visualized on a 1% agarose gel to assess relative band intensity. Samples were normalized and pooled and 25 µl of the pooled library was run on a 1% SYBR Green (Invitrogen) stained gel. The target band was excised and incubated with 30 µl of Milli-Q water overnight at 4˚C. This library was quantified using a Quant-iT PicoGreen dsDNA assay kit (Thermo Fisher) and submitted for paired-end 250bp sequencing on an Illumina Miseq at Tufts University Core Facility (TUCF).

Raw ITS2 data were submitted to SymPortal (B. C. C. Hume et al. 2019) to identify ITS2 type profiles. All samples were successfully sequenced and were analyzed at the level of defining intragenomic variant (DIV) to confirm that all symbiotic corals hosted *B. psygmophilum.* Relative abundance of DIVs across *O. arbuscula* fragments were compared using a bar plot constructed with *phyloseq* (McMurdie and Holmes 2013).

#### *4.3.1.7. Comparing orthologous genes in* Oculina arbuscula *and* Breviolum psygmophilum *in symbiosis*

To compare *O. arbuscula* host (both symbiotic and aposymbiotic) and *B. psygmophilum in hospite* responses to temperature challenges, independent gene expression analyses were completed on orthologous genes. This analysis allowed us to test two predictions, first that symbiotic hosts would respond more to temperature challenge than aposymbiotic hosts, and second that symbiotic hosts would respond more than their photobionts *in hospite*. Orthologous genes were identified following methods presented in

Dixon and Kenkel (2019) with additional specifics for Symbiodiniaceae described here: https://github.com/grovesdixon/symbiodinium_orthologs. Briefly, cd-hit (W. Li and Godzik 2006) clustered sequences in *O. arbuscula* and *B. psygmophilum* reference transcriptomes with a sequence identity threshold of 0.98, alignment coverage of the longer and shorter sequence of at least 0.3, and only the longest sequence was retained. Transdecoder v5.5.0 (Haas et al. 2013) predicted protein coding sequences in the clustered references based on open reading frames (ORFs) and homology to known proteins. Only the longest ORFs (minimum amino acid length=50 bp) were retained and then annotated using a blastp alignment against the Swissprot database and protein domains were identified with scanHmm in HMMER v3.2.1 (S. R. Eddy 2011). FastOrtho assigned these predicted coding sequences to orthologous groups with an e-value cut-off of $1 \times 10^{-10}$ (L. Li, Stoeckert, and Roos 2003). Paralogs (N=9727 groups) were removed, leaving 1951 orthologous groups. Protein sequences for these orthologs were aligned using the multiple sequence alignment program MAFFT (Katoh and Standley 2013) and gene trees were built with FastTree (Price, Dehal, and Arkin 2009), which infers approximately-maximum-likelihood phylogenetic trees from protein sequences. These constructed trees were pruned using the biopython module *Phylo* (Talevich et al. 2012), which facilitated the inclusion of additional orthologous groups as single copy orthologs, for a total of 1962 single-copy orthologs.

*Seqtk* (https://github.com/lh3/seqtk) subsetted *O. arbuscula* and *B. psygmophilum* reference transcriptome fasta files to include only single copy orthologs. These single copy ortholog reference transcriptomes were then concatenated and quality filtered TagSeq

reads were mapped to this ortholog reference using Bowtie2 (-k mode, with k=5, in addition to the flags --no-hd and --no-sq). For each partner, only orthologs with a mean count >2 across samples were retained, leaving 1381 host orthologs and 250 photobiont orthologs. The low number of photobiont counts led to a total of only 185/1962 shared orthologs with high-quality mapped reads across both the host and symbiont ortholog dataset. To directly compare responses to temperature treatment of symbiotic hosts, aposymbiotic hosts, and photobionts *in hospite*, *O. arbuscula* and *B. psygmophilum* count data for these 185 orthologs were included in the same DESeq2 model, which modeled a main effect of the aggregate factor of temperature treatment (cold challenge, heat challenge, or control) and sample type (symbiotic host, aposymbiotic host, or photobiont *in hospite*). Response of the three sample types (symbiotic host, aposymbiotic host, or photobiont *in hospite*) to heat challenge and cold challenge relative to the control was quantified as the number of differentially expressed orthologs with an adjusted p-value <0.1. A two-proportions z-test (*prop.test*) tested for differences in the proportion of differentially expressed orthologs across sample types. Comparisons included symbiotic host vs. aposymbiotic host under heat and cold challenge, symbiotic host vs. *in hospite* photobiont under heat and cold challenge, and aposymbiotic host vs. *in hospite* photobiont under heat and cold challenge.

### *4.3.2. Experiment II.* Breviolum psygmophilum *response in culture* - ex hospite

#### *4.3.2.1. Photobiont cell culture maintenance*

To isolate the response of *Breviolum psygmophilum* to temperature challenge *ex hospite*, the thermal challenge experiment detailed above in *O. arbuscula* holobionts was replicated on cultured *B. psygmophilum* (Figure 4-1d). Symbiont cultures used for this experiment were *B. psygmophilum* cells isolated from *O. arbuscula* from Radio Island, NC on June 29, 2018. Symbiodiniaceae cells were isolated from the host by serially diluting host tissue removed via airbrush into sterile F/2 media (Bigelow NCMA, East Boothbay, ME, USA). The "ancestral culture" was maintained in F/2 media based on artificial seawater (Instant Ocean), with monthly transfers to fresh media, in a Percival incubator (model AL-30L2) at a temperature of 26°C and irradiance of 30 $\mu$mol photons $m^{-2}$ $sec^{-1}$ on a 14:10 hour light:dark cycle. In preparation for the culture experiment, on October 18, 2019, this long-term acclimated ancestral culture was split into three new flasks, each with 100 mL of F/2 media and 0.5 mL of dense cells. On October 26, 2019, these three "daughter cultures" were acclimated to 18°C by decreasing temperatures at a rate of 1°C $day^{-1}$ over a span of nine days, and reached 18°C on November 5, 2019.

#### *4.3.2.2. Semi-continuous culture methodology*

Daughter cultures were acclimated to 18°C for 11 weeks, after which new "test cultures" were created from the daughter cultures (one from each), which were used in a preliminary experiment to determine the timing of when cultures reached the stationary growth phase (Figure A3-3a). This information was leveraged to maintain cultures in

exponential growth phase throughout the temperature challenge experiments. Each test culture initially had a cell density of 10,000 cells $mL^{-1}$ in a total volume of 100 mL F/2 media. Test cultures were maintained at 18°C under a 14:10 hour light:dark cycle when determining timing of exponential and stationary growth phases. Triplicate hemocytometer cell counts were conducted every other day on each flask and were used to calculate cell densities to establish timing of when the stationary growth phase was reached, which was approximately ten days after initial transfer.

#### *4.3.2.3. Checking identity of* Breviolum psygmophilum ex hospite

*Ex hospite* photobiont species identity was confirmed prior to thermal challenge experiments. Daughter cultures were sub-sampled one week before the start of the experiment, on October 23, 2020. DNA was extracted using the DNeasy Plant Mini Kit (Qiagen) following manufacturer's instructions. The ITS2 region was targeted using the same forward and reverse primers and PCR profiles described above: *ITS-DINO* (Pochon et al. 2001) and *ITS2Rev2* (Stat et al. 2009). Amplified samples were sent to Eton Biosciences, where they were purified and sequenced using Sanger sequencing. Sequence quality was checked using *4Peaks*, and sequence identity was confirmed using NCBI Nucleotide BLAST with default parameters.

#### *4.3.2.4. Thermal challenge experiment*

*Breviolum psygmophilum* cultures were exposed to three thermal challenge treatments, which mirrored treatments described for the holobiont *O. arbuscula* experiment detailed in part I (Figure 4-1d). The *ex hospite* photobiont thermal challenge experiment

began on October 30, 2020, after a total acclimation of 51 weeks at 18°C. Experimental cultures (N=4 flasks per treatment) were established from the long-term acclimated daughter flasks, with an initial cell density of 200,000 cells $mL^{-1}$ in 100 mL of F/2 media.

At the start of the experiment, all heat and cold challenge flasks were placed in separate Percival incubators (model AL-30L2), and control flasks were maintained in a temperature-controlled room (Harris Environmental Systems, Andover, MA). Both incubators and the temperature control room started at 18°C and followed a 14:10 hour light:dark cycle at ~50 umol photons $m^{-2}$ $sec^{-1}$. Temperatures were changed in the heat and cold challenge treatments approximately 20 hours after the experimental cultures were created. Each temperature increase in successive days occurred during the dark phase of the light cycle at the same time each day (11:30). All experimental cultures were sub-sampled every other day for hemocytometer counts to track cell growth through time. Experimental cultures were grown semi-continuously, with the timing of transfers determined using the preliminary experiment described above (Figure A3-3). Specifically, on day 7, all cultures were homogenized, half of their volume (50 mL) was transferred to a sterile flask, and an equivalent volume of F/2 media was added. This doubled the number of experimental flasks, from N=12 to N=24 (N=8 replicate flasks per treatment). The 15-day culture experiment mirrored the holobiont experiment and final sample collection and processing was completed on November 13, 2020.

#### *4.3.2.5. Sample processing, RNA extraction, and sequencing*

At the end of the experiment (day 15), all cultures were thoroughly mixed by vortexing, poured into two 50 mL conical tubes and centrifuged at 5000 RPM for 7

minutes. After the supernatant was removed, samples were flash frozen in liquid nitrogen and stored at -80°C until RNA extraction.

To obtain sufficient RNA for TagSeq, replicate cultures in the cold challenge treatment were pooled, such that there were four pooled replicates extracted separately. The limited cell density in the cold challenge was the result of reduced growth under cold challenge (Figure A3-3). The heat challenge and control flasks had sufficient cell density to conduct independent RNA extractions on each of the eight replicate flasks. To extract RNA, flash frozen pellets were ground for three minutes in a mortar and pestle that was pre-chilled with liquid nitrogen. Additional liquid nitrogen was added as needed to keep the cell pellet frozen. Ground cells were then transferred to a 1.5 mL tube, and RNA was extracted using RNAqueous-micro kits (ThermoFisher Scientific) following manufacturer's instructions, except final extracts were eluted in 15 $\mu$L. DNA was removed *via* DNA-free DNA Removal Kit (ThermoFisher Scientific) and RNA quality was visually checked using gel electrophoresis. RNA concentrations were quantified using a Quant-iT PicoGreen dsDNA Assay (ThermoFisher Scientific). Total RNA was sent to the University of Texas at Austin Genome Sequencing and Analysis Facility (GSAF), where it was prepared for TagSeq following Meyer et al. (2011). Samples were sequenced across two lanes of the NovaSeq 6000 machine with single-end 100 bp sequencing.

*4.3.2.6. Gene expression analyses on* ex hospite Breviolum psygmophilum

The generation of *ex hospite B. psygmophilum* TagSeq count data followed methods detailed in part I for the holobiont analyses, except samples were mapped to the *B. psygmophilum* reference transcriptome alone. Principal component analysis (PCAs),

gene expression plasticity, and GO-enrichment analyses were conducted on the culture dataset as detailed in part I. A heat-map of genes with GO annotations related to photosynthesis were conducted on the culture dataset similar to the method in part I, except an unadjusted p-value <0.01 was used to restrict the number of genes included in the heat map. In addition, the same method was used to generate a heatmap of genes with GO annotations related to oxidative stress, as these terms were consistently enriched in *ex hospite* GO analyses.

#### *4.3.3. III. Comparing* Breviolum psygmophilum *response* in *and* ex hospite

To compare the gene expression responses of *B. psygmophilum* to temperature challenge *in* and *ex hospite*, the *in hospite* photobiont TagSeq data from the holobiont experiment (part I) and the *ex hospite* photobiont experiment (part II) were analyzed together. This analysis allowed us to test the prediction that photobionts would respond more to temperature challenge *ex hospite* compared to *in hospite*. First, a batch effect correction was conducted on combined raw count data for both experiments using ComBat-seq (Y. Zhang, Parmigiani, and Johnson 2020), with a specified batch of experiment type (*in hospite* or *ex hospite*) and temperature treatment (heat challenge, cold challenge, or control) as the biological treatment of interest. To directly compare *B. psygmophilum* response to temperature treatment *in* and *ex hospite*, batch-corrected data were included in the same DESeq2 (Love, Huber, and Anders 2014) model, which modeled a main effect of the aggregate factor of temperature treatment (cold challenge, heat challenge, or control) and sample type (*in hospite* or *ex hospite*). Genes were only retained in the analysis if they

were present in at least 80% of samples (33/41 samples) at a mean count of 2 or higher, which left 1885 genes for downstream analyses.

Following PCAs detailed in part I above, the combined photobiont count data were *rlog*-transformed and used as input for a PCA to test the effect of the aggregate factor of temperature treatment and sample type on gene expression. Significance was assessed with PERMANOVA, using the *adonis2* function (package=vegan; Oksanen et al. 2022). Gene expression plasticity was also calculated following methods detailed above.

## 4.4 Results

### *4.4.1. Independent responses of Oculina arbuscula and Breviolum psygmophilum to temperature challenges in symbiosis*

#### *4.4.1.1.* Oculina arbuscula *hosts exhibit stronger gene expression responses to cold challenge than heat challenge regardless of symbiotic state*

The aggregate factor of temperature treatment and symbiotic state had a significant effect on *O. arbuscula* host gene expression patterns (Figure 4-2a; *ADONIS* $p$=0.001). In both symbiotic (*Tukey HSD* $p$=0.013) and aposymbiotic (*Tukey HSD* $p$<0.001) hosts, cold challenge elicited significantly higher gene expression plasticity compared to heat challenge (Figure 4-2b; $p$<0.001). However, symbiotic state did not influence gene expression plasticity within temperature treatments (cold challenge, *Tukey HSD* $p$=0.218; heat challenge, *Tukey HSD* $p$=0.992; Figure 4-2b).

When comparing GO delta ranks of the red ESR module from the meta-analysis of *Acropora* coral stress responses (Dixon, Abbott, and Matz 2020) to symbiotic and

aposymbiotic *O. arbuscula* host delta ranks from the heat and cold challenges, positive relationships were observed for GO terms belonging to the biological processes category for all comparisons (Figure 4-2c). These positive relationships with the red ESR module align with the type "A" response reported in *Acropora* (Figure 4-2c).

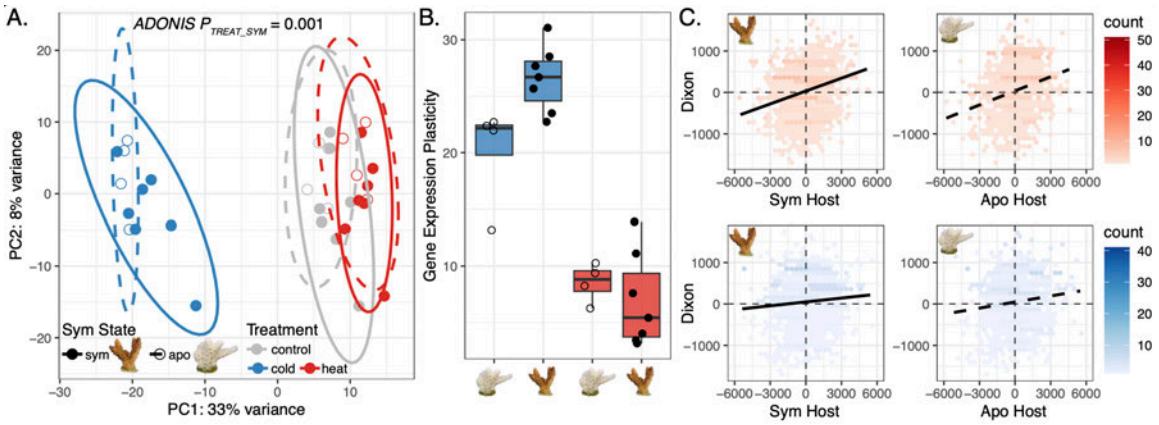


**Figure 4-2.**
**Symbiotic and aposymbiotic *Oculina arbuscula* host gene expression responses to temperature challenges.** (**a**) Principal component (PC) analysis of gene expression of symbiotic (solid point and line) and aposymbiotic (open points, dashed line) coral hosts under control (grey), cold (blue), and heat (red) temperature challenge assessed on day 15. The x- and y-axes represent the % variance explained by the first and second PC, respectively. (**b**) Gene expression plasticity of symbiotic and aposymbiotic coral hosts under cold (blue) and heat (red) challenges. Each point in the boxplot represents the distance in PC space (in panel **a**) between each coral fragment and the average location of control fragments. (**c**) Relationship between gene ontology (GO) delta ranks from biological processes of symbiotic (left) and aposymbiotic (right) coral hosts under heat (top) and cold (bottom) challenge with GO delta ranks from the "red ESR module" from Dixon et al. (2020). The positive slope in all panels represents a "type A" environmental stress response. Coral photos are courtesy of C. Tramonte.

#### *4.4.1.2. Cold challenge induces negative effects on* Breviolum psygmophilum *photosynthetic function*

ITS2 metabarcoding confirmed that all *O. arbuscula* genotypes hosted a majority of defining intragenomic variants (DIVs) associated with *B. psygmophilum* (Figure A3-2). All but one individual hosted 100% *B. psygmophilum,* and all symbiotic *O. arbuscula* fragments hosted the same DIV of *B. psygmophilum* (Figure A3-2). Photosynthetic efficiency (Fv/Fm) of *in hospite B. psygmophilum* was significantly reduced by the interaction of temperature challenge and time (Figure 4-3a; $p<0.001$). By day 8, when target temperatures were 11°C in cold challenge and 25°C in heat challenge, Fv/Fm had significantly declined in the cold challenge relative to control ($p=0.02$), but not in heat challenge relative to control ($p=0.09$). For the remainder of the experiment, Fv/Fm was significantly reduced in both cold and heat challenge relative to the control (Figure 4-3a; $p<0.001$ for all comparisons). Fv/Fm in cold challenge corals was more dramatically reduced than those under heat challenge, with fixed effect parameter estimates on day 14 of -0.065 in heat challenge and -0.24 in cold challenge relative to control (Figure 4-3a).

Temperature challenge treatments had a significant effect on gene expression profiles of *in hospite B. psygmophilum* (Figure 4-3b; *ADONIS p=0.001*). However, in contrast to patterns observed in the coral host, there were no differences in gene expression plasticity between photobionts in cold and heat challenge (Figure 4-3c; *Tukey HSD* $p=0.62$). In line with the negative effects of cold challenge on *B. psygmophilum* Fv/Fm (Figure 4-3a), six GO terms related to photosynthetic processes were significantly underrepresented under cold challenge relative to control conditions (photosystem

[GO:0009521], photosynthesis, light harvesting [GO:0009765], chlorophyll binding [GO:0016168], protein-chromophore linkage [GO:0018298], thylakoid membrane [GO:0042651], and tetrapyrrole binding [GO:0046906]). Six annotated genes assigned to these photosynthetic GO terms were differentially expressed under cold challenge (unadjusted p-value<0.10) relative to control conditions and these genes showcased down-regulation of light-harvesting complex (LHC) and chloroplast under cold challenge relative to both control and heat treatments (Figure 4-3d).

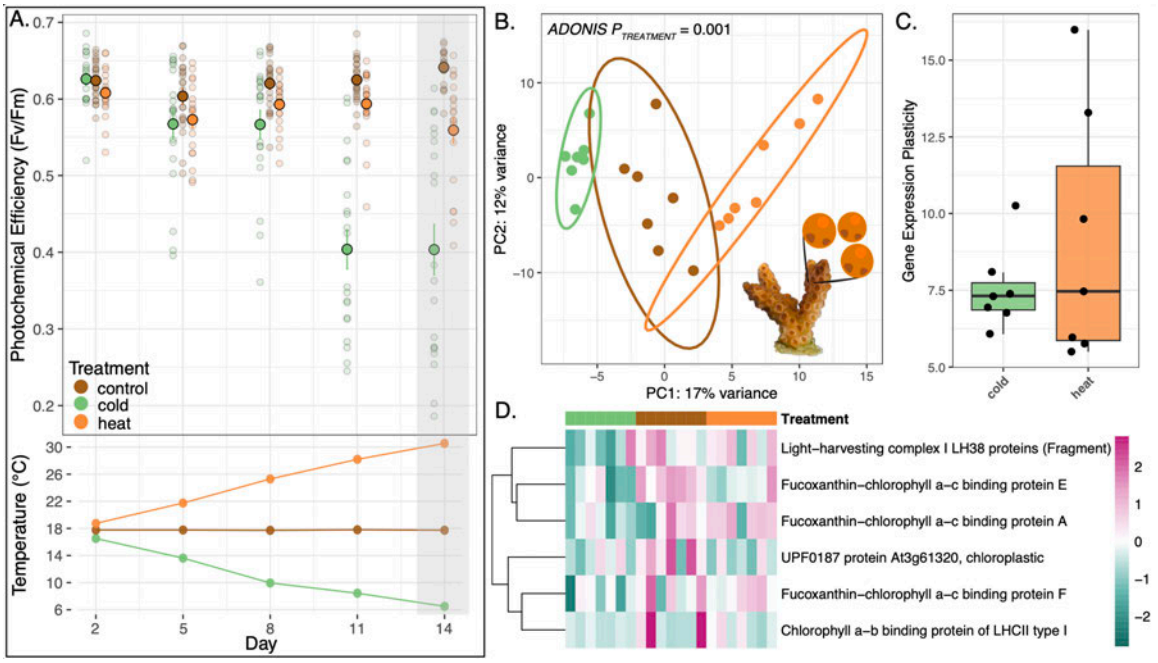


**Figure 4-3.**

***In hospite* photobiont physiology and gene expression responses to temperature challenges.** (**a**) Photochemical efficiency (Fv/Fm, top panel) of *in hospite* photobionts through time as temperatures diverged (bottom panel). Top: Large points represent mean Fv/Fm ± standard error across temperature challenge treatments with smaller transparent points representing an individual coral fragment's average Fv/Fm at each time point. The gray bar indicates the time point immediately prior to sampling for gene expression. (**b**) Principal component (PC) analysis of gene expression of *in hospite* photobionts under control (brown), cold (green), and heat (orange) temperature challenge on day 15. The x- and y-axes represent the % variance explained by the first and second PC, respectively. (**c**) Gene expression plasticity of *in hospite* photobionts under cold (green) and heat (orange) challenge. Each point in the boxplot represents the distance in PC space (in panel **b**) between each coral fragment and the average location of control fragments. Gene expression plasticity was not significantly different between cold and heat challenge (Tukey HSD $p$=0.62). (**d**) Heatmap showing differentially expressed genes (DEGs; unadjusted p-value<0.1) with annotations associated with photosynthesis gene ontology (GO) terms, where each row is a gene and each column is a sample. The color scale represents log2 fold change relative to the gene's mean, where pink represents up-regulation and teal represents down-regulation. Colored blocks above heatmaps indicate temperature challenge treatments. Coral photo is courtesy of C. Tramonte and symbiont shapes were created by G. Puntin.

### *4.4.2. Comparing response of* Oculina arbuscula *and* Breviolum psygmophilum *in symbiosis using orthologous genes*

The number of differentially expressed orthologs was significantly greater in symbiotic hosts compared to aposymbiotic hosts under cold challenge ($X^2$ = 7.27; $p$=0.004), but not heat challenge (Figure 4-4; $X^2$ = 1.82; $p$=0.09). Similarly, the number of differentially expressed orthologs was significantly greater in aposymbiotic *O. arbuscula* hosts compared to *in hospite B. psygmophilum* photobionts under cold challenge ($X^2$ = 68.50; $p$<0.0001), but not heat challenge (Figure 4-4; $X^2$ = 1.82; $p$=0.09). Additionally, aposymbiotic *O. arbuscula* hosts also exhibited more differentially expressed orthologs compared to *in hospite B. psygmophilum* under cold challenge ($X^2$ = 35.17; $p$<0.0001), but not heat challenge (Figure 4-4; $X^2$ = 0; $p$=0.5).

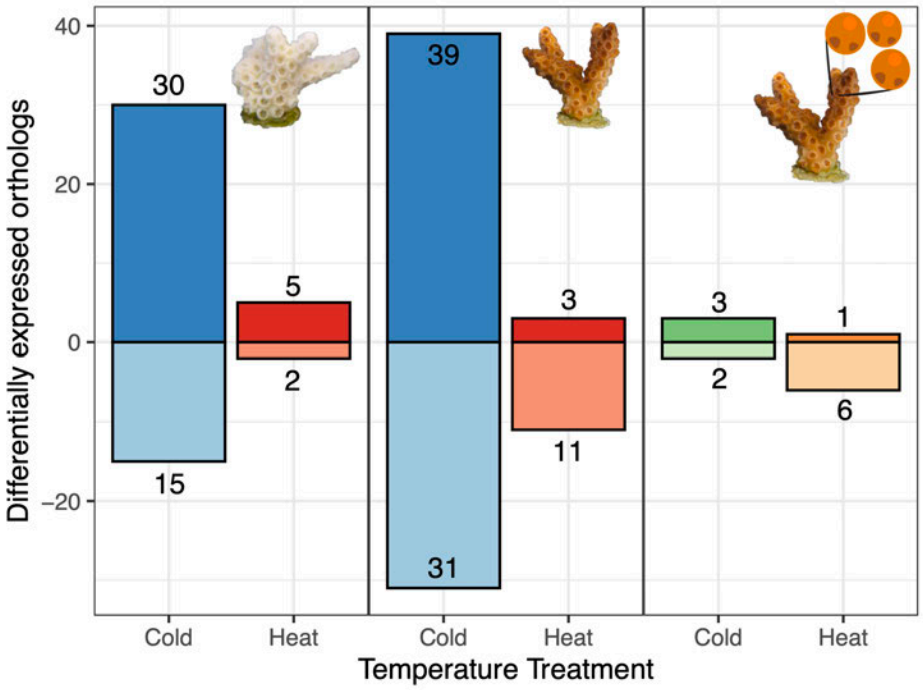


**Figure 4-4.**
**Coral hosts exhibit more differentially expressed orthologs than *in hospite* photobionts under thermal challenges.** Bar plots representing the number of differentially expressed orthologous genes (positive values = up-regulated, negative values = down-regulated) in response to temperature challenges (indicated on x-axis) in aposymbiotic hosts (left), symbiotic hosts (middle), and *in hospite* photobionts (right). Symbiotic *O. arbuscula* had significantly more differentially expressed orthologs than *in hospite B. psygmophilum* under cold challenge ($p<0.0001$), but not heat challenge ($p=0.09$). Aposymbiotic *O. arbuscula* had significantly more differentially expressed orthologs than *in hospite B. psygmophilum* under cold challenge ($p<0.0001$), but not heat challenge ($p=0.5$). Symbiotic *O. arbuscula* had significantly more differentially expressed orthologs than aposymbiotic *O. arbuscula* under cold challenge ($p=0.004$), but not heat challenge ($p=0.09$). Coral photos are courtesy of C. Tramonte and symbiont shapes were created by G. Puntin.

### *4.4.3.* Breviolum psygmophilum *response to temperature challenge out of symbiosis* - ex hospite

Sanger sequencing confirmed that all parent cultures matched *B. psygmophilum* (GenBank Accession ID LK934671.1) with 100% percent identity and 53-87% query coverage. *Breviolum psygmophilum* cultures in all temperature treatments were maintained in exponential growth phase throughout the experiment (Figure A3-3b,c). Temperature treatment had a significant effect on gene expression patterns of *ex hospite B. psygmophilum* (Figure 4-5a; *ADONIS p*=0.001). Additionally, gene expression plasticity was greater in *ex hospite B. psygmophilum* under cold challenge relative to heat challenge (Figure 4-5b; *Tukey HSD p*=0.008), whereas no significant effect was observed *in hospite* (Figure 4-3c).

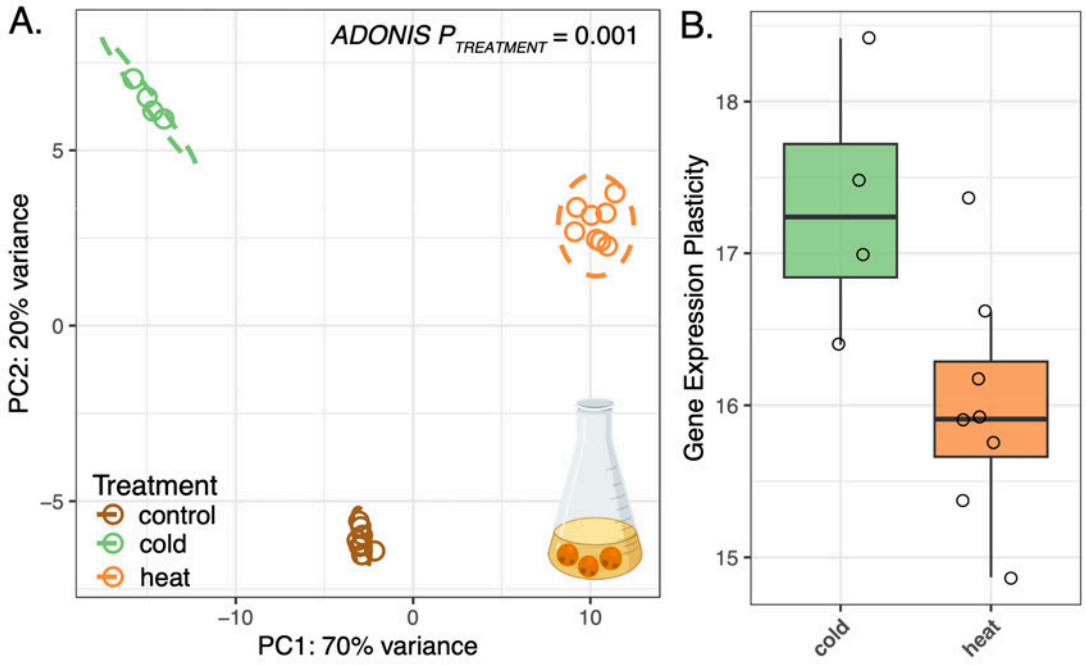


**Figure 4-5.**
***Ex hospite* photobiont gene expression responses to temperature challenges.** (**a**) Principal component (PC) analysis of gene expression of *ex hospite* photobionts under control (brown), cold (green), and heat (orange) temperature challenges. The x- and y-axes represent the % variance explained by the first and second PC, respectively. (**b**) Gene expression plasticity of photobionts *ex hospite* under cold (green) and heat (orange) challenge. Each point in the boxplot represents the distance in PC space (in panel **a**) between each culture replicate and the average location of control cultures. Gene expression plasticity was significantly greater under cold challenge compared to heat challenge (*Tukey HSD p*=0.008). Symbiont shapes were created by G. Puntin and culture icon was created with BioRender.com.

A total of eight GO terms related to photosynthetic processes were significantly underrepresented in *ex hospite B. psygmophilum* under cold challenge (photosystem [GO:0009521], photosynthesis, light harvesting [GO:0009765], chloroplast-nucleus signaling pathway [GO:0010019], photosynthesis [GO:0015979], chlorophyll binding [GO:0016168], protein-chromophore linkage [GO:0018298], thylakoid membrane [GO:0042651], and tetrapyrrole binding [GO:0046906]). A heat map of 59 DEGs

(unadjusted p-value<0.01) under cold challenge belonging to these eight GO terms showcased a small group of up-regulated genes and a larger group of down-regulated genes in response to cold challenge (Figure 4-6a). Up-regulated photosynthesis-related genes included “Pentatricopeptide repeat-containing proteins”, which are involved in RNA editing events in chloroplasts (Barkan and Small 2014). Similar to *B. psygmophilum* in symbiosis (Figure 4-3c), genes involved in the LHC were down-regulated under cold challenge (Figure 4-6a).

Additionally, a total of 5 GO terms commonly associated with stress were differentially enriched in *ex hospite B. psygmophilum* under cold challenge treatment relative to control conditions (protein folding [GO:0006457], cellular response to oxidative stress [GO:0034599], hydrogen peroxide metabolic process [GO:0042743], unfolded protein binding [GO:0051082], cellular response to chemical stress [GO:0062197]). Similar to photosynthesis-related genes, a heat map of 69 DEGs under cold challenge (unadjusted p-value<0.01) assigned to these five stress GO terms and revealed two groups of genes, one down-regulated and one up-regulated under cold challenge relative to control and heat challenge cultures (Figure 4-6b).

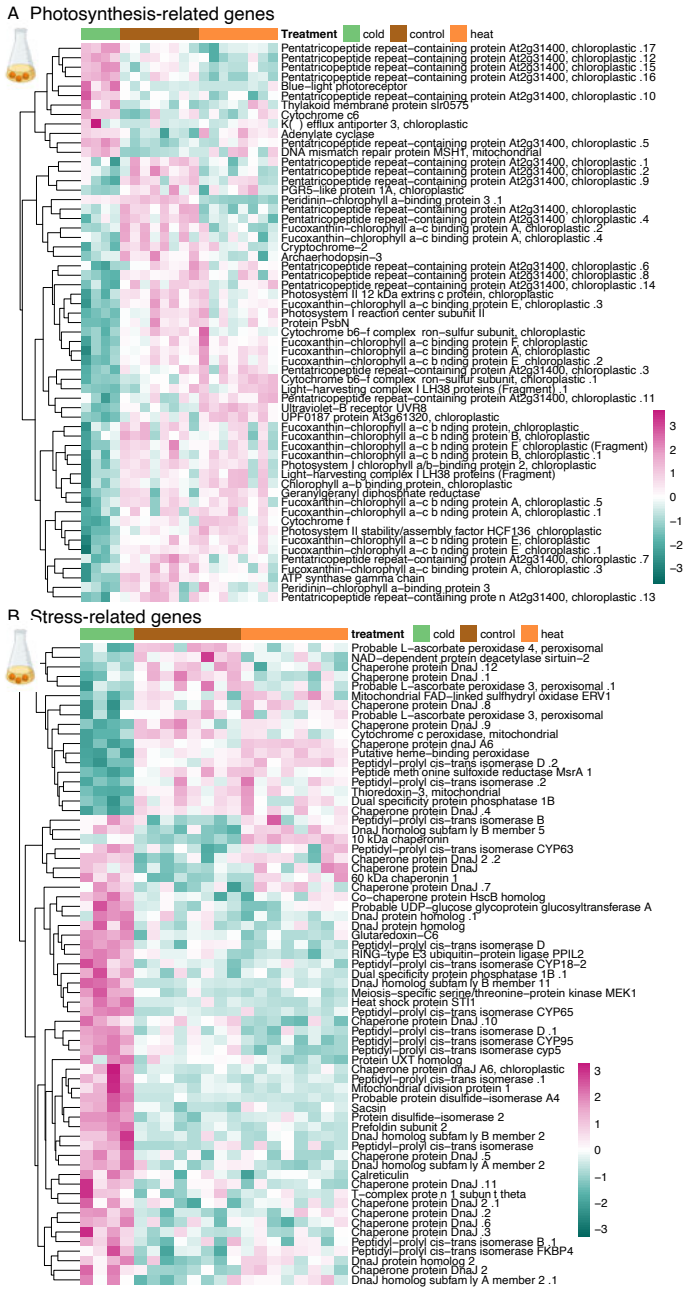


**Figure 4-6.**
***Ex hospite* photobionts exhibit differential expression of photosynthesis and stress-related genes under temperature challenges.** Heatmap showing differentially expressed genes (DEGs; unadjusted p-value<0.01) belonging to photosynthesis (**a**) and stress (**b**) gene ontology (GO) terms, where each row is a gene and each column is a sample. The color scale represents log2 fold change relative to the gene's mean, where pink represents up-regulation and teal represents down-regulation. Colored blocks above heatmaps indicate temperature challenge treatments. Symbiont shapes were created by G. Puntin and culture icons were created with BioRender.com.

### *4.4.4. Comparing responses of* in *and* ex hospite Breviolum psygmophilum

When analyzing *in hospite* and *ex hospite B. psygmophilum* in the same *DESeq2* model, a significant effect of the aggregate factor of temperature treatment and symbiotic state was observed (Figure 4-7a; *ADONIS* $p$=0.001). Temperature and symbiotic state also had a significant effect on gene expression plasticity (Figure 4-7b; $p$<0.0001) with *ex hospite B. psygmophilum* having significantly higher gene expression plasticity compared to *in hospite B. psygmophilum*, both under cold challenge (Tukey HSD $p$<0.0001) and heat challenge (Figure 4-7b; Tukey HSD $p$=0.0001).

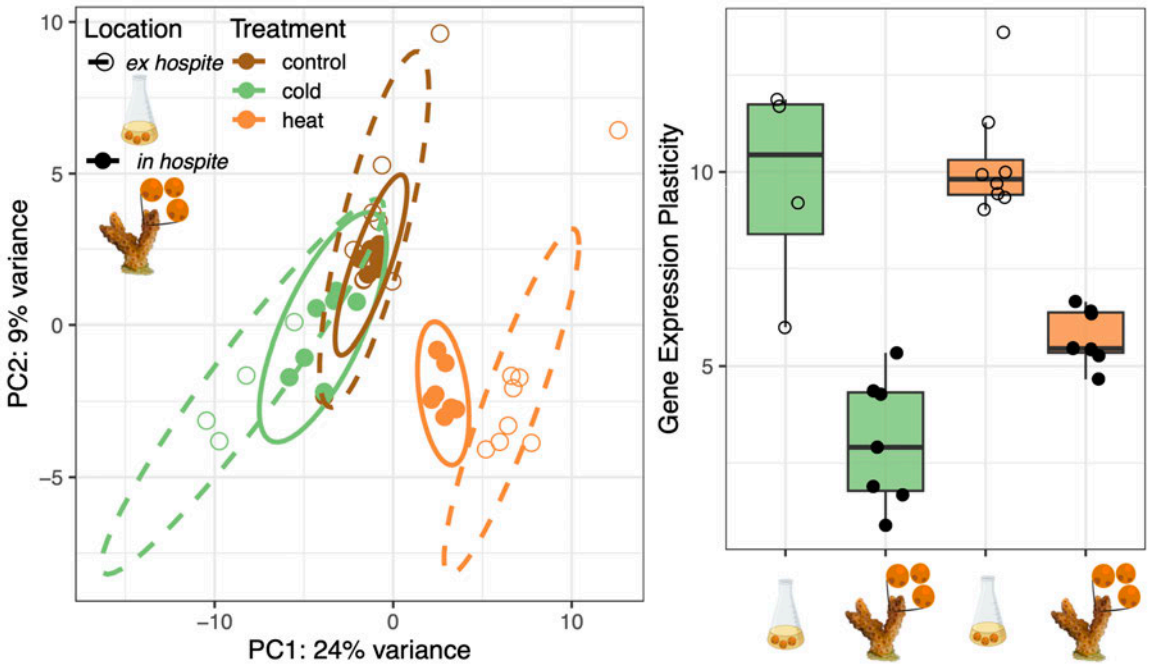


**Figure 4-7.**
***Ex hospite* photobionts respond more strongly to thermal challenges than *in hospite* photobionts.** (**a**) Principal component (PC) analysis of gene expression of *ex hospite* (open circles, dashed lines) and *in hospite* (solid points and lines) photobionts under control (brown), cold (green), and heat (orange) temperatures. The x- and y-axes represent the % variance explained by the first and second PC, respectively. (**b**) Gene expression plasticity of *ex hospite* and *in hospite* photobionts under cold (green) and heat (orange) challenge. Each point in the boxplot represents the distance in PC space (in panel **a**) between each sample and the average location of the respective control treatment (*i.e.,* either *ex hospite* or *in hospite* controls). Gene expression plasticity was significantly greater in *ex hospite* photobionts compared to *in hospite* photobionts under both cold challenge (Tukey HSD $p<0.0001$) and heat challenge (Tukey HSD $p=0.0001$). Coral photos are courtesy of C. Tramonte, symbiont shapes were created by G. Puntin, and culture icons were created with BioRender.com.

## 4.5. Discussion

### *4.5.1. Both aposymbiotic and symbiotic coral hosts exhibit classic environmental stress responses to temperature challenges*

Here, we leveraged genome-wide gene expression profiling of *in* and *ex hospite* facultative coral hosts (*Oculina arbuscula*) and their algal photobionts (*Breviolum psygmophilum*) to disentangle the independent responses of hosts and symbionts to divergent thermal challenges across different symbiotic states. In contrast to our prediction that symbiosis would alter the response of corals to thermal challenge, we found that both heat and cold challenges elicited general ESRs (type A; Dixon, Abbott, and Matz 2020) regardless of symbiotic state. Additionally, both symbiotic and aposymbiotic hosts exhibited greater gene expression plasticity in response to cold challenge compared to heat challenge. This strong response to cold challenge aligns with previous work on the facultatively symbiotic coral, *Astrangia poculata,* when exposed to similar temperature challenges (Wuitchik et al. 2021). Wuitchik et al. (2021) found that aposymbiotic *A. poculata* exposed to cold challenge (6°C) exhibited five times as many DEGs compared to heat challenge (31°C), which corroborates our higher gene expression plasticity and higher number of differentially expressed orthologs observed in corals under cold challenge. Wuitchik et al. (2021) also found that cold challenge elicited a more severe ESR response (type A; Dixon, Abbott, and Matz 2020) while heat challenge elicited a type B response, which contrasts our results where both heat and cold challenge elicited type A responses across both symbiotic states. This suggests that, even though *O. arbuscula* exhibited higher

gene expression plasticity under cold challenge, corals in both temperature challenges were exhibiting stress responses consistent with a tropical coral's ESR.

It is possible that the more consistently severe response in *O. arbuscula* compared to *A. poculata* is due to species differences in thermal breadths, which is consistent with the climate variability hypothesis. The climate variability hypothesis proposes that the greater climatic variability associated with increased latitude selects for organisms with wider thermal tolerances (*i.e.,* greater thermal breadth as you move away from the equator) (Chan et al. 2016; Spicer and Gaston 1999). While *A. poculata's* range extends from the Gulf of Mexico north to Cape Cod, *O. arbuscula* has a restricted, subtropical range only extending to North Carolina (Thornhill et al. 2008). As Wuitchik et al. (2021) studied *A. poculata* collected from its northern range edge in Woods Hole, MA, and *O. arbuscula* were collected from NC, it is possible that *A. poculata* has a wider thermal breadth and was therefore less negatively affected by similar temperature challenges.

The type A response presented in Dixon et al. (2020) is characterized by functional enrichment of processes that characterize the coral ESR, including downregulation of cell division and upregulation of cell death, response to ROS, protein degradation, NF-κB signaling, immune response, and protein folding. Specifically, every type A dataset in the tropical coral *Acropora* showcased upregulation of ROS and protein folding (Dixon, Abbott, and Matz 2020). This informed our hypothesis that temperature challenge would result in an ESR-like response, akin to a type A response, in symbiotic *O. arbuscula* but not in aposymbiotic individuals. Instead, we observed that both symbiotic and aposymbiotic *O. arbuscula* exhibited type A responses under heat and cold challenge,

although the strength of this relationship was weaker under cold challenge. This pattern could be the result of small numbers of background symbionts in aposymbiotic corals (as previously observed in aposymbiotic *Astrangia poculata*; Dimond and Carrington 2008) producing ROS and resulting in the observed type A response. Alternatively, it is possible that aposymbiotic corals were light-stressed as aposymbiotic individuals lack shading from symbionts (*e.g.,* Scheufen, Iglesias-Prieto, and Enríquez 2017). Additionally, the temperature challenges applied here were relatively short (15 days), and it is possible that symbiotic and aposymbiotic *O. arbuscula* would have exhibited differential responses if the challenges had been more extreme or lasted longer (McLachlan et al. 2020). In general, facultatively symbiotic corals are understudied, and future work should explore the responses of symbiotic and aposymbiotic corals under different stressors (*i.e.,* light, nutrients) and for longer time course experiments (as in Aichelman et al. 2021).

### *4.5.2. Evidence of host buffering in O. arbuscula holobionts*

Here, we present three forms of evidence suggesting that *O. arbuscula* hosts are buffering their algal photobionts under thermal extremes: 1. The coral host exhibited greater differential ortholog expression than its photobiont under cold challenge, 2. Stress-related genes were differentially expressed in photobionts *ex hospite* but not *in hospite*, and 3. *Ex hospite* photobionts exhibited higher gene expression plasticity in response to temperature challenges than *in hospite* photobionts. The higher magnitude of differential expression in coral hosts compared to photobionts in symbiosis aligns with previous evidence suggesting that cnidarian hosts and their algal photobionts exhibit strong differences in the magnitude of gene expression responses under environmental challenges.

For example, Davies et al. (2018) reported that when the tropical coral *Siderastrea siderea* was exposed to a 95-day temperature and acidification challenge, coral hosts consistently exhibited greater differential expression of highly conserved genes compared to their photobiont *Cladocopium goreaui.* Barshis et al. (2014) also found no changes in gene expression in either heat-susceptible *Cladocopium* (type C3K) or heat-tolerant *Durusdinium* (type D2) in symbiosis with *Acropora hyacinthus* following three days of high temperature exposure, which contrasted strong gene expression responses in the coral host (Barshis et al. 2013). Consistent with these patterns, Leggat et al. (2011) also observed that Symbiodiniaceae algae (*Cladocopium* C3) exhibited little change in expression of six stress and metabolic genes compared to their hosts (*Acropora aspera*).

In addition to differences between symbiotic partners while in symbiosis, symbiosis itself has been observed to alter gene expression patterns and physiology in Symbiodiniaceae algae. Here, we observed differential regulation of stress-related GO categories under cold challenge *ex hospite*, and within those GO categories included up-regulation of a heat shock protein (heat shock protein STI1) and a ubiquitin-related gene (RING-type E3 ubiquitin-protein ligase PPIL2). These genes are both classic signatures of the tropical coral ESR (Dixon, Abbott, and Matz 2020) and their differential regulation highlights the potential benefits of a symbiotic lifestyle for Symbiodiniaceae. Examples of symbiosis mitigating Symbiodiniaceae stress responses have been previously characterized using gene expression studies. For example, gene expression of *ex hospite Durusdinium trenchii* maintained at 28°C exhibited enrichment for the GO term "response to temperature stimulus" relative to *in hospite D. trenchii* in *Exaiptasia pallida,* which was attributed to

the protective microenvironment of the symbiosome (Bellantuono et al. 2019). Additionally, Maor-Landaw et al. (2020) compared gene expression of *Breviolum minutum* in culture to *B. minutum* freshly isolated from *Exaiptasia diaphana* and observed a signature of down-regulation of genes indicative of the protected and stress-reduced environment of the symbiosome. Specifically, pentatricopeptide repeats (PPR), which have been previously associated with Symbiodiniaceae RNA processing in response to environmental stress and were included in the repertoire of "stress responsive genes" in *Fugacium kawagutii* (S. Lin, Yu, and Zhang 2019), were down-regulated in freshly isolated *B. minutum* (Maor-Landaw, van Oppen, and McFadden 2020). These findings support our third piece of evidence for host buffering, which is the higher magnitude of gene expression responses (*i.e.,* gene expression plasticity) in *ex hospite* photobionts compared to *in hospite.* This suggests that *in hospite* photobionts responded less at the level of gene expression to cope with temperature challenges compared to *ex hospite* photobionts. Taken together, our results provide further evidence that cnidarian hosts exert control over the symbiont's micro-environment under environmental stress. However, one important caveat to the work presented here is that the lower depth of coverage of *in hospite B. psygmophilum* sequencing data could have limited our ability to detect differential expression of stress-related genes. Therefore, future work should implement RNA extraction methods that prioritize obtaining and sequencing equal amounts of genetic material of both host and photobiont.

### *4.5.3. Cold challenge elicited negative effects on photosynthesis of* ex hospite *and* in hospite Breviolum psygmophilum

Although responses of *B. psygmophilum in hospite* were muted (*i.e.,* fewer differentially expressed genes and orthologs) under temperature challenges compared to its response *ex hospite,* we still observed negative effects on photosynthesis at the level of phenotype (*in hospite* Fv/Fm) and gene expression (both *in hospite* and *ex hospite*), particularly under cold challenge. *Ex hospite B. psygmophilum* exhibited differential expression of numerous genes related to photosynthesis and stress, including down-regulation of genes related to the light harvesting complex (LHC) under cold challenge. This aligns with previous work investigating how symbiosis affects Symbiodiniaceae photosynthesis. For example, Bellantuono et al. (2019) found that photosynthetic processes were modified in *D. trenchii* living *in hospite* compared to *ex hospite.* Specifically, GO terms related to photosynthesis (*i.e.*, photosynthesis, photosystem II repair, and light harvesting) were positively enriched *in hospite* compared to *ex hospite*, which the authors proposed may be the result of coral host carbon concentrating mechanisms increasing the availability of $CO_2$ *in hospite*. In addition to overall down-regulation of genes related to the LHC under cold challenge *in hospite*, we observed reduced Fv/Fm of *in hospite B. psygmophilum*. This physiological effect of cold challenge aligns with previous work demonstrating reduced Fv/Fm in cultured *B. psygmophilum* exposed to simulated seasonal temperature declines (cooled from 26°C to 10°C and maintained for two weeks before returning to 26°C) (Thornhill et al. 2008). In that study, *B. psygmophilum* Fv/Fm recovered to pre-challenge values once temperatures were returned to control conditions (26°C),

while other Symbiodiniaceae species that typically associate with tropical coral species failed to regain Fv/Fm following cold challenge (Thornhill et al. 2008). This difference was attributed to *B. psygmophilum's* symbiosis with corals in temperate/subtropical areas where they experience exposure to large annual temperature variation, aligning with a recent report of its wide thermal breadth (16.15°C) compared to six other Symbiodiniaceae isolates (Dilernia et al. 2023). Therefore, Fv/Fm declines and down-regulation of genes related to photosynthesis could be representative of seasonal responses of *B. psygmophilum* to low temperatures, and if the cultures were returned to control condition, they may have recovered.

While we observed strong phenotypic and gene expression responses of *B. psygmophilum* under cold challenge but not heat challenge, links between photosynthetic disruption and transcriptional regulation of photosynthetic machinery found here align with previous work of Symbiodiniaceae under heat stress. This includes evidence that heat stress can inhibit the synthesis and resulting mRNA pool of an antenna protein of the light harvesting complex (acpPC) in Symbiodiniaceae (Takahashi et al. 2008). Additionally, temperature anomalies have been shown to alter thylakoid membrane fluidity, resulting in a decoupling of light harvesting and photochemistry, thereby suppressing NADPH and ATP synthesis, resulting in increased reactive oxygen species (ROS) in Symbiodiniaceae (Tchernov et al. 2004). In addition to transferring absorbed light energy to the photosynthetic reaction center, LHCs play an important role in photoprotection and have been linked to thermal sensitivity in Symbiodiniaceae (Takahashi et al. 2008). It has been proposed that decreasing the number of peripheral LHCs may serve as a photoprotective

mechanism under heat stress, as it ultimately decreases the light reaching photosynthetic reaction centers and reduces the risk of damage to D1 reaction center proteins (Hill and Ralph 2006). It is possible that the down-regulation of LHC-related genes observed here may be representative of a photoprotective mechanism in *B. psygmophilum* under any thermal stress. While we were unable to find published work investigating the effects of cold challenge on Symbiodiniaceae gene expression, there is evidence that cold challenge induces similar photophysiology responses as heat challenge in Symbiodiniaceae (*e.g.,* Marangoni, Rottier, and Ferrier-Pagès 2021; Saxby, Dennison, and Hoegh-Guldberg 2003; Kemp et al. 2011; Thornhill et al. 2008; Roth, Goericke, and Deheyn 2012). It is therefore possible that the heat challenge here was not extreme enough or long enough to elicit a similarly negative response as cold challenge. Indeed, Fv/Fm of *in hospite B. psygmophilum* under heat challenge was declining, but still significantly higher than cold challenge at the end of the experiment. This aligns with the findings of Roth et al. (2012), where cold challenge was more immediately harmful for *Acropora yongei* symbiosis, but heat stress was more harmful in the long term. Although *ex hospite B. psygmophilum* Fv/Fm was not quantified here, the differential regulation of many photosynthesis and stress-related genes discussed above suggests an even more negative impact of cold stress on photosynthesis *ex hospite.* Altogether, future work would benefit from longer and more extreme temperature challenges to ensure that the entire thermal performance curve is investigated. Lastly, future studies quantifying additional phenotypes in both *in* and *ex hospite B. psygmophilum* to determine if such a convergent response to temperature challenge exists are warranted.

### *4.5.4. Alternative hypotheses for "host buffering"*

It is important to acknowledge that transcriptional regulation is just one component of the molecular processes involved in responding to thermal stress. Mounting evidence suggests that a lack of differentially expressed genes under environmental challenges could be the result of post-transcriptional and/or post-translational mechanisms in Symbiodiniaceae. This includes evidence of microRNA (miRNA)-based gene regulatory mechanisms in Symbiodiniaceae (S. Lin et al. 2015; Baumgarten et al. 2013), which aligns with the genomic evidence that dinoflagellates may be more capable of translational rather than transcriptional regulation (S. Lin 2011). Additionally, a study of *Symbiodinium microadriaticum* highlighted that an apparent lack of common transcription factors and few differentially expressed genes could be attributed to small RNA (smRNA) post-transcriptional gene regulatory mechanisms (Baumgarten et al. 2013). It has also been proposed that the lack of transcriptional differences in Symbiodiniaceae could be due to gene duplication as a mechanism to increase transcript and protein levels of genes (Aranda et al. 2016). It is therefore possible that the lack of *in hospite* photobiont response to thermal challenges found here is not evidence of 'host buffering', but instead important post-transcriptional or post-translational regulation is occurring in Symbiodiniaceae and these processes were not quantified here. Another unique aspect of Symbiodiniaceae genomes is *trans*-splicing of spliced leader sequences, which converts polycistronic mRNAs (code for multiple proteins) into monocistronic mRNAs (code for one protein) and potentially regulates gene expression (Bayer et al. 2012; H. Zhang et al. 2007). TagSeq cannot account for splice variation (Meyer, Aglyamova, and Matz 2011), preventing us from considering

splice variant differences. Finally, comparing algae in culture to algae in symbiosis inherently includes a confounding variable of nutritional status, as algae in culture exist in nutrient replete conditions (Maruyama and Weis 2021). For future studies, including nutrient controls (*ex hospite* Symbiodiniaceae in nutrient-depleted media) would be useful to incorporate, in addition to leveraging proteomic and gene expression profiling in parallel (*e.g.,* Camp et al. 2022).

### *4.5.5. Implications of the current study*

The experiments presented here support a scenario in which coral hosts modulate the environment of *in hospite* Symbiodiniaceae algae to buffer their responses to temperature challenges. While understanding the response of subtropical corals to thermal extremes is valuable in its own right, the facultative symbiosis, calcifying nature, and available genomic resources of *O. arbuscula* make it a unique model for linking these results back to tropical coral responses as climate change progresses (Rivera and Davies 2021). If coral hosts are able to regulate the environments of their photobionts, and this regulation in turn can serve to limit stress in the holobiont and ultimately reduce coral bleaching, then this phenotype can be used to identify coral-algal pairings that will be more or less resilient under future global change conditions.

## 4.6. Acknowledgements

We would like to thank Steve Broadhurst for assistance collecting *Oculina arbuscula* colonies from Radio Island, North Carolina and Dr. Joel Fodrie for assistance with collection permits. The symbiont shapes used in figures were created by Giulia Puntin and modified for use (https://github.com/sPuntinG/Coral_stuff). Thank you to Carlos Tramonte for the *Oculina arbuscula* photos used in figures.

## 4.7. Data Availability

All raw data and code associated with analyses presented in Chapter 4 are maintained in a Github repository at the following link: https://github.com/wuitchik/MPCC_2018.

# CHAPTER FIVE: CONCLUSIONS

Since the first documentation of mass coral bleaching events in the literature (Glynn 1984), studies of the causes and consequences of this phenomena have expanded dramatically (Sully et al. 2019). Research efforts have spanned many levels of inquiry, ranging from broad-scale ecosystem influences of mass coral bleaching events (*e.g.,* Stuart-Smith et al. 2018) down to research that requires microsensors to consider the effects of heat stress at the cellular scale (*e.g.,* Wangpraseurt et al. 2017). Despite this vast body of important work, there remains many outstanding questions surrounding what makes a coral resistant or resilient in the face of anthropogenic climate change stressors, including temperature extremes and ocean acidification. Specifically, our understanding of how interactions between diverse members of the coral holobiont drive responses and how these interactions depend upon variability in the abiotic environment across space and time remain unclear. Answering these questions is of critical importance, as climate change continues to threaten the health and functioning of coral reef ecosystems, which in turn threatens the communities that depend upon the resources that these reefs provide (T. D. Eddy et al. 2021).

The aim of this dissertation was to use an integrative approach to address how the role of stress duration, species diversity, reef-scale spatiotemporal variation, and symbiosis influence a coral's response to stress. Broadly, I found species differences in responses to climate change stressors, which were modulated by duration of the exposure as well as thermal history of the corals' natal reef (Chapter 2). In addition to these broad species-level differences found in Chapter 2, Chapter 3 highlighted the importance of cryptic host

diversity, and specifically how unique holobiont pairings (*i.e.,* combination of cryptic host lineage, algal symbiont species, and microbiome) drive physiology and stress responses. Lastly, I took a more mechanistic approach to understanding the independent responses of the coral host and its symbiotic algae by characterizing how these partners responded to temperature challenges in and out of symbiosis, and I found evidence of host modulation of the symbiont's environment (Chapter 4).

The research presented in this dissertation highlights the need for follow-up studies that would clarify the broad-scale applicability of the findings presented here. Specifically, the work described in Chapter 2 would have benefitted from measuring the broad sense heritability ($H_2$) of the coral responses to temperature and ocean acidification stress (following Singh, Ceccarelli, and Hamblin 1993). Measurements of heritability would allow for the estimation of the evolutionary potential and adaptive capacity of coral populations, which would greatly aid in effective management strategies (*e.g.,* Jury, Delano, and Toonen 2019). Future studies incorporating estimates of heritability–either broad sense or narrow sense–into characterizing species-specific responses to climate change stressors are warranted and will be required before effective management plans for coral populations can be implemented.

The experimental design of Chapter 3 left me unable to determine whether the three cryptic lineages of *S. siderea* distributed across the Bocas del Toro archipelago were locally adapted to the distinct environments in which they were sampled. If future work conducted a reciprocal transplant experiment between cryptic lineages across the inshore and offshore environments they inhabit, this would allow us to distinguish whether these lineages are

locally adapted, and would more directly link environmental selection to the lineage distributions (Kawecki and Ebert 2004). Additionally, a deeper understanding of thermal performance curves (TPCs) of *S. siderea* cryptic lineages would place the differences in lineage thermal tolerance observed in Chapter 3 in the context of the coral's thermal limits. If TPCs were coupled with a reciprocal transplant experiment, we would also uncover whether cryptic lineages have the capacity for plasticity in thermal limits following transplantation, which would provide additional context for the roles of adaptation and acclimation in these cryptic lineages and ultimately improve understanding of their ability to persist under future climate change conditions. If evidence of local adaptation of the cryptic lineages is found in future work, whole genome sequencing to uncover the loci driving adaptation to the distinct inshore and offshore environments would be informative, and would have broad-scale applications in identifying the molecular underpinnings that shape coral resilience.

Lastly, the experiments presented in Chapter 4 are confounded by the distinct nutrient environments of photobionts *in hospite* vs. *ex hospite* (Maruyama and Weis 2021), and future work would benefit from including additional nutrient controls to confirm the observed host buffering pattern. Additionally, the global gene expression method leveraged in Chapter 4 ignores the role of post-transcriptional processes in driving response to temperature challenge, which are thought to be prevalent in Symbiodiniaceae (*e.g.,* Baumgarten et al. 2013). Future work integrating proteomics and RNA sequencing to better characterize the role of post-transcriptional and post-translational modifications of Symbiodiniaceae both *in hospite* and *ex hospite* is warranted. Additionally, incorporating

other coral species in these experiments or corals from different locations will determine if the observed 'host buffering' pattern is conserved between species or varies between populations.

The findings of this dissertation improve our understanding of the phenotypic and genotypic characteristics that enable corals to persist under challenging environmental conditions. For example, I found that some species (*Siderastrea siderea*) are more resistant to temperature and acidification stressors than others (*Pseudodiploria strigosa*), and that local adaptation to more stressful environments can modulate within-species responses (Chapter 2). Additionally, I uncovered that specific cryptic host lineage and algal symbiont species pairings are particularly resistant to heat challenge (Chapter 3). These findings have relevant implications to conservation, and protecting these more tolerant lineages are likely to improve reef restoration outcomes under warming oceans. Additionally, uncovering the host's ability to modulate the environment of its symbiont (Chapter 4) opens up a new avenue of inquiry, and understanding whether certain coral hosts are better at protecting their symbionts from environmental stress could have additional implications in identifying corals that are better prepared to withstand future stressful conditions.

# APPENDIX 1: CHAPTER 2 SUPPLEMENT

## A1.1. Supplementary materials and methods

### *A1.1.1. Coral collection and experimental design*

All coral colonies were collected from the Belize Mesoamerican Barrier Reef System (MBRS) in June 2015, and totaled *n*=3/species/site (3 colonies x 2 reef zones x 2 species = 12 putative genotypes). The nearshore (NS) site was Port Honduras Marine Reserve (PHMR; 16°11'23.5314"N, 88°34'21.9360"W) and the forereef (FR) site was Sapodilla Cayes Marine Reserve (SCMR; 16°07'00.0114"N, 88°15'41.1834"W). Colonies were separated by at least 5 m to maximize the likelihood of obtaining genetically distinct individuals.

Following fragmentation at Northeastern University, corals recovered for 23 days in natural flow-through seawater from Massachusetts Bay with salinity and temperature (±SD) of 30.7±0.8 and 28.2±0.5°C, respectively. Following this, temperatures of the elevated temperature treatments were increased by 0.4°C every 3 days and $pCO_2$ was adjusted by 0 μatm (present day), +30 μatm (end of century), and +240 μatm (extreme) every 3 days to achieve target treatment conditions.

Coral fragments were maintained in treatment conditions for a total of 95 days (9 August 2015 – 12 November 2015). Fragments were frozen approximately every 30 days, but actual number of days from the start of the experiment to sampling were 36 ($T_0$ to $T_{30}$), 63 ($T_0$ to $T_{60}$), and 92 ($T_0$ to $T_{95}$). Temperatures were maintained via 50W glass aquarium heaters within each tank and a 75W heater in each sump. Desired $pCO_2$ levels were achieved using high-precision digital solenoid-valve mass flow controllers (Aalborg

Instruments and Controls; Orangeburg, NY, USA) to bubble gas into each tank and sump with either air alone (present day $pCO_2$, 31°C), air in combination with $CO_2$-free air (present day $pCO_2$, 28°C) or air with $CO_2$ gas (end of century and extreme $pCO_2$ treatments at both 28 and 31°C). Experimental gas mixtures were measured using Qubit S151 (range 0-2000 µatm; accuracy ± 1 µatm) and S153 (range 0-10%; accuracy ± 0.3%) infrared $pCO_2$ analyzers (Qubit Systems; Kingston, Ontario, Canada) calibrated with certified air-$CO_2$ gas standards. Temperatures were measured using a partial-immersion glass thermometer (precision ±0.3%; accuracy ±0.4%), salinity was measured with a YSI 3200 conductivity meter (10.0 $cm^{-2}$ cell; Yellow Spring, Ohio, USA), and pH was measured with an AccuFet Solid-State pH probe (Fisher Scientific; Waltham, Massachusetts, USA) calibrated with 4.01, 7.00, and 10.01 NBS buffers maintained at experimental temperatures. In the event of mortality that yielded insufficient coral fragments for sampling at all time points, corals were preferentially sampled at the end of the experiment (long-term exposure: $T_{95}$) instead of after moderate-term exposure ($T_{60}$). Sample sizes are therefore lower for both species at $T_{60}$ compared to the other time points.

### *A1.1.2. Coral host and symbiont physiology*

The buoyant weight and dry weight measurements were correlated for both species (*S. siderea* $R^2$=0.90, $p$<0.001; *P. strigosa* $R^2$=0.81, $p$<0.001), indicating that change in buoyant weight should reflect a proportionate change in dry weight. Fragments of *S. siderea* ($n$=69) and *P. strigosa* ($n$=97) from both this study and Bove et al. (2019) were used to establish this relationship. Equations used to calculate dry weight from buoyant weight are shown below. Dry weight was converted from g to mg, corrected to surface area

of each fragment and to number of days in experimental treatment to calculate calcification rate (mg $cm^{-2}$ $day^{-1}$).

*S. siderea*: Dry weight (g) = 1.95 × BW (g) + 3.60, $R^2$ = 0.90

*P. strigosa*: Dry weight (g) = 1.63 × BW (g) + 6.96, $R^2$ = 0.81

For the total coral host protein content bicinchoninic acid (BCA) protein assay, host tissue slurry was vortexed with glass beads for 15 minutes and then centrifuged for 3 minutes at 4000 RPM. Next, 15 µL of the centrifuged sample was added to 235 µL artificial seawater along with 250 µL of Bradford reagent. After samples were mixed, absorbance was measured in a BioSpectrometer (Eppendorf, Hauppauge, NY, USA) at 562 nm. Coral protein concentrations were calculated using a standard curve of bovine serum albumin ranging from 0 to 1000 µg $mL^{-1}$ and normalized to living coral surface area.

For the total coral host carbohydrates phenol-sulfuric acid method (following Masuko et al. 2005), an aliquot of coral host tissue was diluted to 50 µL with artificial seawater (Instant Ocean Sea Salt), to which 150 µL of sulfuric acid and 30 µL of 5% phenol were added. Following a 5-minute incubation at 90°C and another 5-minute incubation at room temperature, absorbance at 490 nm was measured in a spectrophotometer (Synergy H1 Microplate Reader; BioTek Instruments; VT, USA). Carbohydrate concentrations were calculated using a standard curve of D-glucose solutions ranging from 0.039 to 2 mg $mL^{-1}$ and normalized to living coral surface area.

For the symbiont density hemocytometer count method (following Rodrigues and Grottoli 2007), after vortexing the symbiont pellet, a 1:1 Lugol's iodine and formalin solution was added for contrast and cell preservation. Triplicate 10 µL subsamples were

counted on a hemocytometer using a light microscope, averaged, and normalized to slurry volume and live coral tissue surface area.

For the chlorophyll *a* pigment density method (following Marchetti et al. 2012), 40 mL of 90% acetone was added to the symbiont pellet, homogenized, then stored in the dark for 24 hours. 100 µL of each sample was then diluted in 7.9 mL of 90% acetone. A 10AU Field and Laboratory Fluorometer (Turner Designs, San Jose, CA) was used to measure the initial concentration ($R_b$), then 2 drops of 10% HCl was added to the sample tube, after which a second fluorometer reading was taken ($R_a$). Total Chl *a* content (µg $L^{-1}$) was calculated using the equation below, where 0.548 is a calibration constant specific to the fluorometer used, 40 mL is the volume of acetone left overnight, and 80 is the dilution factor. Total Chl *a* was then normalized to live coral surface area to get units of µg Chl *a* $cm^{-2}$.

$$\text{Chl } a \left(\mu g\ L^{-1}\right) = 0.548 \times (R_b - R_a) \times 40\ mL \times 80$$

### *A1.1.3. Statistical analyses*

For individual physiology parameter linear mixed effects models (except *S. siderea* calcification), the best fit model was derived by starting with the intercept-only model and then using forward-selection to incorporate additional parameters, starting with the most significant parameter, until further addition of parameters did not significantly improve the model fit. Additional parameters were retained in the model if they were significant ($p<0.05$) and produced smaller AIC values (Akaike 1974). Parameter interactions were only considered if those two parameters were already significant and included in the model. For net calcification rate data, multiple fragments of each genotype were represented at

each time point. Because genotype is included in the model as a random effect, multiple fragment numbers do not artificially increase the sample size and instead only increase the precision of the rate measurement for that colony.

Because *S. siderea* calcification data did not meet assumptions of normality even with transformation, a generalized additive model for location scale and shape with a Weibull distribution was implemented (*gamlss*; Rigby and Stasinopoulos 2005). Calcification data were transformed by adding 1.5 to each value so that all rates were positive for model fitting. The *descdist* function (package *fitdistrplus,* version 1.1-3) was used to identify appropriate distributions for the data and the Weibull distribution was selected based on AIC (*fitdist*). The best fit model structure was then determined using forward-selection (*stepGAIC*), with the full model defined as the interactions of temperature, $pCO_2$, time, and reef zone, with a random effect of genotype.

For the Principal Components Analysis (PCA), all physiology parameters were log-transformed, and calcification rates were x+2 log-transformed. Only individual coral fragments for which all physiology parameters were present were included in this analysis, which was run with 10,000 permutations using the model below.

Adonis(scores ~ reef zone * $pCO_2$ * temperature + genotype)

## A1.2. Supplementary Results

### *A1.2.1. Experimental treatments*

At all timepoints, cumulative temperatures were significantly different between all 28 °C and 31 °C treatments ($p<0.05$, Figure A1-1, Table A1-7). At $T_0$, $pCO_2$ conditions were not significantly different between the end of century $pCO_2$, 31 °C and present day

$pCO_2$, 31 °C treatments ($p$=0.99) or between end of century $pCO_2$, 31 °C and present day $pCO_2$, 28 °C treatments ($p$=0.97; Figure A1-2, Table A1-7). This lack of difference in $pCO_2$ at $T_0$, in addition to limited sampling of water quality between $T_0$ and $T_{30}$, drove a lack of significant difference between the same treatments at $T_{30}$, despite these treatments being distinct when considering only $T_{30}$ data (all $p$<0.05). Additionally, $pCO_2$ at the remaining time points was significantly different between treatment levels, as was cumulative $pCO_2$ over the 95-day experiment duration (Figure A1-2, Table A1-7).

### *A1.2.2. Combined species holobiont physiology*

*Siderastrea siderea* and *P. strigosa* had distinct holobiont physiologies at all experimental durations (Adonis $p_{species}$<0.001 for short-term [$T_{30}$], moderate-term [$T_{60}$], and long-term [$T_{95}$]; Figure A1-3; Table A1-5). Although species had a significant main effect on combined physiology through time, *S. siderea* and *P. strigosa* exhibit the most divergent physiologies at $T_{30}$, and then converge to be entirely overlapping at $T_{60}$ and $T_{95}$ (Figure A1-3). There were also significant independent effects of temperature and $pCO_2$ on the combined physiology for both species at each time point (Adonis $p$<0.05 for all time points; Figure A1-3, Table A1-5).

## A1.3. Supplementary Figures

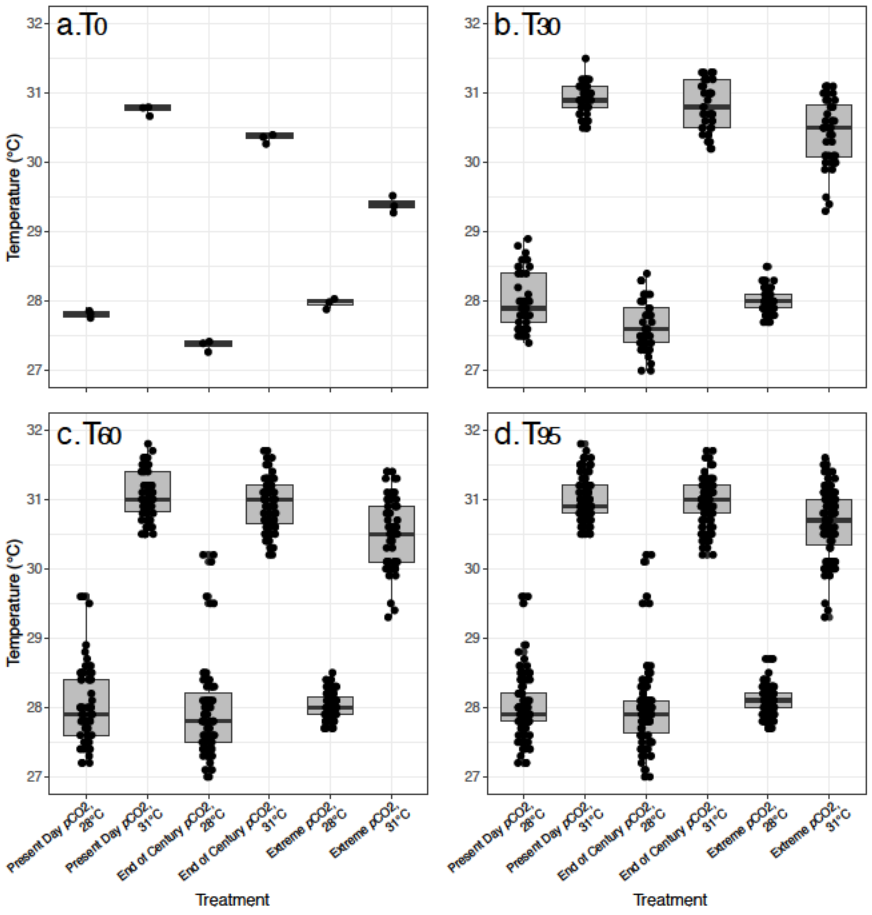


**Figure A1-1.**
Temperature measured cumulatively throughout the experiment. (**a**) $T_0$ ($n$=3/treatment); (**b**) $T_{30}$=short-term exposure, including $T_0$-$T_{30}$ measurements ($n$=40/treatment); (**c**) $T_{60}$=moderate-term exposure, including $T_0$-$T_{60}$ measurements ($n$=67/treatment); (**d**) $T_{95}$=long-term exposure, including all measurements ($n$=106/treatment). Within $pCO_2$ treatment and time point, all temperature treatments are significantly different ($p$<0.05)

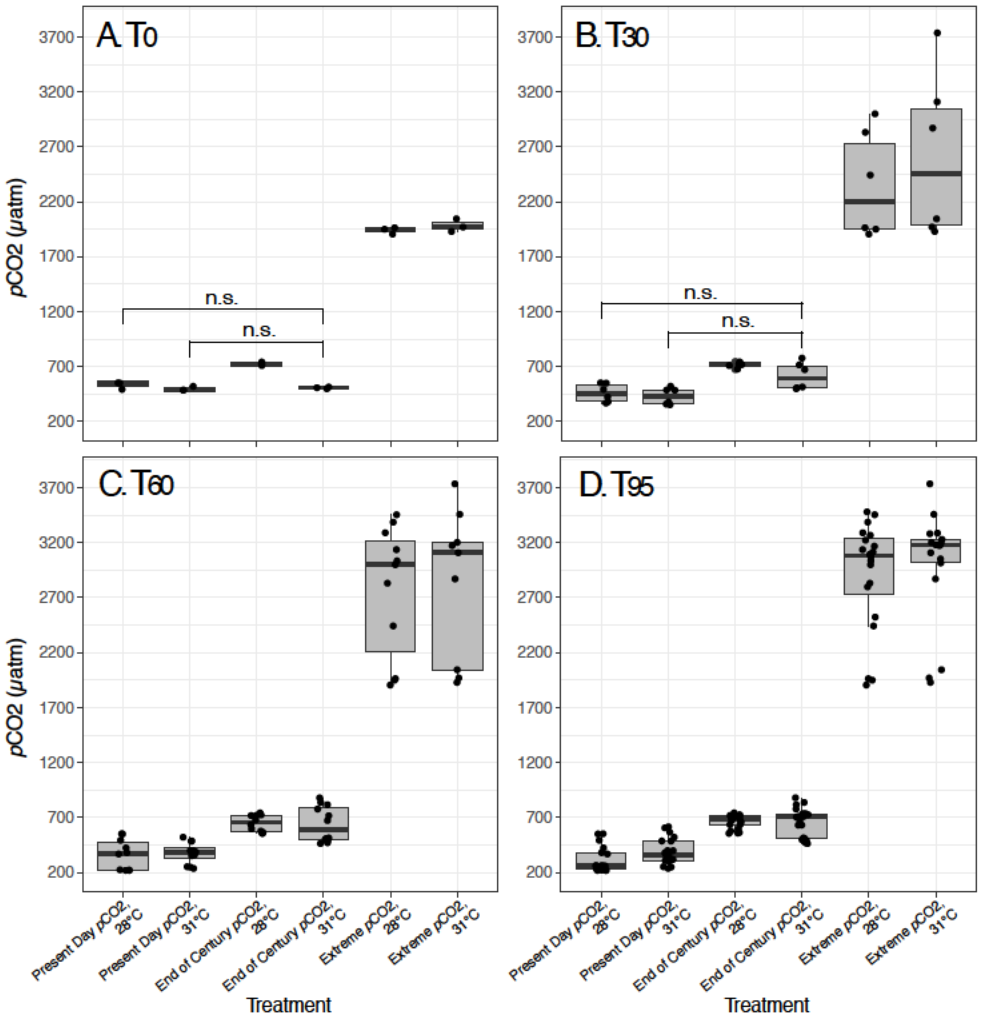


**Figure A1-2.**
Partial pressure of carbon dioxide ($pCO_2$) measured cumulatively throughout the experiment. (**a**) $T_0$ ($n$=3/treatment); (**b**) $T_{30}$=short-term exposure ($n$=6/treatment); (**c**) $T_{60}$=moderate-term exposure ($n$=12/treatment); (**d**) $T_{95}$=long-term exposure ($n$=21/treatment, except $n$=20 for present day $pCO_2$, 28°C). Brackets with "n.s." indicate a lack of significant difference in $pCO_2$ between treatment levels.

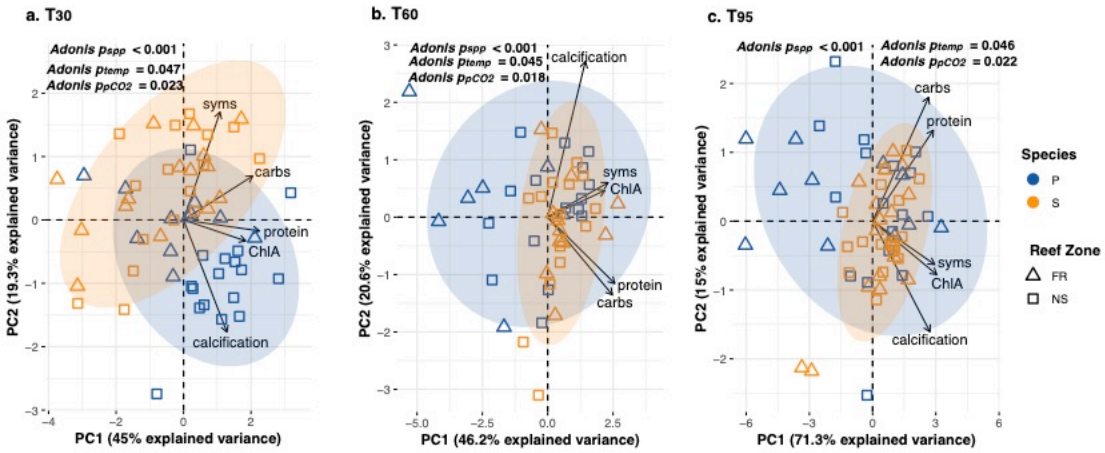


**Figure A1-3.**
Principal Components Analysis (PCA) of *Siderastrea siderea* and *Pseudodiploria strigosa* log-transformed physiology data, including carbohydrate (carbs; mg $cm^{-2}$), protein (protein; mg $cm^{-2}$), symbiont density (syms; cells $cm^{-2}$), chlorophyll *a* (ChlA; µg $cm^{-2}$), and calcification rate (mg $cm^{-2}$ $day^{-1}$). Colors represent species (*S. siderea*=S=orange, *P. strigosa*=P=blue) and shapes represent reef zone (triangle=forereef [FR], square=nearshore [NS]). Points represent an individual coral fragment's combined physiology after each experimental duration (**a**=short-term [$T_{30}$], **b**=moderate-term [$T_{60}$], **c**=long-term [$T_{95}$]). Individuals were only included if they had a measure for each of the five parameters at that time point. The x- and y-axes indicate the variance explained (%) by first and second principal components, respectively.

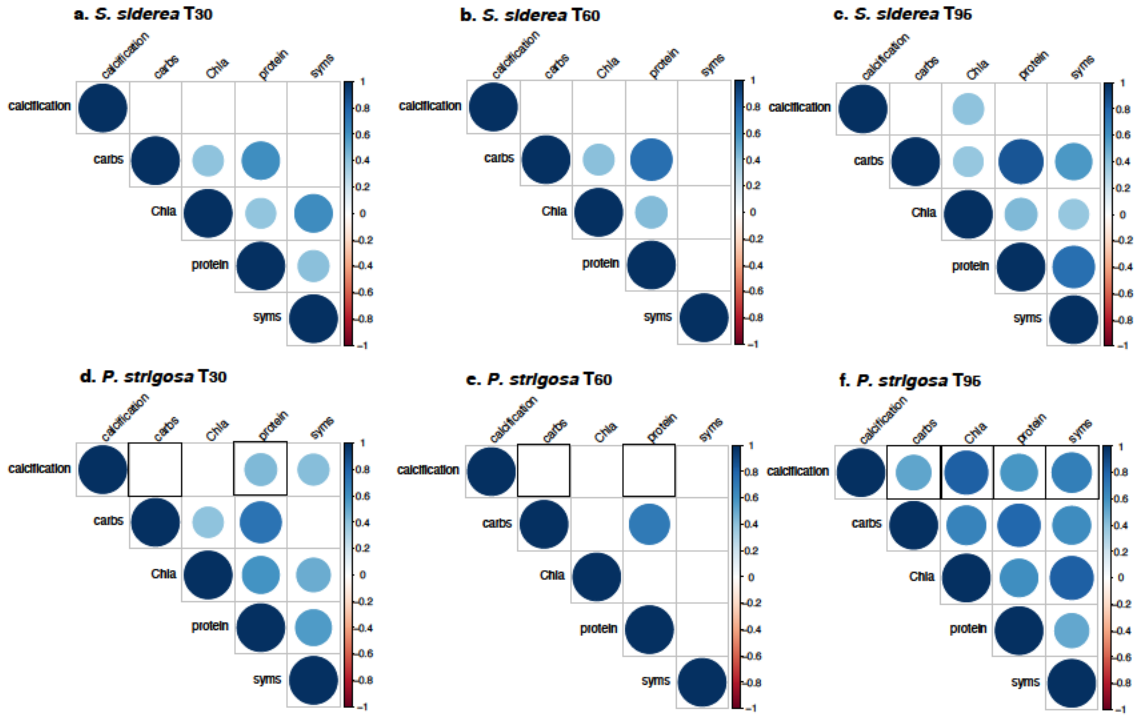


**Figure A1-4.**
Correlation matrices for *S. siderea* (**a-c**) and *P. strigosa* (**d-f**) host and symbiont physiology parameters, including carbohydrates (carbs; mg $cm^{-2}$), proteins (protein; mg $cm^{-2}$), symbiont density (syms; cells $cm^{-2}$), chlorophyll *a* (Chla; µg $cm^{-2}$), and calcification rate (mg $cm^{-2}$ $day^{-1}$) through time (**a,d**=short-term [$T_{30}$], **b,e**=moderate-term [$T_{60}$], **c,f**=long-term [$T_{95}$]). Positive correlations are represented by blue colors and negative correlations are represented by red colors. Circle color intensity and size are proportional to the correlation coefficients. Insignificant correlations ($p$>0.05) are blank. Black boxes indicate correlations that are specifically discussed further (Figures 2-6 and A1-5).

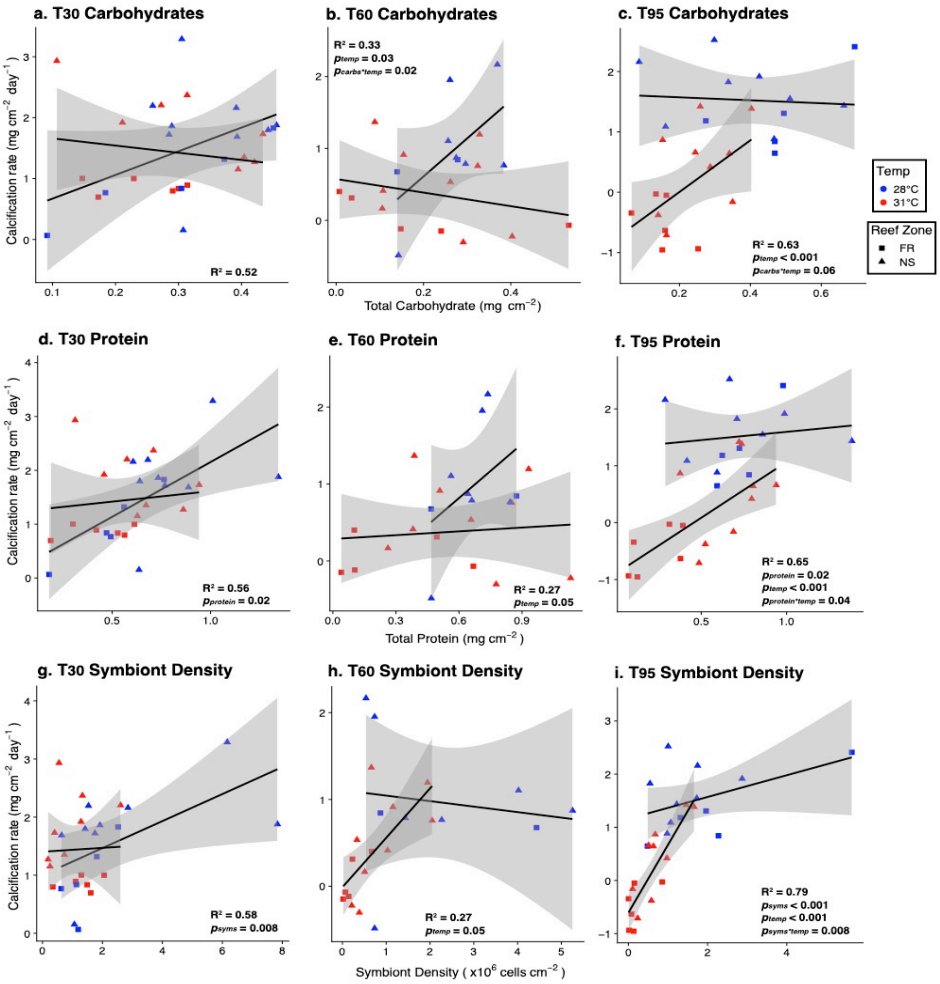


**Figure A1-5.**
Correlations of *Pseudodiploria strigosa* calcification with carbohydrates (**a-c**), proteins (**d-f**), and symbiont density (**g-i**). Points represent an individual coral fragment at each time point (**a,d,g**=short-term [$T_{30}$], **b,e,h**=moderate-term [$T_{60}$], **c,f,i**=long-term [$T_{95}$]). Colors represent temperature treatment (red=31°C, blue=28°C) and shapes represent reef zone (square=forereef [FR], triangle=nearshore [NS]). Significant factors are indicated within each panel. Lines represent linear fits between the physiology parameters by temperature (using ggplot2's *stat_smooth()* method) with gray shading representing 95% confidence intervals for each temperature. Conditional $R^2$ values are reported.

## A1.4. Supplementary Tables

**Table A1-1.**

**Measured water quality parameters.** Average cumulative measured parameters for all experimental treatments: salinity (Sal), temperature (Temp), measured pH ($pH_M$), total alkalinity (TA), and dissolved inorganic carbon (DIC). All values are displayed as average ± standard error, and cumulative sample sizes are indicated under each value. Note that the increase in TA throughout the experiment is a result of using natural seawater in the flow-through system and differences in seawater chemistry across seasons.

| Treatment | Duration | Temp (°C) | Sal (psu) | TA ($\mu$M) | $pH_{M\text{-}NBS}$ | DIC ($\mu$M) |
|---|---|---|---|---|---|---|
| Present Day $pCO_2$, 28°C | $T_0$ | 27.8 ±0.03 *(n=3)* | 32.1 ±0.0 *(n=3)* | 1889±0 *(n=3)* | 8.14±0.005 *(n=3)* | 1688±1 *(n=3)* |
| | $T_{30}$ | 28.0 ±0.07 (n=40) | 31.4 ±0.06 *(n=39)* | 1930 ±19 *(n=6)* | 8.20±0.018 *(n=44)* | 1692±4 *(n=6)* |
| | $T_{60}$ | 27.0 ±0.07 *(n=67)* | 31.4 ±0.03 *(n=66)* | 1969±16 *(n=12)* | 8.24±0.015 *(n=71)* | 1644±17 *(n=12)* |
| | $T_{95}$ | 28.0±0.04 *(n=106)* | 31.5 ±0.03 *(n=105)* | 2008±15 *(n=20)* | 8.27±0.012 *(n=110)* | 1660±11 *(n=20)* |
| Present Day $pCO_2$, 31°C | $T_0$ | 30.8 ±0.03 *(n=3)* | 32.4 ±0.09 *(n=3)* | 1880±0 *(n=3)* | 8.29±0.002 *(n=3)* | 1642±4 *(n=3)* |
| | $T_{30}$ | 30.9 ±0.04 *(n=40)* | 31.3 ±0.07 *(n=38)* | 1949±31 *(n=6)* | 8.19±0.022 *(n=44)* | 1670±13 *(n=6)* |
| | $T_{60}$ | 31.2 ±0.06 *(n=67)* | 31.4 ±0.04 *(n=65)* | 1998±21 *(n=12)* | 8.22±0.016 *(n=71)* | 1677±13 *(n=12)* |
| | $T_{95}$ | 31.1 ±0.04 *(n=106)* | 31.5 ±0.04 *(n=104)* | 2039±16 *(n=21)* | 8.21±0.012 *(n=110)* | 1716±16 *(n=21)* |
| End of Century $pCO_2$, 28°C | $T_0$ | 27.4±0.03 *(n=3)* | 31.8 ±0.04 *(n=3)* | 1874±0 *(n=3)* | 7.98±0.002 *(n=3)* | 1718±1 *(n=3)* |
| | $T_{30}$ | 27.7 ±0.06 *(n=40)* | 31.3 ±0.05 *(n=39)* | 1948±33 *(n=6)* | 7.91±0.030 *(n=44)* | 1783±29 *(n=6)* |
| | $T_{60}$ | 28.0±0.09 *(n=67)* | 31.3 ±0.03 *(n=66)* | 1999±22 *(n=12)* | 7.94±0.020 *(n=71)* | 1809±16 *(n=12)* |
| | $T_{95}$ | 28.0 ±0.02 *(n=106)* | 31.5 ±0.03 *(n=105)* | 2045±17 *(n=21)* | 7.95±0.0133 *(n=110)* | 1852±14 *(n=21)* |
| End of Century $pCO_2$, 31°C | $T_0$ | 30.4 ±0.03 *(n=3)* | 32.0 ±0.02 *(n=3)* | 1936±0 *(n=3)* | 8.21±0.004 *(n=3)* | 1695±1 *(n=3)* |
| | $T_{30}$ | 30.8 ±0.06 *(n=40)* | 31.2 ±0.06 *(n=36)* | 1982±21 *(n=6)* | 7.95±0.038 *(n=44)* | 1765±32 *(n=6)* |
| | $T_{60}$ | 30.9±0.05 *(n=67)* | 31.3 ±0.03 *(n=63)* | 2013±14 *(n=12)* | 7.96±0.025 *(n=71)* | 1795±22 *(n=12)* |
| | $T_{95}$ | 31.0 ±0.03 *(n=106)* | 31.5 ±0.03 *(n=102)* | 2042±11 *(n=21)* | 7.96±0.016 *(n=110)* | 1828±15 *(n=21)* |
| Extreme $pCO_2$, 28°C | $T_0$ | 28.0 ±0.03 *(n=3)* | 32.0 ±0.01 *(n=3)* | 1952±0 *(n=3)* | 7.63±0.002 *(n=3)* | 1915±1 *(n=3)* |
| | $T_{30}$ | 28.0±0.03 *(n=40)* | 31.2 ±0.13 *(n=39)* | 2020±31 *(n=6)* | 7.41±0.034 *(n=44)* | 2003±40 *(n=6)* |
| | $T_{60}$ | 28.0 ±0.02 *(n=67)* | 31.3 ±0.08 *(n=66)* | 2061±19 *(n=12)* | 7.34±0.024 *(n=71)* | 2069±28 *(n=12)* |
| | $T_{95}$ | 28.1 ±0.02 *(n=106)* | 31.5 ±0.06 *(n=105)* | 2092±13 *(n=21)* | 7.33±0.016 *(n=110)* | 2103±18 *(n=21)* |
| | $T_0$ | 29.4±0.06 | 32.3 ±0.01 | 1751±0 | 7.63±0.002 | 1719±2 |

| | | | | | | |
|---|---|---|---|---|---|---|
| Extreme $pCO_2$, 31°C | | *(n=3)* | *(n=3)* | *(n=3)* | *(n=3)* | *(n=3)* |
| | $T_{30}$ | 30.4 ±0.08 *(n=40)* | 31.3 ±0.1 *(n=38)* | 1915±73 *(n=6)* | 7.40±0.037 *(n=44)* | 1906±84 *(n=6)* |
| | $T_{60}$ | 30.6 ±0.09 *(n=67)* | 31.4 ±0.06 *(n=65)* | 2013±46 *(n=12)* | 7.32±0.026 *(n=71)* | 2027±55 *(n=12)* |
| | $T_{95}$ | 30.7 ±0.06 *(n=106)* | 31.5 ±0.04 *(n=104)* | 2062±29 *(n=21)* | 7.30±0.017 *(n=110)* | 2075±33 *(n=21)* |

**Table A1-2.**
**Calculated water quality parameters.** Average cumulative calculated parameters for all treatments: $pCO_2$ of the mixed gases in equilibrium with seawaters ($pCO_{2(gas\text{-}e)}$); calculated pH ($pH_c$); carbonate ion concentration ($[CO_3^{2-}]$); bicarbonate ion concentration ($[HCO_3^-]$); dissolved carbon dioxide ($[CO_2]_{(SW)}$), and aragonite saturation state ($\Omega_A$). All values are displayed as average ± standard error, and cumulative sample sizes are indicated under each value.

| Treatment | Duration | $pCO_{2(gas\text{-}e)}$ ($\mu$atm-v) | $pH_{c\text{-}NBS}$ | $[CO_3^{2-}]$ ($\mu$M) | $[HCO_3^-]$ ($\mu$M) | $[CO_2]_{(SW)}$ ($\mu$M) | $\Omega_A$ |
|---|---|---|---|---|---|---|---|
| Present Day $pCO_2$, 28°C | $T_0$ | 530±19 *(n=3)* | 8.03±0.01 *(n=3)* | 143±1 *(n=3)* | 1531±1 *(n=3)* | 14±0.2 *(n=3)* | 2.3±0.02 *(n=3)* |
| | $T_{30}$ | 460±34 *(n=6)* | 8.09±0.03 *(n=6)* | 169±12 *(n=6)* | 1511±10 *(n=6)* | 12±1 *(n=6)* | 2.8±0.2 *(n=6)* |
| | $T_{60}$ | 332±42 *(n=12)* | 8.24±0.05 *(n=12)* | 226±18 *(n=12)* | 1410±33 *(n=12)* | 9±1 *(n=12)* | 3.7±0.3 *(n=12)* |
| | $T_{95}$ | 298±27 *(n=20)* | 8.28±0.03 *(n=20)* | 242±12 *(n=20)* | 1409±19 *(n=21)* | 8±0.7 *(n=20)* | 4.0±0.2 *(n=20)* |
| Present Day $pCO_2$, 31°C | $T_0$ | 496±12 *(n=3)* | 8.06±0.008 *(n=3)* | 167±2 *(n=3)* | 1463±5 *(n=3)* | 12±0.3 *(n=3)* | 2.8±0.04 *(n=3)* |
| | $T_{30}$ | 429±31 *(n=6)* | 8.13±0.03 *(n=6)* | 196±13 *(n=6)* | 1463±4 *(n=6)* | 10±0.7 *(n=6)* | 3.3±0.2 *(n=6)* |
| | $T_{60}$ | 374±27 *(n=12)* | 8.19±0.03 *(n=12)* | 225±12 *(n=12)* | 1443±18 *(n=12)* | 9±0.6 *(n=12)* | 3.8±0.2 *(n=12)* |
| | $T_{95}$ | 388±25 *(n=21)* | 8.19±0.03 *(n=21)* | 228±9 *(n=21)* | 1479±20 *(n=21)* | 9±0.6 *(n=21)* | 3.8±0.1 *(n=21)* |
| End of Century $pCO_2$, 28°C | $T_0$ | 724±9 *(n=3)* | 7.92±0.005 *(n=3)* | 116±1 *(n=3)* | 1585±1.8 *(n=3)* | 19±0.2 *(n=3)* | 1.9±0.01 *(n=3)* |
| | $T_{30}$ | 714±9 *(n=6)* | 7.94±0.01 *(n=6)* | 125±4 *(n=6)* | 1640±25 *(n=6)* | 18±0.2 *(n=6)* | 2.0±0.06 *(n=6)* |
| | $T_{60}$ | 647±21 *(n=12)* | 7.99±0.02 *(n=12)* | 142±6 *(n=12)* | 1650±12 *(n=12)* | 17±0.6 *(n=12)* | 2.3±0.09 *(n=12)* |
| | $T_{95}$ | 663±13 *(n=21)* | 7.98±0.009 *(n=21)* | 145±3 *(n=21)* | 1690±13 *(n=21)* | 17±0.3 *(n=21)* | 2.4±0.05 *(n=21)* |
| End of Century $pCO_2$, 31°C | $T_0$ | 506±5 *(n=3)* | 8.06±0.003 *(n=3)* | 172±1 *(n=3)* | 1511±2 *(n=3)* | 12±0.1 *(n=3)* | 2.9±0.02 *(n=3)* |
| | $T_{30}$ | 613±50 *(n=6)* | 8.01±0.03 *(n=6)* | 158±6 *(n=6)* | 1592±37 *(n=6)* | 15±1 *(n=6)* | 2.7±0.1 *(n=6)* |
| | $T_{60}$ | 636±47 *(n=12)* | 8.01±0.03 *(n=12)* | 161±7 *(n=12)* | 1619±27 *(n=12)* | 15±0.2 *(n=12)* | 2.7±0.1 *(n=12)* |
| | $T_{95}$ | 662±28 *(n=21)* | 7.99±0.02 *(n=3)* | 159±4 *(n=21)* | 1653±18 *(n=21)* | 16±0.7 *(n=21)* | 2.7±0.07 *(n=21)* |
| Extreme $pCO_2$, 28°C | $T_0$ | 1939±18 *(n=3)* | 7.55±0.03 *(n=6)* | 59±0.4 *(n=3)* | 1807±1 *(n=3)* | 49±0.4 *(n=3)* | 1.0±0.01 *(n=3)* |
| | $T_{30}$ | 2348±198 *(n=6)* | 7.49±0.03 *(n=3)* | 53±3 *(n=6)* | 1891±37 *(n=6)* | 60±5 *(n=6)* | 0.9±0.05 *(n=6)* |
| | $T_{60}$ | 2891±208 *(n=12)* | 7.42±0.03 *(n=12)* | 46±3 *(n=12)* | 1948±25 *(n=12)* | 74±5 *(n=12)* | 0.8±0.04 *(n=12)* |
| | $T_{95}$ | 2973±125 *(n=21)* | 7.41±0.03 *(n=21)* | 46±2 *(n=21)* | 1981±16 *(n=21)* | 76±3 *(n=21)* | 0.8±0.03 *(n=21)* |
| | $T_0$ | 1980±34 | 7.50±0.01 | 52±1 | 1621±2 | 47±0.8 | 0.9±0.01 |

| | | | | | | | |
|---|---|---|---|---|---|---|---|
| Extreme $pCO_2$, 31°C | | *(n=3)* | *(n=3)* | *(n=3)* | *(n=3)* | *(n=3)* | *(n=3)* |
| | $T_{30}$ | 2609±304 *(n=6)* | 7.44±0.03 *(n=6)* | 48±2 *(n=6)* | 1795±78 *(n=6)* | 62±8 *(n=6)* | 0.8±0.03 *(n=6)* |
| | $T_{60}$ | 3228±266 *(n=12)* | 7.38±0.03 *(n=12)* | 44±1.0 *(n=12)* | 1905±50 *(n=12)* | 78±7 *(n=12)* | 0.7±0.03 *(n=12)* |
| | $T_{95}$ | 3245±154 *(n=21)* | 7.38±0.02 *(n=21)* | 45±1 *(n=21)* | 1952±31 *(n=21)* | 78±4 *(n=21)* | 0.8±0.02 *(n=21)* |

**Table A1-3.**
Model results for *Siderastrea siderea* and *Pseudodiploria strigosa* host (calcification rate, total protein, total carbohydrates) and symbiont physiology (cell density and chlorophyll *a* concentration), and generalized additive model results for *S. siderea* calcification. Explicit models were determined from forward model selection, and are listed next to each species for the metric being considered. Sum Sq = sum of squares, Mean Sq = mean square of the error, NumDF = numerator degrees of freedom, DenDF = denominator degrees of freedom, and SE = standard error. Nearshore = NS and forereef = FR in reference to reef zones. *Siderastrea siderea* has unique columns due to the different format of the model.

| CALCIFICATION | | | | | | |
|---|---|---|---|---|---|---|
| **Factor** | **Estimate** | **SE** | **T-value** | **P-value** | | |
| ***Siderastrea siderea*** | Model = gamlss(calcification ~ duration*$pCO_2$*temperature*rz + random(genotype)) | | | | | |
| T60 – T30 | 0.003 | 0.098 | 0.033 | 0.974 | | |
| T30 – T90 | 0.234 | 0.102 | 2.289 | 0.023 | | |
| T60 – T90 | 0.007 | 0.110 | 0.065 | 0.950 | | |
| End of century – Present day $pCO_2$ | -0.065 | 0.082 | -0.797 | 0.426 | | |
| Extreme – Present day $pCO_2$ | -0.253 | 0.082 | -3.097 | 0.002 | | |
| End of century – Extreme $pCO_2$ | 0.231 | 0.123 | 1.874 | 0.063 | | |
| 31°C – 28 °C | 0.085 | 0.080 | 1.069 | 0.287 | | |
| NS – FR reef zone | 0.065 | 0.080 | 0.813 | 0.418 | | |
| | | | | | | |
| **Factor** | **Sum Sq** | **Mean Sq** | **NumDF** | **DenDF** | **F-value** | **P-value** |
| ***Pseudodiploria strigosa*** | Model = lmer(calcification ~ duration + temperature + $pCO_2$ + reef zone + duration*temperature + temperature*$pCO_2$ + temperature*reef zone + 1\|genotype) | | | | | |
| Duration | 20.030 | 10.015 | 2 | 158.130 | 27.226 | <0.0001 |
| Temperature | 17.801 | 17.801 | 1 | 159.190 | 48.392 | <0.0001 |
| $pCO_2$ | 6.628 | 3.314 | 2 | 158.490 | 9.009 | <0.001 |
| Reef zone | 4.460 | 4.460 | 1 | 3.190 | 12.124 | 0.036 |
| Duration:Temperature | 9.014 | 4.507 | 2 | 158.130 | 12.252 | <0.0001 |
| Temperature:$pCO_2$ | 5.359 | 2.681 | 2 | 158.490 | 7.284 | 0.001 |
| Temperature:Reef zone | 1.752 | 1.752 | 1 | 159.370 | 4.764 | 0.031 |
| TOTAL PROTEIN | | | | | | |
| ***Siderastrea siderea*** | Model = lmer(protein ~ duration + temperature + 1\|genotype) | | | | | |
| Duration | 1.288 | 0.429 | 3 | 133 | 10.051 | <0.0001 |
| Temperature | 0.303 | 0.303 | 1 | 133 | 7.091 | 0.009 |

| | | | | | | |
|---|---|---|---|---|---|---|
| ***Pseudodiploria strigosa*** | Model = lmer(protein ~ temperature + 1\|genotype) | | | | | |
| Temperature | 1.476 | 1.476 | 1 | 111.080 | 28.712 | <0.0001 |
| CARBOHYDRATES | | | | | | |
| ***Siderastrea siderea*** | Model = lmer(carbohydrate ~ temperature + 1\|genotype) | | | | | |
| Temperature | 1.589 | 1.589 | 1 | 135 | 8.820 | 0.004 |
| ***Pseudodiploria strigosa*** | Model = lmer(carbohydrate ~ temperature + duration + duration*temperature + 1\|genotype) | | | | | |
| Temperature | 3.363 | 3.363 | 1 | 102.200 | 23.996 | <0.0001 |
| Duration | 2.761 | 0.920 | 3 | 102.080 | 6.567 | <0.0001 |
| Temperature:Duration | 1.604 | 0.535 | 3 | 102.010 | 3.815 | 0.012 |
| SYMBIONT DENSITY | | | | | | |
| ***Siderastrea siderea*** | Model = lmer(symbiont density ~ duration + temperature + $pCO_2$ + duration*$pCO_2$ + 1\|genotype) | | | | | |
| Duration | 7.892 | 2.631 | 3 | 117.400 | 7.303 | <0.001 |
| Temperature | 3.891 | 3.891 | 1 | 117.190 | 10.804 | 0.001 |
| $pCO_2$ | 2.538 | 1.269 | 2 | 117.290 | 3.523 | 0.033 |
| Duration: $pCO_2$ | 7.008 | 1.168 | 6 | 117.290 | 3.243 | 0.006 |
| ***Pseudodiploria strigosa*** | Model = lmer(symbiont density ~ temperature + duration + 1\|genotype) | | | | | |
| Duration | 31.213 | 31.213 | 1 | 105.520 | 30.634 | <0.0001 |
| Temperature | 27.963 | 9.321 | 3 | 105.660 | 9.148 | <0.0001 |
| CHLOROPHYLL A | | | | | | |
| ***Siderastrea siderea*** | Model = lmer(Chl *a* ~ duration + $pCO_2$ + 1\|genotype) | | | | | |
| Duration | 40.553 | 13.518 | 3 | 127.340 | 32.161 | <0.0001 |
| $pCO_2$ | 5.918 | 2.959 | 2 | 127.280 | 7.040 | 0.001 |
| ***Pseudodiploria strigosa*** | Model = lmer(Chl *a* ~ temperature + $pCO_2$ + (1\|genotype) | | | | | |
| Temperature | 28.998 | 28.998 | 1 | 108.200 | 38.734 | <0.0001 |
| $pCO_2$ | 5.739 | 2.870 | 2 | 108.060 | 3.833 | 0.025 |

**Table A1-4.**
Summary of Tukey's HSD post-hoc tests for *Siderastrea siderea* and *Pseudodiploria strigosa* host (calcification, total protein, total carbohydrates) and symbiont physiology (cell density and chlorophyll *a* concentration). Only significant interactions are included. SE = standard error and DF = degrees of freedom. Nearshore = NS and forereef = FR in reference to reef zones. *Siderastrea siderea* net calcification results not shown here because comparisons are output from the generalized additive model and are included in Table A1-3.

| Contrast | Estimate | SE | DF | T-ratio | P-value |
|---|---|---|---|---|---|
| CALCIFICATION | | | | | |
| ***Pseudodiploria strigosa*** | | | | | |
| | Comparison = temperature | | | | |
| 28 – 31 | 0.734 | 0.106 | 159 | 6.939 | <.0001 |
| | Comparison = reef zone | | | | |
| FR – NS | -0.511 | 0.147 | 3.080 | -3.477 | 0.039 |
| | Comparison = $pCO_2$ | | | | |
| Present day – Extreme | 0.480 | 0.115 | 158 | 4.186 | 0.0001 |
| End of century – Extreme | 0.316 | 0.114 | 159 | 2.765 | 0.017 |
| | Comparison = temperature \| duration | | | | |
| 28, T30 – 28, T60 | 0.558 | 0.150 | 158 | 3.726 | 0.004 |
| 31, T30 – 31, T60 | 0.827 | 0.143 | 158 | 5.786 | <.0001 |
| 31, T30 – 31, T95 | 1.301 | 0.181 | 158 | 7.196 | <.0001 |
| 28, T60 – 31, T60 | 0.485 | 0.164 | 159 | 2.958 | 0.041 |
| 28, T60 – 31, T95 | 0.959 | 0.198 | 159 | 4.848 | <.0001 |
| 31, T60 – 28, T95 | -1.028 | 0.198 | 158 | -5.186 | <.0001 |
| 28, T95 – 31, T95 | 1.502 | 0.227 | 158 | 6.616 | <.0001 |
| | Comparison = temperature \| reef zone | | | | |
| 28, FR – 31, FR | 0.944 | 0.160 | 159.800 | 5.914 | <.0001 |
| 31, FR – 31, NS | -0.720 | 0.171 | 5.720 | -4.210 | 0.024 |
| | Comparison = temperature \| $pCO_2$ | | | | |
| 28, Present day – 31, Present day | 1.191 | 0.167 | 158 | 7.137 | <.0001 |
| 28, Present day – 31, End of century | 1.105 | 0.167 | 158 | 6.623 | <.0001 |
| 28, Present day – 28, Extreme | 0.915 | 0.168 | 159 | 5.457 | <.0001 |
| 28, Present day – 31, Extreme | 1.236 | 0.167 | 158 | 7.409 | <.0001 |
| 31, Present day – 28, End of century | -0.776 | 0.164 | 158 | -4.741 | <0.001 |
| 28, End of century – 31, End of century | 0.690 | 0.164 | 158 | 4.216 | <0.001 |

| | | | | | |
|---|---|---|---|---|---|
| 28, End of century – 28, Extreme | 0.500 | 0.166 | 159 | 3.009 | 0.035 |
| 28, End of century – 31, Extreme | 0.821 | 0.164 | 158 | 5.018 | <.0001 |
| | Comparison = reef zone \| duration \| $pCO_2$ \| temperature | | | | |
| Duration = T30, $pCO_2$= Present day, Temperature = 31; FR – NS | -1.036 | 0.341 | -3.036 | 96 | 0.003 |
| Duration = T60, $pCO_2$ = Present day, Temperature = 31; FR – NS | -0.806 | 0.411 | -1.963 | 96 | 0.050 |
| Duration = T95, $pCO_2$ = End of century, Temperature = 31; FR – NS | -1.306 | 0.570 | -2.291 | 96 | 0.024 |
| Duration = T30, $pCO_2$ = Extreme, Temperature = 31; FR – NS | -0.840 | 0.341 | -2.461 | 96 | 0.016 |
| PROTEIN | | | | | |
| ***Siderastrea siderea*** | | | | | |
| | Comparison = temperature | | | | |
| 28 – 31 | 0.094 | 0.035 | 128 | 2.662 | 0.009 |
| | Comparison = duration | | | | |
| T0 – T60 | -0.228 | 0.051 | 129 | -4.462 | 0.0001 |
| T0 – T95 | -0.136 | 0.049 | 128 | -2.785 | 0.031 |
| T30 – T60 | -0.238 | 0.051 | 129 | -4.645 | <.0001 |
| T30 – T95 | -0.145 | 0.049 | 128 | -2.976 | 0.018 |
| ***Pseudodiploria strigosa*** | | | | | |
| | Comparison = temperature | | | | |
| 28 – 31 | 0.225 | 0.042 | 111 | 5.357 | <.0001 |
| CARBOHYDRATES | | | | | |
| ***Siderastrea siderea*** | | | | | |
| | Comparison = temperature | | | | |
| 28 – 31 | 0.215 | 0.073 | 130 | 2.969 | 0.004 |
| ***Pseudodiploria strigosa*** | | | | | |
| | Comparison = temperature | | | | |
| 28 – 31 | 0.347 | 0.071 | 102 | 4.900 | <.0001 |
| | Comparison = duration | | | | |
| T0 – T60 | 0.417 | 0.102 | 102 | 4.099 | 0.001 |
| T30 – T60 | 0.275 | 0.102 | 102 | 2.695 | 0.040 |
| T60 – T95 | -0.370 | 0.102 | 102 | -3.634 | 0.002 |
| | Comparison = duration \| temperature | | | | |
| T0, 28 – T60, 31 | 0.662 | 0.135 | 102 | 4.920 | 0.0001 |
| T0, 28 – T90, 31 | 0.511 | 0.135 | 102 | 3.799 | 0.006 |

| | | | | | |
|---|---|---|---|---|---|
| T30, 28 – T60, 31 | 0.503 | 0.139 | 102 | 3.615 | 0.011 |
| T60, 28 – T90, 28 | -0.589 | 0.151 | 102 | -3.902 | 0.004 |
| T90, 28 – T30, 31 | 0.544 | 0.139 | 102 | 3.905 | 0.004 |
| T90, 28 – T60, 31 | 0.893 | 0.139 | 102 | 6.416 | <.0001 |
| T90, 28 – T90, 31 | 0.742 | 0.139 | 102 | 5.332 | <.0001 |
| T0, 31 – T60, 31 | 0.475 | 0.139 | 102 | 3.406 | 0.021 |
| SYMBIONT DENSITY | | | | | |
| ***Siderastrea siderea*** | | | | | |
| | Comparison = duration | | | | |
| T0 – T30 | 0.418 | 0.145 | 117 | 2.882 | 0.024 |
| T0 – T95 | 0.661 | 0.143 | 117 | 4.634 | 0.0001 |
| | Comparison = temperature | | | | |
| 28 – 31 | 0.341 | 0.104 | 117 | 3.286 | 0.001 |
| | Comparison = $pCO_2$ | | | | |
| End of century – Extreme | 819314 | 336723 | 117 | 2.433 | 0.043 |
| | Comparison = duration \| $pCO_2$ | | | | |
| T0, Extreme – T30, Extreme | 0.996 | 0.245 | 117 | 4.067 | 0.005 |
| T30, Present day – T30, Extreme | 1.099 | 0.245 | 117 | 4.477 | 0.001 |
| T30, Present day – T95, Present day | 0.824 | 0.245 | 117 | 3.357 | 0.047 |
| ***Pseudodiploria strigosa*** | | | | | |
| | Comparison = duration | | | | |
| T30 – T95 | 0.746 | 0.263 | 105 | 2.835 | 0.028 |
| T0 – T60 | 0.977 | 0.275 | 106 | 3.555 | 0.003 |
| T0 – T95 | 1.332 | 0.266 | 106 | 5.004 | <.0001 |
| | Comparison = temperature | | | | |
| 28 – 31 | 1.05 | 0.19 | 105 | 5.53E+00 | <.0001 |
| CHLOROPHYLL A | | | | | |
| ***Siderastrea siderea*** | | | | | |
| | Comparison = duration | | | | |
| T0 – T60 | -1.155 | 0.159 | 127 | -7.258 | <.0001 |
| T0 – T95 | -1.195 | 0.153 | 127 | -7.823 | <.0001 |
| T30 – T60 | -0.947 | 0.160 | 128 | -5.914 | <.0001 |
| T30 – T95 | -0.988 | 0.154 | 127 | -6.414 | <.0001 |
| | Comparison = $pCO_2$ | | | | |
| Present day – Extreme | 0.493 | 0.136 | 127 | 3.621 | 0.001 |
| End of century – Extreme | 0.352 | 0.134 | 127 | 2.634 | 0.026 |

| ***Pseudodiploria strigosa*** | | | | | |
|---|---|---|---|---|---|
| | Comparison = $pCO_2$ | | | | |
| Present day – Extreme | 0.550 | 0.199 | 108 | 2.766 | 0.018 |
| | Comparison = temperature | | | | |
| 28 – 31 | 1 | 0.163 | 106 | 6.16E+00 | <.0001 |

**Table A1-5.**
PCA Adonis summaries associated with Figure 2-2 and Figure A1-3. The Adonis model used to determine results is listed next to each species and time point. All Adonis models were run with 10,000 permutations. Significant *p*-values are bolded. Sum Sq = sum of squares, Mean Sq = mean square of the error, and DF = degrees of freedom.

| **Factor** | **DF** | **Sum Sq** | **Mean Sq** | **F-Model** | $R^2$ | ***P*-value** |
|---|---|---|---|---|---|---|
| ***S. siderea*, $T_{30}$** | Model = Adonis(scores ~ reef zone * $pCO_2$ * temperature * genotype) | | | | | |
| Reef zone | 1 | 0.001 | 0.001 | 0.225 | 0.007 | 0.867 |
| $pCO_2$ | 2 | 0.017 | 0.008 | 2.768 | 0.179 | 0.054 |
| Temperature | 1 | 0.007 | 0.007 | 2.400 | 0.077 | 0.110 |
| Genotype | 4 | 0.013 | 0.003 | 1.079 | 0.139 | 0.399 |
| Reef zone:$pCO_2$ | 2 | 0.005 | 0.002 | 0.782 | 0.050 | 0.520 |
| Reef zone:Temperature | 1 | 0.001 | 0.001 | 0.214 | 0.007 | 0.880 |
| $pCO_2$:Temperature | 2 | 0.003 | 0.001 | 0.434 | 0.028 | 0.779 |
| Reef zone: $pCO_2$:Temperature | 2 | 0.003 | 0.001 | 0.445 | 0.029 | 0.761 |
| ***S. siderea*, $T_{60}$** | Model = Adonis(scores ~ reef zone.* $pCO_2$ * temperature * genotype) | | | | | |
| Reef zone | 1 | 0.0002 | 0.0002 | 0.108 | 0.003 | 0.963 |
| $pCO_2$ | 2 | 0.002 | 0.001 | 0.726 | 0.045 | 0.524 |
| Temperature | 1 | 0.004 | 0.004 | 3.236 | 0.100 | 0.074 |
| Genotype | 4 | 0.011 | 0.003 | 2.019 | 0.250 | 0.125 |
| Reef zone:$pCO_2$ | 2 | 0.006 | 0.003 | 2.037 | 0.126 | 0.144 |
| Reef zone:Temperature | 1 | 0.001 | 0.001 | 0.377 | 0.012 | 0.663 |
| $pCO_2$:Temperature | 2 | 0.002 | 0.001 | 0.765 | 0.047 | 0.513 |
| Reef zone: $pCO_2$:Temperature | 2 | 0.003 | 0.002 | 1.246 | 0.077 | 0.302 |
| ***S. siderea*, $T_{95}$** | Model = Adonis(scores ~ reef zone * $pCO_2$ * temperature * genotype) | | | | | |
| Reef zone | 1 | 0.001 | 0.001 | 1.464 | 0.023 | 0.215 |
| $pCO_2$ | 2 | 0.005 | 0.003 | 5.228 | 0.165 | **0.002** |
| Temperature | 1 | 0.001 | 0.001 | 2.065 | 0.033 | 0.125 |
| Genotype | 4 | 0.007 | 0.002 | 3.440 | 0.217 | **0.004** |
| Reef zone:$pCO_2$ | 2 | 0.002 | 0.001 | 2.055 | 0.065 | 0.100 |
| Reef zone:Temperature | 1 | 0.001 | 0.001 | 1.092 | 0.017 | 0.310 |
| $pCO_2$:Temperature | 2 | 0.006 | 0.003 | 5.457 | 0.172 | **0.001** |
| Reef zone: $pCO_2$:Temperature | 2 | 0.0003 | 0.0001 | 0.282 | 0.009 | 0.953 |
| ***P. strigosa*, $T_{30}$** | Model = Adonis(scores ~ reef zone * $pCO_2$ * temperature * genotype) | | | | | |
| Reef zone | 1 | 0.005 | 0.005 | 1.101 | 0.043 | 0.314 |
| $pCO_2$ | 2 | 0.009 | 0.005 | 1.1225 | 0.088 | 0.349 |

| | | | | | | |
|---|---|---|---|---|---|---|
| Temperature | 1 | 0.009 | 0.009 | 2.127 | 0.083 | 0.149 |
| Genotype | 3 | 0.011 | 0.004 | 0.893 | 0.105 | 0.492 |
| Reef zone: $pCO_2$ | 2 | 0.005 | 0.002 | 0.568 | 0.044 | 0.621 |
| Reef zone:Temperature | 1 | 0.007 | 0.007 | 1.705 | 0.067 | 0.205 |
| $pCO_2$:Temperature | 2 | 0.003 | 0.002 | 0.362 | 0.028 | 0.772 |
| Reef zone: $pCO_2$:Temperature | 2 | 0.003 | 0.002 | 0.411 | 0.032 | 0.739 |
| ***P. strigosa*, $T_{60}$** | Model = Adonis(scores ~ reef zone * $pCO_2$ * temperature * genotype) | | | | | |
| Reef zone | 1 | 0.0154 | 0.015 | 4.040 | 0.093 | 0.062 |
| $pCO_2$ | 2 | 0.036 | 0.018 | 4.640 | 0.214 | **0.029** |
| Temperature | 1 | 0.013 | 0.013 | 3.343 | 0.077 | 0.083 |
| Genotype | 3 | 0.037 | 0.012 | 3.267 | 0.226 | 0.053 |
| Reef zone:$pCO_2$ | 2 | 0.012 | 0.006 | 1.508 | 0.070 | 0.258 |
| Reef zone:Temperature | 1 | 0.010 | 0.010 | 2.518 | 0.058 | 0.139 |
| $pCO_2$:Temperature | 2 | 0.006 | 0.003 | 0.735 | 0.034 | 0.521 |
| Reef zone: $pCO_2$:Temperature | 1 | 0.003 | 0.003 | 0.818 | 0.019 | 0.398 |
| ***P. strigosa*, $T_{95}$** | Model = Adonis(scores ~ reef zone * $pCO_2$ * temperature * genotype) | | | | | |
| Reef zone | 1 | 0.013 | 0.013 | 2.299 | 0.079 | 0.140 |
| $pCO_2$ | 2 | 0.003 | 0.001 | 0.241 | 0.017 | 0.870 |
| Temperature | 1 | 0.024 | 0.024 | 4.247 | 0.146 | **0.045** |
| Genotype | 3 | 0.012 | 0.004 | 0.689 | 0.071 | 0.605 |
| Reef zone:$pCO_2$ | 2 | 0.006 | 0.003 | 0.522 | 0.036 | 0.644 |
| Reef zone:Temperature | 1 | 0.022 | 0.022 | 3.967 | 0.136 | 0.053 |
| $pCO_2$:Temperature | 2 | 0.008 | 0.040 | 0.676 | 0.046 | 0.555 |
| Reef zone: $pCO_2$:Temperature | 2 | 0.004 | 0.002 | 0.316 | 0.022 | 0.789 |
| **Combined Species, $T_{30}$** | Model = Adonis(scores ~ species * reef zone * $pCO_2$ * temperature) | | | | | |
| Species | 1 | 0.055 | 0.055 | 14.407 | 0.205 | **0.0002** |
| $pCO_2$ | 2 | 0.023 | 0.012 | 3.046 | 0.087 | **0.047** |
| Temperature | 1 | 0.020 | 0.020 | 5.211 | 0.074 | **0.023** |
| **Combined Species, $T_{60}$** | Model = Adonis(scores ~ species * reef zone * $pCO_2$ * temperature) | | | | | |
| Species | 1 | 0.055 | 0.055 | 14.407 | 0.205 | **0.0006** |
| $pCO_2$ | 2 | 0.023 | 0.012 | 3.046 | 0.087 | **0.045** |
| Temperature | 1 | 0.020 | 0.020 | 5.211 | 0.074 | **0.019** |
| **Combined Species, $T_{95}$** | Model = Adonis(scores ~ species * reef zone * $pCO_2$ * temperature) | | | | | |
| Species | 1 | 0.055 | 0.055 | 14.407 | 0.205 | **0.0004** |
| $pCO_2$ | 2 | 0.023 | 0.012 | 3.046 | 0.087 | **0.046** |

| | | | | | | |
|---|---|---|---|---|---|---|
| Temperature | 1 | 0.012 | 0.020 | 5.211 | 0.074 | **0.022** |

**Table A1-6.**
Linear model summaries associated with Figures 2-6 and A1-5, including chi square values (Chi-Sq), degrees of freedom (DF) and significance (*P*-value) statistics. All data is associated with *P. strigosa,* and the table is separated by experimental time point (short-term=$T_{30}$, moderate-term=$T_{60}$, long-term=$T_{95}$). Linear models are listed above the summaries for that model for reference.

| Factor | Chi-Sq | DF | *P*-value |
|---|---|---|---|
| ***P. strigosa, $T_{30}$*** | | | |
| PROTEIN | Model = (Calcification ~ Protein * Temperature + 1\|genotype) | | |
| Protein | 5.63 | 1 | 0.02 |
| Temperature | 0.12 | 1 | 0.73 |
| Protein:Temperature | 2.05 | 1 | 0.15 |
| CARBOHYDRATES | Model = (Calcification ~ Carbohydrates * Temperature + 1\|genotype) | | |
| Carbohydrates | 0.94 | 1 | 0.33 |
| Temperature | 0.04 | 1 | 0.83 |
| Carbohydrates:Temperature | 3.23 | 1 | 0.07 |
| SYMBIONT DENSITY | Model = (Calcification ~ Symbionts * Temperature + 1\|genotype) | | |
| Symbionts | 6.95 | 1 | 0.008 |
| Temperature | 0.45 | 1 | 0.50 |
| Symbionts:Temperature | 0.75 | 1 | 0.39 |
| ***P. strigosa, $T_{60}$*** | | | |
| PROTEIN | Model = (Calcification ~ Protein * Temperature + 1\|genotype) | | |
| Protein | 0.70 | 1 | 0.40 |
| Temperature | 3.83 | 1 | 0.05 |
| Protein:Temperature | 2.15 | 1 | 0.14 |
| CARBOHYDRATES | Model = (Calcification ~ Carbohydrates * Temperature + 1\|genotype) | | |
| Carbohydrates | 0.005 | 1 | 0.94 |
| Temperature | 4.53 | 1 | 0.03 |
| Carbs:Temperature | 5.72 | 1 | 0.02 |
| SYMBIONT DENSITY | Model = (Calcification ~ Symbionts * Temperature + 1\|genotype) | | |
| Symbionts | 0.18 | 1 | 0.67 |
| Temperature | 2.73 | 1 | 0.10 |
| Symbionts:Temperature | 5.76 | 1 | 0.02 |
| ***P. strigosa, $T_{95}$*** | | | |
| PROTEIN | Model = (Calcification ~ Protein * Temperature + 1\|genotype) | | |
| Protein | 5.09 | 1 | 0.02 |
| Temperature | 15.70 | 1 | < 0.0001 |
| Protein:Temperature | 4.06 | 1 | 0.04 |
| CARBOHYDRATES | Model = (Calcification ~ Carbohydrates * Temperature + 1\|genotype) | | |
| Carbohydrates | 0.74 | 1 | 0.39 |
| Temperature | 13.75 | 1 | < 0.001 |
| Carbs:Temperature | 3.44 | 1 | 0.06 |
| SYMBIONT DENSITY | Model = (Calcification ~ Symbionts * Temperature + 1\|genotype) | | |
| Symbionts | 13.30 | 1 | 0.0003 |
| Temperature | 15.76 | 1 | < 0.0001 |
| Symbionts:Temperature | 7.09 | 1 | 0.01 |
| CHLOROPHYLL A | Model = (Calcification ~ Chl *a* * Temperature + 1\|genotype) | | |

| | | | |
|---|---|---|---|
| Chl *a* | 13.5 | 1 | 0.0002 |
| Temperature | 4.63 | 1 | 0.03 |
| Chl *a*:Temperature | 1.45 | 1 | 0.22 |

**Table A1-7.**
Summary of Tukey's HSD post-hoc tests for experimental treatment (cumulative temperature and $pCO_2$). Estimate, lower, and upper columns represent the difference between the compared mean values and 95% confidence intervals. Asterisks indicate time points where data were log-transformed to meet ANOVA assumptions of normality.

| **Comparison** | **Estimate** | **Lower** | **Upper** | ***P-value*** |
|---|---|---|---|---|
| ***$pCO_2$*** | Model = measured $pCO2$ ~ temperature * $pCO_2$ | | | |
| **$T_0$** | | | | |
| Present day, 31°C – Present day, 28°C | -34.23 | -129.12 | 60.66 | 0.88 |
| End of century 31°C – Present day, 28°C | -24.77 | -119.66 | 70.12 | 0.97 |
| Extreme, 28°C – Present day, 28°C | 1408.36 | 1313.47 | 1503.25 | <0.0001 |
| Extreme, 31°C – Present day, 28°C | 1449.83 | 1354.95 | 1544.72 | <0.0001 |
| End of century, 28°C – Present day, 31°C | 227.60 | 132.71 | 322.49 | <0.0001 |
| End of century, 31°C – Present day, 31°C | 9.46 | -85.43 | 104.35 | 0.99 |
| Extreme, 28°C – Present day, 31°C | 1442.59 | 1347.70 | 1537.48 | <0.0001 |
| Extreme, 31°C – Present day, 31°C | 1484.06 | 1389.18 | 1578.95 | <0.0001 |
| End of century, 31°C – End of century, 28°C | -218.14 | -313.03 | -123.25 | <0.0001 |
| Extreme, 28°C – End of century, 28°C | 1214.99 | 1120.10 | 1309.88 | <0.0001 |
| Extreme, 31°C – End of century, 28°C | 1256.46 | 1161.57 | 1351.35 | <0.0001 |
| Extreme, 28°C – End of century, 31°C | 1433.13 | 1338.25 | 1528.02 | <0.0001 |
| Extreme, 31°C – End of century, 31°C | 1474.61 | 1379.72 | 1569.50 | <0.0001 |
| Extreme, 31°C – Extreme, 28°C | 41.47 | -53.42 | 136.36 | 0.75 |
| **$T_{30}$*** | | | | |
| Present day, 31°C – Present day, 28°C | -0.07 | -0.43 | 0.29 | 0.99 |
| End of century, 28°C – Present day, 28°C | 0.45 | 0.09 | 0.82 | 0.006 |
| End of century, 31°C – Present day, 28°C | 0.28 | -0.08 | 0.65 | 0.21 |
| Extreme, 28°C – Present day, 28°C | 1.63 | 1.26 | 1.99 | <0.0001 |
| Extreme, 31°C – Present day, 28°C | 1.71 | 1.35 | 2.08 | <0.0001 |
| End of century, 28°C – Present day, 31°C | 0.52 | 0.16 | 0.88 | 0.001 |
| End of century, 31°C – Present day, 31°C | 0.35 | -0.01 | 0.72 | 0.06 |
| Extreme, 28°C – Present day, 31°C | 1.70 | 1.33 | 2.06 | <0.0001 |
| Extreme, 31°C – Present day, 31°C | 1.78 | 1.42 | 2.14 | <0.0001 |
| End of century, 31°C – End of century, 28°C | -0.17 | -0.53 | 0.19 | 0.80 |
| Extreme, 28°C – End of century, 28°C | 1.17 | 0.81 | 1.54 | <0.0001 |
| Extreme, 31°C – End of century, 28°C | 1.26 | 0.90 | 1.63 | <0.0001 |
| Extreme, 28°C – End of century, 31°C | 1.34 | 0.98 | 1.70 | <0.0001 |
| Extreme, 31°C – End of century, 31°C | 1.43 | 1.07 | 1.79 | <0.0001 |
| Extreme, 31°C – Extreme, 28°C | 0.09 | -0.27 | 0.45 | 0.99 |
| **$T_{60}$*** | | | | |
| Present day, 31°C – Present day, 28°C | 0.18 | -0.19 | 0.55 | 0.80 |

| | | | | |
|---|---|---|---|---|
| End of century, 28°C – Present day, 28°C | 0.75 | 0.38 | 1.13 | <0.0001 |
| End of century, 31°C – Present day, 28°C | 0.71 | 0.34 | 1.09 | <0.0001 |
| Extreme, 28°C – Present day, 28°C | 2.23 | 1.85 | 2.60 | <0.0001 |
| Extreme, 31°C – Present day, 28°C | 2.33 | 1.95 | 2.70 | <0.0001 |
| End of century, 28°C – Present day, 31°C | 0.57 | 0.20 | 0.95 | 0.0002 |
| End of century, 31°C – Present day, 31°C | 0.53 | 0.16 | 0.91 | 0.0008 |
| Extreme, 28°C – Present day, 31°C | 2.05 | 1.67 | 2.42 | <0.0001 |
| Extreme, 31°C – Present day, 31°C | 2.15 | 1.77 | 2.52 | <0.0001 |
| End of century, 31°C – End of century, 28°C | -0.04 | -0.41 | 0.33 | 0.99 |
| Extreme, 28°C – End of century, 28°C | 1.47 | 1.10 | 1.85 | <0.0001 |
| Extreme, 31°C – End of century, 28°C | 1.57 | 1.20 | 1.95 | <0.0001 |
| Extreme, 28°C – End of century, 31°C | 1.51 | 1.14 | 1.89 | <0.0001 |
| Extreme, 31°C – End of century, 31°C | 1.61 | 1.24 | 1.99 | <0.0001 |
| Extreme, 31°C – Extreme, 28°C | 0.10 | -0.27 | 0.47 | 0.99 |
| **$T_{95}$*** | | | | |
| Present day, 31°C – Present day, 28°C | 0.29 | 0.06 | 0.52 | 0.005 |
| End of century, 28°C – Present day, 28°C | 0.86 | 0.63 | 1.10 | <0.0001 |
| End of century, 31°C – Present day, 28°C | 0.85 | 0.61 | 1.08 | <0.0001 |
| Extreme, 28°C – Present day, 28°C | 2.35 | 2.11 | 2.58 | <0.0001 |
| Extreme, 31°C – Present day, 28°C | 2.43 | 2.19 | 2.66 | <0.0001 |
| End of century, 28°C – Present day, 31°C | 0.57 | 0.34 | 0.80 | <0.0001 |
| End of century, 31°C – Present day, 31°C | 0.56 | 0.32 | 0.79 | <0.0001 |
| Extreme, 28°C – Present day, 31°C | 2.06 | 1.83 | 2.29 | <0.0001 |
| Extreme, 31°C – Present day, 31°C | 2.14 | 1.91 | 2.37 | <0.0001 |
| End of century, 31°C – End of century, 28°C | -0.02 | -0.25 | 0.22 | 0.99 |
| Extreme, 28°C – End of century, 28°C | 1.49 | 1.25 | 1.72 | <0.0001 |
| Extreme, 31°C – End of century, 28°C | 1.57 | 1.34 | 1.80 | <0.0001 |
| Extreme, 28°C – End of century, 31°C | 1.50 | 1.27 | 1.73 | <0.0001 |
| Extreme, 31°C – End of century, 31°C | 1.58 | 1.35 | 1.81 | <0.000 |
| Extreme, 31°C – Extreme, 28°C | 0.08 | -0.15 | 0.31 | 0.96 |
| **Temperature** | Model = measured temperature ~ temperature * $pCO_2$ | | | |
| **$T_0$*** | | | | |
| Present day, 31°C – Present day, 28°C | 2.93 | 2.74 | 3.13 | <0.0001 |
| End of century, 28°C – Present day, 28°C | -0.47 | -0.66 | -0.27 | <0.0001 |
| End of century, 31°C – Present day, 28°C | 2.53 | 2.34 | 2.73 | <0.0001 |
| Extreme, 28°C – Present day, 28°C | 0.13 | -0.06 | 0.33 | 0.30 |
| Extreme, 31°C – Present day, 28°C | 1.57 | 1.37 | 1.76 | <0.0001 |
| End of century, 28°C – Present day, 31°C | -3.40 | -3.60 | -3.20 | <0.0001 |

| | | | | |
|---|---|---|---|---|
| End of century, 31°C – Present day, 31°C | -0.40 | -0.60 | -0.20 | 0.0001 |
| Extreme, 28°C – Present day, 31°C | -2.80 | -3.00 | -2.60 | <0.0001 |
| Extreme, 31°C – Present day, 31°C | -1.37 | -1.56 | -1.17 | <0.0001 |
| End of century, 31°C – End of century, 28°C | 3.00 | 2.80 | 3.20 | <0.0001 |
| Extreme, 28°C – End of century, 28°C | 0.60 | 0.40 | 0.80 | <0.0001 |
| Extreme, 31°C – End of century, 28°C | 2.03 | 1.84 | 2.23 | <0.0001 |
| Extreme, 28°C – End of century, 31°C | -2.40 | -2.60 | -2.20 | <0.0001 |
| Extreme, 31°C – End of century, 31°C | -0.97 | -1.16 | -0.77 | <0.0001 |
| Extreme, 31°C – Extreme, 28°C | 1.43 | 1.24 | 1.63 | <0.0001 |
| **$T_{30}$** | | | | |
| Present day, 31°C – Present day, 28°C | 2.90 | 2.66 | 3.14 | <0.0001 |
| End of century, 28°C – Present day, 28°C | -0.36 | -0.60 | -0.12 | 0.0002 |
| End of century, 31°C – Present day, 28°C | 2.80 | 2.56 | 3.04 | <0.0001 |
| Extreme, 28°C – Present day, 28°C | -0.02 | -0.26 | 0.22 | 0.99 |
| Extreme, 31°C – Present day, 28°C | 2.40 | 2.16 | 2.64 | <0.0001 |
| End of century, 28°C – Present day, 31°C | -3.27 | -3.51 | -3.02 | <0.0001 |
| End of century, 31°C – Present day, 31°C | -0.10 | -0.34 | 0.14 | 0.91 |
| Extreme, 28°C – Present day, 31°C | -2.92 | -3.16 | -2.68 | <0.0001 |
| Extreme, 31°C – Present day, 31°C | -0.51 | -0.75 | -0.26 | <0.0001 |
| End of century, 31°C – End of century, 28°C | 3.17 | 2.92 | 3.41 | <0.0001 |
| Extreme, 28°C – End of century, 28°C | 0.34 | 0.10 | 0.58 | 0.0005 |
| Extreme, 31°C – End of century, 28°C | 2.76 | 2.52 | 3.00 | <0.0001 |
| Extreme, 28°C – End of century, 31°C | -2.82 | -3.06 | -2.58 | <0.0001 |
| Extreme, 31°C – End of century, 31°C | -0.41 | -0.65 | -0.16 | <0.0001 |
| Extreme, 31°C – Extreme, 28°C | 2.42 | 2.18 | 2.66 | <0.0001 |
| **$T_{60}$** | | | | |
| Present day, 31°C – Present day, 28°C | 3.20 | 2.92 | 3.49 | <0.0001 |
| End of century, 28°C – Present day, 28°C | -0.06 | -0.34 | 0.23 | 0.99 |
| End of century, 31°C – Present day, 28°C | 2.91 | 2.63 | 3.20 | <0.0001 |
| Extreme, 28°C – Present day, 28°C | 0.01 | -0.28 | 0.30 | 1.00 |
| Extreme, 31°C – Present day, 28°C | 2.59 | 2.30 | 2.88 | <0.0001 |
| End of century, 28°C – Present day, 31°C | -3.26 | -3.55 | -2.97 | <0.0001 |
| End of century, 31°C – Present day, 31°C | -0.29 | -0.58 | -0.001 | 0.048 |
| Extreme, 28°C – Present day, 31°C | -3.20 | -3.49 | -2.91 | <0.0001 |
| Extreme, 31°C – Present day, 31°C | -0.61 | -0.90 | -0.33 | <0.0001 |
| End of century, 31°C – End of century, 28°C | 2.97 | 2.68 | 3.26 | <0.0001 |
| Extreme, 28°C – End of century, 28°C | 0.06 | -0.23 | 0.35 | 0.99 |
| Extreme, 31°C – End of century, 28°C | 2.65 | 2.36 | 2.93 | <0.0001 |
| Extreme, 28°C – End of century, 31°C | -2.91 | -3.20 | -2.62 | <0.0001 |

| | | | | |
|---|---|---|---|---|
| Extreme, 31°C – End of century, 31°C | -0.32 | -0.61 | -0.04 | 0.02 |
| Extreme, 31°C – Extreme, 28°C | 2.58 | 2.30 | 2.87 | <0.0001 |
| **$T_{95}$** | | | | |
| Present day, 31°C – Present day, 28°C | 3.11 | 2.92 | 3.31 | <0.0001 |
| End of century, 28°C – Present day, 28°C | -0.03 | -0.22 | 0.17 | 0.99 |
| End of century, 31°C – Present day, 28°C | 2.97 | 2.78 | 3.17 | <0.0001 |
| Extreme, 28°C – Present day, 28°C | 0.08 | -0.11 | 0.27 | 0.91 |
| Extreme, 31°C – Present day, 28°C | 2.73 | 2.53 | 2.92 | <0.0001 |
| End of century, 28°C – Present day, 31°C | -3.14 | -3.33 | -2.95 | <0.0001 |
| End of century, 31°C – Present day, 31°C | -0.14 | -0.33 | 0.05 | 0.34 |
| Extreme, 28°C – Present day, 31°C | -3.03 | -3.23 | -2.84 | <0.0001 |
| Extreme, 31°C – Present day, 31°C | -0.39 | -0.58 | -0.20 | <0.0001 |
| End of century, 31°C – End of century, 28°C | 3.00 | 2.81 | 3.19 | <0.0001 |
| Extreme, 28°C – End of century, 28°C | 0.11 | -0.09 | 0.30 | 0.69 |
| Extreme, 31°C – End of century, 28°C | 2.75 | 2.56 | 2.94 | <0.0001 |
| Extreme, 28°C – End of century, 31°C | -2.89 | -3.09 | -2.70 | <0.0001 |
| Extreme, 31°C – End of century, 31°C | -0.25 | -0.44 | -0.06 | 0.003 |
| Extreme, 31°C – Extreme, 28°C | 2.64 | 2.45 | 2.84 | <0.0001 |

# APPENDIX 2: CHAPTER 3 SUPPLEMENT

## A2.1. Supplementary materials and methods

### *A2.1.1. Experimental conditions*

Throughout the experiment, corals were maintained in 42 L aquaria at salinity of 33 ppt using Instant Ocean Sea Salt artificial seawater (ASW), which was refreshed weekly with 40% water changes. Corals were fed freshly hatched *Artemia sp.* nauplii two to three times weekly and were allowed to feed for one hour before resuming recirculating flow in the aquaria. Nubbins were rotated weekly to ensure even light exposure over the course of the experiment. Salinity was measured in each treatment at least once daily using a YSI 3200 conductivity meter (Yellow Springs, Ohio, USA), and pH was measured 3 times weekly in each treatment using an Orion Star A211 pH meter (calibrated with certified NBS pH buffers of 4.01, 7.00, and 10.01). Temperature was controlled with two 500 W heaters (Eheim) and a chiller (AquaEuroUSA, Los Angeles CA, USA) that were used to maintain DTV profiles in each treatment using the Neptune Systems Apex Classic AquaController with custom coded profiles. Briefly, virtual heating and cooling segments were used to dictate changes in target temperature for each treatment in two-hour intervals and all variability treatments descended to a nighttime minimum of 28.5°C for 9 hours. Heating rates differed to allow all treatments to spend the same amount of time each day at the highest temperature in the profile. Temperature was measured daily using a NIST-calibrated glass thermometer and evaluated against Apex readouts, with twice weekly calibration. Temperature was recorded by the Apex system and at 5-minute intervals with HOBO ProV2 Loggers (Onset, Bourne, MA) throughout the duration of the experiment,

except for the moderate variability treatment, which is missing data for the heat challenge and recovery periods due to a failed logger. Experimental temperature data presented here is HOBO logger data corrected to the calibrated Apex data, as this is the most complete temperature record across all treatments. Differences in daily temperature parameters (variability, mean, maximum, and minimum) across treatments during the 50-day DTV treatment were determined using a one-way ANOVA with Tukey's HSD post-hoc tests (Figure A2-8; Table A2-11).

### *A2.1.2. Profiling of prokaryotic and Symbiodiniaceae communities*

ITS2 primers included the forward SYM_VAR_5.8S2 (5' - TCGTCGGCAGCGTC AGATGTGTATAAGAGACAG *NNNN* **GTGAATTGCAGAACTCCGTG** - 3') (B. Hume et al. 2015) and the reverse SYM_VAR_REV (5' - GTCTCGTGGGCTCGG AGATGTGTATAAGAGACAG *NNNN* **CCTCCGCTTACTTATAGCTT** 3') (B. Hume et al. 2013). 16S primers included the forward Hyb515F (5'-TCGTCGGCAGCGTC AGATGTGTATAAGAGACAG *NNNN* **GTGYCAGCMGCCGCGGTAA**-3′) (Parada, Needham, and Fuhrman 2016) and the reverse Hyb806R (5'-GTCTCGTGGGCTCGG AGATGTGTATAAGAGACAG *NNNN* **GGACTACNVGGGTWTCTAAT**-3') (Apprill et al. 2015). Underlined bases denote adapter linker, bold bases are primer sequences, and the middle bases are spacer sequences. Both ITS2 and 16S PCR reactions totaled 30 µl and included 30 ng of template DNA, 1 µM forward primer, 1 µM reverse primer, 0.2 mM dNTP, 1X ExTaq buffer (Takara), 0.025 U ExTaq enzyme (Takara), and the remaining Milli-Q $H_2O$ (Millipore). For ITS2 primers, the reaction profile cycled at 95°C for 40 seconds, 59°C for 120 seconds, and 72°C for 60 seconds for 28 cycles and a final

elongation step of 72°C for 7 minutes. The reaction profile for 16S primers cycled at 95°C for 40 seconds, 58°C for 120 seconds, and 72°C for 60 seconds for 32 cycles with a final elongation step of 72°C for 5 minutes. For 16S, two negative controls using water were prepared and later used to remove contaminant sequences. PCR products were purified using GeneJET PCR Purification kits (ThermoFisher) eluted in 30 µl. Each PCR product was uniquely barcoded, subjected to five PCR cycles, and visualized on a 1% agarose gel to assess relative concentrations. Samples were pooled in equal concentrations within libraries, and 25 µl of the pooled library was run on a 1% SYBR Green (Invitrogen) stained gel. The target band was excised and incubated with 30 µl of Milli-Q water overnight at 4˚C. The ITS2 and 16S libraries were then quantified using a Quant-iT PicoGreen dsDNA assay kit (Thermo Fisher), pooled based on concentration (1:3 ITS2 and 2:3 16S) and submitted for paired-end 250bp sequencing on an Illumina Miseq at TUCF.

## A2.2. Supplementary Results

### *A2.2.1. Aquaria conditions*

Following the end of DTV conditions, temperatures in all aquaria were brought to the thermal minimum and then increased 1°C per day to an 8-day heat challenge treatment with mean (± standard error) temperature across all treatments of 31.82 (± 0.003) °C. Subsequently, temperatures were decreased by 1°C per day to recovery conditions, which were maintained for 16 days at a mean (± standard error) of 29.42 (± 0.004) °C (Figure 3-1). Following the recovery period, all coral fragments were frozen.

### *A2.2.2. Diel temperature variability did little to structure algal and microbial communities*

The core microbiome consisted of five bacterial ASVs. Dispersion in the core microbiome was not significantly different based on DTV treatment (*Pdis*=0.18; Figure A2-7b) or host lineage (*Pdis*=0.61; Figure A2-6b). Additionally, there was no spatial structure in core microbiome communities based on DTV treatment (*ADONIS p*=0.12; Figure A2-7b) or host lineage (*ADONIS p*=0.70; Figure A2-6b). The accessory microbiome consisted of 636 ASVs. Dispersion of this community was not significantly altered by DTV treatment (*Pdis*=0.20; Figure A2-7c); however, it was significantly more constrained in L1 compared to L2 (*Pdis*=0.012; Figure A2-6c). Additionally, the accessory microbiome community was significantly different across DTV treatments (*ADONIS p*=0.004; Figure A2-7c) and host lineages (*ADONIS p* = 0.006; Figure A2-6c). Similar to the patterns observed with all ASVs, accessory microbiomes of corals in the control treatment were significantly different from those in low (*ADONIS p*=0.007), moderate (*ADONIS p*=0.005), and high variability (*ADONIS p*=0.008) DTV treatments (Figure A2-7c). All microbiome spatial statistics are reported in Table A2-8.

There were four differentially abundant microbial taxa across DTV treatments, all of which were more abundant in control treatment relative to variability treatments (Figure A2-7d). These taxa included two ASVs in the Order "SAR11 clade" (Families "Clade I" and "Clade III"), an ASV of Class "Parcubacteria", and an ASV of the Family "Flavobacteriaceae", classified as *Tenacibaculum mesophilum*. Additionally, there were two differentially abundant taxa identified across host lineages. An ASV in the Order

"SAR11 clade" (Family "Clade III") was more abundant in L2 compared to L1, and an ASV in the family "Rhodanobacteraceae", classified as *Dyella thiooxydans,* was more abundant in L2 compared to L1 (Figure A2-6d).

## A2.3. Supplementary Figures

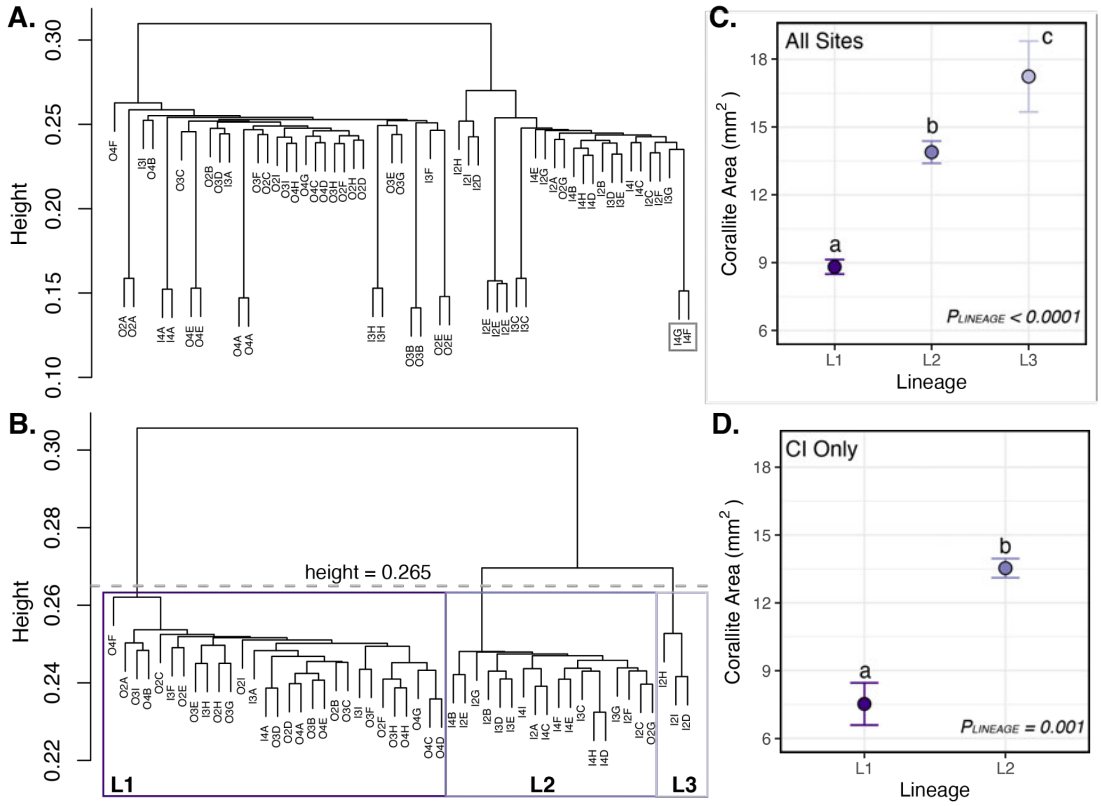


**Figure A2-1.**
**Presence of three cryptic lineages of a *Siderastrea siderea* species complex in Bocas del Toro Reef Complex with distinct phenotypes.** (**a**) Identity by state (IBS) cluster dendrogram of all samples. The gray box highlights one putative clonal pair (I4G and I4F), which occur at the same height as the technical replicates (indicated by identical sample name). (**b**) IBS cluster dendrogram with technical replicates and one putative clone removed (I4F). The dashed line at height = 0.265 represents the cutoff for lineage assignment, with lineages 1-3 (L1, L2, L3) indicated with purple boxes. (**c**) Mean corallite area ($mm^2$) ± standard error from corals from all collection sites showcasing that lineage 1 (L1; n = 29) had the smallest corallite area, followed by lineage 2 (L2; n = 16; Tukey HSD $p < 0.0001$) and then lineage 3 (L3; n = 3; Tukey HSD $p = 0.015$). (**d**) These same differences in mean corallite area ± standard error were observed when considering L1 (n = 4) and L2 (n = 4) that co-occur at Cristobal Island (CI). Letters indicate statistical differences in corallite area between lineages according to Tukey HSD post-hoc tests.

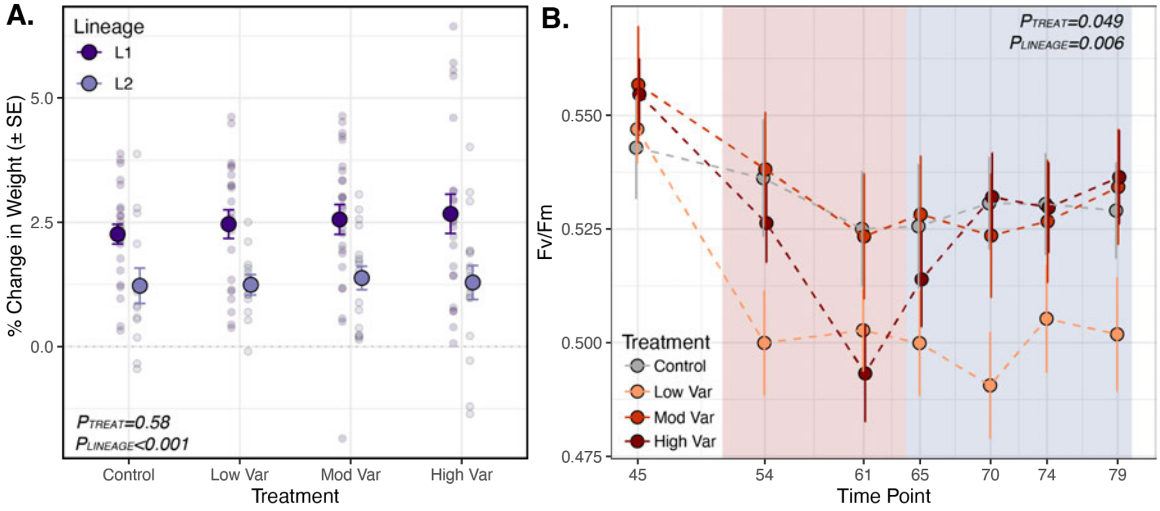


**Figure A2-2.**
**Little effect of prior diel temperature variability (DTV) treatment on growth or photochemical efficiency under heat challenge.** (**a**) Percent change in weight by host cryptic lineage over the course of the heat challenge and recovery portions of the experiment, measured as % change in weight (y-axis) across previous DTV treatment (x-axis). Large points represent mean ± standard error of percent growth for each lineage across the previous DTV treatments, and smaller points represent an individual fragment's growth. (**b**) Photochemical efficiency (Fv/Fm) across seven time points throughout the end of DTV treatment, heat stress (red shaded) and recovery (blue shaded) time points. Points represent mean ± standard error in Fv/Fm for each DTV treatment. Sample sizes for (**a**) and (**b**) are reported in Tables A2-6 and A2-10, respectively.

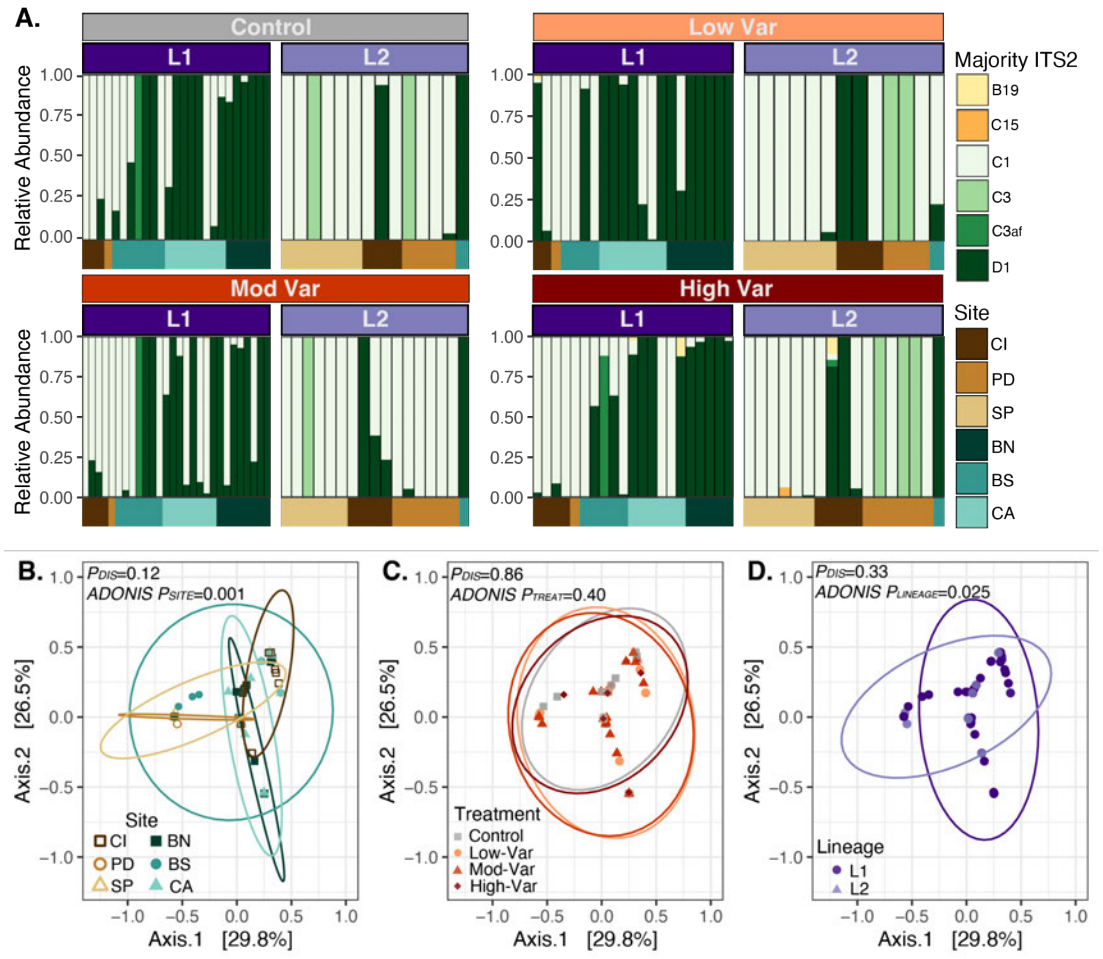


**Figure A2-3.**
**Symbiodiniaceae communities driven by cryptic host lineage and site of origin, not diel temperature variability (DTV).** (**a**) Bar plots of Symbiodiniaceae majority ITS2 sequence relative abundance data, colored by genera. Defining intragenomic variants (DIVs) were summed by majority ITS2 sequence before calculating relative abundances. Nine DIVs matched C1 (*Symbiodinium goreaui*), two DIVs matched C3 (no associated species), five DIVs matched D1 (*Durusdinium trenchii*), and one DIV matched each of the B19, C3af, and C15 majority ITS2 sequences. Bar plots are faceted by lineage (L1 = dark purple, L2 = light purple) within DTV treatment (Control (0°C), Low-Var (2°C), Mod-Var (3°C), and High-Var (4°C)). Each column of the bar plots represents a coral individual, and color blocks under the plots represent the site of origin for each individual (site colors as in Figure 3-2). (**b-d**) Bray-Curtis dissimilarity principal coordinate analyses (PCAs) of Symbiodiniaceae community relative abundance data by site of origin (**b**), DTV treatment (**c**), and host lineage (**d**). DTV treatment colors represent the degree of variability, with darker hues of red representing higher variability treatments, and treatments also being distinguished by shapes.

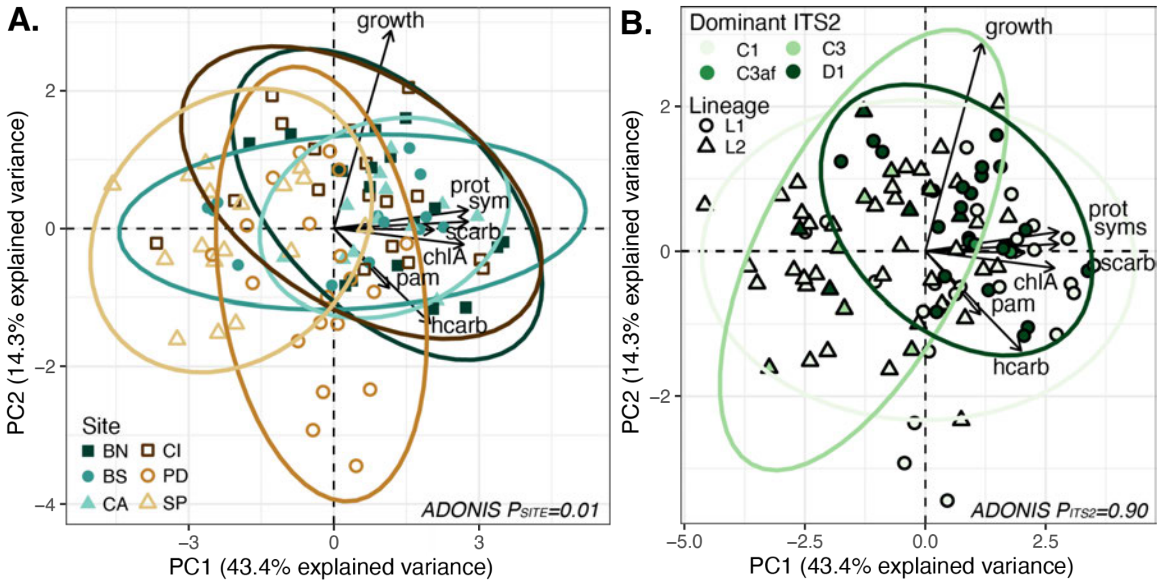


**Figure A2-4.**

**Holobiont phenomes structured by site of origin but not dominant ITS2 type.** Principal component analyses (PCA) of log-transformed holobiont phenomes following 50 days in DTV treatment. Colors represent site of origin (**a**: closed shapes/green shades representing offshore sites and open shapes/brown shades representing inshore sites) or dominant ITS2 type (**b**). In (**b**), shapes represent the cryptic host lineage (L1=open circle, L2=open triangle). Phenotypes include percent change in weight through 50 days in DTV (growth), total protein (prot; mg $cm^{-2}$), host and symbiont carbohydrate (hcarb and scarb, respectively; mg $cm^{-2}$), chlorophyll *a* (chlA; µg $cm^{-2}$), symbiont density (syms; cells $cm^{-2}$), and photochemical efficiency of photosystem II (pam). Only individuals with data for all phenotypes were included (N=97), and x- and y- axes represent the % variance explained by the first and second principal component, respectively.

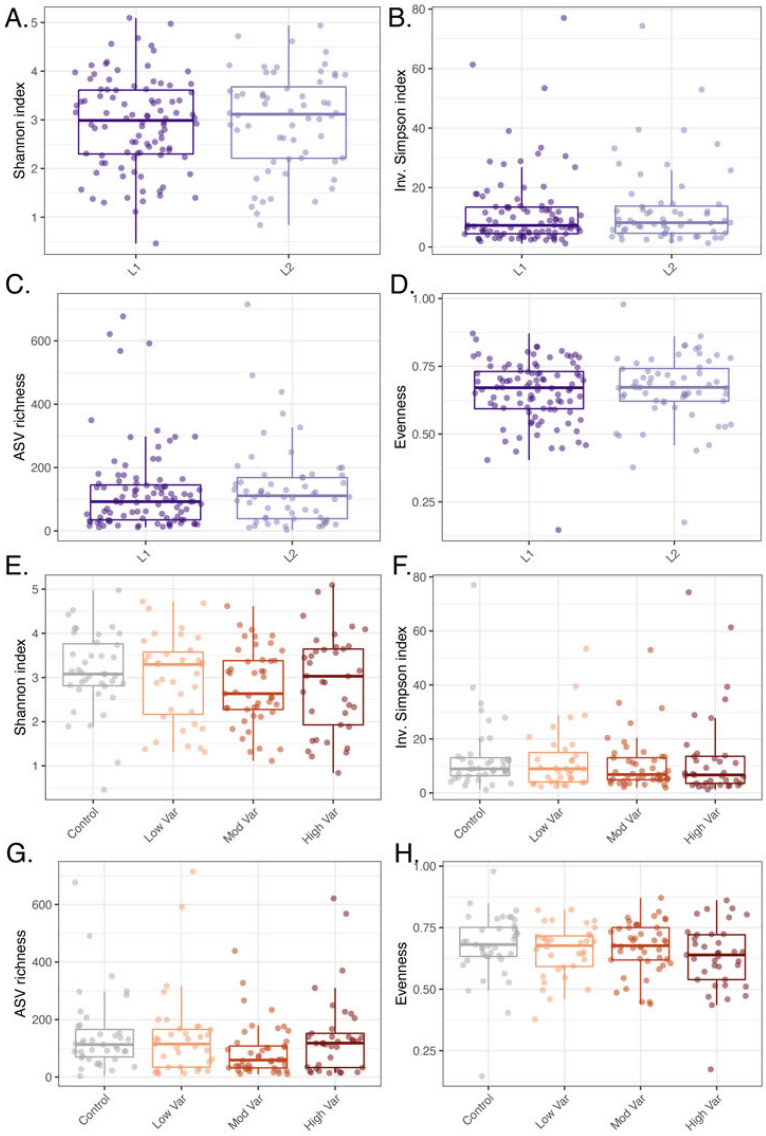


**Figure A2-5.**
**Microbiome diversity is not influenced by cryptic host lineage or diel temperature variability (DTV) treatment.** Diversity metrics, including Shannon index (**a,e**), Inverse Simpson index (**b,f**), ASV richness (**c,g**), and Evenness (**d,h**), presented by cryptic host lineage (**a-d**) and DTV treatment (**e-h**). All diversity metrics were calculated using cleaned data (contaminant ASVs removed, but not trimmed or rarefied). Colors represent lineage (**a-d**: dark purple = L1, light purple = L2) or DTV treatment (**e-h**: control = gray, low variability [Low Var] = light red, moderate variability [Mod Var] = medium red, and high variability [High Var] = dark red). Sample sizes for each lineage are N=96 (L1) and N=60 (L2). Sample sizes for each DTV treatment are N=39 (Control), N=35 (Low Var), N=45 (Mod Var), N=37 (High Var).

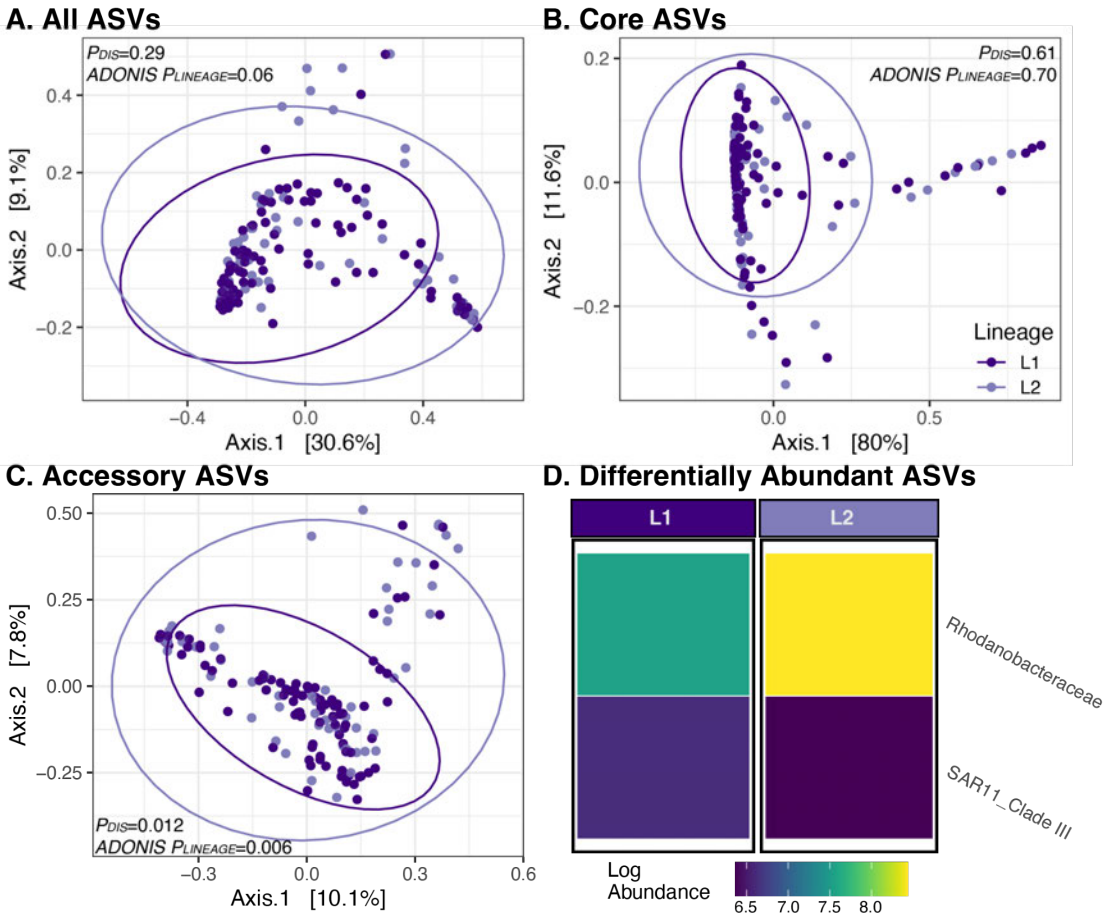


**Figure A2-6.**

**Coral microbiomes are stable across cryptic host lineages.** Bray-Curtis dissimilarity principal coordinate analyses (PCAs) of coral microbiomes for all ASVs (**a**), core ASVs (**b**), and accessory ASVs (**c**). Ellipses in (**a-c**) represent 95% confidence intervals, *ADONIS P*-values indicate significant community differences, and $P_{DIS}$ values compare dispersion across lineages. (**d**) Two differentially abundant ASVs across lineage determined based on ANCOM's W-statistic (>0.6 cut-off), presented at the level of Family. All plots are based on trimmed and rarefied relative abundance data with N=149 samples.

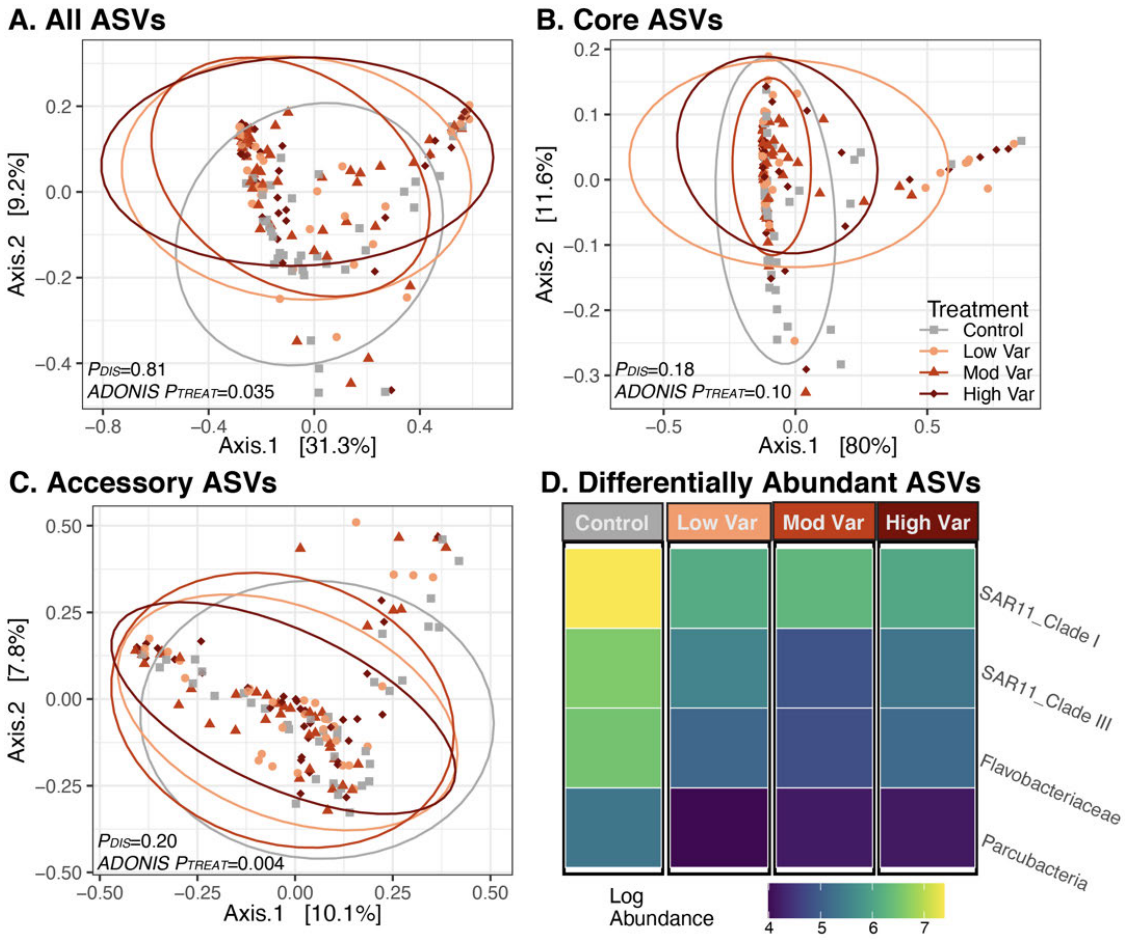


**Figure A2-7.**
**Coral microbiomes shift in response to daily temperature variability (DTV).** Bray-Curtis dissimilarity principal coordinate analyses (PCAs) of coral microbiomes colored by DTV treatment for all ASVs (**a**), core ASVs (**b**), and accessory ASVs (**c**). Ellipses in (**a-c**) represent 95% confidence intervals, *ADONIS P*-values indicate significant community differences, and $P_{DIS}$ values compare dispersion across DTV treatments. (**d**) Four differentially abundant ASVs across DTV treatment determined based on ANCOM's W-statistic (>0.6 cut-off), presented at the level of Family. All plots are based on trimmed and rarefied relative abundance data with N=149 samples.

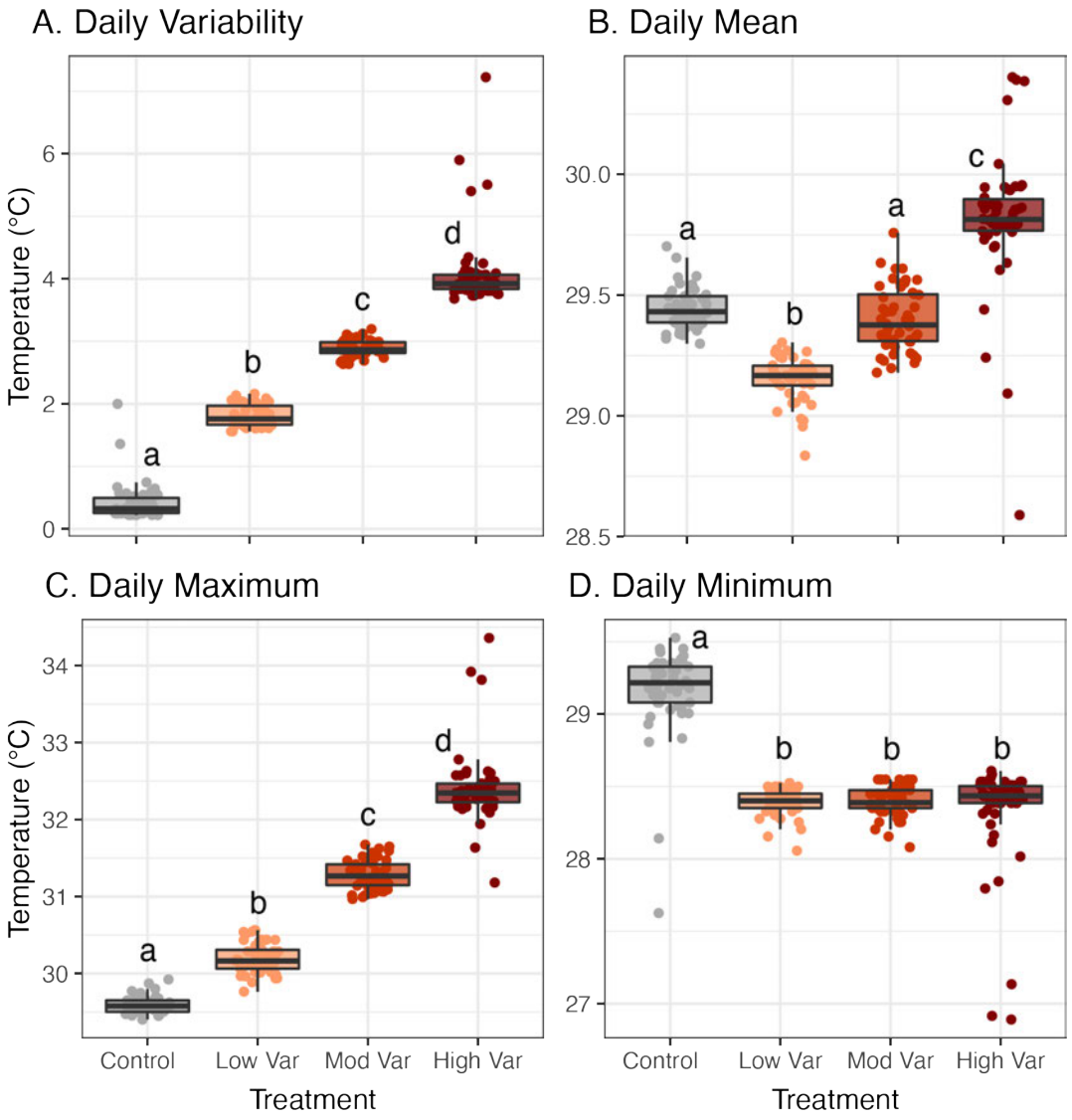


**Figure A2-8.**
**Temperature characteristics of diel temperature variability (DTV) treatments.** Temperature data recorded using HOBO loggers for the duration of the 50-day DTV experiment (September 22, 2016 - November 10, 2016). For all box plots, each point represents one day of temperature data per treatment. Temperature metrics include: (**a**) diel temperature variability (DTV), (**b**) daily mean temperatures, (**c**) daily maximum temperatures, and (**d**) daily minimum temperatures. Distinct letters indicate significant differences in temperature parameters from ANOVA and Tukey's HSD post-hoc tests.

**Table A2-1.**
***In situ* site metadata and *ex situ* experimental treatment conditions.**
**(A)** Site ID, type, and GPS coordinates for sites where *Siderastrea siderea* (N=9 colonies/site) were collected across the Bocas del Toro Reef Complex, Panamá (SP=STRI Point, PD=Punta Donato, CI=Cristobal Island, CA=Cayo de Agua, BN=Bastimentos North, and BS=Bastimentos South). Average, minimum, and maximum daily temperature parameters (°C) are reported for four sites where temperature loggers were recovered (SP, PD, CI, and CA). When error is shown, values represent means ± standard error (SE). When no error is shown, values represent maximum values. **(B)** All values are reported as overall means of the daily mean ± standard deviation of the temperature parameters throughout the 50-day diel temperature variability (DTV) treatments. DTV treatments were statistically distinct (all pairwise comparison *p*-values<0.0001), as were mean temperatures (all pairwise comparison *p*-values<0.0001). Daily maximum temperatures increased with variability treatments (all pairwise comparison *p*-values<0.0001), and daily minimum temperatures were lower in all variability treatments compared to the control.

**A) *In situ* site metadata**

| Site | Type | GPS | Daily Mean | Daily Min | Daily Max | DTV | Max DTV | Overall Max |
|---|---|---|---|---|---|---|---|---|
| SP | Inshore | 9.352434, -82.264553 | 29.32 ± 0.040°C | 29.07 ± 0.040°C | 29.63 ± 0.042°C | 0.56 ± 0.011°C | 1.26°C | 31.59°C |
| PD | Inshore | 9.36924, -82.364037 | 29.71 ± 0.043°C | 29.37 ± 0.043°C | 30.08 ± 0.045°C | 0.70 ± 0.012°C | 1.32°C | 32.15°C |
| CI | Inshore | 9.2654486, -82.243511 | 29.89 ± 0.047°C | 29.39 ± 0.045°C | 30.58 ± 0.056°C | 1.18 ± 0.029°C | 2.86°C | 33.55°C |
| CA | Offshore | 9.193858, -82.053951 | 29.48 ± 0.047°C | 29.02 ± 0.044°C | 29.99 ± 0.052°C | 0.98 ± 0.020°C | 2.41°C | 32.43°C |
| BN | Offshore | 9.348495, -82.176505 | N/A | N/A | N/A | N/A | N/A | N/A |
| BS | Offshore | 9.287438, -82.092315 | N/A | N/A | N/A | N/A | N/A | N/A |

**B) *Ex situ* experimental conditions (Figure A2-8)**

| Treatment | Variability | Mean | Maximum | Minimum |
|---|---|---|---|---|
| Control | 0.43 ± 0.30 | 29.45°C ± 0.084 | 29.59°C ± 0.11 | 28.48°C ± 0.31 |
| Low Var | 1.81°C ± 0.17 | 29.15°C ± 0.092 | 30.20°C ± 0.19 | 27.67°C ± 0.09 |

| | | | | |
|---|---|---|---|---|
| Mod Var | 2.88°C ± 0.13 | 31.28°C ± 0.19 | 31.28°C ± 0.19 | 27.63°C ± 0.11 |
| High Var | 4.10°C ± 0.62 | 32.41°C ± 0.49 | 32.41°C ± 0.49 | 27.61°C ± 0.38 |

**Table A2-2.**
ANOVA and Tukey's HSD results for daily *in situ* temperature data presented in Figure 3-1b. Explicit models are listed under each section for the metric being considered. Sum Sq=sum of squares, Mean Sq=mean square of the error, DF=degrees of freedom. For Tukey HSD outputs, estimate, lower, and upper columns represent the difference between the compared mean values and 95% confidence intervals. Punta Donato=PD, STRI Point=SP, Cristobal Island=CI, Bastimentos North=BN, Bastimentos South=BS, Cayo de Agua=CA.

| **Daily *in situ* Temperature Statistics (Figure 3-1b)** | | | | | |
|---|---|---|---|---|---|
| **Factor/Comparison** | **DF** | **Sum Sq** | **Mean Sq** | **F-value** | **P-value** |
| ***Daily Range*** | **Model = aov(DailyRange ~ site of origin)** | | | | |
| | 3 | 85.08 | 28.359 | 204.6 | <2e-16 |
| ***Tukey HSD*** | | **Estimate** | **Lower** | **Upper** | **P-value** |
| PD-SP | | 0.144 | 0.073 | 0.215 | 1.2e6 |
| CA-SP | | 0.417 | 0.346 | 0.488 | 0 |
| CI-SP | | 0.623 | 0.552 | 0.694 | 0 |
| CA-PD | | 0.273 | 0.202 | 0.344 | 0 |
| CI-PD | | 0.479 | 0.409 | 0.550 | 0 |
| CI-CA | | 0.206 | 0.136 | 0.277 | 0 |
| ***Daily Mean*** | **Model = aov(DailyMean ~ site of origin)** | | | | |
| | 3 | 70.8 | 23.61 | 32.83 | <2e-16 |
| ***Tukey HSD*** | | **Estimate** | **Lower** | **Upper** | **P-value** |
| PD-SP | | 0.390 | 0.229 | 0.551 | 0 |
| CA-SP | | 0.160 | -0.002 | 0.321 | 0.053 |
| CI-SP | | 0.578 | 0.416 | 0.739 | 0 |
| CA-PD | | -0.231 | -0.392 | -0.069 | 0.001 |
| CI-PD | | 0.187 | 0.026 | 0.349 | 0.015 |
| CI-CA | | 0.418 | 0.257 | 0.579 | 0 |

**Table A2-3.**
PERMANOVA results for the effect of site of origin on 2bRAD identity by state (IBS) matrix presented in Figure 3-2b. Explicit model is listed. Sum Sq=sum of squares, $R^2$ indicates the percentage of the variance explained.

| **2bRAD PERMANOVA (Figure 3-2b)** | | | | | |
|---|---|---|---|---|---|
| **Factor/Comparison** | **DF** | **Sum Sq** | **$R^2$** | **F-Value** | **P-Value** |
| | **Model = adonis(IBS_Matrix ~ site_of_origin)** | | | | |
| Site of origin | 5 | 0.40473 | 0.21067 | 2.3487 | 0.001 |

**Table A2-4.**
PERMANOVA results from holobiont phenome data presented in Figure 3-2c, Figure 3-3a-b, and Figure A2-4. Explicit models are listed under each section for the time point being considered (Initial and End of diel temperature variability [DTV] treatment). Sum Sq=sum of squares, Mean Sq=mean square of the error, DF=degrees of freedom, $R^2$=percentage of variance explained, Omega-sq=effect size. N=42 for initial time point and N=97 for end of DTV time point.

| **Holobiont Phenome Physiology PERMANOVA Statistics (Figure 3-2c, Figure 3-3a-b & Figure A2-4)** | | | | | | | |
|---|---|---|---|---|---|---|---|
| **Factor/ Comparison** | **DF** | **Sum Sq** | **Mean Sq** | **F-Value** | **$R^2$** | **Omega-sq** | **P-value** |
| ***Initial (T0)*** | **Model = adonis(scores ~ lineage + site_of_origin)** | | | | | | |
| Lineage | 1 | 0.031 | 0.031 | 20.837 | 0.333 | 0.321 | 9.99e-05 |
| Site of origin | 5 | 0.010 | 0.002 | 1.364 | 0.109 | 0.042 | 0.190 |
| ***End of DTV*** | **Model = adonis(scores ~ lineage + dominant_sym + dtv_treatment + site_of_origin)** | | | | | | |
| Lineage | 1 | 0.032 | 0.032 | 10.67 | 0.088 | 0.091 | 0.0002 |
| Dominant symbiont | 3 | 0.004 | 0.001 | 0.406 | 0.010 | -0.019 | 0.905 |
| Treatment | 3 | 0.036 | 0.014 | 4.57 | 0.113 | 0.099 | 0.0009 |
| Site of origin | 5 | 0.249 | 0.007 | 2.43 | 0.100 | 0.067 | 0.010 |

**Table A2-5.**
Linear model and Tukey's HSD results for corallite area differences across lineages, presented in Figure A2-1. The explicit model is listed. DF=degrees of freedom, SE=standard error. L1=lineage 1, L2=lineage 2, L3=lineage 3.

| **Corallite Area Statistics (Figure A2-1)** | | | | | |
|---|---|---|---|---|---|
| **Factor/Comparison** | **Estimate** | **SE** | **DF** | **T-value** | **P-value** |
| ***Corallite Area*** | | **Model = lmer(corallite_area ~ lineage + (1\|genet))** | | | |
| Intercept | 8.7252 | 0.3435 | 44.7154 | 25.404 | <2e-16 |
| Lineage (L2) | 5.1702 | 0.5718 | 44.8748 | 9.042 | 1.13e-11 |
| Lineage (L3) | 8.5199 | 1.1102 | 44.9221 | 7.674 | 1.04e-09 |
| ***Tukey HSD*** | **Estimate** | **SE** | **DF** | **T-value** | **P-value** |
| L1 – L2 | -5.17 | 0.574 | 44.2 | -9.009 | <0.001 |
| L1 – L3 | -8.52 | 1.111 | 44.5 | -7.666 | <0.001 |
| L2 – L3 | -3.35 | 1.151 | 44.6 | -2.911 | 0.0152 |

**Table A2-6.**
Linear model results for coral growth data presented in Figures 3-3c and A2-2a. Explicit models are listed under each section for the time point being considered (during variability, or during heat stress and recovery). Low Variability=Low Var, Moderate Variability=Mod Var, High Variability=High Var. Sample sizes are as follows during variability: Control DTV (L1=24, L2=15), Low Var (L1=22, L2=14), Mod Var (L1=25, L2=18), High Var (L1=22, L2=17). Sample sizes are as follows during heat stress and recovery: Control DTV (L1=24, L2=13), Low Var (L1=21, L2=12), Mod Var (L1=25, L2=17), High Var (L1=22, L2=17).

| **Coral Growth Statistics (Figure 3-3c & Figure A2-2a)** | | | | | |
|---|---|---|---|---|---|
| **Factor/Comparison** | **Estimate** | **Std. Error** | **DF** | **T-value** | **P-value** |
| ***During Variability*** | **Model = lmer(growth ~ treatment + lineage + (1\|genet))** | | | | |
| Intercept | 1.3703 | 0.238 | 85.13 | 5.77 | 1.25e-07 |
| Treatment(Low Var) | 0.288 | 0.218 | 112.26 | 1.32 | 0.19 |
| Treatment(Mod Var) | 0.580 | 0.207 | 111.54 | 2.80 | 0.006 |
| Treatment(High Var) | 0.581 | 0.214 | 112.33 | 2.72 | 0.008 |
| Lineage(L2) | -0.675 | 0.320 | 45.27 | -2.11 | 0.04 |
| ***During Heat Stress + Recovery*** | **Model = lmer(growth ~ treatment + lineage + (1\|genet))** | | | | |
| Intercept | 2.302 | 0.240 | 94.86 | 9.575 | 1.34e-15 |
| Treatment(Low Var) | 0.085 | 0.249 | 108.97 | 0.339 | 0.735 |
| Treatment(Mod Var) | 0.285 | 0.232 | 107.33 | 1.25 | 0.223 |
| Treatment(High Var) | 0.248 | 0.237 | 107.49 | 1.044 | 0.299 |
| Lineage(L2) | -1.18 | 0.310 | 45.23 | -3.822 | 0.0004 |

**Table A2-7.**
ANOVA results from microbiome diversity data, including separate analyses for Shannon Index, Simpson Index, OTU Richness, and Evenness, presented in Figure A2-5. Explicit models are listed under each section for the data being considered. Sum Sq=sum of squares, DF=degrees of freedom.

| **Microbiome Diversity Statistics (Figure A2-5)** | | | | | |
|---|---|---|---|---|---|
| **Shannon Index** | | | | | |
| **Factor/Comparison** | **DF** | **Sum Sq** | **Mean Sq** | **F-value** | **P-value** |
| | **Model = aov(Shannon ~ DTV treatment + lineage)** | | | | |
| DTV Treatment | 3 | 2.81 | 0.9362 | 1.006 | 0.392 |
| Lineage | 1 | 0.15 | 0.1530 | 0.164 | 0.686 |
| **Simpson Index** | | | | | |
| | **Model = aov(Simpson ~ DTV treatment + lineage)** | | | | |
| DTV Treatment | 3 | 1.40 | 0.4651 | 0.658 | 0.579 |
| Lineage | 1 | 0.39 | 0.3872 | 0.547 | 0.461 |
| **OTU Richness** | | | | | |
| | **Model = aov(Richness ~ DTV treatment + lineage)** | | | | |
| DTV Treatment | 3 | 6.50 | 2.1655 | 2.188 | 0.0918 |
| Lineage | 1 | 0.08 | 0.0800 | 0.081 | 0.7766 |
| **Evenness** | | | | | |
| | **Model = aov(Evenness ~ DTV treatment + lineage)** | | | | |
| DTV Treatment | 3 | 0.0496 | 0.016546 | 1.134 | 0.337 |
| Lineage | 1 | 0.0064 | 0.006379 | 0.437 | 0.509 |

**Table A2-8.**
Betadispersion and PERMANOVA results from microbiome data, including separate analyses for core taxa, accessory taxa, and all ASVs, presented in Figures A2-6 and A2-7. Explicit models are listed under each section for the data being considered. Sum Sq=sum of squares, DF=degrees of freedom, $R^2$=percentage of variance explained.

| **Microbiome Spatial Statistics (Figures A2-6, A2-7)** | | | | | |
|---|---|---|---|---|---|
| **Core Microbiome Dispersion** | | | | | |
| **Factor/Comparison** | **DF** | **Sum Sq** | **Mean Sq** | **F-value** | **P-value** |
| | **Model = betadisper(distance.coretaxa ~ DTV treatment)** | | | | |
| DTV Treatment | 3 | 0.2115 | 0.070495 | 1.6587 | 0.1786 |
| | **Model = betadisper(distance.coretaxa ~ lineage)** | | | | |
| Lineage | 1 | 0.0108 | 0.010836 | 0.2556 | 0.6139 |
| **Core Microbiome Spatial Structure** | | | | | |
| **Factor/Comparison** | **DF** | **Sum Sq** | **$R^2$** | **F-Value** | **P-value** |
| | **Model = adonis(core.taxa ~ DTV treatment + lineage, permutations = 999)** | | | | |
| DTV Treatment | 3 | 0.3886 | 0.03698 | 1.84759 | 0.123 |
| Lineage | 1 | 0.0237 | 0.00226 | 0.33801 | 0.703 |
| **Accessory Microbiome Dispersion** | | | | | |
| **Factor/Comparison** | **DF** | **Sum Sq** | **Mean Sq** | **F-value** | **P-value** |
| | **Model = betadisper(distance.accessorytaxa ~ DTV treatment)** | | | | |
| DTV Treatment | 3 | 0.009255 | 0.0030849 | 1.5509 | 0.2039 |
| | **Model = betadisper(distance.accessorytaxa ~ lineage)** | | | | |
| Lineage | 1 | 0.010496 | 0.0104957 | 6.398 | 0.01248 |
| **Accessory Microbiome Spatial Structure** | | | | | |
| **Factor/Comparison** | **DF** | **Sum Sq** | **$R^2$** | **F-Value** | **P-value** |
| | **Model = adonis(accessory.taxa ~ DTV treatment + lineage, permutations = 999)** | | | | |
| DTV Treatment | 3 | 1.871 | 0.02911 | 1.4571 | 0.004 |
| Lineage | 1 | 0.761 | 0.01185 | 1.7791 | 0.006 |

| **All ASVs Dispersion** | | | | | |
|---|---|---|---|---|---|
| **Factor/Comparison** | **DF** | **Sum Sq** | **Mean Sq** | **F-value** | **P-value** |
| | **Model = betadisper(distance. taxa ~ DTV treatment)** | | | | |
| DTV Treatment | 3 | 0.0346 | 0.011536 | 0.3152 | 0.8144 |
| | **Model = betadisper(distance. taxa ~ lineage)** | | | | |
| Lineage | 1 | 0.0371 | 0.037137 | 1.133 | 0.2889 |
| **All ASVs Spatial Structure** | | | | | |
| **Factor/Comparison** | **DF** | **Sum Sq** | **$R^2$** | **F-Value** | **P-value** |
| | **Model = adonis(accessory.taxa ~ DTV treatment + lineage, permutations = 999)** | | | | |
| DTV Treatment | 3 | 1.196 | 0.03182 | 1.5971 | 0.035 |
| Lineage | 1 | 0.449 | 0.01194 | 1.7988 | 0.060 |

**Table A2-9.**
Betadispersion and PERMANOVA results from Symbiodiniaceae spatial data, presented in Figure A2-3. Explicit models are listed under each section for the data being considered. Sum Sq=sum of squares, DF=degrees of freedom, $R^2$=percentage of variance explained.

| **Symbiodiniaceae Spatial Statistics (Figure A2-3)** | | | | | |
|---|---|---|---|---|---|
| **Symbiodiniaceae Dispersion** | | | | | |
| **Factor/Comparison** | **DF** | **Sum Sq** | **Mean Sq** | **F-value** | **P-value** |
| | **Model = betadisper(distance.its2 ~ DTV treatment)** | | | | |
| DTV Treatment | 3 | 0.00413 | 0.0013761 | 0.2562 | 0.8568 |
| | **Model = betadisper(distance its2 ~ lineage)** | | | | |
| Lineage | 1 | 0.0356 | 0.035633 | 0.9397 | 0.3339 |
| | **Model = betadisper(distance its2 ~ site)** | | | | |
| Site of origin | 5 | 1.3691 | 0.27382 | 1.8048 | 0.1152 |
| **Symbiodiniaceae Spatial Structure** | | | | | |
| **Factor/Comparison** | **DF** | **Sum Sq** | **$R^2$** | **F-Value** | **P-value** |
| | **Model = adonis(core.taxa ~ DTV treatment + site + lineage, permutations = 999)** | | | | |
| DTV Treatment | 3 | 0.973 | 0.01574 | 1.0206 | 0.402 |
| Site of origin | 5 | 13.595 | 0.21989 | 8.5538 | 0.001 |
| Lineage | 1 | 0.849 | 0.01373 | 2.6712 | 0.025 |

**Table A2-10.**
Linear model results for photochemical efficiency (Fv/Fm) data presented in Figures 3-4a,c and Figure A2-2b. Explicit model is listed. Sample sizes for each treatment are as follows: Control (N=27), Low Variability (N=33), Moderate Variability (N=29), High Variability (N=31).

| **Photochemical Efficiency (Fv/Fm) Statistics (Figure 3-4a,c & Figure A2-2b)** | | | |
|---|---|---|---|
| **Factor/Comparison** | **Chi Sq** | **DF** | **P-value** |
| **Model = lmer(fvfm ~ time*lineage*dominant_sym*dtv_treatment + 1\|genet)** | | | |
| Time | 89.69 | 6 | <2e-16 |
| Lineage | 7.517 | 1 | 0.006 |
| Dominant Symbiont | 39.056 | 3 | 1.689e-8 |
| Treatment | 7.866 | 3 | 0.049 |
| Time*Lineage | 8.124 | 6 | 0.229 |
| Time*Dominant Symbiont | 52.16 | 18 | 3.532e-5 |
| Lineage*Dominant Symbiont | 0.043 | 1 | 0.835 |
| Time*Treatment | 34.52 | 18 | 0.011 |
| Lineage*Treatment | 3.944 | 3 | 0.268 |
| Dominant Symbiont *Treatment | 64.92 | 7 | 1.564e-11 |
| Time*Lineage*Dominant Symbiont | 17.65 | 6 | 0.007 |
| Time*Lineage*Treatment | 8.754 | 18 | 0.965 |
| Time*Dominant Symbiont*Treatment | 36.33 | 42 | 0.718 |
| Lineage*Dominant Symbiont*Treatment | 2.782 | 3 | 0.427 |
| Time*Lineage*Dominant Symbiont*Treatment | 16.36 | 18 | 0.567 |

**Table A2-11.**
ANOVA and Tukey's HSD results for *ex situ* experiment temperature data presented in Figure A2-8. Explicit models are listed under each section for the temperature metric being considered. Sum Sq=sum of squares, Mean Sq=mean square of the error, DF=degrees of freedom, SE=standard error. For Tukey HSD outputs, estimate, lower, and upper columns represent the difference between the compared mean values and 95% confidence intervals.

| **Daily DTV Treatment Temperature Statistics (Figure A2-8)** | | | | | |
|---|---|---|---|---|---|
| **Factor/Comparison** | **DF** | **Sum Sq** | **Mean Sq** | **F-value** | **P-value** |
| ***Daily Range*** | **Model = aov(DailyRange ~ treatment)** | | | | |
| DTV Treatment | 3 | 365 | 121.67 | 929.4 | <2e-16 |
| ***Tukey HSD*** | | **Estimate** | **Lower** | **Upper** | **P-value** |
| Low Var - Control | | 1.377 | 1.189 | 1.564 | 0 |
| Mod Var - Control | | 2.453 | 2.265 | 2.640 | 0 |
| High Var - Control | | 3.665 | 3.477 | 3.852 | 0 |
| Mod Var - Low Var | | 1.076 | 0.889 | 1.264 | 0 |
| High Var - Low Var | | 2.288 | 2.100 | 2.475 | 0 |
| High Var - Mod Var | | 1.212 | 1.024 | 1.399 | 0 |
| **Factor/Comparison** | **DF** | **Sum Sq** | **Mean Sq** | **F-value** | **P-value** |
| ***Daily Mean*** | **Model = aov(DailyMean ~ treatment)** | | | | |
| DTV Treatment | 3 | 11.102 | 3.701 | 127.6 | <2e-16 |
| ***Tukey HSD*** | | **Estimate** | **Lower** | **Upper** | **P-value** |
| Low Var - Control | | -0.294 | -0.382 | -0.205 | 0 |
| Mod Var - Control | | -0.046 | -0.134 | 0.043 | 0.540 |
| High Var - Control | | 0.366 | 0.278 | 0.454 | 0 |
| Mod Var - Low Var | | 0.248 | 0.160 | 0.336 | 0 |
| High Var - Low Var | | 0.660 | 0.571 | 0.748 | 0 |
| High Var - Mod Var | | 0.412 | 0.323 | 0.500 | 0 |
| **Factor/Comparison** | **DF** | **Sum Sq** | **Mean Sq** | **F-value** | **P-value** |
| ***Daily Minimum*** | **Model = aov(DailyMin ~ treatment)** | | | | |

| | | | | | |
|---|---|---|---|---|---|
| DTV Treatment | 3 | 23.83 | 7.942 | 121.8 | <2e-16 |
| ***Tukey HSD*** | | **Estimate** | **Lower** | **Upper** | **P-value** |
| Low Var - Control | | -0.769 | -0.902 | -0.637 | 0 |
| Mod Var - Control | | -0.762 | -0.894 | -0.630 | 0 |
| High Var - Control | | -0.849 | -0.981 | -0.716 | 0 |
| Mod Var - Low Var | | 0.007 | -0.125 | 0.139 | 0.999 |
| High Var - Low Var | | -0.079 | -0.212 | 0.053 | 0.408 |
| High Var - Mod Var | | -0.086 | -0.219 | 0.046 | 0.330 |
| **Factor/Comparison** | **DF** | **Sum Sq** | **Mean Sq** | **F-value** | **P-value** |
| ***Daily Maximum*** | | | | **Model = aov(DailyMax ~ treatment)** | |
| DTV Treatment | 3 | 230.94 | 76.98 | 956.1 | <2e-16 |
| ***Tukey HSD*** | | **Estimate** | **Lower** | **Upper** | **P-value** |
| Low Var - Control | | 0.608 | 0.460 | 0.755 | 0 |
| Mod Var - Control | | 1.690 | 1.544 | 1.838 | 0 |
| High Var - Control | | 2.816 | 2.669 | 2.963 | 0 |
| Mod Var - Low Var | | 1.083 | 0.936 | 1.230 | 0 |
| High Var - Low Var | | 2.209 | 2.061 | 2.356 | 0 |
| High Var - Mod Var | | 1.125 | 0.978 | 1.272 | 0 |

# APPENDIX 3: CHAPTER 4 SUPPLEMENT

## A3.1. Supplementary Figures

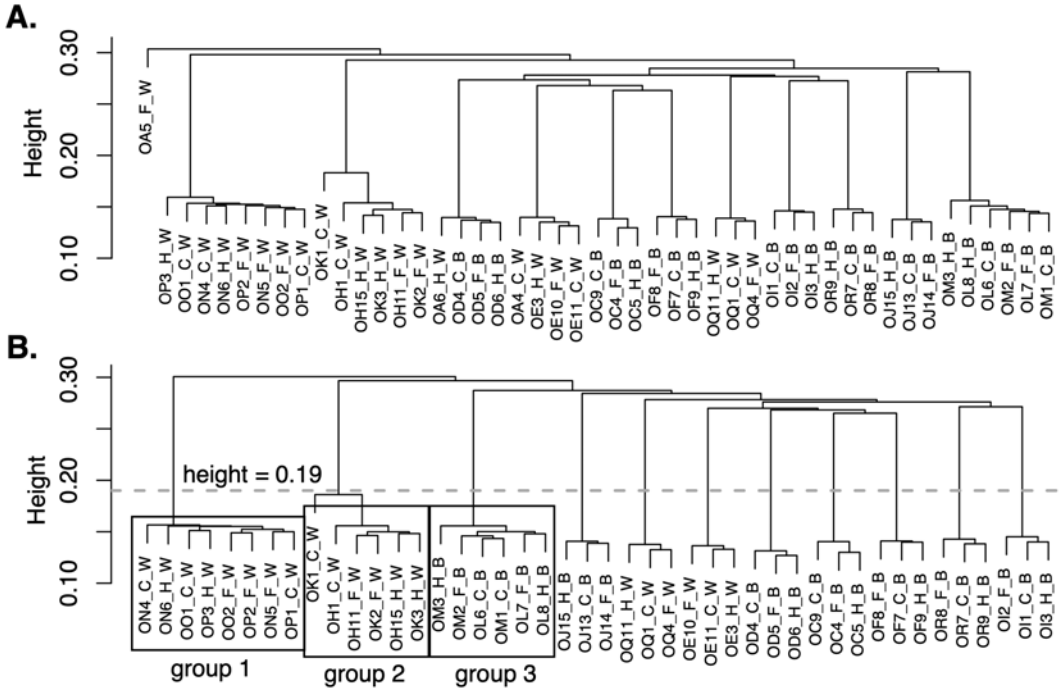


**Figure A3-1.**
Identity by state (IBS) cluster dendrograms of *Oculina arbuscula* fragments, both with (**a**) and without (**b**) genotype A. (**b**) IBS cluster dendrogram indicates three putative clonal groups each containing more than one putative genotype, identified with black boxes. The dashed line at height = 0.19 represents the cutoff for clone assignments, and the remaining groups outside of the three boxes indicate replicate fragments from the same genotype distributed across temperature challenge treatments. Sample IDs include information on genotype, fragment number, temperature challenge treatment, and symbiotic state. All samples start with 'O', indicating the coral species *O. arbuscula*, followed by a second letter denoting genet and a number, which denotes the fragment number. The letter following the first '_' indicates temperature treatment (C = control, F = cold, H = heat) and the final letter indicates symbiotic state (W = aposymbiotic (white), B = symbiotic (brown)).

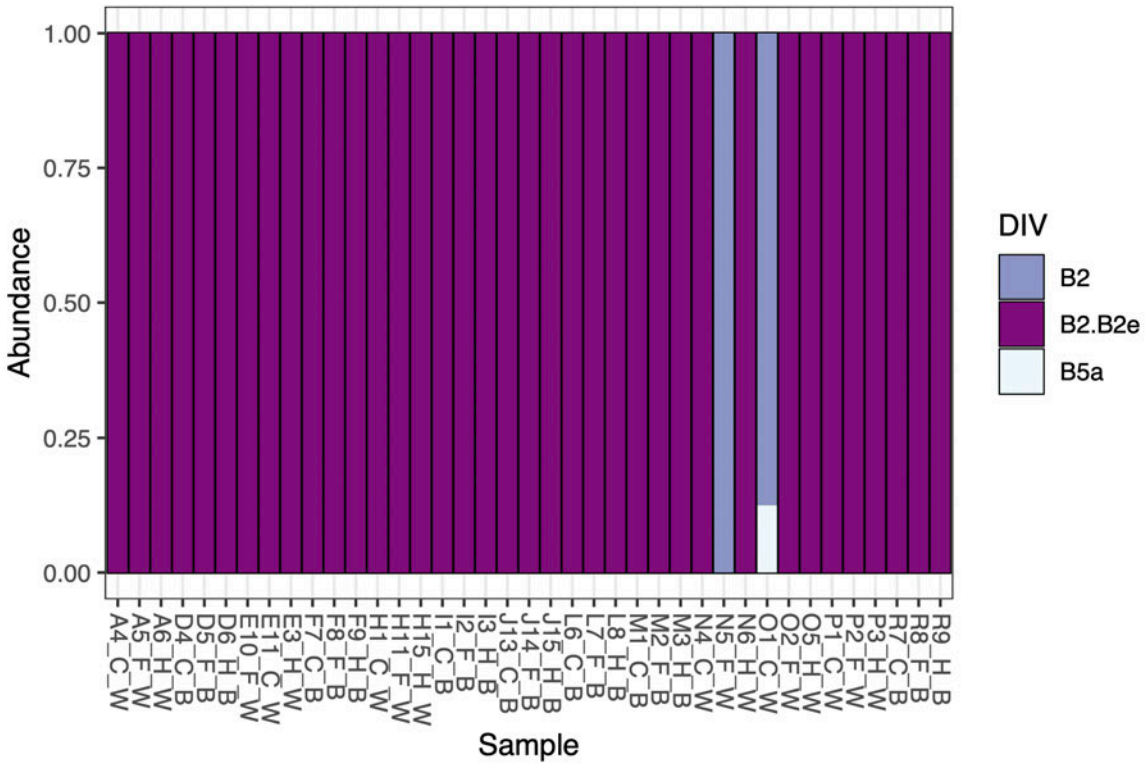


**Figure A3-2.**
Bar plots of Symbiodiniaceae defining intragenomic variants (DIVs) hosted by *Oculina arbuscula*, colored by DIV. Each column of the bar plot represents one *O. arbuscula* fragment. Sample names include genotype, fragment number, temperature treatment (C = control, F = cold challenge, H = heat challenge), and symbiotic state (W = aposymbiotic (white), B = symbiotic (brown)). For example, A4_C_W can be interpreted as follows: genotype A, fragment 4, control treatment, aposymbiotic.

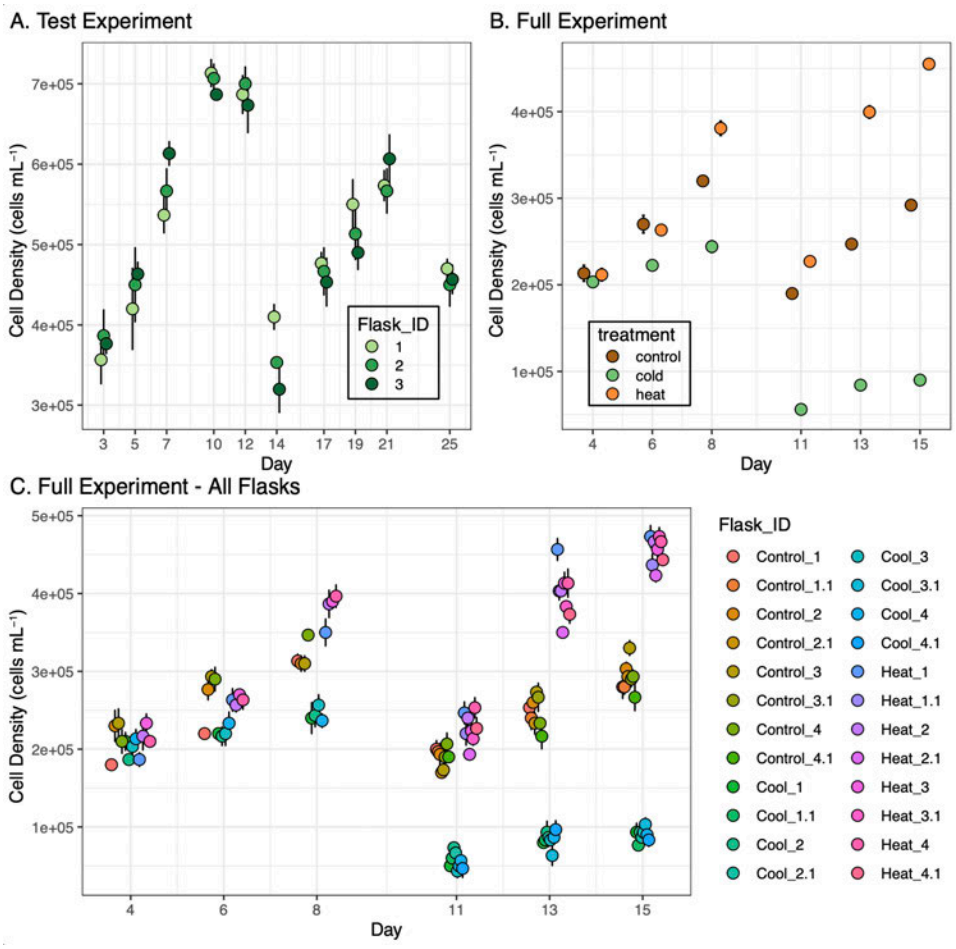


**Figure A3-3.**
***Ex hospite Breviolum psygmophilum* cell growth to establish semi-continuous growth methodology. (a).** Cell density through time during a test experiment to determine timing of exponential and stationary growth phases of *B. psygmophilum* cultures under control conditions (18°C). The three replicate flasks reached stationary phase on approximately day 12, which informed later transfers to fresh media on day 10 (**b,c**) to maintain cultures in the exponential growth phase following semi-continuous culturing methodology. (**b,c**) Cell density through time during the *ex hospite* photobiont experiment, where transfers to fresh media occurred on day 10. The same data are presented in both panels **b** and **c**, but data are aggregated across replicate flasks in panel **b** while data from all individual flasks are shown in panel **c**.

## A3.2. Supplementary Tables

**Table A3-1.**
***Oculina arbuscula* and *Breviolum psygmophilum* holobiont sequencing information.** Sample names (Oculina_ID) indicate genotype, fragment number, temperature treatment (C = control, F = cold challenge, H = heat challenge), and symbiotic state (W = aposymbiotic (white), B = symbiotic (brown)). RawReads indicate the number of reads from the unfiltered fastq file. TrimmedReads indicate the number of reads remaining after filtering. MappedReads are the number of reads aligning one time to the concatenated *O. arbuscula* and *B. psygmophilum* reference transcriptome. HostCounts and SymCounts indicate the *O. arbuscula* and *B. psygmophilum* counts used in DESeq, respectively. Asterisks next to sample ID's indicate samples that were removed, either because they were clones (genotypes O, L, K, A) or because of apparent sequencing failure (genotype A).

| Oculina_ID | RawReads | TrimmedReads | MappedReads | HostCounts | SymCounts |
|---|---|---|---|---|---|
| OA4_C_W* | 713004 | 81024 | 12147 | 18323 | 1089 |
| OA5_F_W* | 3804138 | 957178 | 163218 | 221233 | 40560 |
| OA6_H_W* | 6953917 | 1294706 | 236223 | 344287 | 26010 |
| OC4_F_B | 3129577 | 934048 | 186743 | 288914 | 17844 |
| OC5_H_B | 2795155 | 724676 | 130277 | 180792 | 26135 |
| OC9_C_B | 5259035 | 1208042 | 205301 | 318337 | 22893 |
| OD4_C_B | 3136756 | 951626 | 164800 | 255933 | 21264 |
| OD5_F_B | 6030497 | 1673236 | 334379 | 526111 | 37542 |
| OD6_H_B | 3724669 | 1008182 | 179415 | 271569 | 18113 |
| OE10_F_W | 4196932 | 1245305 | 226276 | 380053 | 16239 |
| OE11_C_W | 3308942 | 909105 | 164122 | 244119 | 26366 |
| OE3_H_W | 4162845 | 1317354 | 232765 | 372206 | 20520 |
| OF7_C_B | 2097443 | 605880 | 115258 | 156872 | 20246 |
| OF8_F_B | 2937370 | 969666 | 179015 | 297083 | 12948 |
| OF9_H_B | 12787828 | 1776900 | 281666 | 438839 | 25337 |
| OH11_F_W | 2126834 | 693351 | 196295 | 209505 | 9177 |
| OH15_H_W | 8292392 | 2165705 | 126032 | 534770 | 43978 |
| OH1_C_W | 3782080 | 1130597 | 354041 | 303477 | 28026 |
| OI1_C_B | 8138535 | 2203496 | 419720 | 657766 | 47404 |
| OI2_F_B | 4702871 | 1418771 | 271742 | 417661 | 39203 |
| OI3_H_B | 3848414 | 897870 | 148130 | 232085 | 13119 |
| OJ13_C_B | 6221360 | 1833913 | 341585 | 525116 | 38777 |

| | | | | | |
|---|---|---|---|---|---|
| OJ14_F_B | 8008008 | 2142125 | 406134 | 640399 | 40860 |
| OJ15_H_B | 2255126 | 724997 | 137730 | 189255 | 32169 |
| OK1_C_W* | 833657 | 321054 | 50955 | 84859 | 4020 |
| OK2_F_W* | 6949550 | 1199628 | 204041 | 354591 | 6864 |
| OK3_H_W* | 1802139 | 660720 | 114659 | 194220 | 6332 |
| OL6_C_B* | 3668299 | 1077721 | 205720 | 304863 | 31519 |
| OL7_F_B* | 4727630 | 1335005 | 256529 | 398154 | 33031 |
| OL8_H_B* | 2466305 | 790985 | 146068 | 216377 | 15962 |
| OM1_C_B | 7295614 | 1938251 | 350216 | 528331 | 37088 |
| OM2_F_B | 1853944 | 619682 | 121936 | 180069 | 15985 |
| OM3_H_B | 2884074 | 871352 | 178897 | 224827 | 49798 |
| ON4_C_W | 4824787 | 1355099 | 244121 | 404358 | 10913 |
| ON5_F_W | 16246514 | 4022360 | 741401 | 1245818 | 16411 |
| ON6_H_W | 4920306 | 790076 | 115833 | 197072 | 4483 |
| OO1_C_W* | 5739490 | 1659319 | 288043 | 492086 | 7458 |
| OO2_F_W* | 3620699 | 1177521 | 216080 | 364733 | 5697 |
| OP1_C_W* | 5471120 | 1520681 | 260562 | 434079 | 13265 |
| OP2_F_W* | 4596831 | 1275987 | 238375 | 409622 | 8280 |
| OP3_H_W* | 6076638 | 1231158 | 209973 | 320730 | 25153 |
| OQ11_H_W | 8004810 | 1825271 | 156895 | 378358 | 38204 |
| OQ1_C_W | 3568498 | 969113 | 253911 | 269162 | 5799 |
| OQ4_F_W | 9668834 | 2864331 | 556904 | 897646 | 49375 |
| OR7_C_B | 3930279 | 1070544 | 180214 | 284083 | 23315 |
| OR8_F_B | 4983180 | 1287597 | 258211 | 392987 | 27428 |
| OR9_H_B | 4230653 | 676034 | 95841 | 149213 | 12362 |

**Table A3-2.**
***Breviolum psygmophilum* in culture (*ex hospite*) sequencing information.** Culture names (Culture_ID) indicate the treatment and replicate number (1-4), and dashes after the replicate number (-1) represent cultures that were split on day 10 to maintain exponential growth using the semi-continuous method. Culture flasks in the cool treatment have four instead of eight replicates because the semi-continuous culture replicates were pooled to get enough RNA for sequencing. RawReads indicate the number of reads from the unfiltered fastq file. TrimmedReads indicate the number of reads remaining after filtering. Mapped reads are the number of reads aligning one time to the reference transcriptome. Counts indicate the *B. psygmophilum* counts used in DESeq, respectively.

| Culture_ID | RawReads | TrimmedReads | MappedReads | Counts |
|---|---|---|---|---|
| Control-1-1 | 8576577 | 3445558 | 1077887 | 1285858 |
| Control-1 | 9322624 | 3355528 | 1056244 | 1259276 |
| Control-2-1 | 8949773 | 3374355 | 1032055 | 1229172 |
| Control-2 | 8092097 | 2439177 | 668422 | 806901 |
| Control-3-1 | 8013989 | 2765579 | 777245 | 931442 |
| Control-3 | 5053389 | 1720274 | 474485 | 571218 |
| Control-4-1 | 6743878 | 2309182 | 610653 | 728048 |
| Control-4 | 6924866 | 2023393 | 505631 | 603137 |
| Cool-1 | 4595701 | 1541637 | 422413 | 484972 |
| Cool-2 | 5492316 | 2006782 | 611776 | 713239 |
| Cool-3 | 6490381 | 2798699 | 968135 | 1113555 |
| Cool-4 | 6515185 | 2871085 | 1015311 | 1184420 |
| Heat-1-1 | 5405332 | 2627373 | 887841 | 1060861 |
| Heat-1 | 7322437 | 2939714 | 975190 | 1144023 |
| Heat-2-1 | 7897004 | 2661411 | 830809 | 983978 |
| Heat-2 | 6252561 | 2847025 | 983662 | 1154335 |
| Heat-3-1 | 6653011 | 2909299 | 980661 | 1154315 |
| Heat-3 | 6055500 | 1875336 | 512730 | 606975 |
| Heat-4-1 | 7074897 | 2946953 | 1006165 | 1186170 |
| Heat-4 | 6879771 | 2115655 | 580844 | 684762 |

**Table A3-3.**
**Ortholog counts.** Counts indicate the ortholog counts for *Oculina arbuscula* (.host Sample Name) and *Breviolum psygmophilum* (.sym Sample Name) counts used in DESeq.

| Sample Name | Counts |
|---|---|
| OC4_F_B.host | 9218 |
| OC4_F_B.sym | 1225 |
| OC5_H_B host | 4509 |
| OC5_H_B.sym | 1171 |
| OC9_C_B.host | 7256 |
| OC9_C_B.sym | 1526 |
| OD4_C_B host | 6254 |
| OD4_C_B.sym | 1287 |
| OD5_F_B host | 17126 |
| OD5_F_B.sym | 2384 |
| OD6_H_B.host | 7742 |
| OD6_H_B.sym | 951 |
| OE10_F_W.host | 11097 |
| OE11_C_W.host | 6058 |
| OE3_H_W host | 9404 |
| OF7_C_B.host | 4402 |
| OF7_C_B.sym | 949 |
| OF8_F_B host | 9618 |
| OF8_F_B.sym | 1194 |
| OF9_H_B host | 10815 |
| OF9_H_B.sym | 1585 |
| OH1_C_W host | 7007 |
| OH11_F_W.host | 6764 |
| OH15_H_W.host | 14051 |
| OI1_C_B host | 16977 |
| OI1_C_B.sym | 2383 |
| OI2_F_B host | 13358 |
| OI2_F_B.sym | 2561 |

| | |
|---|---|
| OI3_H_B.host | 5213 |
| OI3_H_B.sym | 806 |
| OJ13_C_B.host | 12743 |
| OJ13_C_B.sym | 1852 |
| OJ14_F_B.host | 18929 |
| OJ14_F_B.sym | 2834 |
| OJ15_H_B host | 5493 |
| OJ15_H_B.sym | 1250 |
| OM1_C_B.host | 10745 |
| OM1_C_B.sym | 1890 |
| OM2_F_B.host | 5445 |
| OM2_F_B.sym | 930 |
| OM3_H_B host | 5524 |
| OM3_H_B.sym | 2175 |
| ON4_C_W host | 10097 |
| ON5_F_W.host | 36181 |
| ON6_H_W.host | 4600 |
| OQ1_C_W host | 6384 |
| OQ11_H_W.host | 10828 |
| OQ4_F_W.host | 28179 |
| OR7_C_B.host | 7328 |
| OR7_C_B.sym | 1380 |
| OR8_F_B.host | 13392 |
| OR8_F_B.sym | 1677 |
| OR9_H_B host | 3565 |
| OR9_H_B.sym | 740 |

# BIBLIOGRAPHY

Abrego, David, Karin E Ulstrup, Bette L Willis, and Madeleine J.H van Oppen. 2008. "Species–Specific Interactions between Algal Endosymbionts and Coral Hosts Define Their Bleaching Response to Heat and Light Stress." *Proceedings of the Royal Society B: Biological Sciences* 275 (1648): 2273–82. https://doi.org/10.1098/rspb.2008.0180.

Agostini, Sylvain, Hiroyuki Fujimura, Tomihiko Higuchi, Ikuko Yuyama, Beatriz E. Casareto, Yoshimi Suzuki, and Yoshikatsu Nakano. 2013. "The Effects of Thermal and High-CO2 Stresses on the Metabolism and Surrounding Microenvironment of the Coral Galaxea Fascicularis." *Comptes Rendus Biologies* 336 (8): 384–91. https://doi.org/10.1016/j.crvi.2013.07.003.

Aichelman, Hannah E., Colleen B. Bove, Karl D. Castillo, Jessica M. Boulton, Alyssa C. Knowlton, Olivia C. Nieves, Justin B. Ries, and Sarah W. Davies. 2021. "Exposure Duration Modulates the Response of Caribbean Corals to Global Change Stressors." *Limnology and Oceanography* 66 (8): 3100–3115. https://doi.org/10.1002/lno.11863.

Aichelman, Hannah E., Joseph E. Townsend, Travis A. Courtney, Justin H. Baumann, Sarah W. Davies, and Karl D. Castillo. 2016. "Heterotrophy Mitigates the Response of the Temperate Coral Oculina Arbuscula to Temperature Stress." *Ecology and Evolution* 6 (18): 6758–69. https://doi.org/10.1002/ece3.2399.

Albright, Rebecca, Yuichiro Takeshita, David A. Koweek, Aaron Ninokawa, Kennedy Wolfe, Tanya Rivlin, Yana Nebuchina, Jordan Young, and Ken Caldeira. 2018. "Carbon Dioxide Addition to Coral Reef Waters Suppresses Net Community Calcification." *Nature* 555 (7697): 516–19. https://doi.org/10.1038/nature25968.

Altieri, Andrew H., Seamus B. Harrison, Janina Seemann, Rachel Collin, Robert J. Diaz, and Nancy Knowlton. 2017. "Tropical Dead Zones and Mass Mortalities on Coral Reefs." *Proceedings of the National Academy of Sciences* 114 (14): 3660–65. https://doi.org/10.1073/pnas.1621517114.

Anderson, Kristen D., Neal E. Cantin, Jordan M. Casey, and Morgan S. Pratchett. 2019. "Independent Effects of Ocean Warming versus Acidification on the Growth, Survivorship and Physiology of Two Acropora Corals." *Coral Reefs* 38 (6): 1225–40. https://doi.org/10.1007/s00338-019-01864-y.

Anthony, Kenneth R. N., Mia O. Hoogenboom, Jeffrey A. Maynard, Andréa G. Grottoli, and Rachael Middlebrook. 2009. "Energetics Approach to Predicting Mortality Risk from Environmental Stress: A Case Study of Coral Bleaching." *Functional Ecology* 23 (3): 539–50. https://doi.org/10.1111/j.1365-2435.2008.01531.x.

Apprill, A, S McNally, R Parsons, and L Weber. 2015. “Minor Revision to V4 Region SSU RRNA 806R Gene Primer Greatly Increases Detection of SAR11 Bacterioplankton.” *Aquatic Microbial Ecology* 75 (2): 129–37. https://doi.org/10.3354/ame01753.

Aranda, M., Y. Li, Y. J. Liew, S. Baumgarten, O. Simakov, M. C. Wilson, J. Piel, et al. 2016. “Genomes of Coral Dinoflagellate Symbionts Highlight Evolutionary Adaptations Conducive to a Symbiotic Lifestyle.” *Scientific Reports* 6 (1): 39734. https://doi.org/10.1038/srep39734.

Baker, Andrew C., Peter W. Glynn, and Bernhard Riegl. 2008. “Climate Change and Coral Reef Bleaching: An Ecological Assessment of Long-Term Impacts, Recovery Trends and Future Outlook.” *Estuarine, Coastal and Shelf Science* 80 (4): 435–71. https://doi.org/10.1016/j.ecss.2008.09.003.

Banks, Samantha, and Kristi Foster. 2016. “Baseline Levels of Siderastrea Siderea Bleaching under Normal Environmental Conditions in Little Cayman.” *Open Journal of Marine Science* 7 (1): 142–54. https://doi.org/10.4236/ojms.2017.71011.

Barkan, Alice, and Ian Small. 2014. “Pentatricopeptide Repeat Proteins in Plants.” *Annual Review of Plant Biology* 65 (1): 415–42. https://doi.org/10.1146/annurev-arplant-050213-040159.

Barott, Katie L., Alexander A. Venn, Sidney O. Perez, Sylvie Tambutté, and Martin Tresguerres. 2015. “Coral Host Cells Acidify Symbiotic Algal Microenvironment to Promote Photosynthesis.” *Proceedings of the National Academy of Sciences* 112 (2): 607–12. https://doi.org/10.1073/pnas.1413483112.

Barshis, Daniel J., Charles Birkeland, Robert J. Toonen, Ruth D. Gates, and Jonathon H. Stillman. 2018. “High-Frequency Temperature Variability Mirrors Fixed Differences in Thermal Limits of the Massive Coral Porites Lobata.” *Journal of Experimental Biology* 221 (24): jeb188581. https://doi.org/10.1242/jeb.188581.

Barshis, Daniel J., Jason T. Ladner, Thomas A. Oliver, and Stephen R. Palumbi. 2014. “Lineage-Specific Transcriptional Profiles of Symbiodinium Spp. Unaltered by Heat Stress in a Coral Host.” *Molecular Biology and Evolution* 31 (6): 1343–52. https://doi.org/10.1093/molbev/msu107.

Barshis, Daniel J., Jason T. Ladner, Thomas A. Oliver, François O. Seneca, Nikki Traylor-Knowles, and Stephen R. Palumbi. 2013. “Genomic Basis for Coral Resilience to Climate Change.” *Proceedings of the National Academy of Sciences* 110 (4): 1387–92. https://doi.org/10.1073/pnas.1210224110.

Bates, Douglas, Martin Mächler, Ben Bolker, and Steve Walker. 2015. "Fitting Linear Mixed-Effects Models Using Lme4." *Journal of Statistical Software* 67 (October): 1–48. https://doi.org/10.18637/jss.v067.i01.

Baumann, Justin H., Joseph E. Townsend, Travis A. Courtney, Hannah E. Aichelman, Sarah W. Davies, Fernando P. Lima, and Karl D. Castillo. 2016. "Temperature Regimes Impact Coral Assemblages along Environmental Gradients on Lagoonal Reefs in Belize." *PLOS ONE* 11 (9): e0162098. https://doi.org/10.1371/journal.pone.0162098.

Baumgarten, Sebastian, Till Bayer, Manuel Aranda, Yi Jin Liew, Adrian Carr, Gos Micklem, and Christian R. Voolstra. 2013. "Integrating MicroRNA and MRNA Expression Profiling in Symbiodinium Microadriaticum, a Dinoflagellate Symbiont of Reef-Building Corals." *BMC Genomics* 14 (1): 704. https://doi.org/10.1186/1471-2164-14-704.

Bay, Rachael A., and Stephen R. Palumbi. 2014. "Multilocus Adaptation Associated with Heat Resistance in Reef-Building Corals." *Current Biology* 24 (24): 2952–56. https://doi.org/10.1016/j.cub.2014.10.044.

Bayer, Till, Manuel Aranda, Shinichi Sunagawa, Lauren K. Yum, Michael K. DeSalvo, Erika Lindquist, Mary Alice Coffroth, Christian R. Voolstra, and Mónica Medina. 2012. "Symbiodinium Transcriptomes: Genome Insights into the Dinoflagellate Symbionts of Reef-Building Corals." *PLOS ONE* 7 (4): e35269. https://doi.org/10.1371/journal.pone.0035269.

Bellantuono, Anthony J., Katherine E. Dougan, Camila Granados-Cifuentes, and Mauricio Rodriguez-Lanetty. 2019. "Free-Living and Symbiotic Lifestyles of a Thermotolerant Coral Endosymbiont Display Profoundly Distinct Transcriptomes under Both Stable and Heat Stress Conditions." *Molecular Ecology* 28 (24): 5265–81. https://doi.org/10.1111/mec.15300.

Berkelmans, Ray, and Madeleine J.H van Oppen. 2006. "The Role of Zooxanthellae in the Thermal Tolerance of Corals: A 'Nugget of Hope' for Coral Reefs in an Era of Climate Change." *Proceedings of the Royal Society B: Biological Sciences* 273 (1599): 2305–12. https://doi.org/10.1098/rspb.2006.3567.

Berkelmans, Ray, and B. L. Willis. 1999. "Seasonal and Local Spatial Patterns in the Upper Thermal Limits of Corals on the Inshore Central Great Barrier Reef." *Coral Reefs* 18 (3): 219–28. https://doi.org/10.1007/s003380050186.

Bickford, David, David J. Lohman, Navjot S. Sodhi, Peter K. L. Ng, Rudolf Meier, Kevin Winker, Krista K. Ingram, and Indraneil Das. 2007. "Cryptic Species as a Window on Diversity and Conservation." *Trends in Ecology & Evolution* 22 (3): 148–55. https://doi.org/10.1016/j.tree.2006.11.004.

Boilard, Aurélie, Caroline E. Dubé, Cécile Gruet, Alexandre Mercière, Alejandra Hernandez-Agreda, and Nicolas Derome. 2020. “Defining Coral Bleaching as a Microbial Dysbiosis within the Coral Holobiont.” *Microorganisms* 8 (11): 1682. https://doi.org/10.3390/microorganisms8111682.

Bove, Colleen B. 2022. “RandomFun.” https://doi.org/10.5281/zenodo.5961964.

Bove, Colleen B., Katharine Greene, Sharla Sugierski, Nicola Kriefall, Alexa Huzar, Annabel Hughes, Koty Sharp, Nicole Fogarty, and Sarah W. Davies. 2023. “Exposure to Global Change and Microplastics Elicits an Immune Response in an Endangered Coral.” *Frontiers in Marine Science* 9 (January): 1037130. https://doi.org/10.3389/fmars.2022.1037130.

Bove, Colleen B., Maria Valadez Ingersoll, and Sarah W. Davies. 2022. “Help Me, Symbionts, You’re My Only Hope: Approaches to Accelerate Our Understanding of Coral Holobiont Interactions.” *Integrative and Comparative Biology*, September, icac141. https://doi.org/10.1093/icb/icac141.

Bove, Colleen B., Justin B. Ries, Sarah W. Davies, Isaac T. Westfield, James Umbanhowar, and Karl D. Castillo. 2019. “Common Caribbean Corals Exhibit Highly Variable Responses to Future Acidification and Warming.” *Proceedings of the Royal Society B: Biological Sciences* 286 (1900): 20182840. https://doi.org/10.1098/rspb.2018.2840.

Bove, Colleen B., James Umbanhowar, and Karl D. Castillo. 2020. “Meta-Analysis Reveals Reduced Coral Calcification Under Projected Ocean Warming but Not Under Acidification Across the Caribbean Sea.” *Frontiers in Marine Science* 7. https://www.frontiersin.org/articles/10.3389/fmars.2020.00127.

Bradford, Marion M. 1976. “A Rapid and Sensitive Method for the Quantitation of Microgram Quantities of Protein Utilizing the Principle of Protein-Dye Binding.” *Analytical Biochemistry* 72 (1): 248–54. https://doi.org/10.1016/0003-2697(76)90527-3.

Brading, Patrick, Mark E. Warner, Phillip Davey, David J. Smith, Eric P. Achterberg, and David J. Suggett. 2011. “Differential Effects of Ocean Acidification on Growth and Photosynthesis among Phylotypes of Symbiodinium (Dinophyceae).” *Limnology and Oceanography* 56 (3): 927–38. https://doi.org/10.4319/lo.2011.56.3.0927.

Briand, Julia K., Hector M. Guzmán, and Jennifer M. Sunday. 2023. “Spatio-Temporal Patterns in Coral Reef Composition and Function across an Altered Environmental Gradient: A 15-Year Study in the Caribbean.” *Frontiers in Marine Science* 9. https://www.frontiersin.org/articles/10.3389/fmars.2022.977551.

Brown, B. E. 1997. “Coral Bleaching: Causes and Consequences.” *Coral Reefs* 16 (1): S129–38. https://doi.org/10.1007/s003380050249.

Buckley, Lauren B., and Raymond B. Huey. 2016. “How Extreme Temperatures Impact Organisms and the Evolution of Their Thermal Tolerance.” *Integrative and Comparative Biology* 56 (1): 98–109. https://doi.org/10.1093/icb/icw004.

Burns, John A, Huanjia Zhang, Elizabeth Hill, Eunsoo Kim, and Ryan Kerney. 2017. “Transcriptome Analysis Illuminates the Nature of the Intracellular Interaction in a Vertebrate-Algal Symbiosis.” Edited by Debashish Bhattacharya. *ELife* 6 (May): e22054. https://doi.org/10.7554/eLife.22054.

Burriesci, Matthew S., Theodore K. Raab, and John R. Pringle. 2012. “Evidence That Glucose Is the Major Transferred Metabolite in Dinoflagellate–Cnidarian Symbiosis.” *The Journal of Experimental Biology* 215 (19): 3467–77. https://doi.org/10.1242/jeb.070946.

Butchart, Stuart H. M., Matt Walpole, Ben Collen, Arco van Strien, Jörn P. W. Scharlemann, Rosamunde E. A. Almond, Jonathan E. M. Baillie, et al. 2010. “Global Biodiversity: Indicators of Recent Declines.” *Science* 328 (5982): 1164–68. https://doi.org/10.1126/science.1187512.

Callahan, Benjamin J., Paul J. McMurdie, Michael J. Rosen, Andrew W. Han, Amy Jo A. Johnson, and Susan P. Holmes. 2016. “DADA2: High-Resolution Sample Inference from Illumina Amplicon Data.” *Nature Methods* 13 (7): 581–83. https://doi.org/10.1038/nmeth.3869.

Camacho, Christiam, George Coulouris, Vahram Avagyan, Ning Ma, Jason Papadopoulos, Kevin Bealer, and Thomas L. Madden. 2009. “BLAST+: Architecture and Applications.” *BMC Bioinformatics* 10 (1): 421. https://doi.org/10.1186/1471-2105-10-421.

Camp, Emma F., Tim Kahlke, Brandon Signal, Clinton A. Oakley, Adrian Lutz, Simon K. Davy, David J. Suggett, and William P. Leggat. 2022. “Proteome Metabolome and Transcriptome Data for Three Symbiodiniaceae under Ambient and Heat Stress Conditions.” *Scientific Data* 9 (1): 153. https://doi.org/10.1038/s41597-022-01258-w.

Castillo, Karl D., Justin B. Ries, John F. Bruno, and Isaac T. Westfield. 2014. “The Reef-Building Coral Siderastrea Siderea Exhibits Parabolic Responses to Ocean Acidification and Warming.” *Proceedings of the Royal Society B: Biological Sciences* 281 (1797): 20141856. https://doi.org/10.1098/rspb.2014.1856.

Castillo, Karl D., Justin B. Ries, Jack M. Weiss, and Fernando P. Lima. 2012. “Decline of Forereef Corals in Response to Recent Warming Linked to History of Thermal

Exposure." *Nature Climate Change* 2 (10): 756–60. https://doi.org/10.1038/nclimate1577.

Chan, Wei-Ping, I-Ching Chen, Robert K. Colwell, Wei-Chung Liu, Cho-ying Huang, and Sheng-Feng Shen. 2016. "Seasonal and Daily Climate Variation Have Opposite Effects on Species Elevational Range Size." *Science* 351 (6280): 1437–39. https://doi.org/10.1126/science.aab4119.

Cheng, Lijing, John Abraham, Kevin E. Trenberth, John Fasullo, Tim Boyer, Michael E. Mann, Jiang Zhu, et al. 2022. "Another Record: Ocean Warming Continues through 2021 despite La Niña Conditions." *Advances in Atmospheric Sciences* 39 (3): 373–85. https://doi.org/10.1007/s00376-022-1461-3.

Chevin, Luis-Miguel, Russell Lande, and Georgina M. Mace. 2010. "Adaptation, Plasticity, and Extinction in a Changing Environment: Towards a Predictive Theory." *PLOS Biology* 8 (4): e1000357. https://doi.org/10.1371/journal.pbio.1000357.

Chomczynski, Piotr, and Nicoletta Sacchi. 2006. "The Single-Step Method of RNA Isolation by Acid Guanidinium Thiocyanate–Phenol–Chloroform Extraction: Twenty-Something Years On." *Nature Protocols* 1 (2): 581–85. https://doi.org/10.1038/nprot.2006.83.

Comeau, S., C. E. Cornwall, T. M. DeCarlo, S. S. Doo, R. C. Carpenter, and M. T. McCulloch. 2019. "Resistance to Ocean Acidification in Coral Reef Taxa Is Not Gained by Acclimatization." *Nature Climate Change* 9 (6): 477–83. https://doi.org/10.1038/s41558-019-0486-9.

Conti-Jerpe, Inga, Philip Thompson, Cheong Wai Martin Wong, Nara Oliveira, Nicolas Duprey, Molly Moynihan, and David Baker. 2020. "Trophic Strategy and Bleaching Resistance in Reef-Building Corals." *Science Advances* 6 (April): eaaz5443. https://doi.org/10.1126/sciadv.aaz5443.

Cooley, S., D. Schoeman, L. Bopp, P. Boyd, S. Donner, D.Y. Ghebrehiwet, S.I. Ito, et al. 2022. "Ocean and Coastal Ecosystems and Their Services." In *Climate Change 2022: Impacts, Adaptation, and Vulnerability. Contribution of Working Group II to the Sixth Assessment Report of the Intergovernmental Panel on Climate Change.*, 379–550. Cambridge, UK and New York, NY, USA: Cambridge University Press.

Costanza, Robert, Rudolf de Groot, Paul Sutton, Sander van der Ploeg, Sharolyn J. Anderson, Ida Kubiszewski, Stephen Farber, and R. Kerry Turner. 2014. "Changes in the Global Value of Ecosystem Services." *Global Environmental Change* 26 (May): 152–58. https://doi.org/10.1016/j.gloenvcha.2014.04.002.

Cui, Guoxin, Yi Jin Liew, Yong Li, Najeh Kharbatia, Noura I. Zahran, Abdul-Hamid Emwas, Victor M. Eguiluz, and Manuel Aranda. 2019. "Host-Dependent Nitrogen Recycling as a Mechanism of Symbiont Control in Aiptasia." *PLOS Genetics* 15 (6): e1008189. https://doi.org/10.1371/journal.pgen.1008189.

Davies, Sarah W., Adrian Marchetti, Justin B. Ries, and Karl D. Castillo. 2016. "Thermal and PCO2 Stress Elicit Divergent Transcriptomic Responses in a Resilient Coral." *Frontiers in Marine Science* 3. https://www.frontiersin.org/articles/10.3389/fmars.2016.00112.

Davies, Sarah W., Muneeb Rahman, Eli Meyer, Elizabeth A. Green, Emmanual Buschiazzo, Mónica Medina, and Mikhail V. Matz. 2013. "Novel Polymorphic Microsatellite Markers for Population Genetics of the Endangered Caribbean Star Coral, Montastraea Faveolata." *Marine Biodiversity* 43 (2): 167–72. https://doi.org/10.1007/s12526-012-0133-4.

Davies, Sarah W., Justin B. Ries, Adrian Marchetti, and Karl D. Castillo. 2018. "Symbiodinium Functional Diversity in the Coral Siderastrea Siderea Is Influenced by Thermal Stress and Reef Environment, but Not Ocean Acidification." *Frontiers in Marine Science* 5. https://www.frontiersin.org/articles/10.3389/fmars.2018.00150.

Davies, Sarah W., Marie E. Strader, Johnathan T. Kool, Carly D. Kenkel, and Mikhail V. Matz. 2017. "Modeled Differences of Coral Life-History Traits Influence the Refugium Potential of a Remote Caribbean Reef." *Coral Reefs* 36 (3): 913–25. https://doi.org/10.1007/s00338-017-1583-8.

Davies, Spencer. 1989. "Short-Term Growth Measurements of Corals Using an Accurate Buoyant Weighing Technique." *Marine Biology* 101 (3): 389–95. https://doi.org/10.1007/BF00428135.

Davy, Simon K., Denis Allemand, and Virginia M. Weis. 2012. "Cell Biology of Cnidarian-Dinoflagellate Symbiosis." *Microbiology and Molecular Biology Reviews* 76 (2): 229–61. https://doi.org/10.1128/MMBR.05014-11.

Dean, Andrew D., Ewan J. A. Minter, Megan E. S. Sørensen, Christopher D. Lowe, Duncan D. Cameron, Michael A. Brockhurst, and A. Jamie Wood. 2016. "Host Control and Nutrient Trading in a Photosynthetic Symbiosis." *Journal of Theoretical Biology*, Advances in Modelling Biological Evolution: Linking Mathematical Theories with Empirical Realities, 405 (September): 82–93. https://doi.org/10.1016/j.jtbi.2016.02.021.

DeMerlis, Allyson, Amanda Kirkland, Madeline L. Kaufman, Anderson B. Mayfield, Nathan Formel, Graham Kolodziej, Derek P. Manzello, Diego Lirman, Nikki Traylor-Knowles, and Ian C. Enochs. 2022. "Pre-Exposure to a Variable

Temperature Treatment Improves the Response of Acropora Cervicornis to Acute Thermal Stress." *Coral Reefs* 41 (2): 435–45. https://doi.org/10.1007/s00338-022-02232-z.

DeSalvo, Michael K., Shinichi Sunagawa, Christian R. Voolstra, and Mónica Medina. 2010. "Transcriptomic Responses to Heat Stress and Bleaching in the Elkhorn Coral Acropora Palmata." *Marine Ecology Progress Series* 402 (March): 97–113. https://doi.org/10.3354/meps08372.

Dilernia, Nicole J., Emma F. Camp, Natasha Bartels, and David J. Suggett. 2023. "Contrasting the Thermal Performance of Cultured Coral Endosymbiont Photo-Physiology." *Journal of Experimental Marine Biology and Ecology* 561 (April): 151865. https://doi.org/10.1016/j.jembe.2022.151865.

Dimond, J., and E. Carrington. 2008. "Symbiosis Regulation in a Facultatively Symbiotic Temperate Coral: Zooxanthellae Division and Expulsion" 27: 601–4.

Dixon, Groves B., Evelyn Abbott, and Mikhail Matz. 2020. "Meta-Analysis of the Coral Environmental Stress Response: Acropora Corals Show Opposing Responses Depending on Stress Intensity." *Molecular Ecology* 29 (15): 2855–70. https://doi.org/10.1111/mec.15535.

Dixon, Groves B., Sarah W. Davies, Galina V. Aglyamova, Eli Meyer, Line K. Bay, and Mikhail V. Matz. 2015. "Genomic Determinants of Coral Heat Tolerance across Latitudes." *Science* 348 (6242): 1460–62. https://doi.org/10.1126/science.1261224.

Dixon, Groves B., and Carly D. Kenkel. 2019. "Molecular Convergence and Positive Selection Associated with the Evolution of Symbiont Transmission Mode in Stony Corals." *Proceedings of the Royal Society B: Biological Sciences* 286 (1901): 20190111. https://doi.org/10.1098/rspb.2019.0111.

Dominici-Arosemena, Arturo, and Matthias Wolff. 2005. "Reef Fish Community Structure in Bocas Del Toro (Caribbean, Panama): Gradients in Habitat Complexity and Exposure," 613–37.

Doney, Scott C., Victoria J. Fabry, Richard A. Feely, and Joan A. Kleypas. 2009. "Ocean Acidification: The Other CO $_2$ Problem." *Annual Review of Marine Science* 1 (1): 169–92. https://doi.org/10.1146/annurev.marine.010908.163834.

Dougan, Katherine E. 2020. "A Comparative Genomics Exploration of Inter-Partner Metabolic Signaling in the Coral-Algal Symbiosis." FIU Electronic Theses and Dissertations.

Drury, Crawford, Jenna Dilworth, Eva Majerová, Carlo Caruso, and Justin B. Greer. 2022. “Expression Plasticity Regulates Intraspecific Variation in the Acclimatization Potential of a Reef-Building Coral.” *Nature Communications* 13 (1): 4790. https://doi.org/10.1038/s41467-022-32452-4.

Eckert, Ryan J., Michael S. Studivan, and Joshua D. Voss. 2019. “Populations of the Coral Species Montastraea Cavernosa on the Belize Barrier Reef Lack Vertical Connectivity.” *Scientific Reports* 9 (1): 7200. https://doi.org/10.1038/s41598-019-43479-x.

Eddy, Sean R. 2011. “Accelerated Profile HMM Searches.” *PLOS Computational Biology* 7 (10): e1002195. https://doi.org/10.1371/journal.pcbi.1002195.

Eddy, Tyler D., Vicky W. Y. Lam, Gabriel Reygondeau, Andrés M. Cisneros-Montemayor, Krista Greer, Maria Lourdes D. Palomares, John F. Bruno, Yoshitaka Ota, and William W. L. Cheung. 2021. “Global Decline in Capacity of Coral Reefs to Provide Ecosystem Services.” *One Earth* 4 (9): 1278–85. https://doi.org/10.1016/j.oneear.2021.08.016.

Edmunds, Peter J. 2005. “The Effect of Sub-Lethal Increases in Temperature on the Growth and Population Trajectories of Three Scleractinian Corals on the Southern Great Barrier Reef.” *Oecologia* 146 (3): 350–64. https://doi.org/10.1007/s00442-005-0210-5.

Edmunds, Peter J., Darren Brown, and Vincent Moriarty. 2012. “Interactive Effects of Ocean Acidification and Temperature on Two Scleractinian Corals from Moorea, French Polynesia.” *Global Change Biology* 18 (7): 2173–83. https://doi.org/10.1111/j.1365-2486.2012.02695.x.

Enríquez, Susana, Eugenio R. Méndez, Ove Hoegh-Guldberg, and Roberto Iglesias-Prieto. 2017. “Key Functional Role of the Optical Properties of Coral Skeletons in Coral Ecology and Evolution.” *Proceedings of the Royal Society B: Biological Sciences* 284 (1853): 20161667. https://doi.org/10.1098/rspb.2016.1667.

Falkowski, Paul G., Zvy Dubinsky, Leonard Muscatine, and Lawrence McCloskey. 1993. “Population Control in Symbiotic Corals: Ammonium Ions and Organic Materials Maintain the Density of Zooxanthellae.” *BioScience* 43 (9): 606–11. https://doi.org/10.2307/1312147.

Fifer, James E., Nina Yasuda, Takehisa Yamakita, Colleen B. Bove, and Sarah W. Davies. 2022. “Genetic Divergence and Range Expansion in a Western North Pacific Coral.” *Science of The Total Environment* 813 (March): 152423. https://doi.org/10.1016/j.scitotenv.2021.152423.

Fitt, W. K., F. K. McFarland, M. E. Warner, and G. C. Chilcoat. 2000. “Seasonal Patterns of Tissue Biomass and Densities of Symbiotic Dinoflagellates in Reef Corals and Relation to Coral Bleaching.” *Limnology and Oceanography* 45 (3): 677–85. https://doi.org/10.4319/lo.2000.45.3.0677.

Fontaine, Samantha S., Patrick M. Mineo, and Kevin D. Kohl. 2022. “Experimental Manipulation of Microbiota Reduces Host Thermal Tolerance and Fitness under Heat Stress in a Vertebrate Ectotherm.” *Nature Ecology & Evolution* 6 (4): 405–17. https://doi.org/10.1038/s41559-022-01686-2.

França, Filipe M., Cassandra E. Benkwitt, Guadalupe Peralta, James P. W. Robinson, Nicholas A. J. Graham, Jason M. Tylianakis, Erika Berenguer, et al. 2020. “Climatic and Local Stressor Interactions Threaten Tropical Forests and Coral Reefs.” *Philosophical Transactions of the Royal Society B: Biological Sciences* 375 (1794): 20190116. https://doi.org/10.1098/rstb.2019.0116.

Frieler, K., M. Meinshausen, A. Golly, M. Mengel, K. Lebek, S. D. Donner, and O. Hoegh-Guldberg. 2013. “Limiting Global Warming to 2 °C Is Unlikely to Save Most Coral Reefs.” *Nature Climate Change* 3 (2): 165–70. https://doi.org/10.1038/nclimate1674.

Fu, Limin, Beifang Niu, Zhengwei Zhu, Sitao Wu, and Weizhong Li. 2012. “CD-HIT: Accelerated for Clustering the next-Generation Sequencing Data.” *Bioinformatics* 28 (23): 3150–52. https://doi.org/10.1093/bioinformatics/bts565.

Fuller, Zachary L., Veronique J. L. Mocellin, Luke A. Morris, Neal Cantin, Jihanne Shepherd, Luke Sarre, Julie Peng, et al. 2020. “Population Genetics of the Coral Acropora Millepora: Toward Genomic Prediction of Bleaching.” *Science* 369 (6501): eaba4674. https://doi.org/10.1126/science.aba4674.

Galand, Pierre E., Leila Chapron, Anne-Leila Meistertzheim, Erwan Peru, and Franck Lartaud. 2018. “The Effect of Captivity on the Dynamics of Active Bacterial Communities Differs Between Two Deep-Sea Coral Species.” *Frontiers in Microbiology* 9. https://www.frontiersin.org/articles/10.3389/fmicb.2018.02565.

Glynn, Peter W. 1984. “Widespread Coral Mortality and the 1982–83 El Niño Warming Event.” *Environmental Conservation* 11 (2): 133–46. https://doi.org/10.1017/S0376892900013825.

Gnaiger, E., and G. Bitterlich. 1984. “Proximate Biochemical Composition and Caloric Content Calculated from Elemental CHN Analysis: A Stoichiometric Concept.” *Oecologia* 62 (3): 289–98. https://doi.org/10.1007/BF00384259.

Gómez-Corrales, Matías, and Carlos Prada. 2020. “Cryptic Lineages Respond Differently to Coral Bleaching.” *Molecular Ecology* 29 (22): 4265–73. https://doi.org/10.1111/mec.15631.

Green, Elizabeth A., Sarah W. Davies, Mikhail V. Matz, and Mónica Medina. 2014. “Quantifying Cryptic Symbiodinium Diversity within Orbicella Faveolata and Orbicella Franksi at the Flower Garden Banks, Gulf of Mexico.” *PeerJ* 2 (May): e386. https://doi.org/10.7717/peerj.386.

Grottoli, Andréa G., L. J. Rodrigues, and C. Juarez. 2004. “Lipids and Stable Carbon Isotopes in Two Species of Hawaiian Corals, Porites Compressa and Montipora Verrucosa, Following a Bleaching Event.” *Marine Biology* 145 (3): 621–31. https://doi.org/10.1007/s00227-004-1337-3.

Grottoli, Andréa G., Lisa J. Rodrigues, and James E. Palardy. 2006. “Heterotrophic Plasticity and Resilience in Bleached Corals.” *Nature* 440 (7088): 1186–89. https://doi.org/10.1038/nature04565.

Grottoli, Andréa G., Mark E. Warner, Stephen J. Levas, Matthew D. Aschaffenburg, Verena Schoepf, Michael McGinley, Justin Baumann, and Yohei Matsui. 2014. “The Cumulative Impact of Annual Coral Bleaching Can Turn Some Coral Species Winners into Losers.” *Global Change Biology* 20 (12): 3823–33. https://doi.org/10.1111/gcb.12658.

Guillermic, Maxence, Louise P. Cameron, Ilian De Corte, Sambuddha Misra, Jelle Bijma, Dirk de Beer, Claire E. Reymond, Hildegard Westphal, Justin B. Ries, and Robert A. Eagle. 2021. “Thermal Stress Reduces Pocilloporid Coral Resilience to Ocean Acidification by Impairing Control over Calcifying Fluid Chemistry.” *Science Advances* 7 (2): eaba9958. https://doi.org/10.1126/sciadv.aba9958.

Guzmán, Héctor M., Penelope A. G. Barnes, Catherine E. Lovelock, and Ilka C. Feller. 2005. “A Site Description of the CARICOMP Mangrove, Seagrass and Coral Reef Sites in Bocas Del Toro, Panamá.” http://repository.si.edu/xmlui/handle/10088/3878.

Haas, Brian J., Alexie Papanicolaou, Moran Yassour, Manfred Grabherr, Philip D. Blood, Joshua Bowden, Matthew Brian Couger, et al. 2013. “De Novo Transcript Sequence Reconstruction from RNA-Seq Using the Trinity Platform for Reference Generation and Analysis.” *Nature Protocols* 8 (8): 1494–1512. https://doi.org/10.1038/nprot.2013.084.

Hackerott, Serena, Harmony A. Martell, and Jose M. Eirin-Lopez. 2021. “Coral Environmental Memory: Causes, Mechanisms, and Consequences for Future Reefs.” *Trends in Ecology & Evolution* 36 (11): 1011–23. https://doi.org/10.1016/j.tree.2021.06.014.

Harvey, Jeffrey A., Kévin Tougeron, Rieta Gols, Robin Heinen, Mariana Abarca, Paul K. Abram, Yves Basset, et al. 2022. "Scientists' Warning on Climate Change and Insects." *Ecological Monographs* n/a (n/a): e1553. https://doi.org/10.1002/ecm.1553.

Hector, Tobias E., Kim L. Hoang, Jingdi Li, and Kayla C. King. 2022. "Symbiosis and Host Responses to Heating." *Trends in Ecology & Evolution*, Special issue: Symbiosis, 37 (7): 611–24. https://doi.org/10.1016/j.tree.2022.03.011.

Hickling, Rachael, David B. Roy, Jane K. Hill, Richard Fox, and Chris D. Thomas. 2006. "The Distributions of a Wide Range of Taxonomic Groups Are Expanding Polewards." *Global Change Biology* 12 (3): 450–55. https://doi.org/10.1111/j.1365-2486.2006.01116.x.

Hilker, Monika, and Thomas Schmülling. 2019. "Stress Priming, Memory, and Signalling in Plants." *Plant, Cell & Environment* 42 (3): 753–61. https://doi.org/10.1111/pce.13526.

Hill, Ross, and Peter J. Ralph. 2006. "Photosystem II Heterogeneity of in Hospite Zooxanthellae in Scleractinian Corals Exposed to Bleaching Conditions." *Photochemistry and Photobiology* 82 (6): 1577–85. https://doi.org/10.1111/j.1751-1097.2006.tb09814.x.

Hoegh-Guldberg, O., P. J. Mumby, A. J. Hooten, R. S. Steneck, P. Greenfield, E. Gomez, C. D. Harvell, et al. 2007. "Coral Reefs Under Rapid Climate Change and Ocean Acidification." *Science* 318 (5857): 1737–42. https://doi.org/10.1126/science.1152509.

Holcomb, M., A. L. Cohen, and D. C. McCorkle. 2012. "An Investigation of the Calcification Response of the Scleractinian Coral *Astrangia Poculata* to Elevated $pCO_2$ and the Effects of Nutrients, Zooxanthellae and Gender." *Biogeosciences* 9 (1): 29–39. https://doi.org/10.5194/bg-9-29-2012.

Hooidonk, Ruben van, Jeffrey Maynard, Jerker Tamelander, Jamison Gove, Gabby Ahmadia, Laurie Raymundo, Gareth Williams, Scott F. Heron, and Serge Planes. 2016. "Local-Scale Projections of Coral Reef Futures and Implications of the Paris Agreement." *Scientific Reports* 6 (1): 39666. https://doi.org/10.1038/srep39666.

Horvath, Kimmaree M., Karl D. Castillo, Pualani Armstrong, Isaac T. Westfield, Travis Courtney, and Justin B. Ries. 2016. "Next-Century Ocean Acidification and Warming Both Reduce Calcification Rate, but Only Acidification Alters Skeletal Morphology of Reef-Building Coral Siderastrea Siderea." *Scientific Reports* 6 (1): 29613. https://doi.org/10.1038/srep29613.

Hughes, Terry P., James T. Kerry, Mariana Álvarez-Noriega, Jorge G. Álvarez-Romero, Kristen D. Anderson, Andrew H. Baird, Russell C. Babcock, et al. 2017. "Global Warming and Recurrent Mass Bleaching of Corals." *Nature* 543 (7645): 373–77. https://doi.org/10.1038/nature21707.

Hume, B., C. D'Angelo, J. Burt, A. C. Baker, B. Riegl, and J. Wiedenmann. 2013. "Corals from the Persian/Arabian Gulf as Models for Thermotolerant Reef-Builders: Prevalence of Clade C3 Symbiodinium, Host Fluorescence and Ex Situ Temperature Tolerance." *Marine Pollution Bulletin*, Coral reefs of the Gulf: Past, present and the future of a unique ecosystem, 72 (2): 313–22. https://doi.org/10.1016/j.marpolbul.2012.11.032.

Hume, B., C. D'Angelo, E. G. Smith, J. R. Stevens, J. Burt, and J. Wiedenmann. 2015. "Symbiodinium Thermophilum Sp. Nov., a Thermotolerant Symbiotic Alga Prevalent in Corals of the World's Hottest Sea, the Persian/Arabian Gulf." *Scientific Reports* 5 (1): 8562. https://doi.org/10.1038/srep08562.

Hume, Benjamin C. C., Edward G. Smith, Maren Ziegler, Hugh J. M. Warrington, John A. Burt, Todd C. LaJeunesse, Joerg Wiedenmann, and Christian R. Voolstra. 2019. "SymPortal: A Novel Analytical Framework and Platform for Coral Algal Symbiont next-Generation Sequencing ITS2 Profiling." *Molecular Ecology Resources* 19 (4): 1063–80. https://doi.org/10.1111/1755-0998.13004.

Jeffrey, S. W., and F. Haxo. 1968. "PHOTOSYNTHETIC PIGMENTS OF SYMBIOTIC DINOFLAGELLATES (ZOOXANTHELLAE) FROM CORALS AND CLAMS." https://doi.org/10.2307/1539622.

Jokiel, Paul Louis. 2011. "Ocean Acidification and Control of Reef Coral Calcification by Boundary Layer Limitation of Proton Flux." *Bulletin of Marine Science* 87 (3): 639–57. https://doi.org/10.5343/bms.2010.1107.

Jokiel, Paul Louis, and S. L. Coles. 1990. "Response of Hawaiian and Other Indo-Pacific Reef Corals to Elevated Temperature." *Coral Reefs* 8 (4): 155–62. https://doi.org/10.1007/BF00265006.

Josephs, Emily B. 2018. "Determining the Evolutionary Forces Shaping G × E." *New Phytologist* 219 (1): 31–36. https://doi.org/10.1111/nph.15103.

Jury, Christopher P., Mia N. Delano, and Robert J. Toonen. 2019. "High Heritability of Coral Calcification Rates and Evolutionary Potential under Ocean Acidification." *Scientific Reports* 9 (1): 20419. https://doi.org/10.1038/s41598-019-56313-1.

Jury, Christopher P., and Robert J. Toonen. 2019. "Adaptive Responses and Local Stressor Mitigation Drive Coral Resilience in Warmer, More Acidic Oceans."

*Proceedings of the Royal Society B: Biological Sciences* 286 (1902): 20190614. https://doi.org/10.1098/rspb.2019.0614.

Katoh, Kazutaka, and Daron M. Standley. 2013. "MAFFT Multiple Sequence Alignment Software Version 7: Improvements in Performance and Usability." *Molecular Biology and Evolution* 30 (4): 772–80. https://doi.org/10.1093/molbev/mst010.

Kavousi, Javid, Yasuaki Tanaka, Kozue Nishida, Atsushi Suzuki, Yukihiro Nojiri, and Takashi Nakamura. 2016. "Colony-Specific Calcification and Mortality under Ocean Acidification in the Branching Coral Montipora Digitata." *Marine Environmental Research* 119 (August): 161–65. https://doi.org/10.1016/j.marenvres.2016.05.025.

Kawecki, Tadeusz J., and Dieter Ebert. 2004. "Conceptual Issues in Local Adaptation." *Ecology Letters* 7 (12): 1225–41. https://doi.org/10.1111/j.1461-0248.2004.00684.x.

Kemp, Dustin W., Clinton A. Oakley, Daniel J. Thornhill, Laura A. Newcomb, Gregory W. Schmidt, and William K. Fitt. 2011. "Catastrophic Mortality on Inshore Coral Reefs of the Florida Keys Due to Severe Low-Temperature Stress." *Global Change Biology* 17 (11): 3468–77. https://doi.org/10.1111/j.1365-2486.2011.02487.x.

Kenkel, Carly D., Albert T. Almanza, and Mikhail V. Matz. 2015. "Fine-Scale Environmental Specialization of Reef-Building Corals Might Be Limiting Reef Recovery in the Florida Keys." *Ecology* 96 (12): 3197–3212. https://doi.org/10.1890/14-2297.1.

Kenkel, Carly D., G. Goodbody-Gringley, D. Caillaud, Sarah W. Davies, E. Bartels, and M. V. Matz. 2013. "Evidence for a Host Role in Thermotolerance Divergence between Populations of the Mustard Hill Coral ( *Porites Astreoides* ) from Different Reef Environments." *Molecular Ecology* 22 (16): 4335–48. https://doi.org/10.1111/mec.12391.

Kenkel, Carly D., and Mikhail V. Matz. 2016. "Gene Expression Plasticity as a Mechanism of Coral Adaptation to a Variable Environment." *Nature Ecology & Evolution* 1 (1): 1–6. https://doi.org/10.1038/s41559-016-0014.

Kenkel, Carly D., E. Meyer, and M. V. Matz. 2013. "Gene Expression under Chronic Heat Stress in Populations of the Mustard Hill Coral (Porites Astreoides) from Different Thermal Environments." *Molecular Ecology* 22 (16): 4322–34. https://doi.org/10.1111/mec.12390.

Kingsolver, Joel G., Jessica K. Higgins, and Kate E. Augustine. 2015. "Fluctuating Temperatures and Ectotherm Growth: Distinguishing Non-Linear and Time-

Dependent Effects." *Journal of Experimental Biology* 218 (14): 2218–25. https://doi.org/10.1242/jeb.120733.

Klein, Shannon G., Nathan R. Geraldi, Andrea Anton, Sebastian Schmidt-Roach, Maren Ziegler, Maha J. Cziesielski, Cecilia Martin, et al. 2022. "Projecting Coral Responses to Intensifying Marine Heatwaves under Ocean Acidification." *Global Change Biology* 28 (5): 1753–65. https://doi.org/10.1111/gcb.15818.

Kline, David I., Lida Teneva, Daniel K. Okamoto, Kenneth Schneider, Ken Caldeira, Thomas Miard, Aaron Chai, et al. 2019. "Living Coral Tissue Slows Skeletal Dissolution Related to Ocean Acidification." *Nature Ecology & Evolution* 3 (10): 1438–44. https://doi.org/10.1038/s41559-019-0988-x.

Kornder, Niklas A., Bernhard M. Riegl, and Joana Figueiredo. 2018. "Thresholds and Drivers of Coral Calcification Responses to Climate Change." *Global Change Biology* 24 (11): 5084–95. https://doi.org/10.1111/gcb.14431.

Korneliussen, Thorfinn Sand, Anders Albrechtsen, and Rasmus Nielsen. 2014. "ANGSD: Analysis of Next Generation Sequencing Data." *BMC Bioinformatics* 15 (1): 356. https://doi.org/10.1186/s12859-014-0356-4.

Kroeker, Kristy J, Rebecca L Kordas, Ryan Crim, Iris E Hendriks, Laura Ramajo, Gerald S Singh, Carlos M Duarte, and Jean-Pierre Gattuso. 2013. "Impacts of Ocean Acidification on Marine Organisms: Quantifying Sensitivities and Interaction with Warming." *Global Change Biology* 19 (6): 1884–96. https://doi.org/10.1111/gcb.12179.

Ladner, Jason T., and Stephen R. Palumbi. 2012. "Extensive Sympatry, Cryptic Diversity and Introgression throughout the Geographic Distribution of Two Coral Species Complexes." *Molecular Ecology* 21 (9): 2224–38. https://doi.org/10.1111/j.1365-294X.2012.05528.x.

LaJeunesse, Todd C., John Everett Parkinson, Paul W. Gabrielson, Hae Jin Jeong, James Davis Reimer, Christian R. Voolstra, and Scott R. Santos. 2018. "Systematic Revision of Symbiodiniaceae Highlights the Antiquity and Diversity of Coral Endosymbionts." *Current Biology* 28 (16): 2570-2580.e6. https://doi.org/10.1016/j.cub.2018.07.008.

Langmead, Ben, and Steven L. Salzberg. 2012. "Fast Gapped-Read Alignment with Bowtie 2." *Nature Methods* 9 (4): 357–59. https://doi.org/10.1038/nmeth.1923.

Lê, Sébastien, Julie Josse, and François Husson. 2008. "FactoMineR: An R Package for Multivariate Analysis." *Journal of Statistical Software* 25 (March): 1–18. https://doi.org/10.18637/jss.v025.i01.

Leggat, William, Francois Seneca, Kenneth Wasmund, Lubna Ukani, David Yellowlees, and Tracy D. Ainsworth. 2011. “Differential Responses of the Coral Host and Their Algal Symbiont to Thermal Stress.” *PLOS ONE* 6 (10): e26687. https://doi.org/10.1371/journal.pone.0026687.

Lenth, Russell V., Paul Buerkner, Maxime Herve, Jonathon Love, Fernando Miguez, Hannes Riebl, and Henrik Singmann. 2022. “Emmeans: Estimated Marginal Means, Aka Least-Squares Means.” https://CRAN.R-project.org/package=emmeans.

Levas, Stephen, Verena Schoepf, Mark E. Warner, Matthew Aschaffenburg, Justin Baumann, and Andréa G. Grottoli. 2018. “Long-Term Recovery of Caribbean Corals from Bleaching.” *Journal of Experimental Marine Biology and Ecology* 506 (September): 124–34. https://doi.org/10.1016/j.jembe.2018.06.003.

Li, Li, Christian J. Stoeckert, and David S. Roos. 2003. “OrthoMCL: Identification of Ortholog Groups for Eukaryotic Genomes.” *Genome Research* 13 (9): 2178–89. https://doi.org/10.1101/gr.1224503.

Li, Weizhong, and Adam Godzik. 2006. “Cd-Hit: A Fast Program for Clustering and Comparing Large Sets of Protein or Nucleotide Sequences.” *Bioinformatics* 22 (13): 1658–59. https://doi.org/10.1093/bioinformatics/btl158.

Lin, Frederick Huang. 2019. “HuangLin/ANCOM: Third Release of ANCOM.” Zenodo. https://doi.org/10.5281/zenodo.3577802.

Lin, Senjie. 2011. “Genomic Understanding of Dinoflagellates.” *Research in Microbiology*, The genome organisation of eukaryotic microbes, 162 (6): 551–69. https://doi.org/10.1016/j.resmic.2011.04.006.

Lin, Senjie, Shifeng Cheng, Bo Song, Xiao Zhong, Xin Lin, Wujiao Li, Ling Li, et al. 2015. “The Symbiodinium Kawagutii Genome Illuminates Dinoflagellate Gene Expression and Coral Symbiosis.” *Science* 350 (6261): 691–94. https://doi.org/10.1126/science.aad0408.

Lin, Senjie, Liying Yu, and Huan Zhang. 2019. “Transcriptomic Responses to Thermal Stress and Varied Phosphorus Conditions in Fugacium Kawagutii.” *Microorganisms* 7 (4): 96. https://doi.org/10.3390/microorganisms7040096.

Liu, Huanle, Timothy G. Stephens, Raúl A. González-Pech, Victor H. Beltran, Bruno Lapeyre, Pim Bongaerts, Ira Cooke, et al. 2018. “Symbiodinium Genomes Reveal Adaptive Evolution of Functions Related to Coral-Dinoflagellate Symbiosis.” *Communications Biology* 1 (1): 1–11. https://doi.org/10.1038/s42003-018-0098-3.

Liu, Yi-Wei, Jill N. Sutton, Justin B. Ries, and Robert A. Eagle. 2020. “Regulation of Calcification Site PH Is a Polyphyletic but Not Always Governing Response to Ocean Acidification.” *Science Advances* 6 (5): eaax1314. https://doi.org/10.1126/sciadv.aax1314.

Lohman, Brian K., Jesse N. Weber, and Daniel I. Bolnick. 2016. “Evaluation of TagSeq, a Reliable Low-Cost Alternative for RNAseq.” *Molecular Ecology Resources* 16 (6): 1315–21. https://doi.org/10.1111/1755-0998.12529.

Love, Michael I., Wolfgang Huber, and Simon Anders. 2014. “Moderated Estimation of Fold Change and Dispersion for RNA-Seq Data with DESeq2.” *Genome Biology* 15 (12): 550. https://doi.org/10.1186/s13059-014-0550-8.

Lüdecke, Daniel, Mattan S. Ben-Shachar, Indrajeet Patil, Philip Waggoner, and Dominique Makowski. 2021. “Performance: An R Package for Assessment, Comparison and Testing of Statistical Models.” *Journal of Open Source Software* 6 (60): 3139. https://doi.org/10.21105/joss.03139.

Manzello, Derek P., Mikhail V. Matz, Ian C. Enochs, Lauren Valentino, Renee D. Carlton, Graham Kolodziej, Xaymara Serrano, Erica K. Towle, and Mike Jankulak. 2019. “Role of Host Genetics and Heat-Tolerant Algal Symbionts in Sustaining Populations of the Endangered Coral Orbicella Faveolata in the Florida Keys with Ocean Warming.” *Global Change Biology* 25 (3): 1016–31. https://doi.org/10.1111/gcb.14545.

Maor-Landaw, Keren, Madeleine J. H. van Oppen, and Geoffrey I. McFadden. 2020. “Symbiotic Lifestyle Triggers Drastic Changes in the Gene Expression of the Algal Endosymbiont Breviolum Minutum (Symbiodiniaceae).” *Ecology and Evolution* 10 (1): 451–66. https://doi.org/10.1002/ece3.5910.

Marangoni, Laura Fernandes de Barros, Cecile Rottier, and Christine Ferrier-Pagès. 2021. “Symbiont Regulation in Stylophora Pistillata during Cold Stress: An Acclimation Mechanism against Oxidative Stress and Severe Bleaching.” *Journal of Experimental Biology* 224 (3): jeb235275. https://doi.org/10.1242/jeb.235275.

Marchetti, Adrian, David M. Schruth, Colleen A. Durkin, Micaela S. Parker, Robin B. Kodner, Chris T. Berthiaume, Rhonda Morales, Andrew E. Allen, and E. Virginia Armbrust. 2012. “Comparative Metatranscriptomics Identifies Molecular Bases for the Physiological Responses of Phytoplankton to Varying Iron Availability.” *Proceedings of the National Academy of Sciences* 109 (6): E317–25. https://doi.org/10.1073/pnas.1118408109.

Martin, Marcel. 2011. “Cutadapt Removes Adapter Sequences from High-Throughput Sequencing Reads.” *EMBnet.Journal* 17 (1): 10–12. https://doi.org/10.14806/ej.17.1.200.

Maruyama, Shumpei, and Virginia M. Weis. 2021. “Limitations of Using Cultured Algae to Study Cnidarian-Algal Symbioses and Suggestions for Future Studies.” *Journal of Phycology* 57 (1): 30–38. https://doi.org/10.1111/jpy.13102.

Massey, Melanie D., M. Kate Fredericks, David Malloy, Suchinta Arif, and Jeffrey A. Hutchings. 2022. “Differential Reproductive Plasticity under Thermal Variability in a Freshwater Fish (Danio Rerio).” *Proceedings of the Royal Society B: Biological Sciences* 289 (1982): 20220751. https://doi.org/10.1098/rspb.2022.0751.

Masuko, Tatsuya, Akio Minami, Norimasa Iwasaki, Tokifumi Majima, Shin-Ichiro Nishimura, and Yuan C. Lee. 2005. “Carbohydrate Analysis by a Phenol–Sulfuric Acid Method in Microplate Format.” *Analytical Biochemistry* 339 (1): 69–72. https://doi.org/10.1016/j.ab.2004.12.001.

Matias, Ambrocio Melvin A., Iva Popovic, Joshua A. Thia, Ira R. Cooke, Gergely Torda, Vimoksalehi Lukoschek, Line K. Bay, Sun W. Kim, and Cynthia Riginos. 2022. “Cryptic Diversity and Spatial Genetic Variation in the Coral Acropora Tenuis and Its Endosymbionts across the Great Barrier Reef.” *Evolutionary Applications* n/a (n/a). https://doi.org/10.1111/eva.13435.

Matz, Mikhail V., Eric A. Treml, Galina V. Aglyamova, and Line K. Bay. 2018. “Potential and Limits for Rapid Genetic Adaptation to Warming in a Great Barrier Reef Coral.” *PLOS Genetics* 14 (4): e1007220. https://doi.org/10.1371/journal.pgen.1007220.

McLachlan, Rowan H., James T. Price, Sarah L. Solomon, and Andréa G. Grottoli. 2020. “Thirty Years of Coral Heat-Stress Experiments: A Review of Methods.” *Coral Reefs* 39 (4): 885–902. https://doi.org/10.1007/s00338-020-01931-9.

McMurdie, Paul J., and Susan Holmes. 2013. “Phyloseq: An R Package for Reproducible Interactive Analysis and Graphics of Microbiome Census Data.” *PLOS ONE* 8 (4): e61217. https://doi.org/10.1371/journal.pone.0061217.

Melo Clavijo, Jenny, Alexander Donath, João Serôdio, and Gregor Christa. 2018. “Polymorphic Adaptations in Metazoans to Establish and Maintain Photosymbioses.” *Biological Reviews* 93 (4): 2006–20. https://doi.org/10.1111/brv.12430.

Meyer, E., G. V. Aglyamova, and M. V. Matz. 2011. “Profiling Gene Expression Responses of Coral Larvae (Acropora Millepora) to Elevated Temperature and Settlement Inducers Using a Novel RNA-Seq Procedure.” *Molecular Ecology* 20 (17): 3599–3616. https://doi.org/10.1111/j.1365-294X.2011.05205.x.

Morgan, Kyle M., Chris T. Perry, Jamie A. Johnson, and Scott G. Smithers. 2017. "Nearshore Turbid-Zone Corals Exhibit High Bleaching Tolerance on the Great Barrier Reef Following the 2016 Ocean Warming Event." *Frontiers in Marine Science* 4. https://www.frontiersin.org/articles/10.3389/fmars.2017.00224.

Morley, James W., Rebecca L. Selden, Robert J. Latour, Thomas L. Frölicher, Richard J. Seagraves, and Malin L. Pinsky. 2018. "Projecting Shifts in Thermal Habitat for 686 Species on the North American Continental Shelf." *PLOS ONE* 13 (5): e0196127. https://doi.org/10.1371/journal.pone.0196127.

Morrow, K. M., E. Muller, and M. P. Lesser. 2018. "How Does the Coral Microbiome Cause, Respond to, or Modulate the Bleaching Process?" In *Coral Bleaching: Patterns, Processes, Causes and Consequences*, edited by Madeleine J. H. van Oppen and Janice M. Lough, 153–88. Ecological Studies. Cham: Springer International Publishing. https://doi.org/10.1007/978-3-319-75393-5_7.

Mucci, Alfonso. 1983. "The Solubility of Calcite and Aragonite in Seawater at Various Salinities, Temperatures, and One Atmosphere Total Pressure." *American Journal of Science* 283 (7): 780–99. https://doi.org/10.2475/ajs.283.7.780.

Muscatine, L. 1990. "The Role of Symbiotic Algae in Carbon and Energy Flux in Reef Corals." *Ecosystems of the World*. https://www.semanticscholar.org/paper/The-role-of-symbiotic-algae-in-carbon-and-energy-in-Muscatine/40b336effe682ec15dbe77436da337f7d94491b0.

Muscatine, L., L. R. McCloskey, and R. E. Marian. 1981. "Estimating the Daily Contribution of Carbon from Zooxanthellae to Coral Animal Respiration1." *Limnology and Oceanography* 26 (4): 601–11. https://doi.org/10.4319/lo.1981.26.4.0601.

Noonan, Sam H. C., and Katharina E. Fabricius. 2016. "Ocean Acidification Affects Productivity but Not the Severity of Thermal Bleaching in Some Tropical Corals." *ICES Journal of Marine Science* 73 (3): 715–26. https://doi.org/10.1093/icesjms/fsv127.

Nunes, Flavia L. D., Richard D. Norris, and Nancy Knowlton. 2011. "Long Distance Dispersal and Connectivity in Amphi-Atlantic Corals at Regional and Basin Scales." *PLoS ONE* 6 (7): e22298. https://doi.org/10.1371/journal.pone.0022298.

Okazaki, Remy R., Erica K. Towle, Ruben van Hooidonk, Carolina Mor, Rivah N. Winter, Alan M. Piggot, Ross Cunning, et al. 2017. "Species-Specific Responses to Climate Change and Community Composition Determine Future Calcification Rates of Florida Keys Reefs." *Global Change Biology* 23 (3): 1023–35. https://doi.org/10.1111/gcb.13481.

Oksanen, Jari, Gavin L. Simpson, F. Guillaume Blanchet, Roeland Kindt, Pierre Legendre, Peter R. Minchin, R. B. O'Hara, et al. 2022. "Vegan: Community Ecology Package." https://CRAN.R-project.org/package=vegan.

Oliver, T. A., and S. R. Palumbi. 2011. "Do Fluctuating Temperature Environments Elevate Coral Thermal Tolerance?" *Coral Reefs* 30 (2): 429–40. https://doi.org/10.1007/s00338-011-0721-y.

Parada, Alma E., David M. Needham, and Jed A. Fuhrman. 2016. "Every Base Matters: Assessing Small Subunit RRNA Primers for Marine Microbiomes with Mock Communities, Time Series and Global Field Samples." *Environmental Microbiology* 18 (5): 1403–14. https://doi.org/10.1111/1462-2920.13023.

Parmesan, Camille. 2006. "Ecological and Evolutionary Responses to Recent Climate Change." *Annual Review of Ecology, Evolution, and Systematics* 37 (1): 637–69. https://doi.org/10.1146/annurev.ecolsys.37.091305.110100.

Parmesan, Camille, and Gary Yohe. 2003. "A Globally Coherent Fingerprint of Climate Change Impacts across Natural Systems." *Nature* 421 (6918): 37–42. https://doi.org/10.1038/nature01286.

Pochon, X., J. Pawlowski, L. Zaninetti, and R. Rowan. 2001. "High Genetic Diversity and Relative Specificity among Symbiodinium-like Endosymbiotic Dinoflagellates in Soritid Foraminiferans." *Marine Biology* 139 (6): 1069–78. https://doi.org/10.1007/s002270100674.

Pörtner, H, DC Roberts, V Masson-Delmotte, P Zhai, M Tignor, E Poloczanska, K Mintenbeck, et al. 2019. "IPCC Special Report on the Ocean and Cryosphere in a Changing Climate." IPCC. https://www.ipcc.ch/srocc/.

Prada, Carlos, and Michael E. Hellberg. 2021. "Speciation-by-Depth on Coral Reefs: Sympatric Divergence with Gene Flow or Cryptic Transient Isolation?" *Journal of Evolutionary Biology* 34 (1): 128–37. https://doi.org/10.1111/jeb.13731.

Price, Morgan N., Paramvir S. Dehal, and Adam P. Arkin. 2009. "FastTree: Computing Large Minimum Evolution Trees with Profiles Instead of a Distance Matrix." *Molecular Biology and Evolution* 26 (7): 1641–50. https://doi.org/10.1093/molbev/msp077.

Puntin, Giulia, Michael Sweet, Sebastian Fraune, Mónica Medina, Koty Sharp, Virginia M. Weis, and Maren Ziegler. 2022. "Harnessing the Power of Model Organisms To Unravel Microbial Functions in the Coral Holobiont." *Microbiology and Molecular Biology Reviews* 86 (4): e00053-22. https://doi.org/10.1128/mmbr.00053-22.

Putnam, Hollie M., Katie L. Barott, Tracy D. Ainsworth, and Ruth D. Gates. 2017. "The Vulnerability and Resilience of Reef-Building Corals." *Current Biology* 27 (11): R528–40. https://doi.org/10.1016/j.cub.2017.04.047.

Quast, Christian, Elmar Pruesse, Pelin Yilmaz, Jan Gerken, Timmy Schweer, Pablo Yarza, Jörg Peplies, and Frank Oliver Glöckner. 2013. "The SILVA Ribosomal RNA Gene Database Project: Improved Data Processing and Web-Based Tools." *Nucleic Acids Research* 41 (D1): D590–96. https://doi.org/10.1093/nar/gks1219.

Quigley, Kate M., Line K. Bay, and Bette L. Willis. 2017. "Temperature and Water Quality-Related Patterns in Sediment-Associated Symbiodinium Communities Impact Symbiont Uptake and Fitness of Juveniles in the Genus Acropora." *Frontiers in Marine Science* 4. https://www.frontiersin.org/articles/10.3389/fmars.2017.00401.

R Core Team. 2017. "R Core Team (2017). R: A Language and Environment for Statistical Computing." *R Found. Stat. Comput. Vienna, Austria*.

———. 2022. "R: A Language and Environment for Statistical Computing." Vienna, Austria: R Foundation for Statistical Computing. https://www.R-project.org/.

Rädecker, Nils, Claudia Pogoreutz, Christian R. Voolstra, Jörg Wiedenmann, and Christian Wild. 2015. "Nitrogen Cycling in Corals: The Key to Understanding Holobiont Functioning?" *Trends in Microbiology* 23 (8): 490–97. https://doi.org/10.1016/j.tim.2015.03.008.

Rahmstorf, Stefan, and Dim Coumou. 2011. "Increase of Extreme Events in a Warming World." *Proceedings of the National Academy of Sciences* 108 (44): 17905–9. https://doi.org/10.1073/pnas.1101766108.

Reynaud, Stéphanie, Nicolas Leclercq, Samantha Romaine-Lioud, Christine Ferrier-Pagés, Jean Jaubert, and Jean-Pierre Gattuso. 2003. "Interacting Effects of CO2 Partial Pressure and Temperature on Photosynthesis and Calcification in a Scleractinian Coral." *Global Change Biology* 9 (11): 1660–68. https://doi.org/10.1046/j.1365-2486.2003.00678.x.

Ries, J. B., A. L. Cohen, and D. C. McCorkle. 2010. "A Nonlinear Calcification Response to CO2-Induced Ocean Acidification by the Coral Oculina Arbuscula." *Coral Reefs* 29 (3): 661–74. https://doi.org/10.1007/s00338-010-0632-3.

Ries, Justin B. 2011. "A Physicochemical Framework for Interpreting the Biological Calcification Response to CO2-Induced Ocean Acidification." *Geochimica et Cosmochimica Acta* 75 (14): 4053–64. https://doi.org/10.1016/j.gca.2011.04.025.

Rigby, R. A., and D. M. Stasinopoulos. 2005. “Generalized Additive Models for Location, Scale and Shape.” *Journal of the Royal Statistical Society: Series C (Applied Statistics)* 54 (3): 507–54. https://doi.org/10.1111/j.1467-9876.2005.00510.x.

Rippe, John P., Groves B. Dixon, Zachary L. Fuller, Yi Liao, and Mikhail Matz. 2021. “Environmental Specialization and Cryptic Genetic Divergence in Two Massive Coral Species from the Florida Keys Reef Tract.” *Molecular Ecology* 30 (14): 3468–84. https://doi.org/10.1111/mec.15931.

Rivera, Hanny E., Hannah E. Aichelman, James E. Fifer, Nicola G. Kriefall, Daniel M. Wuitchik, Sara J. S. Wuitchik, and Sarah W. Davies. 2021. “A Framework for Understanding Gene Expression Plasticity and Its Influence on Stress Tolerance.” *Molecular Ecology* 30 (6): 1381–97. https://doi.org/10.1111/mec.15820.

Rivera, Hanny E., and Sarah W. Davies. 2021. “Symbiosis Maintenance in the Facultative Coral, Oculina Arbuscula, Relies on Nitrogen Cycling, Cell Cycle Modulation, and Immunity.” *Scientific Reports* 11 (1): 21226. https://doi.org/10.1038/s41598-021-00697-6.

Robidart, Julie C., Shellie R. Bench, Robert A. Feldman, Alexey Novoradovsky, Sheila B. Podell, Terry Gaasterland, Eric E. Allen, and Horst Felbeck. 2008. “Metabolic Versatility of the Riftia Pachyptila Endosymbiont Revealed through Metagenomics.” *Environmental Microbiology* 10 (3): 727–37. https://doi.org/10.1111/j.1462-2920.2007.01496.x.

Rodas, Andrea M., Rachel M. Wright, Logan K. Buie, Hannah E. Aichelman, Karl D. Castillo, and Sarah W. Davies. 2020. “Eukaryotic Plankton Communities across Reef Environments in Bocas Del Toro Archipelago, Panamá.” *Coral Reefs* 39 (5): 1453–67. https://doi.org/10.1007/s00338-020-01979-7.

Rodolfo-Metalpa, R., F. Houlbrèque, É. Tambutté, F. Boisson, C. Baggini, F. P. Patti, R. Jeffree, et al. 2011. “Coral and Mollusc Resistance to Ocean Acidification Adversely Affected by Warming.” *Nature Climate Change* 1 (6): 308–12. https://doi.org/10.1038/nclimate1200.

Rodrigues, Lisa J., and Andréa G. Grottoli. 2007. “Energy Reserves and Metabolism as Indicators of Coral Recovery from Bleaching.” *Limnology and Oceanography* 52 (5): 1874–82. https://doi.org/10.4319/lo.2007.52.5.1874.

Rose, Noah H., Rachael A. Bay, Megan K. Morikawa, and Stephen R. Palumbi. 2018. “Polygenic Evolution Drives Species Divergence and Climate Adaptation in Corals.” *Evolution* 72 (1): 82–94. https://doi.org/10.1111/evo.13385.

Rose, Noah H., Rachael A. Bay, Megan K. Morikawa, Luke Thomas, Elizabeth A. Sheets, and Stephen R. Palumbi. 2021. "Genomic Analysis of Distinct Bleaching Tolerances among Cryptic Coral Species." *Proceedings of the Royal Society B: Biological Sciences* 288 (1960): 20210678. https://doi.org/10.1098/rspb.2021.0678.

Rosenberg, Eugene, and Ilana Zilber-Rosenberg. 2018. "The Hologenome Concept of Evolution after 10 Years." *Microbiome* 6 (1): 78. https://doi.org/10.1186/s40168-018-0457-9.

Roth, Melissa S. 2014. "The Engine of the Reef: Photobiology of the Coral–Algal Symbiosis." *Frontiers in Microbiology* 5. https://www.frontiersin.org/articles/10.3389/fmicb.2014.00422.

Roth, Melissa S., Ralf Goericke, and Dimitri D. Deheyn. 2012. "Cold Induces Acute Stress but Heat Is Ultimately More Deleterious for the Reef-Building Coral Acropora Yongei." *Scientific Reports* 2 (1): 240. https://doi.org/10.1038/srep00240.

Roy, Rabindra N, Lakshimi N Roy, Kathleen M Vogel, C Porter-Moore, Tara Pearson, Catherine E Good, Frank J Millero, and Douglas M Campbell. 1993. "The Dissociation Constants of Carbonic Acid in Seawater at Salinities 5 to 45 and Temperatures 0 to 45°C." *Marine Chemistry*, Marine Physical Chemistry - in memory of the contributions made to the field by Dr. Ricardo Pytkowicz, 44 (2): 249–67. https://doi.org/10.1016/0304-4203(93)90207-5.

Ruel, Jonathan J., and Matthew P. Ayres. 1999. "Jensen's Inequality Predicts Effects of Environmental Variation." *Trends in Ecology & Evolution* 14 (9): 361–66. https://doi.org/10.1016/S0169-5347(99)01664-X.

Russel, Jakob. 2021. "Russel88/MicEco: V0.9.15." https://doi.org/10.5281/zenodo.4733747.

Safaie, Aryan, Nyssa J. Silbiger, Timothy R. McClanahan, Geno Pawlak, Daniel J. Barshis, James L. Hench, Justin S. Rogers, Gareth J. Williams, and Kristen A. Davis. 2018. "High Frequency Temperature Variability Reduces the Risk of Coral Bleaching." *Nature Communications* 9 (1): 1671. https://doi.org/10.1038/s41467-018-04074-2.

Sagan, Lynn. 1967. "On the Origin of Mitosing Cells." *Journal of Theoretical Biology* 14 (3): 225-IN6. https://doi.org/10.1016/0022-5193(67)90079-3.

Saxby, Tracey, William C. Dennison, and Ove Hoegh-Guldberg. 2003. "Photosynthetic Responses of the Coral Montipora Digitata to Cold Temperature Stress." *Marine*

*Ecology Progress Series* 248 (February): 85–97. https://doi.org/10.3354/meps248085.

Scheufen, Tim, Roberto Iglesias-Prieto, and Susana Enríquez. 2017. "Changes in the Number of Symbionts and Symbiodinium Cell Pigmentation Modulate Differentially Coral Light Absorption and Photosynthetic Performance." *Frontiers in Marine Science* 4. https://www.frontiersin.org/articles/10.3389/fmars.2017.00309.

Schneider, Caroline A., Wayne S. Rasband, and Kevin W. Eliceiri. 2012. "NIH Image to ImageJ: 25 Years of Image Analysis." *Nature Methods* 9 (7): 671–75. https://doi.org/10.1038/nmeth.2089.

Schoepf, Verena, Andréa G. Grottoli, Mark E. Warner, Wei-Jun Cai, Todd F. Melman, Kenneth D. Hoadley, D. Tye Pettay, et al. 2013. "Coral Energy Reserves and Calcification in a High-CO2 World at Two Temperatures." *PLOS ONE* 8 (10): e75049. https://doi.org/10.1371/journal.pone.0075049.

Schoepf, Verena, Maria U. Jung, Malcolm T. McCulloch, Nicole E. White, Michael Stat, and Luke Thomas. 2020. "Thermally Variable, Macrotidal Reef Habitats Promote Rapid Recovery From Mass Coral Bleaching." *Frontiers in Marine Science* 7. https://www.frontiersin.org/articles/10.3389/fmars.2020.00245.

Schoepf, Verena, Hermione Sanderson, and Ellis Larcombe. 2022. "Coral Heat Tolerance under Variable Temperatures: Effects of Different Variability Regimes and Past Environmental History vs. Current Exposure." *Limnology and Oceanography* 67 (2): 404–18. https://doi.org/10.1002/lno.12000.

Sheldon, Kimberly S., and Michael E. Dillon. 2016. "Beyond the Mean: Biological Impacts of Cryptic Temperature Change." *Integrative and Comparative Biology* 56 (1): 110–19. https://doi.org/10.1093/icb/icw005.

Shoguchi, Eiichi, Chuya Shinzato, Takeshi Kawashima, Fuki Gyoja, Sutada Mungpakdee, Ryo Koyanagi, Takeshi Takeuchi, et al. 2013. "Draft Assembly of the Symbiodinium Minutum Nuclear Genome Reveals Dinoflagellate Gene Structure." *Current Biology* 23 (15): 1399–1408. https://doi.org/10.1016/j.cub.2013.05.062.

Siebeck, U. E., N. J. Marshall, A. Klüter, and Ove Hoegh-Guldberg. 2006. "Monitoring Coral Bleaching Using a Colour Reference Card." *Coral Reefs* 25 (3): 453–60. https://doi.org/10.1007/s00338-006-0123-8.

Silverstein, Rachel N., Ross Cunning, and Andrew C. Baker. 2015. "Change in Algal Symbiont Communities after Bleaching, Not Prior Heat Exposure, Increases Heat

Tolerance of Reef Corals." *Global Change Biology* 21 (1): 236–49. https://doi.org/10.1111/gcb.12706.

Singh, M., S. Ceccarelli, and J. Hamblin. 1993. "Estimation of Heritability from Varietal Trials Data." *Theoretical and Applied Genetics* 86 (4): 437–41. https://doi.org/10.1007/BF00838558.

Skotte, Line, Thorfinn Sand Korneliussen, and Anders Albrechtsen. 2013. "Estimating Individual Admixture Proportions from Next Generation Sequencing Data." *Genetics* 195 (3): 693–702. https://doi.org/10.1534/genetics.113.154138.

Smale, Dan A., Thomas Wernberg, Eric C. J. Oliver, Mads Thomsen, Ben P. Harvey, Sandra C. Straub, Michael T. Burrows, et al. 2019. "Marine Heatwaves Threaten Global Biodiversity and the Provision of Ecosystem Services." *Nature Climate Change* 9 (4): 306–12. https://doi.org/10.1038/s41558-019-0412-1.

Smith, Schuyler. 2019. "Schuyler-Smith/Phylosmith: Initial Release." https://doi.org/10.5281/zenodo.3251024.

Somero, G. N. 2010. "The Physiology of Climate Change: How Potentials for Acclimatization and Genetic Adaptation Will Determine 'Winners' and 'Losers.'" *Journal of Experimental Biology* 213 (6): 912–20. https://doi.org/10.1242/jeb.037473.

Speare, Lauren, Sarah W. Davies, John P. Balmonte, Justin Baumann, and Karl D. Castillo. 2020. "Patterns of Environmental Variability Influence Coral-Associated Bacterial and Algal Communities on the Mesoamerican Barrier Reef." *Molecular Ecology* 29 (13): 2334–48. https://doi.org/10.1111/mec.15497.

Spencer Davies, P. 1989. "Short-Term Growth Measurements of Corals Using an Accurate Buoyant Weighing Technique." *Marine Biology* 101 (3): 389–95. https://doi.org/10.1007/BF00428135.

Spicer, John I., and Kevin J. Gaston. 1999. *Physiological Diversity and Its Ecological Implications*. Oxford, United Kingdom: Blackwell Science Limited. https://doi.org/10.1093/auk/118.1.279.

Stat, Michael, Dee Carter, and Ove Hoegh-Guldberg. 2006. "The Evolutionary History of Symbiodinium and Scleractinian Hosts—Symbiosis, Diversity, and the Effect of Climate Change." *Perspectives in Plant Ecology, Evolution and Systematics* 8 (1): 23–43. https://doi.org/10.1016/j.ppees.2006.04.001.

Stat, Michael, and Ruth D. Gates. 2010. "Clade D *Symbiodinium* in Scleractinian Corals: A 'Nugget' of Hope, a Selfish Opportunist, an Ominous Sign, or All of the

Above?" *Journal of Marine Sciences* 2011 (October): e730715. https://doi.org/10.1155/2011/730715.

Stat, Michael, Xavier Pochon, Rebecca O. M. Cowie, and Ruth D. Gates. 2009. "Specificity in Communities of Symbiodinium in Corals from Johnston Atoll." *Marine Ecology Progress Series* 386 (July): 83–96. https://doi.org/10.3354/meps08080.

Stevens, George C. 1989. "The Latitudinal Gradient in Geographical Range: How so Many Species Coexist in the Tropics." *The American Naturalist* 133 (2): 240–56.

Stocker, T.F., D. Qin, G.-K. Plattner, M. Tignor, S.K. Allen, J. Boschung, A. Nauels, Y. Xia, V. Bex, and P.M. Midgley. 2013. "IPCC, 2013: Climate Change 2013: The Physical Science Basis. Contribution of Working Group I to the Fifth Assessment Report of the Intergovernmental Panel on Climate Change." https://www.ipcc.ch/report/ar5/wg1/.

Stuart-Smith, Rick D., Christopher J. Brown, Daniela M. Ceccarelli, and Graham J. Edgar. 2018. "Ecosystem Restructuring along the Great Barrier Reef Following Mass Coral Bleaching." *Nature* 560 (7716): 92–96. https://doi.org/10.1038/s41586-018-0359-9.

Sully, S., D. E. Burkepile, M. K. Donovan, G. Hodgson, and R. van Woesik. 2019. "A Global Analysis of Coral Bleaching over the Past Two Decades." *Nature Communications* 10 (1): 1264. https://doi.org/10.1038/s41467-019-09238-2.

Szabó, Milán, Anthony W. D. Larkum, and Imre Vass. 2020. "A Review: The Role of Reactive Oxygen Species in Mass Coral Bleaching." In *Photosynthesis in Algae: Biochemical and Physiological Mechanisms*, edited by Anthony W.D. Larkum, Arthur R. Grossman, and John A. Raven, 459–88. Advances in Photosynthesis and Respiration. Cham: Springer International Publishing. https://doi.org/10.1007/978-3-030-33397-3_17.

Takahashi, Shunichi, Spencer Whitney, Shigeru Itoh, Tadashi Maruyama, and Murray Badger. 2008. "Heat Stress Causes Inhibition of the de Novo Synthesis of Antenna Proteins and Photobleaching in Cultured Symbiodinium." *Proceedings of the National Academy of Sciences* 105 (11): 4203–8. https://doi.org/10.1073/pnas.0708554105.

Talevich, Eric, Brandon M. Invergo, Peter JA Cock, and Brad A. Chapman. 2012. "Bio.Phylo: A Unified Toolkit for Processing, Analyzing and Visualizing Phylogenetic Trees in Biopython." *BMC Bioinformatics* 13 (1): 209. https://doi.org/10.1186/1471-2105-13-209.

Tchernov, Dan, Maxim Y. Gorbunov, Colomban de Vargas, Swati Narayan Yadav, Allen J. Milligan, Max Häggblom, and Paul G. Falkowski. 2004. "Membrane Lipids of Symbiotic Algae Are Diagnostic of Sensitivity to Thermal Bleaching in Corals." *Proceedings of the National Academy of Sciences* 101 (37): 13531–35. https://doi.org/10.1073/pnas.0402907101.

Thomas, Luke, Noah H. Rose, Rachael A. Bay, Elora H. López, Megan K. Morikawa, Lupita Ruiz-Jones, and Stephen R. Palumbi. 2018. "Mechanisms of Thermal Tolerance in Reef-Building Corals across a Fine-Grained Environmental Mosaic: Lessons from Ofu, American Samoa." *Frontiers in Marine Science* 4. https://www.frontiersin.org/articles/10.3389/fmars.2017.00434.

Thornhill, Daniel J., Dustin W. Kemp, Brigitte U. Bruns, William K. Fitt, and Gregory W. Schmidt. 2008. "Correspondence Between Cold Tolerance and Temperate Biogeography in a Western Atlantic Symbiodinium (Dinophyta) Lineage1." *Journal of Phycology* 44 (5): 1126–35. https://doi.org/10.1111/j.1529-8817.2008.00567.x.

Towle, Erica K., Ian C. Enochs, and Chris Langdon. 2015. "Threatened Caribbean Coral Is Able to Mitigate the Adverse Effects of Ocean Acidification on Calcification by Increasing Feeding Rate." *PLOS ONE* 10 (4): e0123394. https://doi.org/10.1371/journal.pone.0123394.

Trachsel, Julian. n.d. "Funfuns." Funfuns. https://github.com/Jtrachsel/funfuns/.

Urban, Mark C. 2015. "Accelerating Extinction Risk from Climate Change." *Science* 348 (6234): 571–73. https://doi.org/10.1126/science.aaa4984.

Vuuren, Detlef P. van, Jae Edmonds, Mikiko Kainuma, Keywan Riahi, Allison Thomson, Kathy Hibbard, George C. Hurtt, et al. 2011. "The Representative Concentration Pathways: An Overview." *Climatic Change* 109 (1): 5. https://doi.org/10.1007/s10584-011-0148-z.

Wall, Christopher B., R. A. B. Mason, W. R. Ellis, R. Cunning, and R. D. Gates. 2017. "Elevated $pCO_2$ Affects Tissue Biomass Composition, but Not Calcification, in a Reef Coral under Two Light Regimes." *Royal Society Open Science* 4 (11): 170683. https://doi.org/10.1098/rsos.170683.

Wall, Christopher B., Contessa A. Ricci, Grace E. Foulds, Laura D. Mydlarz, Ruth D. Gates, and Hollie M. Putnam. 2018. "The Effects of Environmental History and Thermal Stress on Coral Physiology and Immunity." *Marine Biology* 165 (3): 56. https://doi.org/10.1007/s00227-018-3317-z.

Wang, Shi, Eli Meyer, John K McKay, and Mikhail V Matz. 2012. “2b-RAD: A Simple and Flexible Method for Genome-Wide Genotyping.” *Nature Methods* 9 (8): 808–10. https://doi.org/10.1038/nmeth.2023.

Wangpraseurt, Daniel, Jacob B. Holm, Anthony W. D. Larkum, Mathieu Pernice, Peter J. Ralph, David J. Suggett, and Michael Kühl. 2017. “In Vivo Microscale Measurements of Light and Photosynthesis during Coral Bleaching: Evidence for the Optical Feedback Loop?” *Frontiers in Microbiology* 8. https://www.frontiersin.org/articles/10.3389/fmicb.2017.00059.

Weis, Virginia M. 2008. “Cellular Mechanisms of Cnidarian Bleaching: Stress Causes the Collapse of Symbiosis.” *Journal of Experimental Biology* 211 (19): 3059–66. https://doi.org/10.1242/jeb.009597.

Wernegreen, Jennifer J. 2012. “Endosymbiosis.” *Current Biology* 22 (14): R555–61. https://doi.org/10.1016/j.cub.2012.06.010.

West-Eberhard, Mary Jane. 2005. “Developmental Plasticity and the Origin of Species Differences.” *Proceedings of the National Academy of Sciences* 102 (suppl_1): 6543–49. https://doi.org/10.1073/pnas.0501844102.

Worner, Susan P. 1992. “Performance of Phenological Models Under Variable Temperature Regimes: Consequences of the Kaufmann or Rate Summation Effect.” *Environmental Entomology* 21 (4): 689–99. https://doi.org/10.1093/ee/21.4.689.

Wright, Rachel M., Galina V. Aglyamova, Eli Meyer, and Mikhail V. Matz. 2015. “Gene Expression Associated with White Syndromes in a Reef Building Coral, Acropora Hyacinthus.” *BMC Genomics* 16 (1): 371. https://doi.org/10.1186/s12864-015-1540-2.

Wuitchik, Daniel M., Adeline Almanzar, Brooke E. Benson, Sara Brennan, Juan D. Chavez, Mary B. Liesegang, Jennifer L. Reavis, et al. 2021. “Characterizing Environmental Stress Responses of Aposymbiotic Astrangia Poculata to Divergent Thermal Challenges.” *Molecular Ecology* 30 (20): 5064–79. https://doi.org/10.1111/mec.16108.

Xiang, Tingting, Erik Lehnert, Robert E. Jinkerson, Sophie Clowez, Rick G. Kim, Jan C. DeNofrio, John R. Pringle, and Arthur R. Grossman. 2020. “Symbiont Population Control by Host-Symbiont Metabolic Interaction in Symbiodiniaceae-Cnidarian Associations.” *Nature Communications* 11 (1): 108. https://doi.org/10.1038/s41467-019-13963-z.

Zhang, Huan, Yubo Hou, Lilibeth Miranda, David A. Campbell, Nancy R. Sturm, Terry Gaasterland, and Senjie Lin. 2007. “Spliced Leader RNA Trans-Splicing in

Dinoflagellates." *Proceedings of the National Academy of Sciences* 104 (11): 4618–23. https://doi.org/10.1073/pnas.0700258104.

Zhang, Yuqing, Giovanni Parmigiani, and W Evan Johnson. 2020. "ComBat-Seq: Batch Effect Adjustment for RNA-Seq Count Data." *NAR Genomics and Bioinformatics* 2 (3): lqaa078. https://doi.org/10.1093/nargab/lqaa078.

Ziegler, Maren, Carsten G. B. Grupstra, Marcelle M. Barreto, Martin Eaton, Jaafar BaOmar, Khalid Zubier, Abdulmohsin Al-Sofyani, Adnan J. Turki, Rupert Ormond, and Christian R. Voolstra. 2019. "Coral Bacterial Community Structure Responds to Environmental Change in a Host-Specific Manner." *Nature Communications* 10 (1): 3092. https://doi.org/10.1038/s41467-019-10969-5.

Ziegler, Maren, Francois O. Seneca, Lauren K. Yum, Stephen R. Palumbi, and Christian R. Voolstra. 2017. "Bacterial Community Dynamics Are Linked to Patterns of Coral Heat Tolerance." *Nature Communications* 8 (1): 14213. https://doi.org/10.1038/ncomms14213.

**CURRICULUM VITAE**